

UNCLASSIFIED

AD 222 928

*Reproduced
by the*

**ARMED SERVICES TECHNICAL INFORMATION AGENCY
ARLINGTON HALL STATION
ARLINGTON 12, VIRGINIA**



UNCLASSIFIED

NOTICE: When government or other drawings, specifications or other data are used for any purpose other than in connection with a definitely related government procurement operation, the U. S. Government thereby incurs no responsibility, nor any obligation whatsoever; and the fact that the Government may have formulated, furnished, or in any way supplied the said drawings, specifications, or other data is not to be regarded by implication or otherwise as in any manner licensing the holder or any other person or corporation, or conveying any rights or permission to manufacture, use or sell any patented invention that may in any way be related thereto.

Office of Ordnance Research

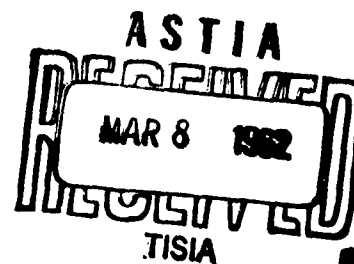
TRANSACTIONS OF THE SECOND CONFERENCE
OF
ARSENAL MATHEMATICIANS

UNANNOUNCED

AD NO. - 222 928

ASTIA FILE COPY

FILE COPY
Return to
ASTIA
ARLINGTON HALL STATION
ARLINGTON 12, VIRGINIA
Attn: TIRS



OFFICE OF ORDNANCE RESEARCH, U.S. ARMY
BOX CM, DUKE STATION
DURHAM, NORTH CAROLINA

OFFICE OF ORDNANCE RESEARCH

Report No. 57-2

July 1957

TRANSACTIONS OF THE SECOND CONFERENCE
OF ARSENAL MATHEMATICIANS

FOREIGN ANNOUNCEMENT AND DISSEMINATION
OF THIS REPORT BY ASTIA IS LIMITED

held at the Ballistic Research Laboratories
February 24, 1956

Office of Ordnance Research
Ordnance Corps, U. S. Army
Box CM, Duke Station
Durham, North Carolina

FOREWORD

The Ballistic Research Laboratories served as host to the Second Conference of Arsenal Mathematicians. This one-day meeting was held 24 February 1956. Colonel A. R. del Campo, Director of the Laboratories, extended a welcome to those in attendance, and then commented on the contributions which mathematicians are making in various specific areas. He also mentioned a few of the training programs currently active at the Aberdeen Proving Ground. Following the talk by Colonel del Campo, Sessions A and B of contributed papers were started and these continued until noon. Session A was chairmanned by Professor H. H. Goldstine of the Institute for Advanced Study, while Associate Technical Director of the Ballistic Research Laboratories, R. H. Kent, served in a similar capacity for Session B. Following lunch more contributed papers were presented at Sessions C and D. Dr. George Glockler, Chief Scientist of the Office of Ordnance Research, and Mr. R. R. Kuebler, of the Office of the Chief of Ordnance, served as Chairmen of these two phases of the program which continued until mid-afternoon. At 1500 the group of some seventy-five scientists in attendance at the conference came together to hear an invited address by Dr. C. B. Tompkins of the University of California. His address was entitled Linear Programming and High Speed Computer Applications. Colonel P. N. Gillon, Commanding Officer of the Office of Ordnance Research, was the Chairman of this final portion of the conference.

Fourteen scientific papers ^{on ordnance problems are} presented ~~by several personnel~~. Boundary layer problems, stress analysis, ballistic equations, stability and heat conduction problems, computer and automatic weapon analysis were some of the many topics in applied mathematics that were ~~discussed during the conference~~.

While it was gratifying to the committee on arrangements to have an over supply of program material, it was unfortunate that time did not permit presentation of all the submitted papers. A two-day conference would have been organized had it been possible to foresee the amount and the quality of the available talent.

Initial Distribution

The initial distribution list of the Transactions of the Second Conference of Arsenal Mathematicians includes those who attended the meeting and/or the government installations with which they are associated. For economy, only a limited number of copies have been sent to each. Additional copies will be transmitted upon request.

TABLE OF CONTENTS

	Page
Foreword	iii
Program	vii
Three-Dimensional Boundary Layers*	
By R. Sedney	
A Numerical Solution of Boundary Value Problems for Nonlinear Ordinary Differential Equations	
By Erwin Fehlberg	1
The Measurement of Nonlinear Forces and Moments by Free Flight Tests	
By C. H. Murphy	9
An Analogue Computer Study of Interior Ballistic Equations	
By William Dittrich	21
The Response of a Tapered Cantilever Beam When a Transient Force is Applied at the End	
By A. S. Elder	35
Analysis of an Infinite Plate Containing Radial Cracks Originating at the Boundary of an Internal Circular Hole	
By O. L. Bowie	67
Analysis of the N-Wave of a Slender Supersonic Projectile	
By D. Steininger and F. D. Bennett.	87
Engraving Pressures for Rotating Bands - An Estimate of Contact Pressure for Continued Normal Engraving of Rectangular Bands	
By E. W. Ross, Jr.	113
Stability of a Liquid-Filled Shell	
By Pvt. L. E. Schmidt**	
Analog Computer Simulation of Automatic Weapons	
By E. H. Jakubowski	137
The Solidification of Molten Material in Finite Regions	
By A. Nordio	157
Fly-Off Rotation Bands Under Centrifugal Loading	
By F. I. Baratta and J. I. Bluhm.	181

* This paper was presented at the Conference. It is not published in these Transactions.

** This paper can be found in a classified security information (SECRET) Appendix of this Report.

TABLE OF CONTENTS

	Page
The Effect of Particle Suspensions on the Flow of a Gas By H. N. Brown*	211
Determination of Elastic Stresses in Chamber Sections of Recoilless Rifles By P. R. Radkowski.	225
Linear Programming and High Speed Computer Applications By C. B. Tompkins	249
Basic Principles of a Two-Dimensional Slide Rule By C. R. White	283

* On the Program a paper with a similar title was presented under the joint authorship of H. Brown and R. Makino.

PROGRAM
 CONFERENCE OF ORDNANCE MATHEMATICIANS
 BALLISTIC RESEARCH LABORATORIES

24 February 1956

Sessions A and B on Friday morning will run concurrently. Sessions C and D on Friday afternoon will also run concurrently. The first paper listed in Session C is classified SECRET. From 1450 to 1550, Session E will be the only session in order.

MORNING

(All times shown are Eastern Standard Time)

Room

0745-0835	259	REGISTRATION
0835-0850	259	WELCOMING REMARKS - Col. A. R. del Campo, Director, Ballistic Research Laboratories
0900-1130	259	SESSION A - Chairman: H. H. Goldstine, The Institute for Advanced Study
0900-0930 - Three-Dimensional Boundary Layers		
R. Sedney Ballistic Research Laboratories		
0930-1000 - A Numerical Solution of Boundary Value Problems for Nonlinear Ordinary Differential Equations		
Erwin Fehlberg, Redstone Arsenal		
1000-1030 INTERMISSION		
1030-1100 - Measurement of Nonlinear Forces and Moments by Free Flight Tests		
C. H. Murphy Ballistic Research Laboratories		
1100-1130 - An Analogue Computer Study of Interior Ballistic Equations		
William Dittrich Frankford Arsenal		

	<u>Room</u>	
0900-1130	211	SESSION B - Chairman: R. H. Kent, Ballistic Research Laboratories
		0900-0930 The Response of Tapered Cantilever Beams When a Transient Force is Applied to the End A. S. Elder, Ballistic Research Laboratories
		0930-1000 Analysis of an Infinite Plate Containing Radial Cracks Originating at the Boundary of an Internal Circular Hole O. L. Bowie, Watertown Arsenal
		1000-1030 INTERMISSION
		1030-1100 Analysis of the N-Wave of a Slender Supersonic Projectile D. Steininger and F. D. Bennett Ballistic Research Laboratories
		1100-1130 Engraving Pressures for Rotating Bands - An Estimate of Contact Pressure for Continued Normal Engraving of Rectangular Bands E. W. Ross, Jr., Watertown Arsenal
1130-1300		LUNCHEON
		AFTERNOON
1300-1430	259	SESSION C - In this session the paper by Pvt. L. E. Schmidt carries a classification of SECRET Chairman: George Glockler, Office of Ordnance Research
		1300-1330 Stability of a Liquid-Filled Shell Pvt. L. E. Schmidt, Picatinny Arsenal
		1330-1400 Analog Computer Simulation of Automatic Weapons E. H. Jakubowski, Springfield Armory
		1400-1430 The Solidification of Molten Material in Finite Regions A. Nordio, Picatinny Arsenal

	<u>Room</u>	
1300-1430	211	SESSION D - Chairman: Roy R. Kuebler, Office of the Chief of Ordnance
		1300-1330 Fly-Off Rotation Bands J. I. Bluhm and F. I. Baratta Watertown Arsenal
		1330-1400 The Effect of Suspensions on Unsteady Gas Flow H. Brown and R. Makino Ballistic Research Laboratories
		1400-1430 Determination of Elastic Stresses in Chamber Sections of Recoilless Rifles P. R. Radowski, Watertown Arsenal
1430-1450		INTERMISSION
1450-1550	259	SESSION E - Chairman: Colonel P. N. Gillon, Ordnance Corps Commanding Officer Office of Ordnance Research
		1450-1550 Linear Programming and High Speed Computer Applications C. B. Tompkins University of California

SUPPLEMENTARY PROGRAM

(To be presented by title)

A Physical Explanation of an Anomaly in a Radar Energy Study

L. M. Court, Diamond Ordnance Fuze Laboratories

Approximate Solutions of Non-Linear Differential Equations Arising in
Ballistics

A. S. Galbraith, Eglin Air Force Base

Stability of the Solution to Differential Equations Arising in Ballistics

A. S. Galbraith, Eglin Air Force Base

Basic Principles of a Two-Dimensional Slide Rule

C. R. White, Ballistic Research Laboratories

Problems in Interferogram Reduction

F. D. Bennett, Ballistic Research Laboratories

x

Refraction Operators in Ray Tracing Through Cones of Constant Index

F. D. Bennett, Ballistic Research Laboratories

Refraction of Light in Conical Flow Fields

R. Sedney and N. Gerber

A NUMERICAL SOLUTION OF BOUNDARY VALUE PROBLEMS FOR NONLINEAR ORDINARY DIFFERENTIAL EQUATIONS

By
Erwin Fehlberg
Redstone Arsenal, Huntsville, Alabama

Introduction. This paper presents a numerical approach to the iteration method as applied to boundary value problems for ordinary differential equations.

Instead of using a numerical integration procedure for the iteration method, expansions in series are applied. In this way the solution is obtained in an analytical form and can easily be computed for any value of the argument. In article 1 the method will be explained in detail for the second- order differential equation. In article 2 the results for the third- and fourth- order differential equation are summarized.

This paper is not concerned with the investigation of criteria for the convergence of the iteration method, but it is always assumed that the considered boundary value problem has a solution and that the iteration procedure converges to this solution.

1. Second- order differential equation. We assume the differential equation has the form:

$$y'' = f(x, y, y'), \quad (1.1)$$

and we are interested in an integral of this equation that solves the following boundary value problem:

$$\begin{aligned} x = -1 : y &= y(-1), \\ x = +1 : y &= y(+1). \end{aligned} \quad (1.2)$$

A linear substitution on x will transform any finite interval $a \leq x \leq b$ into $-1 \leq x \leq +1$. Therefore, our choice of the x -values in (1.2) does not mean any restriction.

According to the iteration procedure we have to introduce into the right-hand side of (1.1) an approximate solution of (1.1) which satisfies (1.2). By this introduction the right-hand side of (1.1) reduces to a function of x alone:

$$y'' = f(x). \quad (1.3)$$

Integrating twice we get the next approximation for our solution, the constants of integration being determined by the boundary values (1.2).

To perform in a convenient way this integration procedure of successive approximation, we make use of expansions in Legendre series. Let us put in (1.3):

$$y'' = f(x) = \sum_n F_n \cdot P_n(x), \quad (1.4)$$

the Legendre coefficients F_n being given in well-known manner by:

$$F_n = \frac{2n+1}{2} \cdot \int_{-1}^{+1} f(x) P_n(x) dx. \quad (1.5)$$

For the required solution $y(x)$ of (1.4) we similarly put:

$$y(x) = \sum_n Y_n \cdot P_n(x) \quad (1.6)$$

with unknown coefficients. However, these unknown coefficients Y_n can easily be expressed by the well-known coefficients F_n of the right-hand side of (1.4).

Denoting the integral $\int f(x) dx$ by $^{(1)}f(x)$ and the integral $\int ^{(1)}f(x) dx$ by $^{(2)}f(x)$, from (1.4) follows:

$$y = ^{(2)}f(x). \quad (1.7)$$

The coefficients Y_n in (1.6) are then given by:

$$Y_n = \frac{2n+1}{2} \int_{-1}^{+1} ^{(2)}f(x) P_n(x) dx. \quad (1.8)$$

Integration by parts reduces (1.8) in the following manner:

$$\begin{aligned} Y_n &= \frac{2n+1}{2} \left[^{(2)}f(x) \cdot ^{(1)}P_n(x) \right]_{-1}^{+1} - \frac{2n+1}{2} \int_{-1}^{+1} ^{(1)}f(x) \cdot ^{(1)}P_n(x) dx \\ Y_n &= \frac{2n+1}{2} \left[^{(2)}f(x) ^{(1)}P_n(x) \right]_{-1}^{+1} - \frac{2n+1}{2} \left[^{(1)}f(x) ^{(2)}P_n(x) \right]_{-1}^{+1} + \frac{2n+1}{2} \cdot \\ &\quad \int_{-1}^{+1} f(x) \cdot ^{(2)}P_n(x) dx. \end{aligned} \quad (1.9)$$

We assume $n \geq 2$ and compute Y_0 and Y_1 later by means of the boundary values.

Then the first two terms on the right-hand side of (1.9) are zero. This follows for the first term from the well-known relation:

$$(2n+1) \cdot ^{(1)}P_n(x) = P_{n+1}(x) - P_{n-1}(x) \quad (1.10)$$

for Legendre's polynomials. For the second term this follows by integrating (1.10):

$$\begin{aligned} (2n+1) ^{(2)}P_n(x) &= ^{(1)}P_{n+1}(x) - ^{(1)}P_{n-1}(x) \\ (2n+1) ^{(2)}P_2(x) &= \frac{1}{2n+3} \left[P_{n+2}(x) - P_n(x) \right] - \frac{1}{2n-1} \cdot \\ &\quad \left[P_n(x) - P_{n-2}(x) \right]. \end{aligned} \quad (1.11)$$

The equation (1.9) then reduces to:

$$Y_n = \frac{2n+1}{2} \int_{-1}^{+1} f(x) {}^{(2)}P_n(x) dx \quad (n \geq 2) \quad (1.12)$$

or, using (1.11):

$$Y_n = \frac{1}{2n+3} \cdot \frac{1}{2} \int_{-1}^{+1} f(x) P_{n+2}(x) dx - \frac{2n+1}{(2n+3)(2n-1)} \int_{-1}^{+1} f(x) P_n(x) dx +$$

$$\frac{1}{2n-1} \cdot \frac{1}{2} \int_{-1}^{+1} f(x) P_{n-2}(x) dx \quad (n \geq 2)$$

or:

$$Y_n = \frac{F_{n-2}}{(2n-3)(2n-1)} - \frac{2F_n}{(2n-1)(2n+3)} + \frac{F_{n+2}}{(2n+3)(2n+5)} \quad (n \geq 2) \quad (1.13)$$

By (1.13) the coefficients Y_n ($n \geq 2$) of our approximate solution $y(x)$ can immediately be computed as soon as the Legendre coefficients F_n of (1.4) are known. However, the determination of the F_n is a relatively easy problem and comparable e.g. to the determination of the coefficients of a Fourier series. As to the technique of the determination of the F_n , the reader may be referred to two former papers of the author*).

We still have to determine Y_0 and Y_1 . From (1.2) follows:

$$Y_0 + Y_1 + Y_2 + \dots + Y_n + \dots = y(+1) \quad (1.14)$$

$$Y_0 - Y_1 + Y_2 + \dots + (-1)^n Y_n + \dots = y(-1).$$

Introducing the abbreviations:

$$\frac{1}{2} [y(+1) + y(-1)] = \bar{y}(1)$$

$$\frac{1}{2} [y(+1) - y(-1)] = \bar{\bar{y}}(1), \quad (1.15)$$

we obtain from (1.14) by addition or subtraction:

$$Y_0 + Y_2 + Y_4 + \dots + Y_{2n} + \dots = \bar{y}(1)$$

$$Y_1 + Y_3 + Y_5 + \dots + Y_{2n+1} + \dots = \bar{\bar{y}}(1). \quad (1.16)$$

* Zeitschr. f. angew. Math. Mech. 24 (1944), p. 71/76

" " " " 31 (1951), p. 104/114.

From the first equation (1.16) and from (1.13) follows:

$$Y_0 = \bar{y}(1) - \sum_{v=1} Y_{2v} = \bar{y}(1) - \sum_{v=1} \left\{ \frac{F_{2v-2}}{(4v-3)(4v-1)} - \frac{2F_{2v}}{(4v-1)(4v+3)} + \frac{F_{2v+2}}{(4v+3)(4v+5)} \right\}$$

or:

$$Y_0 = \bar{y}(1) - \frac{1}{3} F_0 + \frac{1}{15} F_2. \quad (1.17)$$

From the second equation (1.16) and from (1.13) follows in quite the same manner:

$$Y_1 = \bar{y}'(1) - \frac{1}{15} F_1 + \frac{1}{35} F_3. \quad (1.18)$$

By the coefficients (1.17), (1.18), and (1.13) our approximate solution of (1.1) and (1.2) is completely determined.

We then have to substitute this approximate solution and its first derivative into the right-hand side of (1.1) and have to repeat the procedure. For the actual substituting it is useful to express the Legendre coefficients Y_n of the first derivative $y'(x)$ also by the F_v .

In quite the same way as in the case of the Y_n we find:

$$Y_n' = \frac{F_{n-1}}{2n-1} - \frac{F_{n+1}}{2n+3} \quad (n \geq 1) \quad (1.19)$$

and:

$$Y_0' = \bar{y}'(1). \quad (1.20)$$

2. Third- and fourth-order differential equations. We can here restrict ourselves to a short summary of the results which can be obtained in quite the same way as in article 1 for the second-order differential equation.

a. Third-order Differential Equation

Differential equation:

$$y''' = f(x, y, y', y'') \quad (2.1)$$

Boundary values:

$$\begin{aligned} x = -1 : y &= y(-1) \\ x = -1 : y' &= y'(-1) \\ x = +1 : y &= y(+1). \end{aligned} \quad (2.2)$$

Coefficients for the approximate solution:

$$Y_n = \frac{F_{n-3}}{(2n-5)(2n-3)(2n-1)} - \frac{3F_{n-1}}{(2n-3)(2n-1)(2n+3)} + \frac{3F_{n+1}}{(2n-1)(2n+3)(2n+5)} - \frac{F_{n+3}}{(2n+3)(2n+5)(2n+7)} \quad (n \geq 3)$$

$$Y_0 = \bar{y}(1) - \frac{1}{3} \bar{y}'(1) + \frac{1}{3} y'(-1) - \frac{1}{9} F_0 + \frac{1}{45} F_1 + \frac{4}{315} F_2 - \frac{1}{105} F_3$$

$$Y_1 = \bar{y}(1) - \frac{1}{15} F_0 + \frac{2}{105} F_2 - \frac{1}{315} F_4 \quad (2.3)$$

$$Y_2 = \frac{1}{3} \bar{y}(1) - \frac{1}{3} y'(-1) + \frac{1}{9} F_0 - \frac{2}{63} F_1 - \frac{4}{315} F_2 + \frac{1}{63} F_3 - \frac{1}{693} F_5$$

Coefficients for the first derivative of the approximate solution:

$$\left. \begin{aligned} Y_n' &= \frac{F_{n-2}}{(2n-3)(2n-1)} - \frac{2F_n}{(2n-1)(2n+3)} + \frac{F_{n+2}}{(2n+3)(2n+5)} \quad (n \geq 2) \\ Y_0' &= \bar{y}(1) \\ Y_1' &= \bar{y}(1) - y'(-1) + \frac{1}{3} F_0 - \frac{1}{15} F_1 - \frac{4}{105} F_2 + \frac{1}{35} F_3 \end{aligned} \right\} \quad (2.4)$$

Coefficients for the second derivative of the approximate solution:

$$\left. \begin{aligned} Y_n'' &= \frac{F_{n-1}}{2n-1} - \frac{F_{n+1}}{2n+3} \quad (n \geq 1) \\ Y_0'' &= \bar{y}(1) - y'(-1) + \frac{1}{3} F_0 - \frac{2}{70} F_2 + \frac{1}{35} F_3 \end{aligned} \right\} \quad (2.5)$$

b. Fourth-order Differential Equation:

Differential equation:

$$y'''' = f(x, y, y', y'', y'''). \quad (2.6)$$

Boundary values:

$$\begin{aligned} x = -1 : y &= y(-1), \quad y' = y'(-1) \\ x = +1 : y &= y(+1), \quad y' = y'(+1). \end{aligned} \quad (2.7)$$

Coefficients for the approximate solution:

$$\begin{aligned}
 Y_n = & \frac{F_{n-4}}{(2n-7)(2n-5)(2n-3)(2n-1)} - \frac{4F_{n-2}}{(2n-5)(2n-3)(2n+1)(2n+3)} \\
 & + \frac{6F_n}{(2n-3)(2n-1)(2n+3)(2n+5)} - \frac{4F_{n+2}}{(2n-1)(2n+3)(2n+5)(2n+7)} \\
 & + \frac{F_{n+4}}{(2n+3)(2n+5)(2n+7)(2n+9)} \quad (n \geq 4)
 \end{aligned} \tag{2.8}$$

$$Y_0 = \bar{y}(1) - \frac{1}{3} \bar{y}'(1) + \frac{1}{45} F_0 - \frac{2}{315} F_2 + \frac{1}{945} F_4$$

$$Y_1 = \frac{6}{5} \bar{y}(1) - \frac{1}{5} \bar{y}'(1) + \frac{1}{525} F_1 - \frac{2}{1575} F_3 + \frac{1}{3465} F_5$$

$$Y_2 = \frac{1}{3} \bar{y}'(1) - \frac{2}{63} F_0 + \frac{1}{105} F_2 - \frac{4}{2079} F_4 + \frac{1}{9009} F_6$$

$$Y_3 = \frac{1}{5} \bar{y}'(1) - \frac{1}{5} \bar{y}(1) - \frac{2}{675} F_1 + \frac{37}{17325} F_3 - \frac{4}{6435} F_5 + \frac{1}{19305} F_7$$

If, similar to (1.16) the following abbreviations are introduced:

$$\left. \begin{aligned}
 \frac{1}{2} [y'(+1) + y'(-1)] &= \bar{y}'(1) \\
 \frac{1}{2} [y'(+1) - y'(-1)] &= \bar{y}(1)
 \end{aligned} \right\} \tag{2.9}$$

We obtain coefficients for the first derivative of the approximate solution:

$$\begin{aligned}
 Y_n' = & \frac{F_{n-3}}{(2n-5)(2n-3)(2n-1)} - \frac{3F_{n-1}}{(2n-3)(2n-1)(2n+3)} + \frac{3F_{n+1}}{(2n-1)(2n+3)(2n+5)} \\
 & - \frac{F_{n+3}}{(2n+3)(2n+5)(2n+7)} \quad (n \geq 3)
 \end{aligned}$$

$$Y_0' = \bar{y}(1) \tag{2.10}$$

$$Y_1' = \bar{y}'(1) - \frac{1}{15} F_0 + \frac{2}{105} F_2 - \frac{1}{315} F_4$$

$$Y_2' = \bar{y}'(1) - \bar{y}(1) - \frac{1}{105} F_1 + \frac{2}{315} F_3 + \frac{1}{693} F_5$$

Coefficients for the second derivative of the approximate solution:

$$\begin{aligned}
 Y_n'' &= \frac{F_{n-2}}{(2n-3)(2n-1)} - \frac{2F_n}{(2n-1)(2n+3)} + \frac{F_{n+2}}{(2n+3)(2n+5)} \quad (n \geq 2) \\
 Y_0'' &= \bar{y}'(1) \\
 Y_1'' &= 3\bar{y}'(1) - 3\bar{y}(1)
 \end{aligned} \tag{2.11}$$

Coefficients for the third derivative of the approximate solution:

$$\begin{aligned}
 Y_n''' &= \frac{F_{n-1}}{2n-1} - \frac{F_{n+1}}{2n+3} \quad (n \geq 1) \\
 Y_0''' &= 3\bar{y}'(1) - 3\bar{y}(1) + \frac{1}{15} F_1 - \frac{1}{35} F_3
 \end{aligned} \tag{2.12}$$

Note: In this paper we have considered only the simplest boundary conditions. However, our method can also be applied to more involved boundary problems. For these boundary conditions, of course, affect the determination of only the first ν coefficients $Y_0, Y_1, \dots, Y_{\nu-1}$, if ν is the order of the differential equation.

THE MEASUREMENT OF NON-LINEAR FORCES AND
MOMENTS BY MEANS OF FREE FLIGHT TESTS

C. H. Murphy
Ballistic Research Laboratories
Aberdeen Proving Ground, Maryland

An important technique of the exterior ballisticians is the determination of the aerodynamic forces and moments acting on a model by measurements of its free flight motion. Since this technique has been traditionally handicapped by a restriction to linear force systems, considerable importance has been attached to the extension of the technique to non-linear force systems. Although great success has been achieved in the application of the methods of non-linear mechanics to the analysis of non-linear problems, this work is usually restricted to one degree of freedom systems. In exterior ballistics, however, we are faced with the problem of the angular motion of a missile and must contend with two degrees of freedom.

In this paper we will first discuss the problem of one degree of freedom and then describe the extension to two degrees of freedom. A general class of non-linear equations in one dependent variable may be written in the form:

$$\ddot{x} + ax = \mu f(x, \dot{x}) \text{ and } a > 0. \quad (1)$$

The general solution of the linearized equation ($\mu = 0$) is $x = A \cos(\sqrt{a} x + \delta)$. Poincaré¹ has shown that, for "small" values of μ , periodic solutions of (1) exist near solutions of the linearized solution. Poincaré's work was modified

by Gylden and Lindstedt to eliminate certain secular terms. Although the Lindstedt process is an iterative one, the first step is often sufficiently accurate. A rather simple method for performing this first step is embodied in the Kryloff and Bogolinboff method of equivalent linearization.²

In this process Equation (1) is approximated by an equivalent linear one of the form.

$$\ddot{x} + 2k\dot{x} + \omega^2 x = 0 \quad (2)$$

with the solution $x = A e^{-kt} \cos(\omega t + \delta)$. The coefficients of Equation (2) are determined by averaging $\mu f(x, \dot{x})$ over a period of the motion. Kryloff and Bogolinboff, replace the parent non-linear equation by a family of equivalent linear equations. The coefficients of these linear equations depend on the amplitude and, hence, are functions of initial conditions. In particular, if we consider the motion of a unit mass attached to a cubic spring with restoring force $-ax + bx^3$, ^{then} $\mu f(x, \dot{x}) = bx^3$ and the parameters of the equivalent linear equation are

$$k = 0 \quad (3)$$

$$\omega^2 = a + b(3/4 A^2) \quad (4)$$

For this special case Equation (1) can be solved exactly in terms of an elliptic integral of the first type. The exact frequency has been compared with that predicted by Equation (4) and almost amazing agreement has been observed.

In the case of a weak spring ($b > 0$) for which the cubic component can actually reverse the direction of the spring force, Equation (4) was accurate to 1-1/2% up to amplitudes which would make the cubic component half as big as the linear component. For the strong spring ($b < 0$), Equation (4) retained this accuracy of 1-1/2% for amplitudes of oscillation which make the cubic component six times bigger than the linear component. Thus we see that the method of equivalent linearization is good for non-linearities which are definitely not "small".

Equation (4) can not only be used for the prediction of the motion of a mass acted on by a cubic spring, but it can be used in the dynamic measurement of this cubic force. We can disturb the spring and compute values of amplitude and frequency from the resulting motion. If a series of different disturbances are used, we can obtain/number of different values of A and ω . Using Equation (4), ω^2 is plotted versus the effective squared amplitude, $3/4 A^2$, and a line fitted. The slope of this line is b , the coefficient of the cubic term, and its intercept is a , the coefficient of the linear term.

The situation for the angular motion of a missile is quite similar. If we ~~can~~ make use of a Cartesian coordinate system with 1-axis along the trajectory, the 2-axis in the horizontal plane, and the 3-axis determined by the right hand rule, the direction cosines may be denoted by $\sqrt{1 - \lambda_H^2 - \lambda_V^2}$, λ_H , λ_V . For good missiles, the angle between the missile's axis and the trajectory, which is called the yaw angle, is small and λ_H and λ_V are then projections of this angle on horizontal and vertical planes respectively.

For simplicity we will consider an aerodynamic moment of the same form as the cubic spring. The magnitude of this moment is, therefore, a cubic function of the angle between the missile's axis and the trajectory.

$$|\text{Moment}| = |K_{M_0} + K_{M_0 2} \delta^2| \delta \quad C \quad (5)$$

where $\delta^2 = \lambda_H^2 + \lambda_V^2$,

K_{M_0} and $K_{M_0 2}$ are dimensionless aerodynamic coefficients, and

C is a dimensional constant.

In Reference 3 it is shown that the angular motion must satisfy the following second order differential equation in the complex variable $\lambda = \lambda_H + i\lambda_V$.

$$\lambda' - i\left(\frac{A\omega_1}{B}\right)\lambda - \frac{C}{B}(K_{M_0} + K_{M_0 2} \delta^2)\lambda = 0 \quad (6)$$

where A = axial moment of inertia

B = transverse moment of inertia, and

ω_1 = axial spin.

The solution of the linearized form of Equation (6) is

$$\lambda = K_1 e^{i\phi_1} + K_2 e^{i\phi_2} \quad (7)$$

where $\phi_1 = \phi_{10} + \dot{\phi}_1 t$

$$\dot{\phi}_1 = \frac{1}{2} \left[\frac{A\omega_1}{B} \pm \sqrt{\left[\frac{A\omega_1}{B} \right]^2 - 4C K_{M_0}} \right] \text{ and}$$

K_1 are complex constants.

Thus we see that the solution is generated by two complex vectors with magnitudes K_1 and rotating with frequencies $\dot{\phi}_1$. In Reference 3 the equivalent linearization process is applied to Equation (6) and it is found that the solution has the same form as Equation (7). The frequencies $\dot{\phi}_1$'s are now functions of the amplitudes K_1 's. In particular, Equation (4) has the following generalization

$$K_{M_{\text{range}}} = \frac{1}{C} \dot{\phi}_1 \cdot \dot{\phi}_2 = K_{M_0} + K_{M_0^2} \delta_e^2 \quad (8)$$

$$\delta_e^2 = K_1^2 + K_2^2 + \frac{K_1^2 \dot{\phi}_1 - K_2^2 \dot{\phi}_2}{\dot{\phi}_1 - \dot{\phi}_2}.$$

According to Equation (8), from a number of different firings the measured amplitudes of oscillation and frequencies should be combined to yield pairs of $\dot{\phi}_1 \cdot \dot{\phi}_2$ and δ_e^2 and these data points fitted by a line. In Figure 1* this is done for a body of revolution. In this case three center of mass positions were tested and so three different values of K_{M_0} and $K_{M_0^2}$ were obtained. These values showed excellent internal consistency when they were compared with the usual center of mass transformations. Independent wind tunnel tests of this model were made and good agreement with flight tests was obtained.

Next this technique was applied to a large yaw program in which angles up to 30° had been obtained. In Figure 2* these data are plotted and we see that two lines are needed to fit the points! A little reflection showed that each line corresponds to a cubic segment in the moment plane. An examination of

* See end of this paper

the individual firings showed that all rounds possess yawing motions which made use of one or the other segments but not both and this interpretation of the data was, therefore, valid. In Figure 3 the actual moment plane is plotted. (For large angles, δ is actually the sine of the yaw angle and not that angle itself.) The physical explanation for the "corner" at 23° was found to lie in the fact that the flow separates from the lee side of the model at about 23° . Comparison with direct wind tunnel measurement showed excellent agreement.

Because of this success in treating a non-linear static moment, the effect of non-linear Magnus and damping moments was considered. In Reference 3 it was found that these moments cause both modes of oscillation to damp exponentially. The exponential coefficients are functions of amplitude and plots similar to Figure 1 are possible. A number of measurements of non-linear Magnus moments have been made and this extension to damped oscillations has proven extremely valuable.

REFERENCES

1. Peincare, H., Les methodes nouvelles de la mecanique celeste, Vol. I, Chapter III and IV, Paris, 1892.
2. Minorsky, N., Introduction to Non-linear Mechanics, Chapter XII, J. W. Edwards, Ann Arbor, 1947.
3. Murphy, C. H., Measurement of Non-linear Forces and Moments by Means of Free Flight Tests, BRL Report 974, February 1956.

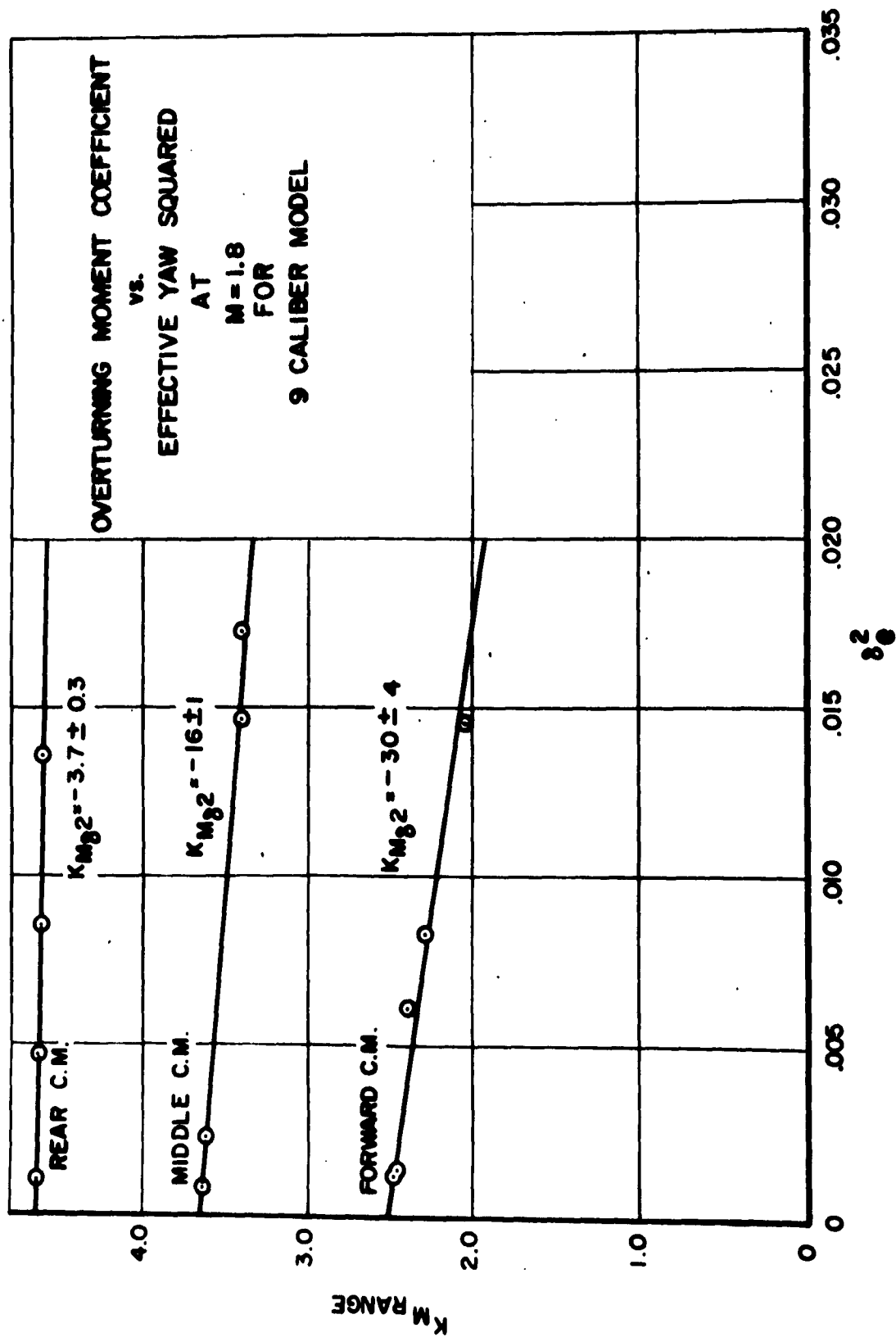


Fig. 1

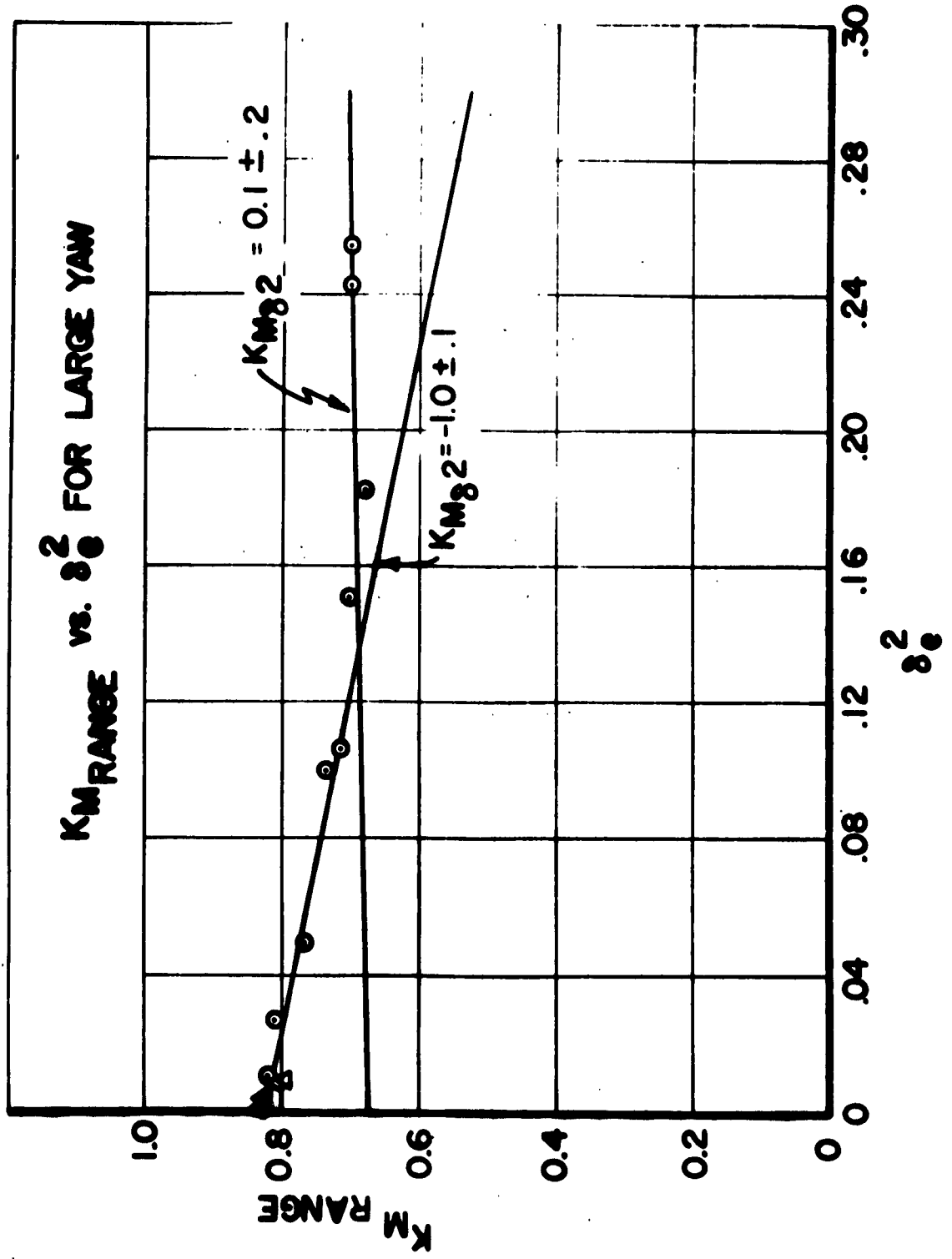


Fig. 2

$K_M \delta$ vs. δ FOR LARGE YAW



Fig. 3

AN ANALOG COMPUTER STUDY OF INTERIOR BALLISTIC EQUATIONS

By

William A. Dittrich
Frankford Arsenal

A study has been undertaken at Frankford Arsenal to simulate the interior ballistic performance of a recoilless rifle by solving a set of simultaneous differential equations describing the system on an analog computer. It was desired to make use of the computer as a development tool to investigate the effects on system performance of varying certain parameters. This provides weapon system development with an intermediate step between theoretical calculations and firing a test weapon, its simulation on an analog computer, making possible a large reduction in the number of test firings necessary to develop a weapon.

The object of the study, then was:

First, to establish the validity and limitations of the equations proposed.

Second, if the validity of the equations proposed were established, to show the use of the computer as a development tool by investigating the changes in muzzle velocity, peak pressure, and the like produced by varying certain propellant and physical design parameters.

The initial weapon studied was a 57 mm recoilless rifle, chosen because of the large amount of experimental data available for it. The equations of motion for this weapon are a modified form of those derived by Hirschfelder and others for a conventional weapon, familiar to many of us.

Equation of State:

$$PV = (1 + \frac{B}{V}) \frac{12 N^1 F T}{T_0} \quad V = V_{c_0} + AX + \frac{N}{\bar{e}} - \frac{C}{\bar{e}}$$

Where:

P = pressure (lb/in²)

V = volume (in³)

N¹ = gas in weapon (lb)

F = impetus of propellant ($\frac{\text{ft. lb}}{\text{lb}}$)

T = gas temperature (°K)

X = travel (in)

C = charge (lb)

T₀ = isochoric flame temperature (K)

B = virial coefficient for gases

A = area of bore (in²)

N = total gas produced (lb)

P = density of propellant $\frac{\text{Lb}}{\text{in}^3}$

PROJECTILE VELOCITY EQUATION

$$V = A/M \int P dt$$

where V = velocity

M = mass of projectile

PROJECTILE TRAVEL EQUATION

$$X = \int V dt$$

BURNING RATE EQUATION

$$N = 2 \frac{c\gamma}{W} \int p^{.7} dt$$

where γ = burning rate constant ($\frac{\text{in}}{\text{sec}}$)

W = web (in)

nozzle discharge equation

$$N'' = C_D A_T \sqrt{\frac{T_o}{T}} \int P dt$$

where:

C_D = nozzle discharge coefficient

A_T = throat area (in²)

N = gas flowing from nozzle (lb)

ENERGY EQUATION:

$$N' C_v T = N C_v T_o - C_D C_p \frac{A_T}{A} \sqrt{T_o T} M V - \frac{(1 + \beta) M V^2}{2}$$

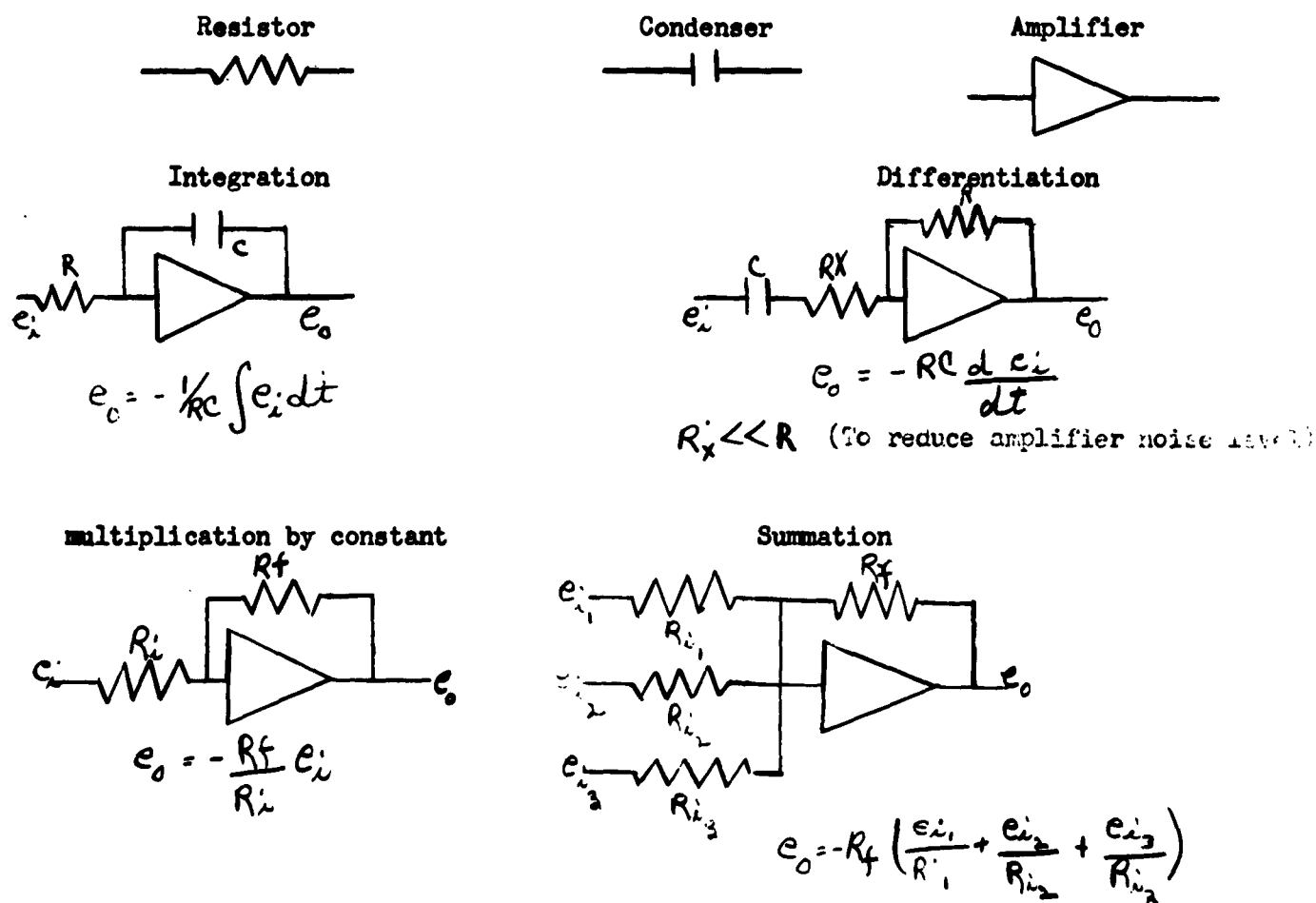
where:

C_v = constant volume spec. ht. of gases

C_p = constant pressure spec. ht. of gases

β = heat loss coefficient

These, then, were the equations set upon the computer. I suppose a short explanation of the analog computer operation would be in order here. The analog computer found its first major use in the field of guided missiles where the cost of test firing made necessary a means of performing all possible research by theoretical means. Recently its use has been rapidly increasing in other science and engineering fields. The analog computer uses such electronic components as amplifiers, resistor capacitor networks, and potentiometers set up in a circuit which obeys the same set of equations as the dynamic system under study. Voltage fluctuates as pressures or displacements, for example, in the physical section and the dynamic response of the simulated system can be recorded. The analog computer has the advantage of simplicity of setup and operation, and speed of solution, however its accuracy seldom exceeds 1 percent. In interior ballistics problems this is normally adequate; the accuracy of measurement equipment used in experiments seldom is more accurate. A few of the basic circuits for various mathematical operations are shown below:



The circuit schematic for the equations given earlier to represent the interior ballistics of a recoilless rifle is shown in figure₁. (At the end of this paper).

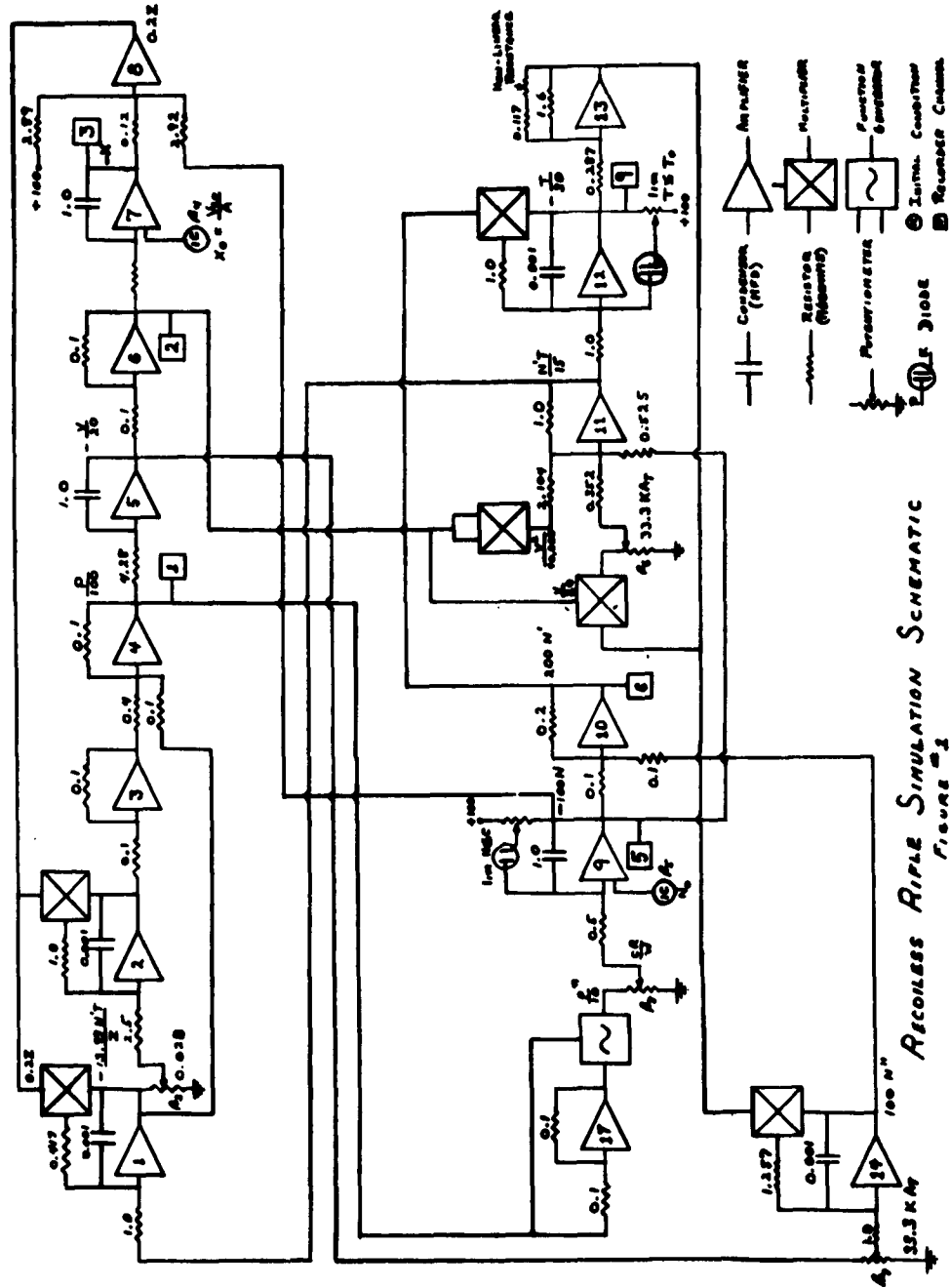
A total of 18 amplifiers, six multipliers and some nonlinear function generators were used. Six channels of information were recorded.

A typical computer run is shown in Figure 2.

It can be seen that peak pressure is 6100 lb/in² and muzzle velocity is 1175 ft/sec. Since the initial charge is 1 lb. it can be seen in (N) and that only 70 percent was burned and only 30 percent went to propelling the projectile. These values agreed quite closely with experimental test results as can be seen in fig. 3. Peak pressures of experimental test results were within 5 percent of computer values. Muzzle velocities came within 5 ft/sec. of each other as shown in figure 4.

Having shown the equations to be representative of the actual physical system it was then decided to vary certain design parameters to discover the effects on interior ballistic performance. Variations of such parameters as web of propellant, burning rate constant, throat area, and nozzle discharge coefficient was made and effects on weapon performance noted. Although time does not permit a complete listing of results of varying such parameters, I can say that it was found that the web size, charge weight, burning rate constant exerted the greatest effect on peak pressures and muzzle velocities of weapon while virial coefficient, nozzle discharge coefficient and specific heat ratio of gases has little effect on the ballistic cycle. The effect of nozzle variations might greatly effect recoil, however, a point not investigated in this study. An example of results obtained, the effect of a linear burning rate equation on weapon pressure is shown in fig. 5.

Since the completion of this study other weapons have been analyzed by this means and suggestions made for ways to improve their performance. Once the analog computer is set up, it is possible to make a hundred or more solutions for different parameter values within one day. The feasibility of certain new weapon systems, such as rocket assisted guns, have also been investigated by this method, resulting in quite a saving over experimental studies. It is hoped in the future that the computer simulation will become one of the standard steps in the creation of a new weapon system.



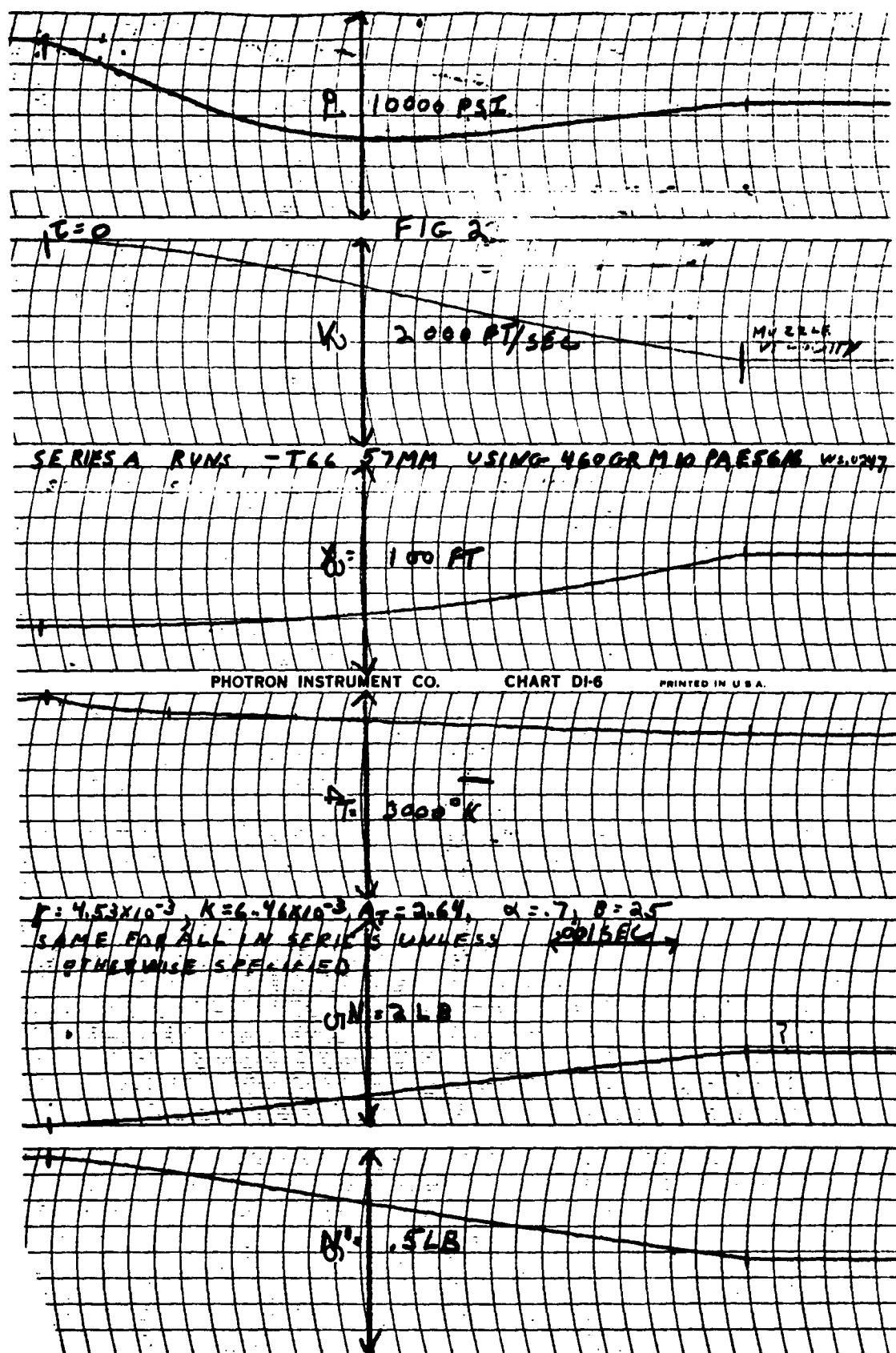


FIG. 2

Fig. #26681-4

Pressure-time curves for 57 mm type 966 recoilless rifle

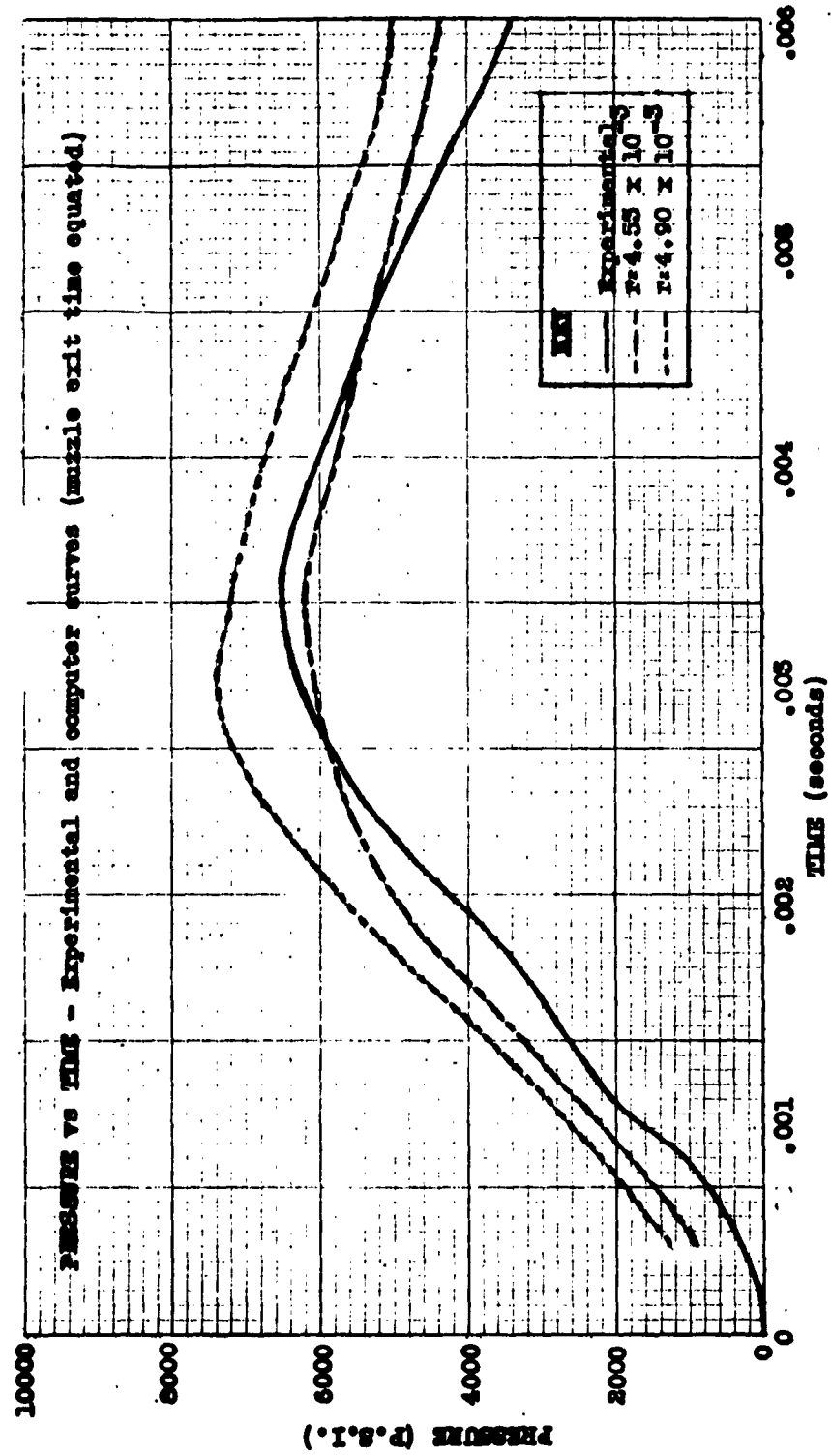


Figure No. 5b

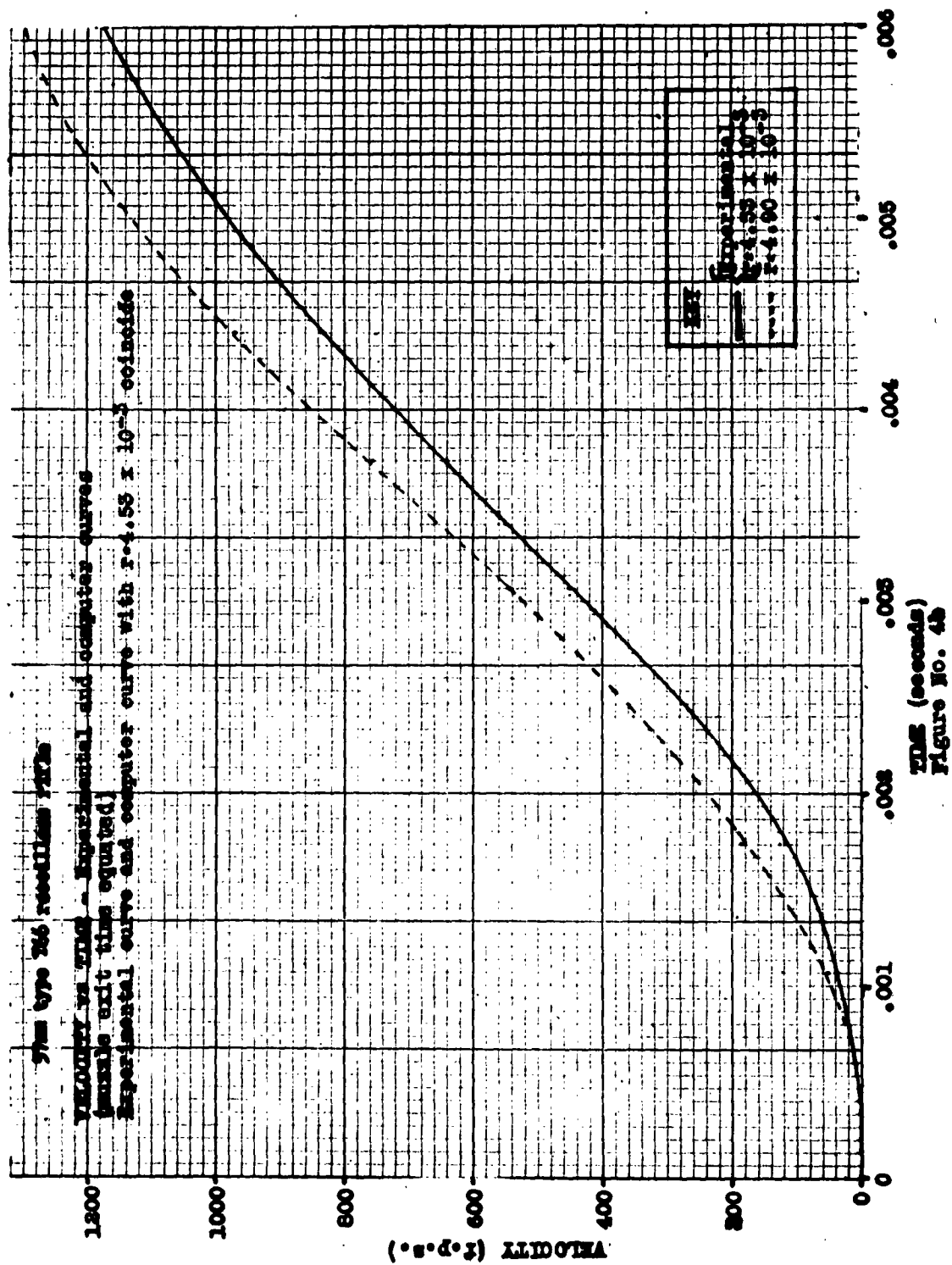
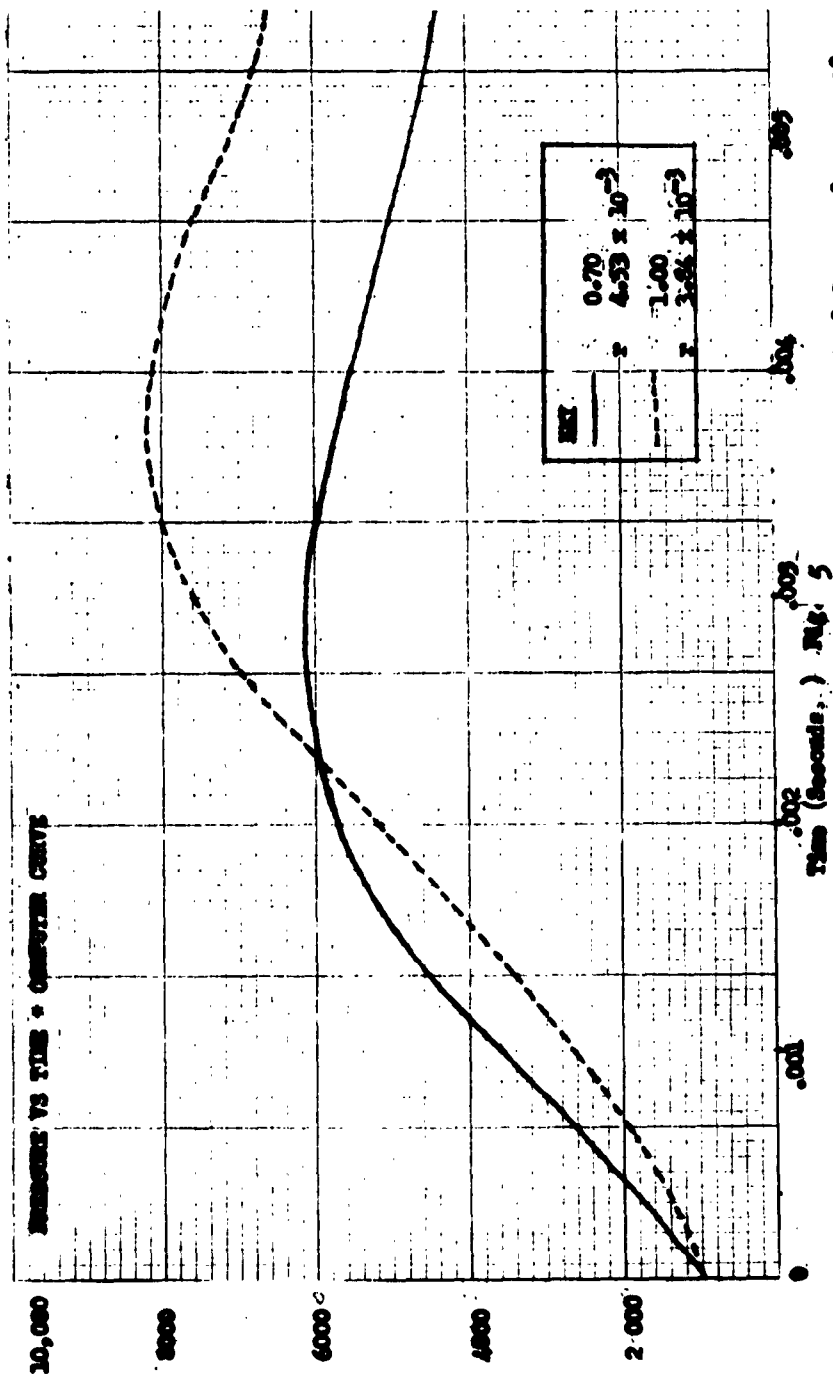


Fig. #266B1-8



Effect of using simplified burning rate equation where pressure exponent is 1.0 on performance of 57 mm type M66 recoilless rifle.

THE RESPONSE OF A TAPERED CANTILEVER BEAM WHEN
A TRANSIENT FORCE IS APPLIED AT THE END

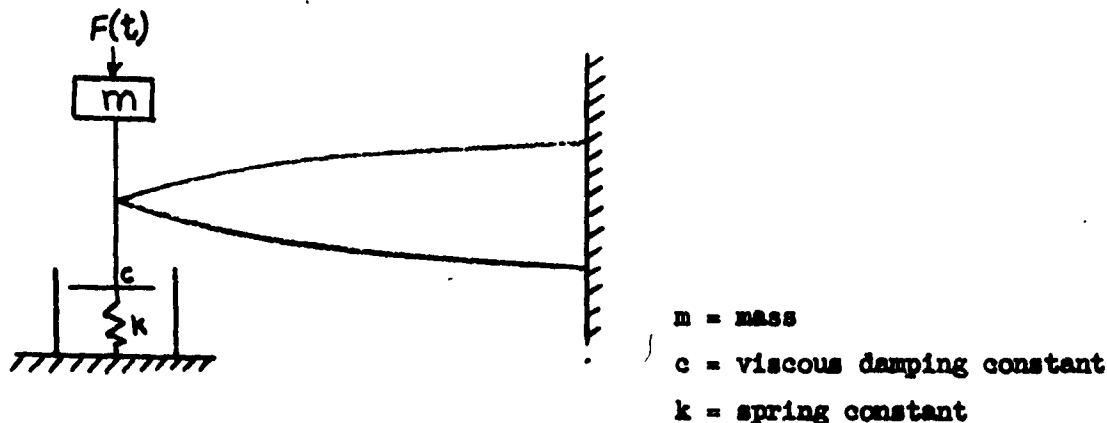
by
A. S. Elder
Ballistic Research Laboratories

INTRODUCTION

In recent years several authors have investigated the vibrations of a beam attached to a mechanical system having lumped physical constants. McBride¹ determined the normal modes and natural frequencies of a uniform cantilever beam with a terminal dashpot. Young² calculated the response of a cantilever beam attached to springs and masses. We will determine the response of a cantilever beam with linear terminal constraints when an arbitrary transient force is applied at the end. We will restrict our investigation initially to beams having a power law variation of section properties, as beams of this description have been considered by several authors, and their results form a convenient point of departure for the present study.^{3,4,5}

I. RESPONSE OF A TAPERED CANTILEVER BEAM WITH
A TERMINAL SPRING, MASS, AND DASHPOT

Consider the mechanical system shown in the diagram below:



The equation of motion is

$$\frac{\partial^2}{\partial x^2} \left(EI \frac{\partial^2 Y}{\partial x^2} \right) + \rho A \frac{\partial^2 Y}{\partial t^2} = 0 \quad (1)$$

The boundary conditions are

$$Y(l, t) = 0 \quad (2)$$

$$Y_x(l, t) = 0 \quad (3)$$

$$EIY_{xx}(0, t) = 0 \quad (4)$$

$$mY_{tt}(0, t) + cY_t(0, t) + kY(0, t) = F(t) - [EIY_{xx}(0, t)]_x \quad (5)$$

$$F(t) = 0, t \leq 0 \quad (6)$$

$$F(t) = F, t > 0 \quad (7)$$

$$Y(x, 0) = 0 \quad (8)$$

$$Y_t(x, 0) = 0 \quad (9)$$

The Laplace transform, defined by the equation

$$y(x, s) = \int_0^{\infty} e^{-st} Y(x, t) dt,$$

was used to remove the time variable from the above system of equations.⁶

$$[EIY_{xx}(x, s)]_{xx} + s^2 \rho A y(x, s) = 0 \quad (10)$$

$$y(l, s) = 0 \quad (11)$$

$$y_x(l, s) = 0 \quad (12)$$

$$EIY_{xx}(0, s) = 0 \quad (13)$$

$$(ms^2 + cs + k)y(0, s) + [EIY_{xx}(0, s)]_x = \frac{F}{s} \quad (14)$$

Consider a cantilever beam in which the section properties vary as a power of the distance from the tip.

$$EI(x) = EI(l) \cdot \left(\frac{x}{l}\right)^\alpha \quad (15)$$

$$\rho A(x) = \rho A(l) \cdot \left(\frac{x}{l}\right)^\beta \quad (16)$$

The mass of the beam is

$$m_b = \int_0^l \rho A(x) dx = \frac{l \rho A(l)}{\beta + 1} \quad (17)$$

The static deflection curve due to a terminal load F is

$$y_0(x) = \frac{F l^3}{EI(l)(2 - \alpha)(3 - \alpha)} \left\{ \left(\frac{x}{l}\right)^{3-\alpha} - (3 - \alpha)\left(\frac{x}{l}\right) + (2 - \beta) \right\} \quad (18)$$

The static spring rate is given by

$$k_b = \frac{F}{y(0)} = \frac{(3 - \alpha)EI(l)}{l^3} \quad (19)$$

For beams of rectangular cross section, the section modulus is given by

$$Z(x) = Z(l) \cdot \left(\frac{x}{l}\right)^{\frac{1}{2}(\alpha + \beta)} \quad (20)$$

The stress at the outside fiber of the beam is

$$\sigma(x) = \frac{F l}{Z(l)} \left(\frac{x}{l}\right)^{1 - \frac{1}{2}(\alpha + \beta)} \quad (21)$$

These equations show that the parameters α and β are subject to certain restrictions:

$\beta > -1$ Finite mass of beam.

$\alpha < +2$ Finite deflection.

$\alpha + \beta \leq 2$ Finite bending stress.

The problem may be rendered dimensionless by the following series of substitutions:

$$\xi = qx$$

$$\lambda = ql$$

$$q^4 = -s^2 \lambda^{\alpha-\beta} \frac{\rho A(l)}{EI(l)}$$

$$\text{or } s^2 = -\lambda^{-\alpha+\beta+4} \cdot \frac{EI(l)}{\rho A(l) \cdot l^4}$$

$$\mu = \frac{m}{l \rho A(l)} = \frac{m}{(\beta+1)m_b}$$

$$\gamma = \frac{cl}{\sqrt{\rho A(l)EI(l)}} = \frac{c}{\sqrt{m_b k_b}} \sqrt{\frac{3-\alpha}{\beta+1}}$$

$$\tau = \frac{kl^3}{EI(l)} = \frac{(3-\alpha)k}{k_b}$$

Equation (8) now becomes

$$[\epsilon^\alpha y_{\epsilon\epsilon}]_{\epsilon\epsilon} - \epsilon^\beta y = 0 \quad (22)$$

Let $\delta = \beta - \alpha + 4$

Then the series solutions of (22) are

$$y_1(\epsilon) = 1 + \frac{\epsilon^\delta}{\delta(\delta-1)(\delta+\alpha-2)(\delta+2-\beta)} + \dots + \quad (23)$$

$$y_2(\epsilon) = \epsilon + \frac{\epsilon^{\alpha+1}}{(\delta+1)(\delta)(\delta+\alpha-1)(\delta+\alpha-2)} + \dots + \quad (24)$$

$$y_3(\epsilon) = \epsilon^{3-\alpha} + \frac{\epsilon^{3-\alpha+\delta}}{(\delta+3-\alpha)(\delta+2-\alpha)(\delta+1)(\delta)} + \dots + \quad (25)$$

$$y_4(\epsilon) = \epsilon^{2-\alpha} + \frac{\epsilon^{2-\alpha+\delta}}{(\delta-1)(\delta)(\delta+2-\alpha)(\delta+1-\alpha)} + \dots + \quad (26)$$

If $\alpha = 1$, y_2 and y_4 coincide, and y_4 must be replaced by the logarithmic solution

$$y_4(\epsilon) = y_2(\epsilon) \log \epsilon + \left(\frac{1}{\delta-1} + \frac{2}{\delta} + \frac{1}{\delta+1} \right) \frac{\epsilon^{\delta+1}}{\delta^2(\delta+1)(\delta-1)} + \dots + \quad (27)$$

These solutions satisfy the following boundary conditions at the origin:

	$y_1(\epsilon)$	$\frac{dy_1(\epsilon)}{d\epsilon}$	$\epsilon^\alpha \frac{d^2 y_1(\epsilon)}{d\epsilon^2}$	$\frac{d}{d\epsilon} \left[\epsilon^\alpha \frac{d^2 y_1(\epsilon)}{d\epsilon^2} \right]$
$y_1(\epsilon)$	1	0	0	0
$y_2(\epsilon)$	0	1	0	0
$y_3(\epsilon)$	0	0	0	$(3 - \alpha)(2 - \alpha)$
$y_4(\epsilon)$ (Eq. 26)	0	0	$(2 - \alpha)(1 - \alpha)$	0
$y_4(\epsilon)$ (Eq. 27)	0	0	1	0

(28)

The transform of $Y(x, t)$ is of the form

$$y(x, s) = c_1(s)y_1(\epsilon) + c_2(s)y_2(\epsilon) + c_3(s)y_3(\epsilon) + c_4(s)y_4(\epsilon)$$

On referring to (13) and (28), we see that

$$c_4(s) = 0$$

The remaining coefficients are readily obtained by applying Cramer's rule. On combining the results according to the rules for adding determinants, we find

$$y(x, s) = \frac{F L^3}{s E I (2)} \cdot \begin{vmatrix} y_1(\epsilon) & y_2(\epsilon) & y_3(\epsilon) \\ y_1(\lambda) & y_2(\lambda) & y_3(\lambda) \\ y_1'(\lambda) & y_2'(\lambda) & y_3'(\lambda) \\ (-\mu\lambda^8 + 17\lambda \frac{1}{2}^3 + \tau) & 0 & (2 - \alpha)(3 - \alpha)\lambda^{3-\alpha} \\ y_1(\lambda) & y_2(\lambda) & y_3(\lambda) \\ y_1'(\lambda) & y_2'(\lambda) & y_3'(\lambda) \end{vmatrix} \quad (29)$$

The deflection $Y(x, t)$ may be found by using the Bromwich inversion integral. Let $s = \psi + i\omega$, $\psi_0 > 0$; then

$$Y(x, t) = \lim_{\omega \rightarrow \infty} \frac{1}{2\pi i} \int_{\gamma_0 - i\omega}^{\gamma_0 + i\omega} e^{st} y(x, s) ds$$

The integral is an analytic function of s . The only singularities are poles which occur at $s = 0$ and at the roots of the frequency equation

$$\Delta(\lambda) = 0$$

where

$$\Delta(\lambda) = \begin{vmatrix} (-\mu\lambda^3 + i\gamma\lambda \frac{1}{2}\lambda^3 + \tau) & 0 & (2 - \alpha)(3 - \alpha)\lambda^{3-\alpha} \\ y_1(\lambda) & y_2(\lambda) & y_3(\lambda) \\ y_1'(\lambda) & y_2'(\lambda) & y_3'(\lambda) \end{vmatrix} \quad (31)$$

It will be shown subsequently that all the poles of $y(x, s)$ in the s plane lie on or to the left of the imaginary axis. Let $\lambda_1, \lambda_2 \dots \lambda_n$ be the roots of this equation in order of increasing modulus and let $s_n = \lambda_n + i\omega_n$;

$$(\lambda_n + i\omega_n)^2 = s_n^2 = -\lambda_n^3 \frac{EI(\lambda)}{\lambda^4 \rho A(\lambda)} \quad (32)$$

The residue at the origin is

$$\lim_{s \rightarrow 0} sy(x, s)$$

If the damping constant γ is sufficiently small, the remaining poles are simple and the residues may be found by differentiation. Let

$$p(s) = \begin{vmatrix} y_1(\epsilon) & y_2(\epsilon) & y_3(\epsilon) \\ y_1(\lambda) & y_2(\lambda) & y_3(\lambda) \\ y_1'(\lambda) & y_2'(\lambda) & y_3'(\lambda) \end{vmatrix}$$

and let

$$q(s) = s\Delta(\lambda)$$

Then the residue at the pole $s = s_n$ in the upper half plane is

$$\frac{F\lambda^3}{EI(l)} \frac{p(s)}{\frac{\partial q(\lambda)}{\partial s}} e^{s_n t}$$

or

$$\frac{F\lambda^3}{2EI(l)} \cdot \frac{\begin{vmatrix} y_1(\epsilon) & y_2(\epsilon) & y_3(\epsilon) \\ y_1(\lambda) & y_2(\lambda) & y_3(\lambda) \\ y_1'(\lambda) & y_2'(\lambda) & y_3'(\lambda) \end{vmatrix}}{\frac{\lambda \partial \Delta(\lambda)}{\partial \lambda}} \left[\cos \omega_n t + i \sin \omega_n t \right] e^{s_n t}$$

since

$$s \frac{\partial \Delta}{\partial s} = -\frac{\lambda}{s} \frac{\partial \Delta}{\partial \lambda}$$

Let

$$r(\epsilon, \lambda_n) = \frac{p(s)}{\frac{\partial q(s)}{\partial s}}$$

when $s_n = \psi_n + i\omega_n$; then the residue at $\bar{s}_n = \psi_n - i\omega_n$ in the lower half plane is

$$\bar{r}(\epsilon, \lambda_n) e^{\bar{s}_n t}$$

The sum of these residues is real. Let

$\text{Re}(r_n)$, $\text{Im}(r_n)$ be the real and imaginary parts of $r(\epsilon, \lambda_n)$. On

combining the above results, we find

$$Y(x, t) = \frac{F l^3}{(3 - \alpha)(2 - \alpha)(1 + \frac{k}{k_b})EI(l)} \cdot \left[\left(\frac{x}{l}\right)^{3-\alpha} - (3 - \alpha)\left(\frac{x}{l}\right) + (2 - \alpha) \right] - \frac{F l^3}{EI(l)} \sum_{n=1}^{\infty} \left[\operatorname{Re}(r_n) \cos \omega_n t - \operatorname{Im}(r_n) \sin \omega_n t \right] e^{\psi_n t} \quad (33)$$

If the damping constant γ is zero, ψ and $\operatorname{Im}(r_n)$ are both zero, and the series solution has the simpler form

$$Y(x, t) = \frac{F l^3}{(3 - \alpha)(2 - \alpha)(1 + \frac{k}{k_b})EI(l)} \cdot \left[\left(\frac{x}{l}\right)^{3-\alpha} - (3 - \alpha)\left(\frac{x}{l}\right) + (2 - \alpha) \right] - \frac{F l^3}{EI(l)} \sum_{n=1}^{\infty} \frac{\begin{vmatrix} y_1(\epsilon) & y_2(\epsilon) & y_3(\epsilon) \\ y_1(\lambda) & y_2(\lambda) & y_3(\lambda) \\ y_1'(\lambda) & y_2'(\lambda) & y_3'(\lambda) \end{vmatrix}}{\lambda \frac{\partial \Delta(\lambda)}{\partial \lambda} \Big|_{\lambda = \lambda_n}} \cos \omega_n t \quad (34)$$

The characteristic root λ_1 may be found approximately by truncating the ascending series for $\Delta(\lambda)$ with the term in $\lambda^{3-\alpha+\delta}$. Let

$$u_3 = \begin{vmatrix} y_1(\lambda) & y_2(\lambda) \\ y_1'(\lambda) & y_2'(\lambda) \end{vmatrix} = 1 - \frac{2\lambda^\delta}{8(8 + \alpha - 1)(8 + \alpha - 2)(8 + \alpha - 3)} + \dots$$

$$u_1 = \begin{vmatrix} y_2(\lambda) & y_3(\lambda) \\ y_2'(\lambda) & y_3'(\lambda) \end{vmatrix} = (2 - \alpha)\lambda^{3-\alpha} \left\{ 1 - \frac{2\lambda^\delta}{8(8 + 1)(8 + \alpha - 1)(8 + \alpha - 3)} + \dots \right\}$$

$$\Delta(\lambda) = (-\mu\lambda^\delta + 17\lambda \frac{1}{2}^\delta + k)u_1(\lambda) + (2 - \alpha)(3 - \alpha)\lambda^{3-\alpha} u_3(\lambda) \quad (35)$$

If the tip of the beam is free, the frequency equation reduces to

$$u_3(\lambda_1) = 0 \quad (36)$$

or

$$\lambda_1^8 \approx \frac{2}{8(8 + \alpha - 1)(8 + \alpha - 2)(8 + \alpha - 3)} \quad (37)$$

If on the other hand the tip is hinged, we have

$$u_1(\lambda_1) = 0 \quad (38)$$

or

$$\lambda_1^8 \approx \frac{2}{8(8 + 1)(8 + \alpha - 1)(8 - \alpha + 3)} \quad (39)$$

Let

$$\mu_1 = \mu + \frac{2\tau}{8(8 + 1)(8 + \alpha - 1)(8 - \alpha + 3)} + \frac{6 - 3\alpha}{8(8 + \alpha - 1)(8 + \alpha - 2)(8 + \alpha - 3)}$$

and

$$\tau_1 = \tau + 3 - \alpha$$

Then, approximately,

$$\begin{aligned} -\mu_1 \lambda^8 + i\gamma \lambda^{\frac{1}{2}} + \tau_1 &= 0, \\ \lambda^{\frac{1}{2}} &\approx \frac{i\gamma \pm \sqrt{-\gamma^2 + 4\tau_1\mu_0}}{2\mu_0} \end{aligned} \quad (40)$$

On referring to Eq. (32), we see that

$$v_1 \sim -\frac{\gamma}{2\mu_1\tau_1} \sqrt{\frac{EI(s)}{\rho A(s) \cdot s^4}} \quad \text{if } 4\tau_1\mu_1 > \gamma^2 \quad (41)$$

$$\omega_1 \sim \pm \frac{\sqrt{4\tau_1\mu_1 - \gamma^2}}{2\mu_1} \sqrt{\frac{EI(s)}{\rho A(s) \cdot s^4}} \quad \text{if } 4\tau_1\mu_1 > \gamma^2 \quad (42)$$

Critical damping occurs when

$$4\tau_1\mu_1 \sim \gamma^2$$

The first characteristic root s_1 is then repeated giving rise to a double pole in the transform $y(x, s)$. Terms of the form $t \cos \omega_1 t$

and $t \sin \omega_1 t$ will then occur in Eq. (33). If $4\tau_1\mu_1 < \gamma^2$, Eq. (40) will have two real, unequal roots, and the system will be overdamped in the first mode.*

Orthogonal function theory may be used to show that $\psi_n < 0$ when the damping constant c is > 0 . Let $y(x, s_n)$ be a normal function satisfying Eqs. (10-13) and the homogeneous boundary condition

$$(ms^2 + cs + k)y(0, s) + [EIy_{xx}(0, s)]_x = 0 \quad (43)$$

Then the complex conjugate of $y(x, s_n)$ will satisfy Eqs. (11-13), the differential equation

$$[EI\bar{y}_{xx}(x, s_n)]_{xx} + \bar{s}^2 \rho A \bar{y}(x, s_n) = 0, \quad (44)$$

and the boundary condition

$$(\bar{m}\bar{s}^2 + c\bar{s} + k)\bar{y}(0, s_n) + [EI\bar{y}_{xx}(0, s_n)]_x = 0 \quad (45)$$

We may show that

$$\begin{aligned} & -(s_n^2 - \bar{s}_n^2) \int_0^l \rho A y(x, s_n) \bar{y}(x, s_n) dx \\ & = y(0, s_n) \frac{d}{dx} \left[EI \frac{d^2 \bar{y}(0, s_n)}{dx^2} \right] - \bar{y}(0, s_n) \frac{d}{dx} \left[EI \frac{d^2 y(0, s_n)}{dx^2} \right] \end{aligned}$$

* In the case of a uniform cantilever beam with a terminal dashpot, McBride has shown that critical damping and over-damping cannot occur in modes higher than the first. This fact is probably true of cantilever beams of non-uniform cross-section with a terminal mass, spring, and dashpot.

Now $s_n = \psi_n + i\omega_n$, $\bar{s}_n = \psi_n - i\omega_n$, so that

$$s_n - \bar{s}_n = 2i\omega_n$$

$$s_n^2 - \bar{s}_n^2 = 4i\psi_n\omega_n$$

On using the boundary conditions (13 and (45), we find after some reduction

$$\psi_n = - \frac{cy(0, s_n)\bar{y}(0, s_n)}{2 \left[my(0, s_n)\bar{y}(0, s_n) + \int_0^l \rho Ay(x, s_n)\bar{y}(x, s_n)dx \right]} \quad (46)$$

Now a complex number times its conjugate is real and positive; therefore

$$\psi_n < 0 \quad \text{if } c > 0$$

and

$$\psi_n = 0 \quad \text{if } c = 0 \quad (47)$$

This result would be expected on physical grounds.

By means of a similar analysis we find that

$$\left\{ \frac{1}{s_n^2} - \frac{1}{\bar{s}_n^2} \right\} \int_0^l EI \frac{d^2 y(x, s_n)}{dx^2} \frac{d^2 \bar{y}(x, s_n)}{dx^2} dx + ky(0, s_n)\bar{y}(0, s_n) = c \left\{ \frac{1}{s_n} - \frac{1}{\bar{s}_n} \right\} y(0, s_n)\bar{y}(0, s_n) \quad (48)$$

On comparing the coefficients of c in Eqs. (46) and (48), we find

$$\psi_n^2 + \omega_n^2 = \frac{ky(0, s_n)\bar{y}(0, s_n) + \int_0^l EI \frac{d^2 y(0, s_n)}{dx^2} \frac{d^2 \bar{y}(0, s_n)}{dx^2} dx}{my(0, s_n)\bar{y}(0, s_n) + \int_0^l \rho Ay(0, s_n)\bar{y}(0, s_n)dx} \quad (49)$$

Then

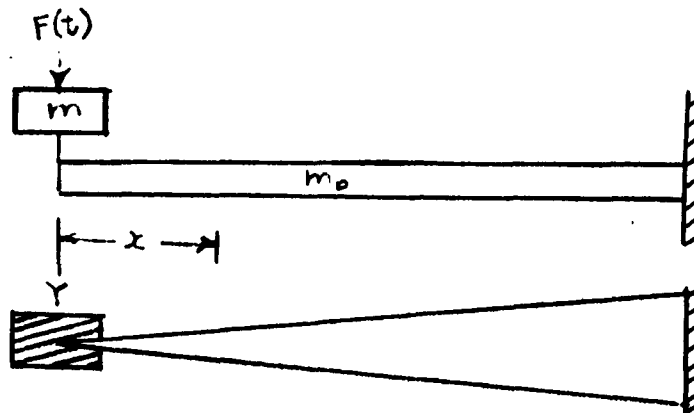
$$\omega_n^2 = \frac{ky^2(0, s_n) + \int_0^l EI \left[\frac{d^2 y(0, s_n)}{dx^2} \right]^2 dx}{my^2(0, s_n) + \int_0^l \rho A y^2(0, s_n) dx} \quad (50)$$

Equation (50) is the usual energy equation for the circular frequency; (49) is the corresponding equation for the modulus of the complex circular frequency $\omega_n + i\psi_n$.

DYNAMIC EFFICIENCY OF BEAMS

The present study is the outgrowth of a design problem which arose in the Ballistic Research Laboratories at Aberdeen Proving Ground. A spring device was required to respond accurately to large forces of rapidly varying magnitude. In order to apply approximate engineering analysis to the test results, it was necessary for the spring device to respond essentially with a single degree of freedom. Due to the high forces and relatively low spring rates encountered, the spring element was fairly heavy, and it was suspected that the distributed mass might cause appreciable response in the higher modes.

The beam-type spring device built at the Ballistic Research Laboratories is represented schematically in the figure below:



We will consider only the response to a step function of force applied to the mass, m , as the response to other terminal forces may be found by using Duhamel's integral.

Equations (1-9) of Part I apply provided we set $k = 0$, $c = 0$ in Eq. (5). We may find the normal elastic curves by setting $Y_n(x, t) = y_n(x) \cos \omega_n t$;

$$\frac{d^2}{dx^2} \left[EI \frac{d^2 y_n}{dx^2} \right] - \omega_n^2 \rho A y_n = 0 \quad (51)$$

$$\frac{d}{dx} \left[EI \frac{d^2 y_n(0)}{dx^2} \right] - \omega_n^2 m y_n(0) = 0 \quad (52)$$

$$EI \frac{d^2 y_n(0)}{dx^2} = 0 \quad (53)$$

$$y_n(l) = 0 \quad (54)$$

$$\frac{dy_n(l)}{dx} = 0 \quad (55)$$

It is convenient to use the influence function and its bilinear expansion in terms of normal elastic curves to solve this problem. The response coefficients are expressed in terms of energy integrals and other parameters of the system. The effects of a change in system parameters upon the response of the first mode may then be determined.

The influence function $G(x, \epsilon)$ is the equilibrium displacement of a point x caused by a unit load at ϵ . It satisfies the differential equations

$$\frac{d}{dx} \left[EI \frac{d^2 G}{dx^2} \right] = 1 \quad 0 \leq \epsilon \leq x < l$$

$$\frac{d}{dx} \left[EI \frac{d^2 G}{dx^2} \right] = 0 \quad 0 \leq x < \epsilon \leq l$$

The influence function and static deflection curve $y_0(x)$ satisfy the boundary conditions (52-55).

Under fairly general conditions, the influence function will possess the absolutely and uniformly convergent bilinear expansion

$$G(x, \epsilon) = \sum_{n=1}^{\infty} \frac{y_n(x)y_n(\epsilon)}{\omega_n^2 \left[my_n^2(0) + \int_0^l \rho A y_n^2 dx \right]} \quad (56)$$

It is evident that $y_0(x) = FG(x, 0)$. The final expression for the dynamic deflection is

$$Y(x, t) = y_0(x) - \sum_{n=1}^{\infty} \frac{F y_n(0) y_n(x)}{\omega_n^2 \left[my_n^2 + \int_0^l \rho A y_n^2 dx \right]} \cos \omega_n t \quad (57)$$

The response coefficients for cantilever beams may be defined as follows:

$$Y(0, t) = y_0(0) \left[1 - \sum_{n=1}^{\infty} A_n \cos \omega_n t \right] \quad (58)$$

$$Y_{tt}(0, t) = \frac{F}{m} \sum_{n=1}^{\infty} B_n \cos \omega_n t \quad (59)$$

$$Y_{xx}(x, t) = \frac{Fx}{EI(x)} \sum_{n=1}^{\infty} \left[1 - \sum_{n=1}^{\infty} C_n(x) \cos \omega_n t \right] \quad (60)$$

A comparison of equations (57) and (59) shows that

$$B_n = \frac{my_n^2(0)}{my_n^2(0) + \int_0^l \rho A y_n^2 dx} \quad (61)$$

This coefficient has an obvious interpretation in terms of kinetic energy. In cases of interest B_1 differs far more from unity than either A_1 or C_1 , and forms a convenient basis of comparison in measuring how far a beam-mass system departs from single degree-of-freedom action. In order to find B_1 exactly, the complete solution of the Bernoulli-Euler equation is required. Reasonable bounds, however, may be derived from the influence function, which is the solution of a much simpler equation.

The notion of reduced mass is frequently used to account for the effects of the distributed mass upon the fundamental frequency and kinetic energy of a beam-mass system. It is defined as

$$m_r = \frac{\int_0^l \rho A y_1^2 dx}{y_1^2(0)}$$

We see that

$$B_1 = \frac{m}{m + m_r}$$

We may show that

$$\frac{mG(0, 0)}{mG(0, 0) + \int_0^l \rho AG(x, x) dx} < B_1 < \frac{m y_0^2(0)}{m y_0^2(0) + \int_0^l \rho A y_0^2 dx} \quad (62)$$

and

$$\frac{1}{G(0, 0)} \int_0^l \rho AG(x, x) dx > m_r > \frac{1}{y_0^2(0)} \int_0^l \rho A y_0^2(x) dx \quad (63)$$

The above relations were derived for a cantilever beam. Nevertheless, they hold for more general conditions of constraint, provided the assumptions which underlie this development are still valid. No energy must pass between the beam-mass system and the supporting structure and this structure must restrain the beam against rigid body motion. In the table below, a comparison is made between the exact and approximate values of B_1 for certain uniform beams.

VALUES OF B_1 AND $\frac{m_r}{m_b}$ FOR CERTAIN UNIFORM BEAMS

$$\frac{m}{m_b} = \frac{3}{2}$$

	<u>Cantilever</u>	<u>Central Mass Ends Hinged</u>	<u>Central Mass Ends Built In</u>
B_1 Exact	.863	.754*	.800*
B_1 Upper Bound	.864	.755	.802
B_1 Lower Bound	.857	.738	.766
$\frac{m_r}{m_b}$ Upper Bound	1/4	8/15	16/35
$\frac{m_r}{m_b}$ Lower Bound	33/140	17/35	13/35

In the above equations, m corresponds to a terminal mass fixed by the conditions of the test. The kinetic energy of the beam must be reduced in order to improve the dynamic response of the beam-mass system. This is done by increasing the stressing efficiency and at the same time minimizing the reduced mass of the beam. However, the strength and energy requirements of the beam-mass system must be maintained, and the beam should be readily fabricated. The last condition sets a practical limit to the improvement in response which may be obtained by redesigning the beam.

Let

- F = maximum load
- S = maximum stress
- σ = stress at given point
- E = Young's modulus
- k = spring rate
- ρ = density (mass per unit volume)
- V = volume of beam

*These figures are derived from data given by H. P. Gay, Reference (8).

The static efficiency, a , is defined as

$$a = \frac{1}{VS^2} \int \sigma^2 dV$$

By equating the internal strain energy to the work done on the beam, we may show the minimum mass of the beam is

$$m_b = \frac{1}{a} \left(\frac{F}{S} \right)^2 \frac{\rho E}{k}$$

All the factors but a are determined by the characteristics of the beam material and the required characteristics of the special spring device.

Consider again a cantilever beam in which the section properties vary as a power of the distance from the tip (15-21). The static efficiency is

$$a = \frac{1}{3} \frac{1 + \beta}{3 - \alpha}$$

The mass of the beam is

$$m_b = \int_0^L \rho A dx = \frac{\rho A(L)}{1 + \beta}$$

The reduced mass ratio is

$$b = \frac{m_r}{m_b}$$

and the net efficiency ratio is $\frac{b}{a}$:

Let $\tau = \frac{x}{L}$, $\delta = \beta - \alpha + 4$; then, on referring to Eq. (63) we find that

$$\frac{6(3 - \alpha)^2}{(\delta + \alpha - 3)(\delta + \alpha - 2)(\delta + \alpha - 1)\delta} > \frac{b}{a} > \int_0^1 \tau^\delta (\tau^{3-\alpha} - (3 - \alpha)\tau + (2 - \alpha))^2 d\tau$$

When α is fixed, the extremes of this inequality are decreasing functions of δ . We should take δ as large as possible subject to the condition

$\alpha + \beta \leq 2$. Let $\delta = 2 - \alpha$; then for cantilever beams of uniform static bending strength we have

$$\frac{3}{(4 - \alpha)(5 - \alpha)} > \frac{b}{a} > \int_0^1 \tau^{2-\alpha} \left\{ \tau^{3-\alpha} - (3 - \alpha)\tau + (2 - \alpha) \right\}^2 d\tau$$

We see that $\frac{b}{a}$ may be made as small as we please by taking α large and negative. However, the only values of α which are practical for engineering purposes lie in the interval

$$1 \leq \alpha \leq 1\frac{1}{2}$$

In the table below, the mass ratio $\frac{m}{m_b}$ is taken to be $\frac{9}{2}$.

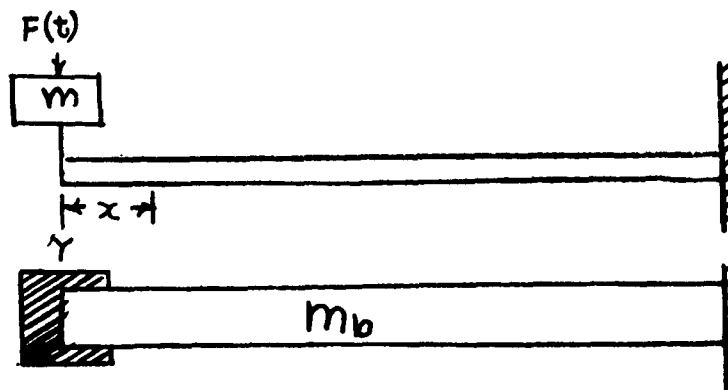
VALUES OF THE REDUCED MASS RATIO AND B_1 FOR
CANTILEVER BEAMS OF UNIFORM STRENGTH

α	$b(\alpha)$		$B_1, \frac{m}{m_b} = \frac{9}{2}$	
	Lower Bound	Upper Bound	Upper Bound	Lower Bound
1.0	.0667	.0833	.985	.982
1.1	.0706	.0884	.984	.981
1.2	.0749	.0940	.984	.980
1.3	.0796	.1001	.983	.978
1.4	.0848	.1068	.982	.976
1.5	.0905	.1143	.980	.975

The combined effects of increased stressing efficiency and more favorable mass distribution decreases the net efficiency ratio $\frac{b}{a}$ from $\frac{1}{4}$ for a uniform cantilever beam ($\alpha = \beta = 0$) to $1/36$ for a linearly tapered cantilever beam ($\alpha = \beta = 1$) having the same strength and energy characteristics.

THE RESPONSE OF UNIFORM AND LINEARLY TAPERED CANTILEVER BEAMS

Cantilever beams of uniform cross section were used in the first special spring device constructed at the Ballistic Research Laboratories. A diagram is shown below.



The response to a step function of force may be obtained by setting $\alpha = 0$, $\beta = 0$, $c = 0$, $k = 0$ in Eq. (1-9). The series (23-25) are then expressed in terms of hyperbolic and circular functions. The characteristic equation is

$$-\frac{m}{m_b} \lambda (\cosh \lambda \sin \lambda - \cos \lambda \sinh \lambda) + (1 + \cos \lambda \cosh \lambda) = 0$$

The circular frequencies are given by

$$\omega_n = \lambda_n^2 \sqrt{\frac{EI}{m_b}}$$

where λ_n is the n^{th} positive root of the frequency equation. The motion at the free end is

$$Y(l, t) = \frac{1}{3} \frac{F l^3}{EI} \left[1 - \sum_{n=1}^{\infty} \lambda_n \cos \omega_n t \right]$$

where

$$A_n = \frac{12 [\coth \lambda_n - \cot \lambda_n]}{\lambda_n^4 \left[2 \frac{m}{m_b} \lambda_n + \left(\frac{m}{m_b} + 1 \right) (\coth \lambda_n - \cot \lambda_n) \right]}$$

The acceleration of the mass m is given by

$$Y_{tt} = \frac{F}{m} \sum_{n=1}^{\infty} B_n \cos \omega_n t$$

where

$$B_n = \frac{4m}{m_b} \frac{\coth \lambda_n - \cot \lambda_n}{2\lambda_n \frac{m}{m_b} + \left(1 + \frac{m}{m_b} \right) (\coth \lambda_n - \cot \lambda_n)}$$

The strain at the built-in end is given by the series

$$Y_{xx}(l, t) = \frac{lF}{EI} \left[1 - \sum_{n=1}^{\infty} C_n(l) \cos \omega_n t \right]$$

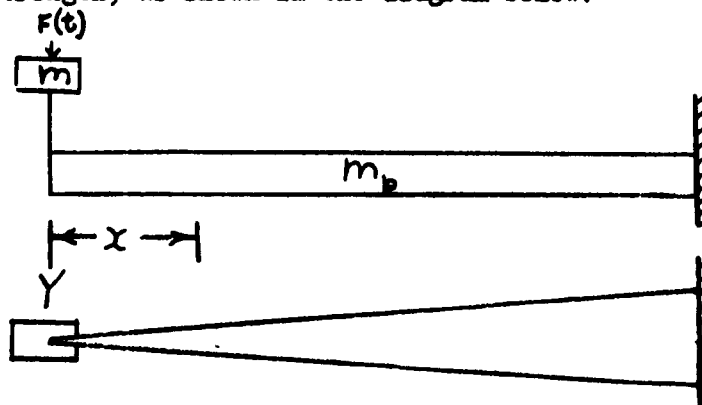
Calculations were carried out for the mass ratio $\frac{m}{m_b} = \frac{3}{2}$, as this was considered the most unfavorable ratio that would occur in practice. The results are tabulated below:

RESPONSE COEFFICIENTS FOR A UNIFORM CANTILEVER BEAM

$$\frac{m}{m_b} = \frac{3}{2}$$

n	λ_n	ω_n/ω_1	A_n	B_n	C_n
1	1.14644338	1.0000	.999461111	.863269	+1.022259
2	3.99951130	12.171	.00051740	.066194	- .026047
3	7.1132135	38.497	.00001859	.023801	+ .0049776
4	10.241683	79.806	.000002159	.011874	- .001694
5	13.376078	136.13	.000000442	.007074	+ .000767

We see that only the acceleration coefficient B_1 differs markedly from unity. The approximate analysis of Part II indicates that a linearly tapered cantilever beam should respond more faithfully to a transient force applied at the end. Accordingly, the second spring device was constructed of linearly tapered beams of constant static bending strength, as shown in the diagram below:



The response to a step function of force may be found by setting $c = 0$, $k = 0$ in Eqs. (1-9) and $\alpha = 1$, $\beta = 1$ in the equations of Part I. The deflection may be expressed in terms of the functions

$$y_1 = 1 + \frac{1}{3} \frac{\epsilon^4}{4!} + \frac{1 \cdot 5}{3 \cdot 7} \frac{\epsilon^8}{8!} + \dots$$

$$y_2 = \epsilon + \frac{2}{4} \frac{\epsilon^5}{5!} + \frac{2 \cdot 6}{4 \cdot 8} \frac{\epsilon^9}{9!} + \dots$$

$$y_3 = \frac{1}{2} \epsilon^2 + \frac{3}{5} \frac{\epsilon^6}{6!} + \frac{3 \cdot 7}{5 \cdot 9} \frac{\epsilon^{10}}{10!} + \dots$$

which are solutions of the differential equation

$$\epsilon y_{\epsilon\epsilon\epsilon\epsilon} + 2y_{\epsilon\epsilon\epsilon} - \epsilon y = 0$$

These series were first given by A. Ono in his study of turbine blades.

The frequency equation is

$$\Delta(\lambda) = 0$$

where

$$\Delta(\lambda) = \begin{vmatrix} \frac{m}{2m_0} \lambda^2 & 0 & -1 \\ y_1(\lambda) & y_2(\lambda) & y_3(\lambda) \\ y_1'(\lambda) & y_2'(\lambda) & y_3'(\lambda) \end{vmatrix}$$

The circular frequency of the n^{th} mode is

$$\omega_n = \frac{\lambda_n^2}{l^2} \sqrt{\frac{EI(l)}{\rho A(l)}}$$

where λ_n is the n^{th} positive root of the frequency equation. The deflection is

$$Y(x, t) = \frac{Fl^3}{2EI(l)} (l - x)^2 - \frac{4Fl^3}{EI(l)} \sum_{n=1}^{\infty} \frac{\begin{vmatrix} y_1(\epsilon) & y_2(\epsilon) & y_3(\epsilon) \\ y_1(\lambda_n) & y_2(\lambda_n) & y_3(\lambda_n) \\ y_1'(\lambda_n) & y_2'(\lambda_n) & y_3'(\lambda_n) \end{vmatrix}}{\lambda_n^3 \frac{\partial \Delta(\lambda_n)}{\partial \lambda}} \cos \omega_n t$$

The displacement at the free end is given by

$$Y(0, t) = \frac{Fl^3}{2EI(l)} (1 - \lambda_n \cos \omega_n t)$$

where

$$A_n = \frac{8 \begin{vmatrix} y_2(\lambda_n) & y_3(\lambda_n) \\ y_2'(\lambda_n) & y_3'(\lambda_n) \end{vmatrix}}{\lambda_n^3 \frac{\partial \Delta(\lambda_n)}{\partial \lambda}}$$

The corresponding acceleration is given by

$$Y_{tt}(0, t) = \frac{F}{m} \sum B_n \cos \omega_n t$$

where

$$B_n = \frac{\lambda_n^4 m}{m_b} A_n = \frac{2\lambda_n^m \begin{vmatrix} y_2(\lambda_n) & y_3(\lambda_n) \\ y_2'(\lambda_n) & y_3'(\lambda_n) \end{vmatrix}}{m_b \frac{\partial \Delta(\lambda_n)}{\partial \lambda}}$$

The strain at the free end is given by

$$Y_{xx}(0, t) = \frac{Fs}{EI(l)} \left[1 - \sum_{n=1}^{\infty} c_n \cos \omega_n t \right]$$

where

$$c_n = \frac{4 \begin{vmatrix} y_1(\lambda_n) & y_2(\lambda_n) \\ y_1'(\lambda_n) & y_2'(\lambda_n) \end{vmatrix}}{\lambda_n \frac{\partial \Delta(\lambda_n)}{\partial \lambda}}$$

On referring the characteristic equation, we see that

$$B_n = c_n$$

for all values of n . A similar formula is true for all beams of uniform static bending strength.

The functions y_1 , y_2 , and y_3 , together with their first three derivatives, were calculated by the Computing Laboratory of the Ballistic Research Laboratories. The characteristic roots and Fourier coefficients were then found by desk calculation. The values of these constants for a mass ratio $\frac{m}{m_b} = \frac{3}{2}$ are given below.

RESPONSE COEFFICIENTS FOR A LINEARLY TAPERED BEAM

$$\frac{m}{m_b} = \frac{3}{2}$$

<u>n</u>	<u>λ_n</u>	<u>$\frac{\omega_n}{\omega_1}$</u>	<u>A_n</u>	<u>$B_n = c_n$</u>
1	1.26397436	1	.99969708	.9563696
2	4.10791986	10.563	.00029522	.0315259
3	7.13977	31.908	.00000680	.0066287
4	10.25647	65.844	.00000054	.0022484
5	13.3853	112.144	.00000008	.0010133
Sum			.9999997	.9977859

This table shows how a more favorable mass distribution reduces the kinetic energy of the beam. The estimated value of B_1 estimated by Rayleigh's method is .9574, an error of only 1/10 of 1%.

The response coefficients were also calculated for a mass ratio of $\frac{m}{m_b} = \frac{9}{2}$. This constant strength characteristics as a uniform

cantilever beam having a mass ratio of $\frac{m}{m_b} = \frac{3}{2}$.

RESPONSE COEFFICIENTS FOR A LINEARLY TAPERED BEAM

$$\frac{m}{m_b} = \frac{9}{2}$$

<u>n</u>	<u>λ_n</u>	<u>$\frac{\omega_n}{\omega_1}$</u>	<u>A_n</u>	<u>$B_n = c_n$</u>
1	.96741174	1	.99996478	.98523
2	4.08611	17.840	.00003439	.01078
3	7.13179	54.347	.00000076	.00222
4	10.25263	112.32	.00000006	.00075
5	13.38315	138.34	.00000001	.00034
Sum			1.00000000	.99934

We see that the acceleration response of the tapered cantilever beam closely approximates the response of a massless spring for the mass ratio used here. The figure $B_1 = .863$ obtained for the cantilever beam of uniform cross section should be compared with the value $B_1 = .985$ shown in the table above. There is a corresponding improvement in the A_1 coefficient.

Normal deflection curves for uniform beams subject to various end constraints have been published by Den Hartog and others. It was convenient to graph the normal deflection curves for the tapered beam in dimensionless form. The length of the beam equals the characteristic root; the deflection scale is arbitrary. The base of the beam is built in; the tip was either hinged or free. These correspond to the

limiting values of the ratio $\frac{m}{m_b} \rightarrow 0$ and $\frac{m}{m_b} \rightarrow \infty$. The deflection equation is:

$$y(\epsilon) = S_{e,n} \cdot \begin{vmatrix} y_1(\epsilon) & y_2(\epsilon) & y_3(\epsilon) \\ y_1(\lambda_n) & y_2(\lambda_n) & y_3(\lambda_n) \\ y_1'(\lambda_n) & y_2'(\lambda_n) & y_3'(\lambda_n) \end{vmatrix}$$

$$= S_{0,n} [S_{1,n} y_1(\epsilon) + S_{2,n} y_2(\epsilon) + S_{3,n} y_3(\epsilon)]$$

The characteristic roots, the scaling constant $S_{0,n}$, and the constants $S_{1,n}$ are tabulated below.

DEFLECTION CONSTANTS FOR A TAPERED CANTILEVER BEAM

$$S_{3,n} = 0$$

<u>n</u>	<u>λ_n</u>	<u>$S_{0,n}$</u>	<u>$S_{1,n}$</u>	<u>$S_{2,n}$</u>
1	2.6752	1.0000	2.83354	1.50406
2	5.5718	.2000	-20.84760	+12.57850
3	8.6883	.0200	+297.42400	-178.12100
4	11.8152	.0010	-4931.18000	+2954.16000
5	14.9494	.0001	+90799.60000	-54395.30000

From this table, it is found that $\lambda_1^2 = 7.1567$, which may be compared with the value 7.16 given by Ono. The remaining roots apparently have not been given previously, even in the extensive tabulation of characteristic roots published by D. Wrinch.

Similar calculations were made for a tapered beam hinged at the tip.

DEFLECTION CONSTANTS FOR A TAPERED BEAM TIP HINGED - BASE BUILT IN

$$S_{1,n} = 0$$

<u>n</u>	<u>λ_n</u>	<u>$S_{0,n}$</u>	<u>$S_{2,n}$</u>	<u>$S_{3,n}$</u>
1	4.0750	1.000	+3.92382	-2.90119
2	7.1278	.100	-46.00510	+35.14440
3	10.2507	.010	+715.68100	-545.85500
4	13.3820	.005	-12452.30000	+9498.11000

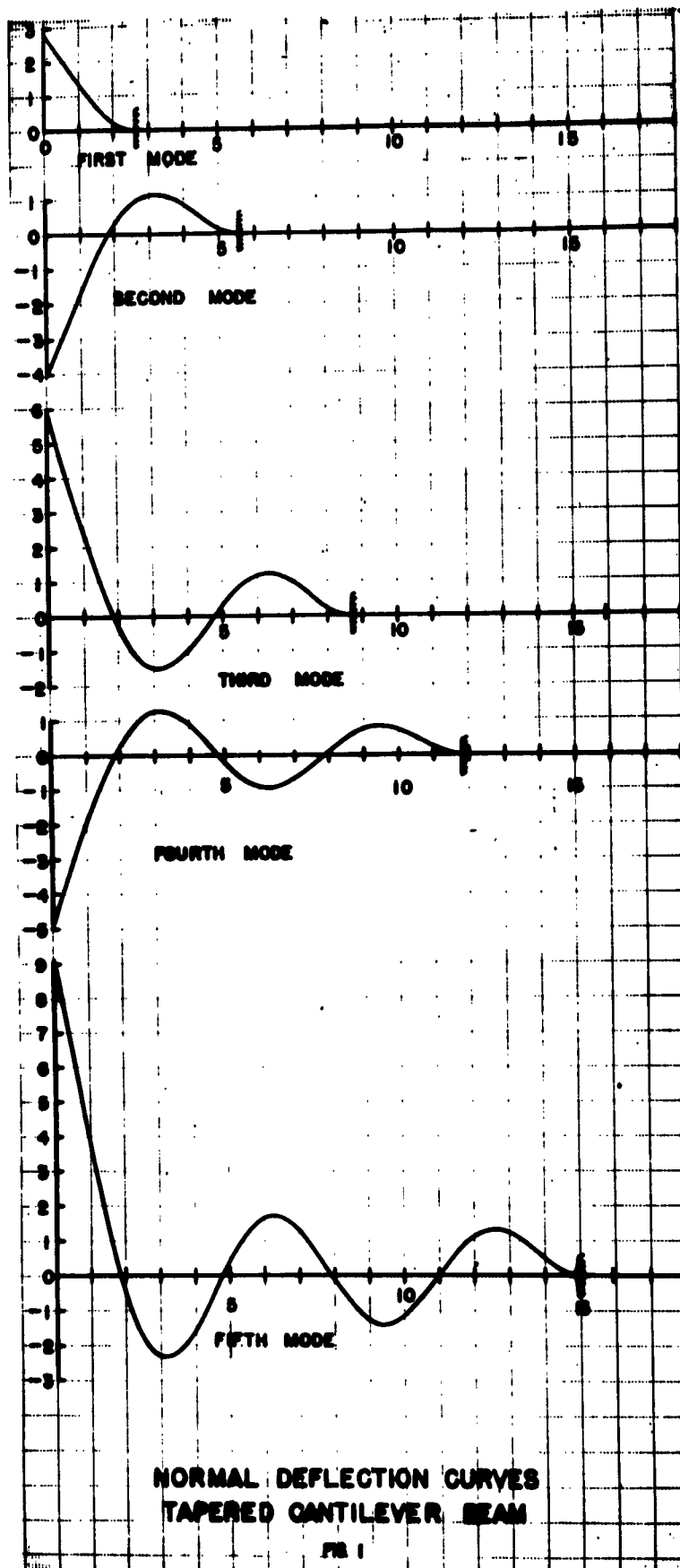
These deflection curves are shown in Fig. 1 and 2.

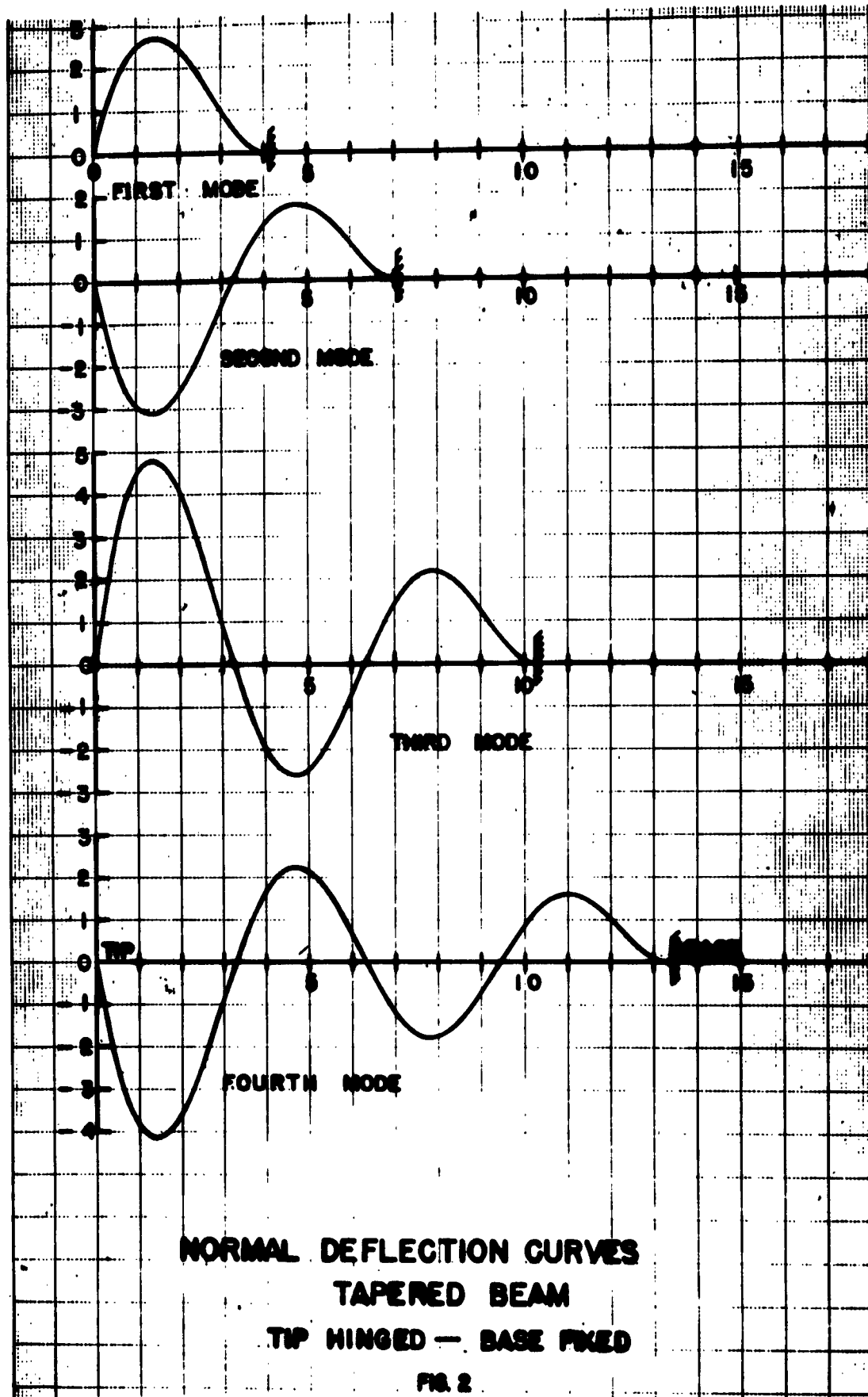
BIBLIOGRAPHY

1. The Free Lateral Vibrations of a Cantilever Beam with a Terminal Dashpot, E. J. McBride, Jour. of Applied Mech. Vol. 10, No. 3, Sept. 1943.
2. Vibration of a Beam with Concentrated Mass, Spring and Dashpot. Dana Young. A.S.M.E. pp. 47-A-9.
3. Forced Vibration of Uniform and Tapered Beams with General Edge Conditions and Loads, C. J. Thorne, L. J. Deveral, P. V. Lothrop, No. 12, Studies in Applied Mathematics, University of Utah, Salt Lake City, Utah.
4. On the Lateral Vibrations of Rods of Variable Cross-Section, D. M. Wrinch, Phil, Mag. S. 6 Vol. 46, No. 272, and Aug. 1923, pp. 273-291.
5. Lateral Vibrations of Tapered Bars, Akinasa Ono, Journal of the Society of Mechanical Engineers, Vol. XXVIII, No. 99, July 1925, pp. 429-441.
6. Modern Operational Mathematics in Engineering, R. V. Churchill, McGraw Hill Book Co., Inc., New York, First Edition, 1944.
7. The Response of Tapered Cantilever Beams with a Terminal Mass when a Constant Force is Applied Instantaneously at the Mass, A. S. Elder, BRL Report No. 979, April 1956.
8. The Response of Simple Beams with a Central Mass to a Constant Force Applied Instantaneously at the Center, H. P. Gay, BRL Memorandum Report No. 837, Oct. 1954.

A. S. Elder

A. S. ELDER





ANALYSIS OF AN INFINITE PLATE CONTAINING RADIAL CRACKS
ORIGINATING AT THE BOUNDARY OF AN INTERNAL CIRCULAR HOLE

by
O. L. Bowie
Watertown Arsenal

I. INTRODUCTION

Considerable advance has been made in recent years in the application of energy type theories in determining the influence of cracks in the specimen geometry on the strength of the specimen. In order to apply theories such as that developed by A. A. Griffith [(1)]*, it is necessary to calculate the elastic strain energy of the system. Although only the boundary stresses and displacements are actually necessary for this calculation, one must nevertheless formally solve the problem as a whole to obtain this information.

This paper is concerned with the solution of a particular class of plane problems in elasticity arising from a distribution of radial cracks of finite length originating at the boundary surface of a circular hole in an infinite plate under the two load systems shown in Figure 1. The geometry of the internal boundary, ζ , can be conveniently described by considering the plate as the complex z - plane where $z = x + iy = re^{i\theta}$. Then, if the center of the hole is chosen as $z = 0$, we specify that the radial cracks lie along $\theta = 0, 2\pi/K, \dots, (K-1)2\pi/K$ where $K \geq 1$ is an integer. For $K \geq 2$, we further restrict our attention to cracks of equal length.

Two load systems will be considered in detail. The first of these (illustrated in Figure 1a) is the case of uniform tension at infinity with ζ free from applied load. In addition to its plane stress applications, this case enables us to study the plane strain problem corresponding to internal pressure acting in hollow cylinders of very large wall thickness with longitudinal cracks originating at the inside surface. Indeed, this latter problem can be studied by superimposing the solution corresponding to uniform hydrostatic pressure. The second load system will be taken as tension (in one direction) at infinity as illustrated in Figure 1b, again with ζ considered as free from applied load. This latter case arises in the plane stress problem of radial cracks at the boundary of a circular hole in a very large thin plate under tension.

The problems described above can be most conveniently handled by the complex variable method of Muskhelishvili [(2)] for solving plane problems of elasticity.

* Numbers in brackets refer to the references at the end of the paper.

II. STRESS ANALYSIS

A. Formulation of the Problem

The complex variable method of Muskhelishvili depends upon the representation of Airy's stress function, $U(x, y)$, in terms of two analytic functions of the complex variable, z , namely, $\phi(z)$ and $\psi(z)$, where

$$U(x, y) = \operatorname{Re} \left[\bar{z} \phi(z) + \int \bar{z} \psi(z) d\bar{z} \right] \quad (1)$$

With this representation the stress components in rectangular coordinates can be written as

$$\sigma_y + \sigma_x = 2 [\phi'(z) + \overline{\phi'(z)}] = 4 \operatorname{Re} [\phi'(z)] \quad (2)$$

$$\sigma_y - \sigma_x + 2i \tau_{xy} = 2 [\bar{z} \phi''(z) + \psi'(z)] \quad (3)$$

where the prime notation denotes differentiation with respect to z and the bars denote the complex conjugates. The condition that a boundary τ be load-free can be expressed as

$$\phi(z) + z \overline{\phi'(z)} + \overline{\psi(z)} = 0, \quad z \in \tau \quad (4)$$

It is convenient for the purpose of enforcing the boundary condition (4) to introduce an auxiliary complex plane, the ξ -plane, such that the unit circle, $\sigma = e^{i\theta}$, and its exterior in the ξ -plane are mapped into τ and its exterior, respectively, by the analytic function

$$z = \omega(\xi) \quad (5)$$

The stress functions $\phi(z)$ and $\psi(z)$ can be considered as functions of the parameter ξ ; in fact, to simplify the notation we shall designate

$$\phi(z) \equiv \phi[\omega(\xi)] \equiv \phi(\xi) \quad (6)$$

$$\psi(z) \equiv \psi[\omega(\xi)] \equiv \psi(\xi)$$

Thus, $\phi'(z) \equiv \phi'(\xi)/\omega'(\xi)$, etc. and the boundary condition (4) can be written as

$$\phi(\sigma) + \omega(\sigma) \overline{\phi'(\sigma)/\omega'(\sigma)} + \overline{\psi(\sigma)} = 0 \quad (7)$$

The analysis of the problem requires the determination of the functions $\phi(\xi)$ and $\psi(\xi)$ which are analytic for $|\xi| > 1$, and satisfy the loading conditions at infinity and on the unit circle.

B. The Mapping Function

The mapping function (5) for this problem can be expressed in differential form as

$$dz/z = (1 - \zeta^{-k})d\zeta / \zeta (1 + 2\epsilon\zeta^{-k} + \zeta^{-2k})^{\frac{1}{2}} \quad (8)$$

where ϵ is a real constant such that $0 \leq |\epsilon| < 1$ and the denominator is considered positive at $\zeta = 1$ in order to define the proper branch. By varying ϵ , the crack depth can be adjusted to assigned values. The integer K determines the number of radial cracks. It is evident from the structure of Equation (8) that the exterior of the unit circle in the ζ -plane is mapped conformally into the exterior of the corresponding boundary in the z -plane. Finally, from symmetry it is clear that the unit circle is mapped into a circular boundary interrupted by K symmetrically distributed radial cracks of equal depth.

The mapping function defined in differential form by (8) can, in general, be found in closed form by quadrature. For $K = 1$, it can be shown that

$$z = \omega(\zeta) = c \left[\zeta + \zeta^{-1} + (\epsilon + 1) + (1 + \zeta^2) / \sqrt{\zeta^2 - 2\epsilon\zeta + 1} \right] \quad (9)$$

The form of the mapping function, however, increases in complexity with larger integers, K .

For the purpose of the subsequent stress analysis, it is desirable to find a series representation of $\omega(\zeta)$ converging on and exterior to the unit circle. The form of such a series is evidently

$$z = \omega(\zeta) = c \left[\zeta + \sum_{n=1}^{\infty} A_n \zeta^{1-Kn} \right] \quad (10)$$

where c and the A_n 's are real coefficients. The coefficients A_n can be conveniently computed from the following recursive formulae, determined by expanding both sides of (8) in series and equating coefficients of equal powers of ζ

$$\begin{aligned} -K A_1 &= \beta_1 \\ -2K A_2 &= \beta_2 + A_1 \beta_1 \\ -3K A_3 &= \beta_3 + A_1 \beta_2 + A_2 \beta_1 \end{aligned} \quad (11)$$

where

$$\begin{aligned} 2B_1 &= \alpha_1 \\ 2B_2 + B_1^2 &= \alpha_2 \\ 2B_3 + B_1 B_2 &= \alpha_3 \\ 2B_4 + 2B_1 B_3 + B_2^2 &= \alpha_4 \end{aligned} \quad (12)$$

and

$$\alpha_K = -2(1 - \cos \alpha) \sin K\alpha / \sin \alpha, \quad \cos \alpha = -\epsilon$$

The unit circle in the ζ -plane is the circle of convergence of the series (10) since singularities occur on the unit circle at the roots of

$$\zeta^{2K} + 2\zeta^K + 1 = 0 \quad (13)$$

It can be shown⁽¹⁾ that $\lim_{n \rightarrow \infty} A_n = 0$; thus, by a well-known

theorem [8], the series (10) converges at all points on the circle of convergence except at the singular points described above. This property is useful in that it provides for a systematic scheme for obtaining polynomial approximations of the mapping function.

C. Method of Solution

Were it not for the unknown character of the singularities of $\phi(\zeta)$ and $\psi(\zeta)$ on the unit circle, the problem could be solved by simply assuming a series development of the two functions with the proper conditions at infinity, substituting into the condition (7), and determining the numerical values of the coefficients from the set of relations obtained by equating coefficients of equal powers of ζ . This approach would lead to immediate difficulties as it will be shown that $\psi(\zeta)$ must admit simple poles on the unit circle at those points corresponding to the notch roots. Furthermore, certain singularities appear to exist at the points on the unit circle corresponding to the junction of the cracks and the circle. The forms of these latter singularities appear too difficult to establish a priori. A completely rigorous solution of the problem would require that a series expansion of $\phi(\zeta)$ and $\psi(\zeta)$, in which terms corresponding to simple poles at the crack roots be added to the series for $\psi(\zeta)$, be examined for convergence on the unit circle. Although there is every reason to believe that this procedure is possibly theoretically, severe practical difficulties

1. The proof is particularly simple for $K = 1$. From (9), it can be seen that the A_n 's behave essentially as the Legendre polynomials. The proof is more difficult for $K > 2$.

immediately are encountered. Although the infinite system of linear simultaneous equations which determine the coefficients of the series is amenable to numerical solution, it is difficult to determine rigorously the properties of the coefficients necessary to examine convergence.

The method of solution which will be used in this analysis circumvents direct consideration of the second type of singularity mentioned above by considering polynomial approximations of the mapping function. An accurate description of the stress distribution at the crack roots is obtained by introducing cusps to describe the crack roots and their neighborhoods. Convergence of the polynomial approximation to the exact problem can then be considered a matter of choosing a sufficiently accurate polynomial approximation of the mapping function such that a closer approximation will not affect appreciably the values for the information desired.

In the following analysis, we shall denote polynomial approximations of the mapping function by

$$z = \omega(\zeta) = c \left[\zeta + \sum_{n=1}^N \epsilon_n \zeta^{1-\kappa n} \right] \quad (14)$$

The existence of cusps at locations corresponding to the crack roots is ensured by demanding

$$dz/d\zeta = \omega'(\zeta) = (1 - \zeta^{-\kappa}) g(\zeta) \quad (15)$$

where $g(\zeta)$ is a polynomial with coefficients such that the roots of $g(\zeta) = 0$ fall inside the unit circle. Due to the convergence of (10), suitable approximations can be obtained by setting $\epsilon_n = A_n$; modifications of the A_n 's being made to satisfy (15).

D. The Case of "All-Around" Tension at Infinity

For uniform tension at infinity, illustrated in Figure 1a, the applied loading can be expressed as $\sigma_x = \sigma_y = T$ on $|z| = R$, where R is very large. It can be shown² that for this loading condition, the stress functions $\phi(\zeta)$ and $\psi(\zeta)$ behave as $cT R^{1/2}$ and $cT R^{-1}$, respectively, for large $|z|$.

2. A detailed discussion of the stress functions for infinite regions can be found in [4].

The singularities in the stress functions due to the existence of cusps can be determined by the following argument. If there were no boundary irregularities in (14), it can be shown³ that the stress function $\phi(\zeta)$ is a polynomial of the form

$$\phi(\zeta) = CT \left[\zeta/2 + \sum_{n=1}^N \alpha_n \zeta^{1-Kn} \right]. \quad (16)$$

By regarding the solution for polynomial mappings with cusps as a limiting case of this solution, it is evident that $\phi(\zeta)$ will still retain the form of (16) even though cusps are permitted. To determine the form of $\psi(\zeta)$, it is convenient first to express the boundary condition (7) as

$$\omega'(\sigma) \psi(\sigma) = -\omega'(\sigma) \overline{\phi(\sigma)} - \overline{\omega(\sigma)} \phi'(\sigma). \quad (17)$$

The function $\omega'(\zeta) \psi(\zeta)$ is analytic exterior to the unit circle and is given as a continuous function on the unit circle by (17). If the coefficients, α_n , are chosen so that the coefficients of all positive powers of ζ in the Laurent expansion of

$$\omega'(\zeta) \phi(1/\zeta) + \omega(1/\zeta) \phi'(\zeta) \quad (18)$$

vanish, we can determine $\psi(\zeta)$ explicitly in terms of the mapping function and $\phi(\zeta)$. Multiplying both sides of (17) by $1/2\pi i (\sigma - \zeta)$ and integrating around the unit circle, we obtain by a well-known theorem⁴

$$\omega'(\zeta) \psi(\zeta) = -\omega'(\zeta) \phi(1/\zeta) - \omega(1/\zeta) \phi'(\zeta). \quad (19)$$

Thus, the stress function $\psi(\zeta)$ has simple poles, each located at a cusp root.

All that is required to complete the analysis is the determination of the coefficients α_n in the series expansion (16) for $\phi(\zeta)$. Equating coefficients of all positive powers of ζ in the series expansion of (18) yields the following system of linear simultaneous equations for the determination of the α_n :

$$\alpha_p + \sum_{n=1}^{N-p} \alpha_{p+n} \epsilon_n (1 - nK) + \sum_{n=1}^{N-p} \epsilon_{p+n} \alpha_n (1 - nK) + \epsilon_p / 2 = 0 \quad (20)$$

$p = 1, 2, \dots, N$

3. E.g., the case for $K = 2$, $N = 2$ has been discussed by Morkovin [5] in some detail.

4. Reference [4], p. 145.

It is evident that the state of stress is not affected by the addition of a linear expression of the form $C'iz + \beta' i + \alpha'$ to $\phi(z)$ or a complex constant, $\alpha' + i\beta'$, to $\psi(z)$. The constants C' , β' and α' may be considered as zero in this problem. For $K \geq 2$, the constant α' has been chosen as zero; thus, a value of α' is necessary to identically satisfy (7). For $K = 1$, the constant α' is established as zero by the equation $\beta = 1$ in (20); thus, $\alpha = \alpha_1$ is determined to satisfy (7).

E. The Case of Tension in One Direction at Infinity

For the loading $\sigma_y = T$, illustrated in Figure 1b, the analysis is quite parallel to that of Section D. It can be shown [14] that for this loading condition, the stress functions $\phi(\zeta)$ and $\psi(\zeta)$ approach $CT\zeta/4$ and $CT\zeta/2$, respectively, for large $|\zeta|$. The stress function $\phi(\zeta)$ is again a polynomial and has the form

$$\phi(\zeta) = CT \left[\zeta/4 + \sum_{n=1}^{KN} \alpha_n \zeta^{1-n} \right] \quad (21)$$

The constant α_1 does not contribute to the stresses; instead, it is determined in the sense of the last paragraph of Section D.

To determine $\psi(\zeta)$, we note that $\omega'(\zeta)\psi(\zeta)$ has a simple pole at infinity; in fact, $\omega'(\zeta)\psi(\zeta) \approx C^2T\zeta/2$. With the exception of the point at infinity, $\omega'(\zeta)\psi(\zeta)$ is analytic exterior to the unit circle and is given as a continuous function on the unit circle by

$$\omega'(\sigma)\psi(\sigma) = -\omega'(\sigma)\overline{\phi(\sigma)} - \overline{\omega(\sigma)}\phi'(\sigma) \quad (17')$$

If the coefficients α_n are chosen so that the function

$-\omega'(\zeta)\phi(1/\zeta) - \omega(1/\zeta)\phi'(\zeta) \approx C^2T\zeta/2$ for large $|\zeta|$, we can again determine the function $\psi(\zeta)$ in terms of the mapping function and $\phi(\zeta)$; in fact, again we find

$$\omega'(\zeta)\psi(\zeta) = -\omega'(\zeta)\phi(1/\zeta) - \omega(1/\zeta)\phi'(\zeta) \quad (19')$$

Due to the relative lack of stress symmetry for this case, it is difficult to present the linear systems of simultaneous equations for the determination of the α_n 's in a compact manner for an arbitrary integer K . Therefore, only the systems for the

single crack ($K = 1$) and the two crack ($K = 2$) cases will be explicitly formulated.

For $K = 1$,

$$\alpha_p + \sum_{n=1}^{N-p} \alpha_{n+p} \epsilon_n (1-n) + \sum_{n=1}^{N-p} \epsilon_{n+p} \alpha_n (1-n) + \epsilon_p/4 = \begin{cases} -\frac{1}{2} & P=2 \\ 0 & P \neq 2 \end{cases} \quad (22)$$

$P = 1, 2, \dots, N$

For $K = 2$,

$$\alpha_{2p} + \sum_{n=1}^{N-p} \alpha_{2(n+p)} \epsilon_n (1-2n) + \sum_{n=1}^{N-p} \epsilon_{n+p} \alpha_{2n} (1-2n) + \epsilon_p/4 = \begin{cases} -\frac{1}{2} & P=1 \\ 0 & P>1 \end{cases} \quad (23)$$

$P = 1, 2, \dots, N$

$\alpha_{2p-1} = 0$

III. APPLICATION OF THE GRIFFITH CRITERION

The critical stress for which the radial cracks begin to spread will now be determined from general considerations of the total energy of the system as developed by A. A. Griffith [1] in his theory of rupture of brittle⁵ materials, such as glass and cast iron.

This theory is based on the existence of cracks on the surface or in the interior of the solid; thus, rupture is assumed to be conditioned primarily by the extension of an existing crack. The spreading of a crack is accompanied by an increase in energy proportional to the increase in surface; on the other hand, under the action of a given external stress, the potential energy of a cracked solid is lower than if there were no crack. If an extension of the crack leads to a decrease in total energy, the system becomes unstable, the crack spreads, and the material fractures.

The critical stress is that value of the applied load for which the total energy contribution of the cracks is a maximum. Its value can be obtained from the condition

$$\frac{dV}{dl} = -2K h G dl \quad (24)$$

5. Modifications of this theory to account for local plastic deformation occurring in ductile metals have been made by several authors, e.g., Orowan, Reference [6].

where

$V = V_c - V_0$ = Reduction of the potential energy due to the introduction of radial cracks

V_c = Potential energy of the system with radial cracks

V_0 = Potential energy of the system without cracks

K = Number of radial cracks

h = Thickness of the specimen (axially)

G = Surface tension per unit area

ℓ = Length of the radial crack (s)

A. Calculation of the Reduction in Potential Energy, V

1. Uniform tension, T, at infinity.

For the case of uniform tension, T, at infinity, the potential energy for the cracked solid, V_c , is given by

$$V_c = \lim_{r \rightarrow \infty} -\frac{h}{2} \int_0^{2\pi} R(\sigma_r U_r + \tau_{r\theta} U_\theta) d\theta \quad (25)$$

where σ_r , $\tau_{r\theta}$, U_r and U_θ are the stress and displacement components in polar coordinates.

In order to compare the difference in potential energy with and without radial cracks, it is reasonable to refer to the exact geometry rather than polynomial approximations. This will now be carried out by referring the stress functions to the original z coordinate system. The application of the results obtained by polynomial approximation of the boundary will then be carried out.

The integrand in (25) can be expressed in terms of the stress functions $\phi(z)$ and $\psi(z)$ by observing that

$$\sigma_r - i\tau_{r\theta} = \phi'(z) + \overline{\phi'(z)} - e^{2i\theta} [\overline{z} \phi''(z) + \psi'(z)] \quad (26)$$

and

$$2\mu(U_r + iU_\theta) = e^{-i\theta} [\phi(z) - z\overline{\phi'(z)} - \overline{\psi(z)}] \quad (27)$$

where, in terms of Young's Modulus, E, and Poisson's ratio, σ

$$\mu = E/2(1 + \sigma) \quad (28)$$

and

$$\begin{aligned} \mu &= (3 - \sigma)/(1 + \sigma) \text{ for plane stress} \\ \mu &= 3 - 4\sigma \text{ for plane strain} \end{aligned} \quad (29)$$

Thus, but for the constant factor 2μ , the real part of the product of (26) and (27) yields the bracketed portion of the integrand for the potential energy.

For the case of uniform tension at infinity, the stress functions have the forms

$$\phi(z) = T [a_0 + z/2 + a_1 z^{-1} + \dots] \quad (30)$$

$$\psi(z) = T [\beta_0' + \beta_0 z^{-1} + \beta_1 z^{-2} + \dots] \quad (31)$$

After some algebra, it follows that, for plane stress,

$$V_c = \lim_{R \rightarrow \infty} - \frac{\pi T^2 h}{E} \{ (1 - \sigma) R^2 - 2\sigma \beta_0 \} \quad (32)$$

In order to calculate the potential energy for the uncracked plate, V_0 , the stress analysis for a concentric ring with inner radius R_1 and outer radius R loaded on the outer boundary by the same applied load must be carried out. It is necessary to retain secondary effects in order to arrive at the correct value of the energy difference. The actual distribution of applied load including secondary terms can be determined by substituting (30) and (31) into (26) and evaluating $\sigma_r = i T r_0$ at $z = R e^{i\theta}$. The solution of the corresponding boundary value problem for a concentric ring can be found in a straightforward manner⁶ and for plane stress,

$$V_0 = \lim_{R \rightarrow \infty} - \frac{\pi T^2 h}{E} \left(\frac{R^2 + \beta_0}{R^2 - R_1^2} \right)^2 [(1 - \sigma) R^2 + 2\sigma R_1^2] \quad (33)$$

The reduction in potential energy, $V = V_0 - V_c$, is in the limit

$$V = \frac{2\pi T^2 h}{E} (\beta_0 + R_1^2) \quad (34)$$

for the case of plane stress.

We now proceed to interpret this result in terms of the previous analysis based on conformal mapping. The stress function $\psi(\zeta)$ given by (17) can be expanded in a series

$$\psi(\zeta) = CT [\gamma_0' + \gamma_0 \zeta^{-1} + \gamma_1 \zeta^{-2} + \dots] \quad (35)$$

⁶ Reference [4], pp. 291-296.

from which it follows that

$$\beta_0 = C^2 \gamma_0 \quad (36)$$

The hitherto unspecified parameter C occurring in the mapping function will now be chosen so that the radius of the circular hole is adjusted to a fixed unit distance. If $\sigma = \sigma_1$ is defined as that point on the unit circle in the ζ -plane which corresponds to the junction of the crack and the circle in the z -plane, then C will be chosen so that

$$R_1 = \omega(\sigma_1) = 1 \quad (37)$$

Thus,

$$V = \frac{2\pi T^2 h}{E} \left\{ \gamma_0 / [\omega(\sigma_1)/C]^2 + 1 \right\} \quad (38)$$

The crack length, l , measured in units of the radius of the circular hole, can be expressed as

$$l = \omega(1)/\omega(\sigma_1) - 1 \quad (39)$$

from which it follows;

$$V = \frac{2\pi T^2 h}{E} f(l) \quad (40)$$

where

$$f(l) = \gamma_0 [(l+1)/\omega(1)/C]^2 + 1 \quad (41)$$

for the case of plane stress.

For plane strain, the second form of a in (29) must be used. The results are identical but for a factor of $1 - \sigma^2$ with those of plane stress. In fact, for plane strain

$$V = \frac{2\pi T^2 h (1 - \sigma^2)}{E} f(l) \quad (42)$$

where $f(l)$ is again given by (41).

2. Tension in one direction at infinity.

The calculation of V for the case of simple tension at infinity, $\sigma_y = T$, can be carried out in a manner similar to that

of the preceding section. For the case of plane stress, we find

$$v = \frac{2\pi T^2 h}{E} g(l) \quad (43)$$

$$\text{where } g(l) = (\gamma_0 + 2\alpha_2 - A) \left[(l+1)/w(1)/\bar{c} \right]^2 / 2 + 3/4 \quad (44)$$

In (44),

γ_0 = coefficient of ζ^{-1} in the expansion of $\psi(\zeta)$,
e.g., Equation (35)

$$\alpha_2 = \text{coefficient defined by Equation (21)} \quad (45)$$

ϵ_A = coefficient of ζ^{-1} in the mapping function (14).
Thus, $A = \epsilon_2$ for $K = 1$; $A = \epsilon_1$ for $K = 2$;
 $A = 0$ for $K \geq 3$.

B. The Critical Stress by the Griffith Criterion

The critical applied tension, T_0 , can now be calculated for the different cases by substituting (40), (42) and (43) into the condition expressed by (24).

For plane stress,

$$T_0^* = \sqrt{\frac{-KEG}{\pi f(l)}} \quad \text{For uniform tension, } T \quad (46)$$

$$T_0^{**} = \sqrt{\frac{-KEG}{\pi g(l)}} \quad \text{For simple tension, } \sigma_y = T \quad (47)$$

For plane strain,

$$T_0 = \sqrt{\frac{-KEG}{\pi(1-\sigma^2)f(l)}} \quad \text{For uniform tension, } T \quad (48)$$

Thus, if $T > T_0$, the crack will become unstable and lead to failure.

The plane strain criterion (48) is intended for the study of radial cracks in cylinders under internal pressure. Such a load system is obtained by superimposing a hydrostatic pressure of magnitude $P = T$ on the load system corresponding to the uniform tension case. Since it can be shown that the superposition of a hydrostatic stress state will not affect the above critical stress, the critical internal pressure, P_0 , is given by (48).

IV. NUMERICAL RESULTS

The analysis indicated in the previous sections was numerically evaluated for the case of two cracks as shown in Figure 1. In particular, the stress functions were evaluated for nine values of the parameter $\bar{\epsilon}$. From these results, the functions $f(\ell)$ and $g(\ell)$ in the Griffith criterion were found in tabular form. These data in turn were numerically differentiated with respect to the crack length, ℓ , and the critical stresses according to (46) and (47) were obtained.

A. Uniform Tension at Infinity

In order to apply the Griffith criterion to this case, it is necessary to numerically evaluate the coefficient γ_0 in (41). From the definition of γ_0 , it can easily be shown by expanding (17) that

$$\gamma_0 = - \left[1 + 2 \sum_{n=1}^{\infty} \bar{\epsilon}_n \alpha_n (1 - 2n) \right] \quad (49)$$

It was found that γ_0 can be obtained to three significant figure accuracy if thirty terms of the polynomial approximation of the mapping function are retained. The system (20) for the determination of the α_n 's was solved for each choice of $\bar{\epsilon}$ by iteration. The pertinent results of this calculation are listed in Table I.

TABLE I

Calculation of $f(\ell)$ for Uniform Tension at Infinity

$\bar{\epsilon}$	ℓ	$w(\ell)/c$	γ_0	$f(\ell)$
- 1.000	0.000	1.000	- 1.000	0.000
- 0.866	0.303	1.259	-1.975	- 0.159
- 0.707	0.497	1.383	- 1.160 ✓	- 0.359
- 0.500	0.732	1.500	- 1.267 ✓	- 0.694
0.000	1.414	1.707	- 1.509 ✓	- 2.018
+ 0.500	2.732	1.866	- 1.752	- 6.008
+ 0.707	4.027	1.924	- 1.852	-11.640
+ 0.866	6.596	1.966	- 1.933	-27.860
+ 1.000	∞	2.000	- 2.000	- ∞

For large values of ℓ , the solution approaches the form corresponding to the case of a single crack in an infinite plate. In fact,

$$f(\ell) \approx -(\ell + 1)^2 / 2 + 1 \quad (50)$$

An examination of the tabulated values of $f(\ell)$ indicates that for $\ell > 1$ there is very good agreement with Equation (50).

B. Tension in One Direction at Infinity

In order to apply the Griffith criterion to this case, it is necessary to calculate the function $g(\ell)$ given in (44). It can be shown by expanding (19') that, for this case, with $K = 2$

$$\gamma_0 = \epsilon_{1/2} - \left[1/2 + 2 \sum_{n=1}^N \epsilon_n \tau_{2n} (1 - 2n) \right] \quad (51)$$

The system (23) was solved by iteration for the determination of the τ_n 's for the same values of ϵ as previously chosen. The pertinent information obtained for this case is listed in Table II.

TABLE II

Calculation of $g(\ell)$ for Simple Tension at Infinity

ϵ	ϵ_1	τ_2	γ_0	$g(\ell)$
-1.000	0.00	-0.50	-0.50	0.00
-0.866	0.07	-0.61	-0.62	-0.28
-0.707	0.15	-0.69	-0.74	-0.57
-0.500	0.25	-0.75	-0.87	-1.00
-0.000	0.50	-0.83	-1.13	-2.53
+0.500	0.75	-0.82	-1.33	-6.69
+0.707	0.85	-0.80	-1.41	-12.40
+0.866	0.93	-0.78	-1.46	+28.80
+1.000	1.00	-0.75	-1.50	$-\infty$

C. The Critical Stresses

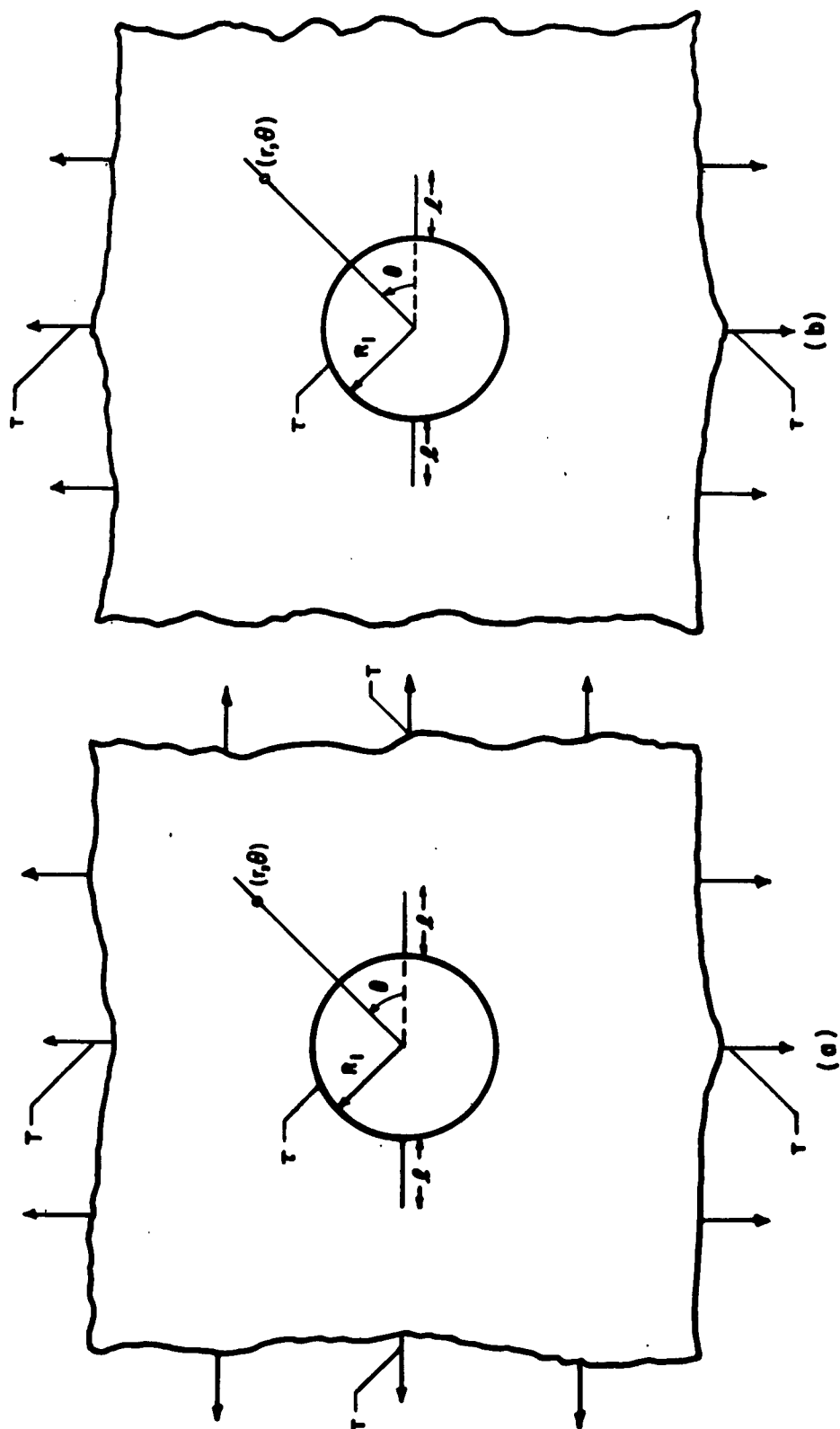
The critical stresses for the cases of uniform and simple tension, T_0^* and T_0^{**} , respectively, can now be found by differentiating numerically the tabular functions $f(l)$ and $g(l)$ and observing Equations (46) and (47). These results are shown in Figure 2.

For sufficiently large values of l , the critical stresses for both loading conditions are proportional to $(1+l)^{-1/2}$; as would be expected from the solution of a single crack of length $2(1+l)$. In Figure 2, it can be seen that for $l > .7$ such an approximation becomes increasingly good. For $l < .7$, the behavior of the solution becomes complicated by the presence of the circular hole.

Finally, the critical internal pressure, P_0 , for the plane strain problem of a circular cylinder with the corresponding plane geometry loaded by internal pressure is proportional to the curve for T_0^* , as indicated by (48) and the paragraph following (48).^o

BIBLIOGRAPHY

- [1] Griffith, A. A., "Theory of Rupture", Proc. of the First Int. Cong. for Appl. Mech., (1924, April), pp. 55 - 63
- [2] Mushelisvili, N., Mathematische Annalen, Vol. 107, (1932-33), pp. 282 - 312
- [3] Titchmarsh, E. C., Theory of Functions, Oxford, (1939), p. 218
- [4] Sokolnikoff, I. S., "Mathematical Theory of Elasticity", (Brown University Lecture Notes), (1941), pp. 243-319
- [5] Morkovin, V., Quart. Appl. Math., Vol. II, No. 4, (1944), pp. 350 - 352
- [6] Orowan, E., Fatigue and Fracture of Metals, Wiley & Sons, Inc., New York, (1950), pp. 139 - 167

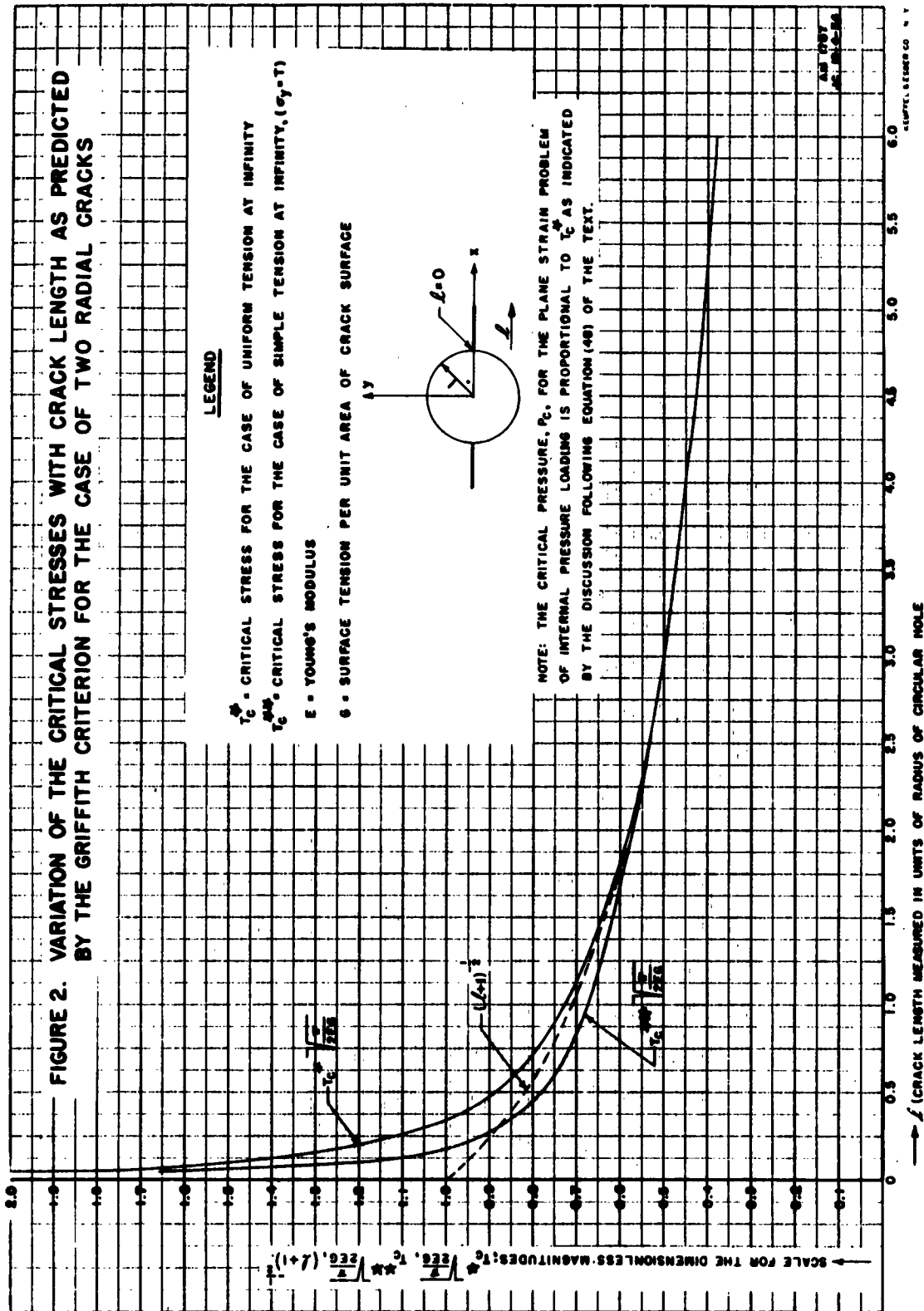


GEOMETRY AND LOADING FOR THE CASE OF TWO CRACKS $K=2$.

FIGURE 1

WATERTOWN ARSENAL LABORATORY

Wtn. 639-13,178



ANALYSIS OF THE N-WAVE OF A SLENDER SUPERSONIC PROJECTIVE

by
D. H. Steininger and F. D. Bennett
Ballistic Research Laboratories

1. INTRODUCTION

1.1 Interferometric Method of Analysis

Interferometric investigation of the fluid flow around a supersonic projectile in free flight gives a quantitative record of the density over the entire flow field.^{1/} Experience shows that the reduction of fringe

^{1/} R. Ladenburg, High Speed Aerodynamics and Jet Propulsion, (Princeton University Press, 1954) Vol. 9, Section A, 3.

shift to density values for an axisymmetric flow is a cumbersome and time consuming process because, in general, the relationship between fringe shift and density at a particular point is not simple. It is useful, therefore, to find flow regions for which some intrinsic property can be determined directly from the measurements of fringe shift.

An interferogram of a supersonic cone-cylinder shows two regions which have conspicuous symmetry of fringe shape, suggesting the possibility of a simplified analysis. The first of these is the well studied^{2,3,4,5/} region

^{2/} J. H. Giese, F. D. Bennett, and V. E. Bergdolt, J. Appl. Phys. 21, 1226 (1950)

^{3/} J. H. Giese and V. E. Bergdolt, J. Appl. Phys. 24, 1389 (1953)

^{4/} V. E. Bergdolt, J. Aeronaut. Sci. 20, 751 (1953)

^{5/} J. D. Cole, G. E. Solomon, and W. W. Willmarth, J. Aeronaut. Sci. 20, 627 (1953)

near the cone in which the fringes are nearly straight and parallel. The flow here is characterized theoretically by the fact that the physical variables are constant along straight lines through the vertex. Assumption of this flow regularity leads to a method of plotting fringe shift which verifies in many instances the close approximation of real flows to idealized conical flow.

The second of these regions lies between the front and rear shock waves at rather large distances from the projectile axis. Here the fringes have a gentle curvature and a similarity of shape which changes only slowly as the distance from the axis increases. This similarity suggests an underlying simplicity of the fundamental flow field. Experiments of Du Mond et al^{6/} show

^{6/} J. W. Du Mond, E. R. Cohen, W. K. H. Panofsky, and E. Deeds, J. Acoust. Soc. Am. 18, 97 (1946)

that at large radial distances and parallel to the axis, the pressure profile consists of a sudden rise at the front shock followed by a linear decrease to a value below free stream and then a sudden rise at the rear shock. The curve so generated has the shape of a capital N, hence is given the name "N-wave".

1.2 Scope of the Paper

Using the results obtained by G. B. Whitham in his improved linearized theory for slender, supersonic projectiles^{7/}, we derive here an analytical

^{7/} G. B. Whitham, Comm. Pure and Appl. Math. 5, 301 (1952)

expression for the fringe shift in the M-wave region. We investigate the more obvious properties of this function and close with an account of preliminary experiments designed to test its validity.

2. THEORY

2.1 The Fringe Shift Integral

If x, r are the polar cylindrical coordinates of the axisymmetric disturbance, and the front tip of the projectile is at the origin with the line of flight along the positive x -axis, then the fringe shift $\delta(x, r)$ is related to the density ρ at (x, r) by^{8/}

$$\delta(x, r) = \frac{2K}{\lambda} \int_r^{r_N} \frac{(\rho - \rho_0) t dt}{(t^2 - r^2)^{1/2}}. \quad (2-1)$$

^{8/} F. D. Bennett, W. C. Carter, and V. E. Bergdolt, J. Appl. Phys. 23, 453 (1952)

K is the Gladstone-Dale constant, λ the wave length of the light in vacuum, ρ_0 the free stream density, and r_N is the outer radius of the disturbance at x . t is the variable of integration in the r direction. As in Figure 1 the fringe shift at (x, r) is determined by an integration of the density values found along the line from r to r_N .

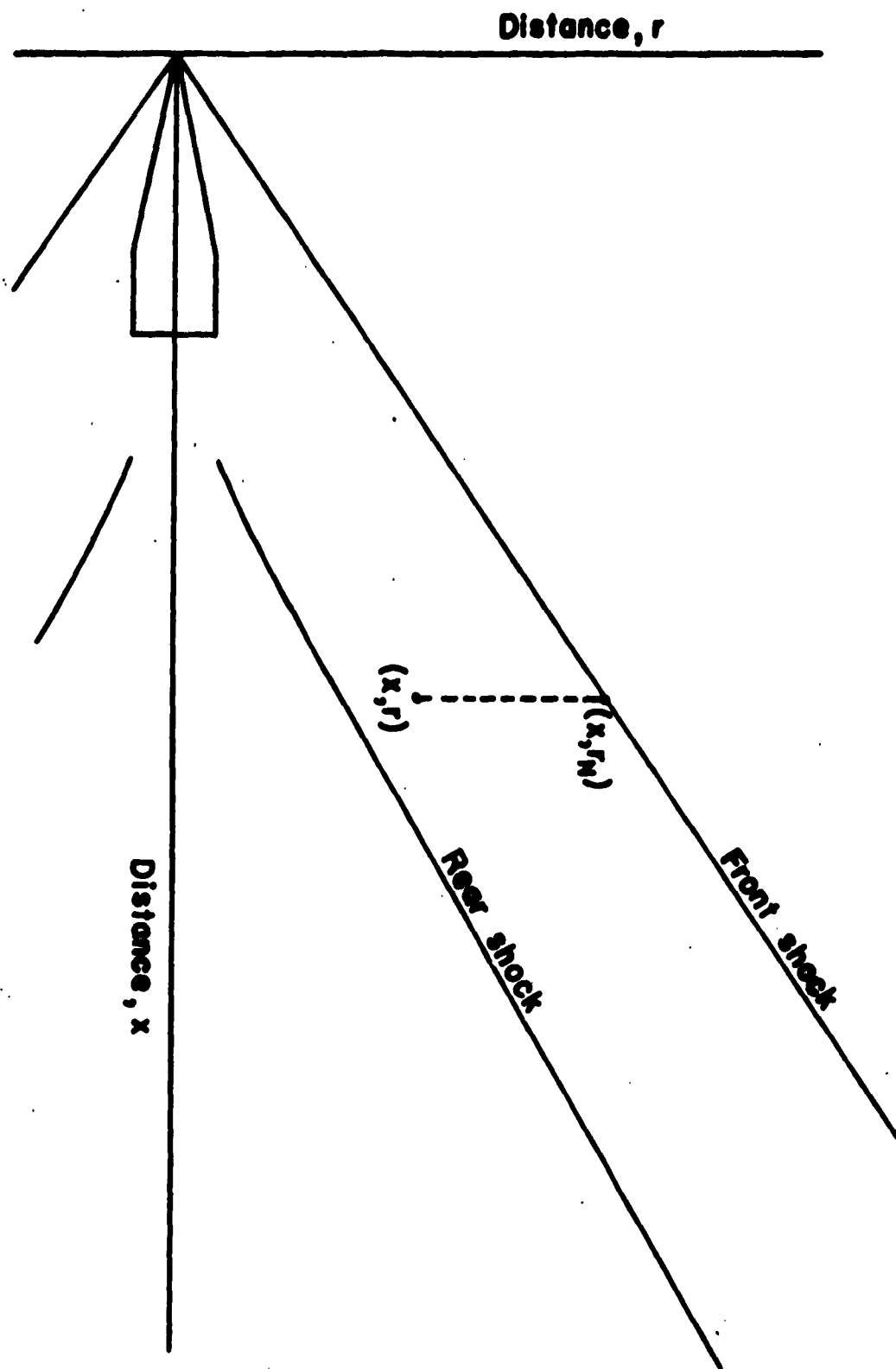


Figure 1. Path of integration of the fringe shift integral for a supersonic projectile.

An inversion of Equation (2-1) allows the reduction of fringe shift measurements to density throughout the flow field^{8/}. Such a reduction does not interest us here; for our purpose is to obtain in the N-wave a functional description of $(\rho - \rho_0)$ and from it derive an expression for the fringe shift in that region.

2.2 Improved Linearized Theory

The linearized theory of von Karman and Moore^{9/} for a slender, supersonic

^{9/} Th. von Karman and N. B. Moore, A.S.M.E. Trans. 54, 303 (1932)

projectile gives solutions which are good first approximations to the actual conditions at the surface of the projectile but which fail as the distance r increases. This failure arises from the fact that the Mach lines are parabolae in second approximation, while the linear approximations to them are straight; and although a curved Mach line intersects a straight one at the surface of the body, the curves diverge with increasing r . The improved theory offered by G. B. Whitham^{7/} makes the linear solutions uniformly valid over the entire field by associating them with the appropriate second order Mach lines. This improved theory still is based upon a first approximation to the potential flow equations and, like linear theory, neglects terms of order u^2 , v^2 , where u and v are the small perturbation velocities in the x and r directions. Nevertheless it has the additional advantage over linear theory that the existence and position of the shock waves are predicted.

With this background, we now list and discuss those results of Whitham which we intend to use. Equations which appear in Whitham's paper will be identified by the notation Wh ().

1. The shock waves. At great distances from its axis the supersonic projectile produces two shock waves, both extending to infinity. The equations for the shock waves at large r are from Wh (43)

$$x = \alpha r + y_0 \pm A r^{1/4} \quad (2-2)$$

where the upper sign represents the front shock and the lower sign the rear shock ($\alpha = (M^2 - 1)^{1/2}$ and A and y_0 are constants related to the body shape). The straight line $x = \alpha r + y_0$ and the two shock waves intersect the x -axis at y_0 . By inspection of Equation (2-2) one sees that the front shock wave lies ahead, and the rear shock behind the straight line by the amount $A r^{1/4}$. Thus the horizontal distance between the two shocks is $2A r^{1/4}$. If the projectile is slender, both A and y_0 can be calculated theoretically from body shape (Cf. Wh (21) and Wh (43)).

2. The pressure distribution. When r is large the pressure distribution between the shock waves is by Wh (71)

$$(p - p_0)/p_0 = \gamma M^2 k^{-1} (2\alpha)^{-1/2} r^{-1} (\alpha r - x + y_0) \quad (2-3)$$

where $k = (\gamma + 1) M^2 2^{-1/2} \alpha^{-3/2}$. p is the disturbed, and p_0 the free stream pressure. Notice that along a trace of constant r the pressure difference, $p - p_0$, decreases linearly with x from a positive value at the front shock

to an equal negative value at the rear shock wave. Midway between the shocks on the straight characteristic $x = \alpha r + y_0$, $p = p_0$. The pressure slope, $\gamma M^2(kr)^{-1}(2\alpha)^{-1/2}$, depends only on the flow constants and the distance from the axis, and not upon the shape of the body producing the disturbance.

2.3 Density Distribution in the N-wave

We now relate $p - p_0$ of Equation (2-3) to $\rho - \rho_0$ of Equation (2-1). Despite the seeming simplicity of this program, some care must be exercised to assure an approximation consistent with that of linear theory.

It can be shown^{10/} that the entropy may be considered constant across a

^{10/} M. A. Heaslet and H. Lomax, High Speed Aerodynamics and Jet Propulsion, (Princeton University Press, 1954) Vol. 9, Section D, 32, p 330

shock wave if third and higher order powers of the perturbation velocities are neglected. We neglect second and higher powers and may, therefore, assume that the flow behind the shock is isentropic. The adiabatic gas law applies, thus

$$\rho/\rho_0 = (p/p_0)^{1/\gamma}. \quad (2-4)$$

Expanding (2-4) in Taylor series around $p = p_0$,

$$(p/p_0)^{1/\gamma} = 1 + \frac{1}{\gamma} \left(\frac{p - p_0}{p_0} \right) + \frac{(1 - \gamma)}{2\gamma^2} \left(\frac{p - p_0}{p_0} \right)^2 + O \left[\left(\frac{p - p_0}{p_0} \right)^3 \right].$$

In Wh (66) Whitham finds that

$$\frac{p - p_0}{p_0} = O(u);$$

so to the linear approximation

$$\rho/\rho_0 = (p/p_0)^{1/\gamma} = 1 + \frac{1}{\gamma} \left(\frac{p - p_0}{p_0} \right)$$

and

$$\frac{\rho - \rho_0}{\rho_0} = \frac{1}{\gamma} \left(\frac{p - p_0}{p_0} \right). \quad (2-5)$$

If we substitute Equation (2-3) into Equation (2-5), we find that

$$\rho - \rho_0 = \rho_0 M^2 k^{-1} (2\alpha)^{-1/2} r^{-1} (\alpha r - x + y_0). \quad (2-6)$$

This is the density distribution in the N-wave region. Along a trace of constant r , its profile has the same characteristic shape as the pressure curve.

2.4 Fringe Shift in the N-wave

Combining Equations (2-6) and (2-1), we obtain

$$\delta(x, r) = \frac{\sqrt{2} K \rho_0 M^2}{\lambda k \alpha^{1/2}} \int_r^{r_N} \left(\frac{\alpha t - x + y_0}{t} \right) \frac{t dt}{(t^2 - r^2)^{1/2}}. \quad (2-7)$$

Here x is constant along the path of integration from r to r_N . Regrouping terms and using Pierce's Equations (133) and (126b) we find

$$\delta(x,r) = \frac{\sqrt{2} K_0 M^2 \alpha^{1/2}}{\lambda k} r \left\{ \left[\left(\frac{r_N}{r} \right)^2 - 1 \right]^{1/2} - \left(\frac{x - y_0}{\alpha r} \right) \ln \left[\frac{r_N}{r} + \left(\left(\frac{r_N}{r} \right)^2 - 1 \right)^{1/2} \right] \right\} \quad (2-8)$$

\underline{r}_N is related to x by means of the front shock equation

$$x = \alpha r_N + y_0 - A r_N^{1/4}. \quad (2-9)$$

Equations (2-8) and (2-9) predict the fringe shift in the N-wave.

2.5 Behavior of the Fringe Shift Expression

We examine the variation of $\delta(x,r)$ along a trace $r = \text{constant}$ as x increases from x_N to x_B . x_N and x_B lie on the front and rear shocks, respectively. \underline{x}_0 lies on the line $x - \alpha r = y_0$, halfway between x_N and x_B (See Figure 2)

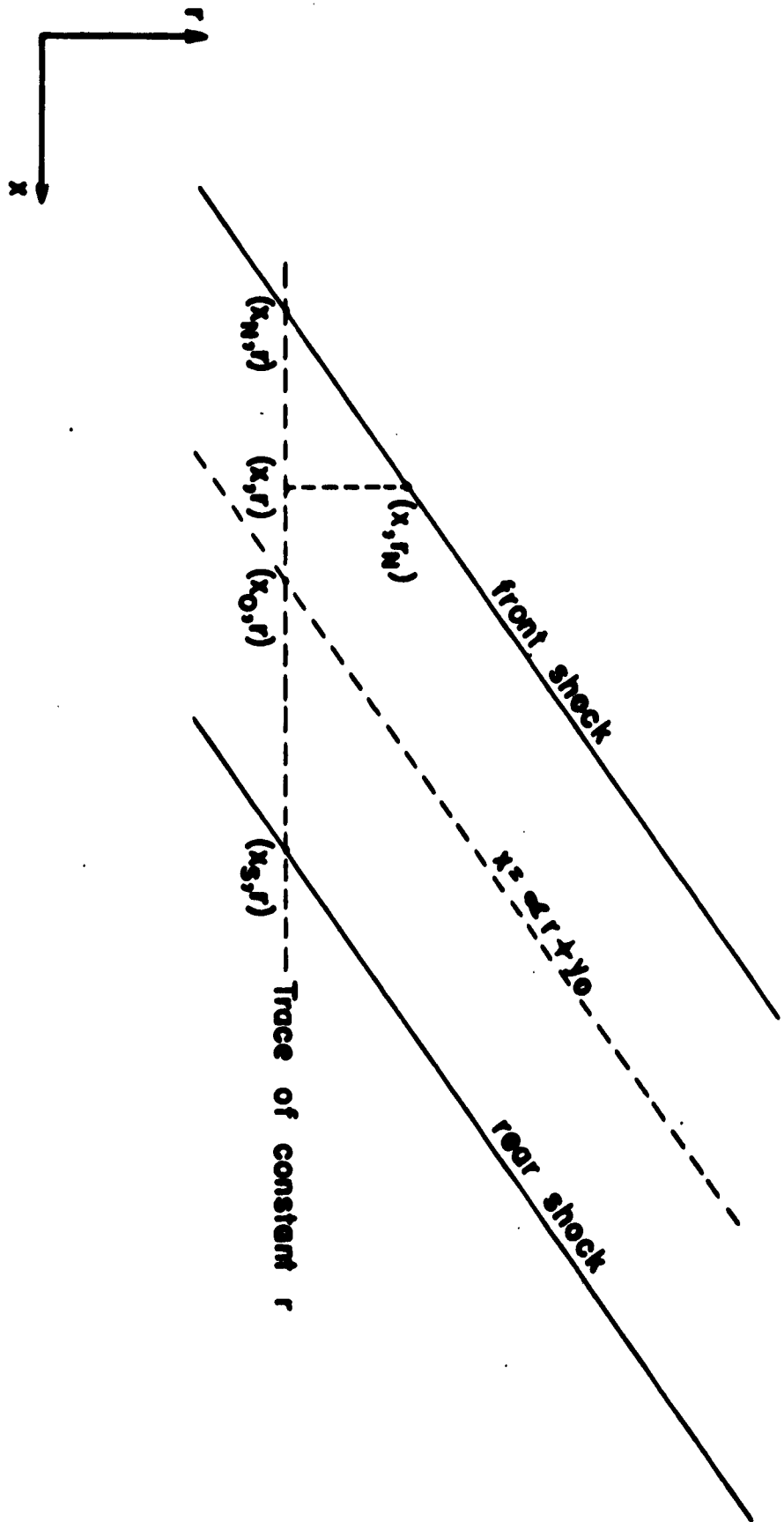


Figure 2. The region between the two shock waves.

Let $f(\xi) = (\xi^2 - 1)^{1/2}$, $g(\xi) = \ln \left[\xi + (\xi^2 - 1)^{1/2} \right]$ and $R = (x - y_0)/\alpha r$,

where $\xi = r_N/r$. For a particular flow the magnitude and sign of f is

determined from Equation (2-8) by the term in the curly brackets viz.

$$\{f - Rg\}.$$

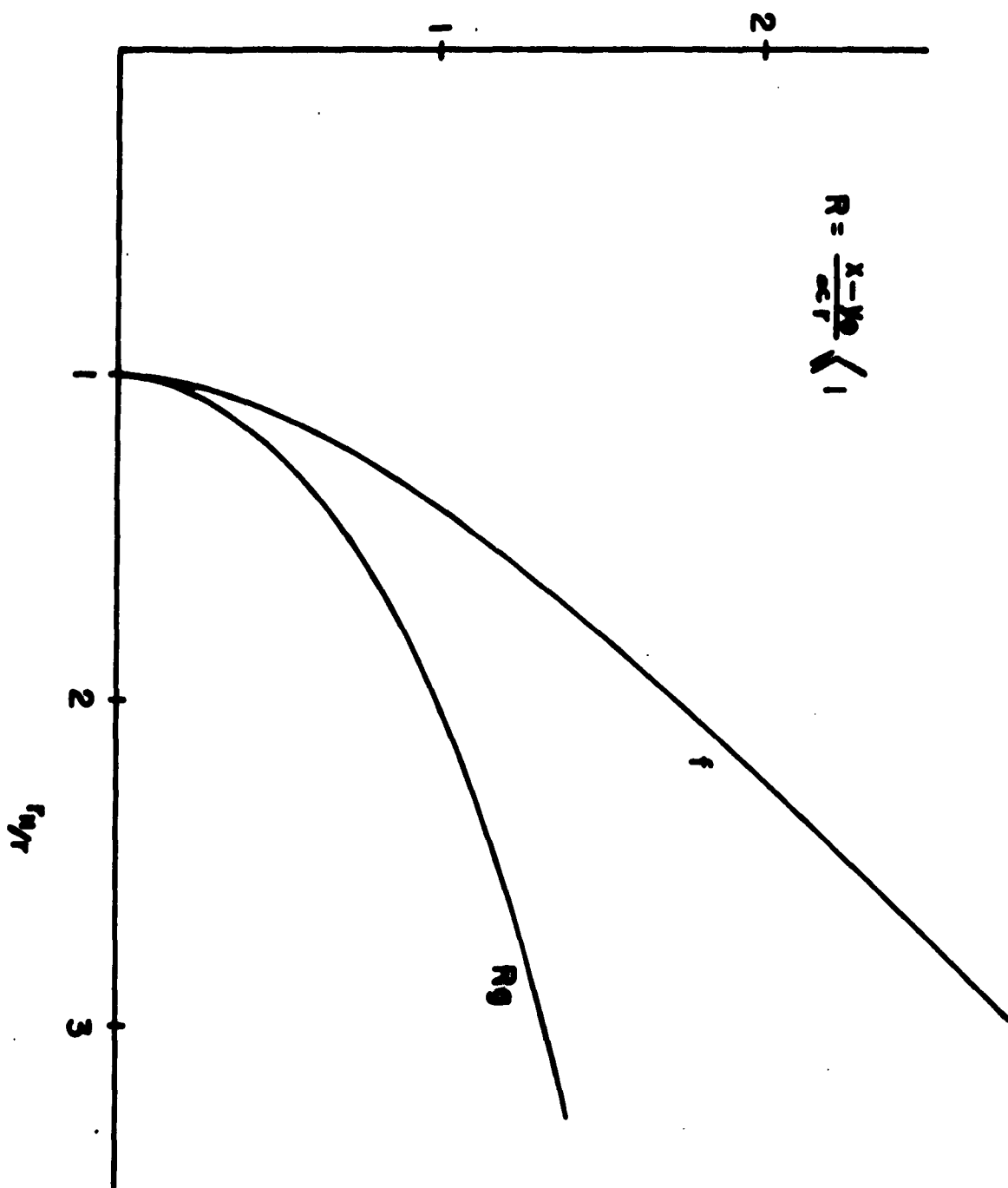
Examine R. By comparison with the equation of the straight characteristic

$$R \begin{cases} < 1 & \text{if } x < x_0 \\ = 1 & \text{if } x = x_0 \\ > 1 & \text{if } x > x_0 \end{cases}$$

Thus R increases monotonically with x from a value less than 1 at the front shock to a value greater than 1 at the rear shock. From the equation of the front shock wave

$$1 - (A/\alpha)r^{-3/4} \leq R \leq 1 + (A/\alpha)r^{-3/4}.$$

The variation of $f(\xi)$ and $Rg(\xi)$ with ξ is shown in Figure 3 for $R \leq 1$.

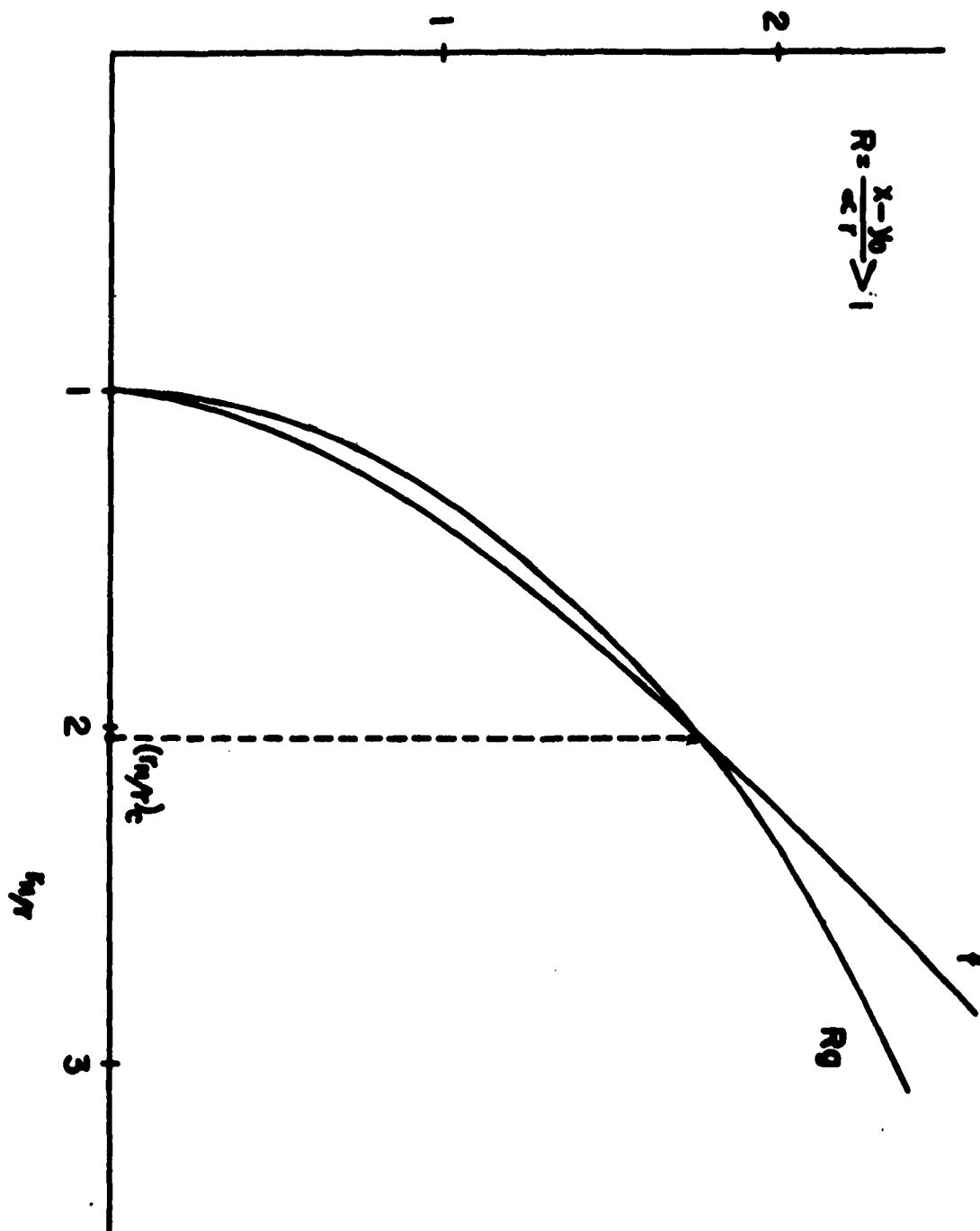
The Functions f and Rg Figure 3. Variation of the functions f and Rg when $R \leq 1$.

The curves have vertical tangents at $\xi = 1$ and intersect at no other point.

When $R > 1$, they are related as in Figure 4. In addition to their intersection and common vertical tangent at $\xi = 1$, they intersect at one point, say $\xi = \xi_0$. ξ_0 increases as R increases.

We can now examine the combination of functions $\{f - Rg\}$. As x increases, so does ξ , R , and ξ_0 (when $R > 1$).

When $x_H \leq x \leq x_0$, $R \leq 1$, so $f > Rg$. Therefore, δ is positive in the forward portion of the N-wave.

The Functions f and Rg Figure 4. Variation of the functions f and Rg when $R > 1$.

When $x_0 < x \leq x_g$, $R > 1$ and

$$r \begin{Bmatrix} > \\ = \\ < \end{Bmatrix} Rg \text{ if } \xi \begin{Bmatrix} > \\ = \\ < \end{Bmatrix} \xi_c.$$

When x is just greater than x_0 , $\xi > \xi_c$, so δ is positive. But it is possible that as x increases, ξ_c increases faster than ξ . If it does, then the conditions $\xi < \xi_c$ can occur and δ will pass through zero to negative values near the rear shock wave. The proof that $\frac{\partial}{\partial x}(\xi_c) > \frac{\partial}{\partial x}(\xi)$ is too complicated to be attempted here. We resort to calculation to establish the behavior of δ in the rear portion of the N-wave.

A calculation of δ vs. x from Equation (2-8), using representative values of A , y_0 and the flow constants, yields a curve that is similar in shape to the dashed line in Figure 6. Computations made at several values of r show that the curve decreases in amplitude as r increases. The zero of the δ curve occurs about 3/4 of the way between x_N and x_g , no matter what the value of r . This fact and the occurrence of the negative fringe shift will be clarified by a deeper analysis now being prepared for publication.

3. PRELIMINARY EXPERIMENTAL RESULTS

3.1 The Slender Cone-Cylinder

We select for this investigation a cylinder of .225-inch diameter with a conical tip of 20° included angle. This projectile is both stable in flight and slender enough to meet the requirements of slender body theory. A comparison of the results of Whitham's theory and the exact adiabatic theory of flow past a cone shows reasonably good agreement for included cone angles up to 20° .¹¹

3.2 Instrumentation

To obtain quantitative data the projectile is fired from a caliber .22 rifle approximately along the axis of an inclosed free flight range. The flow is observed through optical glass windows at the interferometer station of the range by a Mach-Zehnder interferometer with an 8" x 10" working field. For the experiments reported here an interferogram (Figure 5)^{*} is taken of the flow around the cone-cylinder at a Mach number of 2.25.

In order to record the disturbance as far from the axis as possible the gun is aimed to place the projectile near the edge of the picture. Fringes are adjusted to lie parallel to the trajectory.

Projectile velocity is measured between a pair of stations served by 0.1 - Mc chronograph counters triggered by impulses from photocells which respond to fluctuations in light screens through which the missile passes.

*The caption for this figure should read as follows: Interferogram of 20° included angle, cal. .225 cone-cylinder at $M = 2.25$, $p_o = 1$ atmos.



Figure 5

3.3 Measurement of the Interferogram

To interpret the interferogram we measure fringe shift δ along the path traced by a fringe between the shock waves. If r is the radial distance to the disturbed fringe at a certain point (x, r) and r_0 the distance to the same fringe in the undisturbed region in front of the shock, then $\delta = (r - r_0)/\Delta$, where Δ is the average distance between undisturbed fringes. The measurements have an estimated accuracy of $\pm .06$ of a fringe. Although fringe shift along a constant r trace is discussed in § 2.5, it is more convenient to measure fringe shift along a fringe curve. Because the fringe curve deviates from $r = \text{constant}$ by only a small percentage of r , the behavior of δ along the fringe is qualitatively much the same as that along the line $r = \text{constant}$.

3.4 Results

A comparison is given for $r_0 \sim 10$ diameters (Figure 6) between δ measured along the fringe curve and δ as it is predicted by Equation (2-8). The measured δ is about .2 of a fringe greater than the predicted δ at the positive

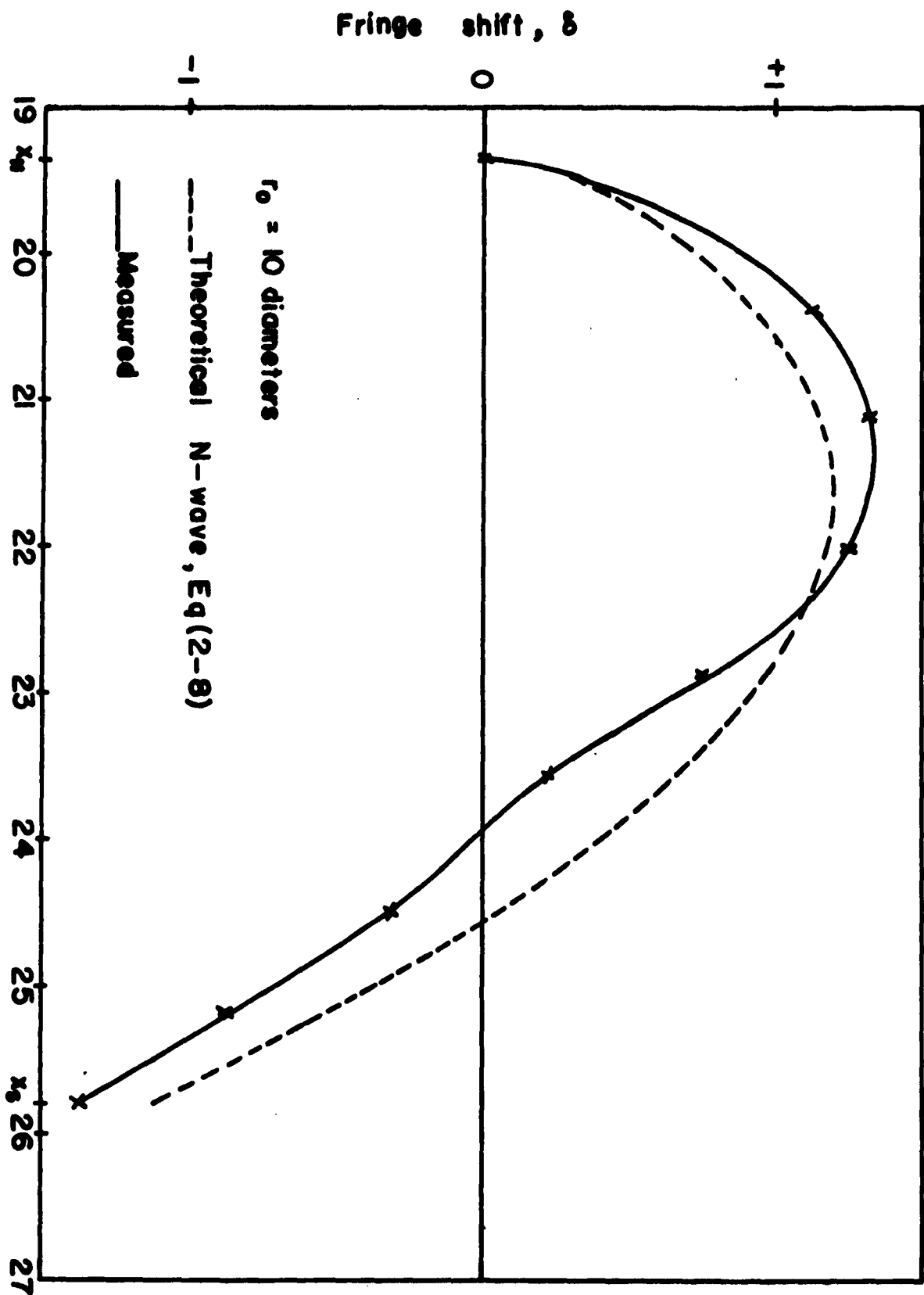
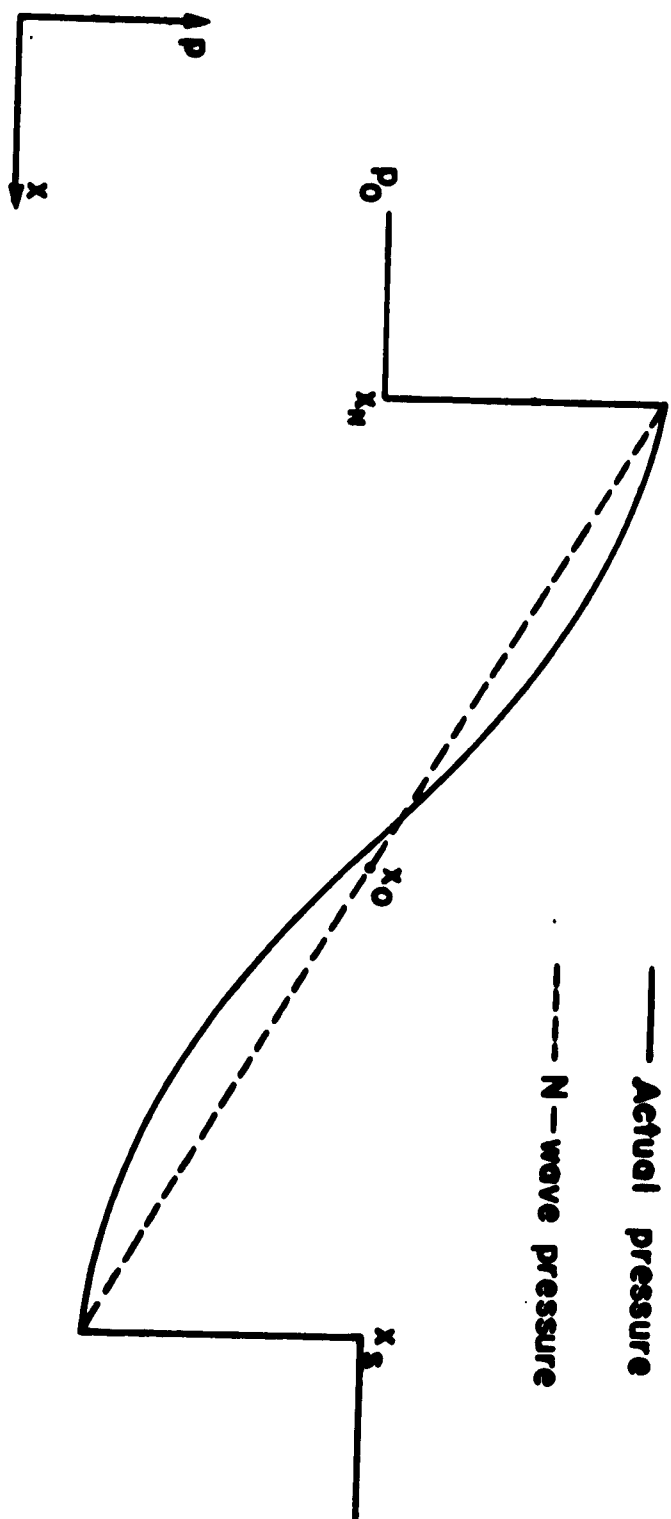


Figure 6. Comparison of measured fringe shift and predicted N-wave fringe shift.

Peak and .3 of a fringe lower than predicted at the rear shock; it becomes zero one half unit ahead of the predicted curve. These discrepancies give the impression that the actual pressure profile in this region is shaped as in Figure 7, the curve lying above the N-wave profile near the front shock and below at the rear shock. A pressure profile taken along a trace only a few diameters from the body and passing through the conical region would show the pressure rising for a short distance behind the front shock and then falling rapidly below free stream in the expansion region coming off the shoulder of the projectile. As this profile degenerates with increasing r to the final linear shape of the N-wave, it passes through the intermediate shape of Figure 10. Evidently we must make observations still farther away from the projectile axis to measure fringe shift in the fully developed N-wave.

Figure 2. Pressure profile between the shock waves.



3.5 Future Experiments

Experiments are under way to launch a very small diameter projectile (on the order of $1/16$ inch) in order that the disturbance can be measured interferometrically in regions at least 50 diameters from the axis. Sub-caliber (less than .225 inch in this case) projectiles are made to fit the rifle bore by encasement in a plastic holder, called a sabot, which separates from the projectile after leaving the muzzle of the rifle. Difficulties arise because during separation the sabot imparts a certain amount of angular momentum and initial yaw to the projectile, and causes a body of borderline stability (such as the 20° cone-cylinder) to yaw violently or tumble in flight. This problem makes it desirable to use a more stable projectile than the cone-cylinder. A sphere is a practical choice. It is stable, easily sabotaged, and can be readily obtained in almost any size.

From a theoretical standpoint it seems possible to use the disturbance from a sphere to verify the predicted N-wave fringe shift. Whitham, in an earlier paper^{11/}, shows that the pressure profile between the shocks far

^{11/} G. B. Whitham, Proc. Roy. Soc. A201, 89 (1950)

enough away from any supersonic body is linear and that the equation of the front shock is similar in form to Equation (2-2). We infer, as Lighthill has done^{12/}, that Equations (2-2) and (2-3) from Whitham's slender body theory

^{12/} M. J. Lighthill, High Speed Aerodynamics and Jet Propulsion, (Princeton University Press, 1954) Vol. 9, Section E, 6, 429

apply to the disturbance sufficiently far from the axis of any supersonic projectile. We will attempt to substantiate this inference in proposed experiments with spheres. A future paper will give a complete account of the the results of these investigations.

ENGRAVING PRESSURES FOR ROTATING BANDS

An Estimate of Contact Pressure for Continued Normal Engraving of Rectangular Bands

by
E. W. Ross, Jr.
Watertown Arsenal

SUMMARY

The principal new result of this report concerns the normal engraving of a narrow inset band of rectangular cross-section by a flat, rigid die. An estimate has been found for the average normal pressure required to continue the engraving process in the early stages. This estimate depends on the initial dimensions of die and band and the yield strength of the band material.

INTRODUCTION

In this report we shall consider the behavior of a rotating band under the engraving action of the rifling in the forcing-cone region of a gun tube. In order to gain insight into the fundamental forces at work during this engraving action, we idealize the problem in the following ways:

- (a) The band is imagined as unwrapped and laid out flat.
- (b) The band is taken as a solid rectangular block, of infinite length in what would be the circumferential direction of the shell.
- (c) Since the forcing cone angle is small, we assume that the rigid lands of the rifling move vertically downward onto the band.
- (d) The lands and grooves of the rifling occur periodically in the circumferential direction; consequently, it is only necessary to consider one band and a half groove width on either side of it as the fundamental zone.

Thus we consider the geometry shown in Figure (1). A solid band of ductile material is set into a surrounding rigid encasement, and a rigid, rectangular die is pushed down into it by some outside agency. We want to find out how much pressure must be exerted in order to push the die any desired distance into the band. The coordinate system (fixed in space) is shown in Figure (1a). (Figure near end of this manuscript.)

We shall assume that the band material behaves as an ideally plastic solid (no work-hardening), and that the loading takes place slowly enough so that inertia effects may be neglected. Further, the material is assumed to obey Tresca's yield criterion and flow rule, and, finally, we suppose that there are no friction forces between the land and band material.

In a previous report, [4]^{*}, we used the limit design theorems of ideal plasticity to find an upper bound on the pressure required to initiate normal engraving of a band of any width and any clearance above the surrounding shell body. In general, this upper bound depended on the band width and clearance as shown in Figure (2). Since publication of [4], a slight improvement has been made in the upper bound for wider bands, and this is incorporated into Figure (2). In the present report we are concerned with estimating the pressure required to keep the engraving process going at any stage of indentation, i.e. not only the initial engraving pressure, but also the pressure at any later time is sought.

^{*}See Bibliography.

In the next section we state the limit design theorems of ideal plasticity, and the third section gives the principal new result of this report, namely the derivation of an estimate of the normal pressure needed to continue indentation of narrow bands in the early stages. That is, it gives a complete prediction of the engraving pressure during the early history of the engraving process. Section IV gives a short discussion of the results and the method used to obtain them.

THE LIMIT DESIGN THEOREMS

We state these theorems in the somewhat restricted form that they take when applied to inset bands of an ideally plastic material obeying Tresca's yield condition and flow rule and loaded normally by a flat die which exerts no friction force on the band material. More general statements and proofs of these theorems may be found in [1] and [2] and some additional remarks are available in [3].

First we must make some definitions. Collapse is defined as the state in which, for the first time during the loading, the die can appreciably indent the band under constant normal pressure, provided the geometrical changes in the band are ignored. A kinematically admissible state is defined as a state of velocity which satisfies 1) all boundary conditions on velocities, 2) the incompressibility condition and 3) the condition that the rate of work of the external applied load equals or exceeds the internal rate of energy dissipation. If, (as in the present report) the assumed velocity state consists of zones of rigid body motion separated by surfaces of tangential velocity discontinuity, the internal dissipation rate is $\int_{S_D} K \Delta V dS_D$, where K is the yield stress in pure shear, ΔV is the magnitude of the vector velocity change across a surface of discontinuity and the integral is taken over all discontinuity surfaces. A statically admissible state is defined as a state of stress, which satisfies 1) the equilibrium conditions, 2) the yield condition and 3) the boundary conditions on stresses.

The two limit design theorems are as follows:

(I) Collapse will not occur until the largest values of the surface loads have been reached for which it is possible to find a statically admissible stress state.

(II) Collapse will occur under the smallest value of the surface loads for which it is possible to find a kinematically admissible velocity state.

Thus, the load corresponding to any statically admissible stress state is a lower bound on the true collapse load, and the load corresponding to any kinematically admissible velocity state is an upper bound on the true collapse load.

We point out in passing that these theorems only apply to problems having certain general types of boundary conditions, and that these conditions are satisfied by the band both in its initial configuration and in the assumed deformed configurations. As stated these theorems consider collapse to occur at constant load and neglect the change in boundary shape as time goes on; that is, they give bounds on the load at the first instant of uncontained plastic deformation.

THE PRESSURE HISTORY IN NORMAL ENGRAVING OF NARROW BANDS

In this section we restrict our attention to bands that are narrow enough so that during engraving the displaced material moves out the ends of the band and does not flow up around the sides of the die, i.e., the material always and everywhere deforms without motion in the x-direction, see Figure (1a). We may also add that if some outside agency prevents the material from flowing up around the sides of the die, the displaced material will all flow out the ends of even a wide band. This is not a far-fetched situation in practice, for most guns in current use have

(III.1) diameter of groove bottoms \geq band diameter.

That is, there is no clearance at all between the groove bottoms and the top of the band. In such cases almost all the flow during engraving will be longitudinal; the only transverse flow will occur in the later stages of engraving and will involve the metal which has at an earlier stage flowed longitudinally into the cannellures.

In estimating the pressure necessary to continue engraving at any stage, we shall use the second limit design theorem at successive instants of engraving, just as we used it in [4] for the initial instant of engraving. We recall again that this theorem gives us an upper bound on the load that produces collapse, collapse being defined as a state in which for the first time during the loading program uncontained plastic flow can take place under constant loads if the simultaneous geometrical changes are ignored, see, for example, [2]. Suppose we know the correct deformed geometry of the band at any instant (say, t); then we choose a kinematically admissible state of deformation, and this gives us an upper bound on the collapse load for that instant. If the kinematically admissible velocity state is a good approximation to the true mode of deformation, the upper bound will be a good estimate of the collapse load and the accompanying change in shape of the band will be accurately given to us for a brief ensuing interval of time by the chosen velocity state. This leads us to a new deformed geometry at time $t + \Delta t$, and we may imagine the whole process, choosing a kinematically admissible state, finding the new estimated collapse load and mode of deformation to be repeated at time $t + \Delta t$. If this can be done starting from the initial moment of collapse and kept up for a number of intervals of length Δt , the pressure

history curve will be approximated by a discontinuous set of horizontal lines. If the analysis can be carried out letting $\Delta t \rightarrow 0$, we shall get in the limit a continuous approximation to the pressure-history curve; if, fortuitously, we should happen to guess the true velocity state at each stage, we would get the true pressure history curve.

We shall use the idea sketched above to get an approximate pressure history curve. In deriving our estimates, we shall use at every stage velocity states like those used for narrow bands in [4].

Call L_1 and H_1 , respectively, the band's initial half-width and clearance; similarly L and H are the half-width and clearance at any later stage. During engraving the value of H decreases from H_1 , and the value of L increases from L_1 . We define $G = \frac{L_1}{a}$ and $C = \frac{H_1}{a}$. If for any G , C is sufficiently small the state of deformation will at any later time be chosen as shown in Figure (3). For larger values of G , however, the state of deformation will be chosen as shown in Figure (4), for a short time after the beginning, but, as the die descends further, the overhanging lip will eventually strike the surrounding shell body see Figure (5), and the state of deformation becomes as shown in Figure (3) again. It is then clear that two types of deformation may be distinguished depending on whether the deformed metal comes into contact with the shell body or not. When it does not, as illustrated in Figure (4), we shall call it an optimum flow, and when it does, as illustrated in Figure (3), we shall speak of constrained flow. We shall call $\xi = \frac{H}{H_1}$ and the time-like variable which measures the progress of events will be chosen as the penetration, $\eta = 1 - \xi$.

We first deal with the case where the flow is initially constrained. The mode of flow at any stage is shown in Figure (3). Internal dissipation, calculated for a half-land width and half-band width, takes place on the bottom and side of the zone of flow.

$$\text{Bottom:} \quad \Delta V = V_0 \csc \alpha$$

$$\text{Area of the Bottom} = a L \sec \alpha$$

$$\text{Dissipation} = \frac{K a L V_0}{\sin \alpha \cos \alpha}$$

$$\text{Side:} \quad \Delta V = V_0 \csc \alpha$$

$$\text{Area of the side} = \frac{1}{2} L_1^2 \tan \alpha$$

$$\text{Dissipation} = \frac{K V_0 L_1^2}{2 \cos \alpha}$$

$$\text{External work rate} = p V_0 a L$$

Therefore the pressure required for continued indentation satisfies

$$(III.2) \quad \frac{p}{k} \leq \frac{1}{\cos a} \left[\frac{1}{\sin a} + \frac{1}{2} \frac{L}{a} \frac{L_1}{L} \right]$$

Incompressibility requires that

$$(III.3) \quad HL = H_1 L_1,$$

and the angle a is given by

$$(III.4) \quad a = \tan^{-1} \left(\frac{H}{L} \right).$$

Combining these results gives (after some algebra)

$$(III.5) \quad \frac{p}{k} \leq \frac{G}{C\xi^2} \frac{1}{\xi^2} + \frac{C}{G} \xi^2 + \frac{G\xi^4}{2} \sqrt{1 + \frac{C}{G^2} \xi^4}$$

These results are plotted for $G = 1, 2$ and 3 in Figures (6), (7) and (8) in the form of curves of P against $\eta = 1 - \xi$ with G as parameter. It is almost obvious that if the flow is constrained initially, it can never become optimum under the assumed modes of deformation, but a simple proof may be desirable and will be given shortly.

We now deal with the somewhat more complex case where the flow is optimum to begin with. In this case we assume the state of deformation looks as in Figure (4). The dissipation is as follows:

$$\text{Side zone dissipation} = kV_0 \csc a \cdot \frac{L_1^2}{2} \tan a$$

$$\text{Bottom zone dissipation} = kV_0 \csc a \cdot aL_1 \sec a$$

$$\text{External work rate} = pV_0 aL$$

The pressure required to continue indentation therefore satisfies

$$(III.6) \quad \frac{p}{k} \leq \left(\frac{L_1}{L} \right) \frac{1}{\cos a} \left[\frac{G}{2} + \frac{1}{\sin a} \right]$$

The value of α is found by setting the partial derivative of the right-hand side equal to zero, giving

$$(III.7) \quad \frac{G}{2} \sin^3 \alpha + 2 \sin^2 \alpha - 1 = 0,$$

the same result as was obtained for the initial indentation problem in [4].

We call the solution of (III.7) α_0 . The value of L during the optimum stage of indentation is given at any time by

$$(III.8) \quad L = L_1 + (H_1 - H) \cot \alpha_0.$$

This type of deformation continues until the overhanging lip strikes the rigid shell body, i.e. until

$$(III.9) \quad L_1 \tan \alpha_0 = H$$

or

$$(III.10) \quad \xi = \frac{G \tan \alpha_0}{C} = \xi_0$$

From this point on the flow is constrained. The value of α jumps to the value given by

$$(III.11) \quad \alpha_c = \tan^{-1} \left(\frac{H}{L} \right)$$

or, (using (III.8) and (III.10)),

$$(III.12) \quad \alpha_c = \tan^{-1} (\xi_0 \tan \alpha_0).$$

From this point on the pressure obeys equation (III.5), and L is given by (III.3).

The complete pressure history estimate is shown in Figures (6), (7) and (8) for $G = 1, 2$ and 3 respectively. It will be noted that a discontinuity in pressure occurs for all flows that are optimum at the start, the magnitude and time of the jump depending on the original geometry of the band. Analytically, the time of the jump is given by (III.9) where α_0 is the solution of (III.7); the magnitude of the jump is given by

$$(III.13) \quad \frac{\Delta p}{k} = \frac{C}{G} \cot^2 \alpha_0 + \frac{G}{C} \tan^2 \alpha_0 + \frac{1}{2} \frac{G^2}{C} \tan \alpha_0 \sqrt{1 + \frac{G^2}{C^2} \tan^4 \alpha_0} - \frac{G \sin \alpha_0}{C \cos^3 \alpha_0} \left[\frac{G}{2} + \frac{1}{\sin \alpha_0} \right]$$

In order to facilitate the calculation of the total load on the land, given by

$$(III.14) \quad Q = 4paL,$$

we have included on Figures (6), (7) and (8) curves of $\frac{L}{a}$ as a function of

η . When the flow is optimum, we have (see III.5)).

$$(III.15) \quad \frac{L}{a} = G + c\eta \cot \alpha_0;$$

we see that $\frac{L}{a}$ varies linearly with η . When the flow is constrained, we have (see III.3)).

$$(III.16) \quad \frac{L}{a} = \frac{G}{\xi},$$

and the variation of (L/a) does not depend on G . For given G and C values, the curve for constrained flow of course intersects the optimum flow line at the point of pressure discontinuity (provided a discontinuity occurs).

We now give a simple proof that if the flow is constrained initially, it can never become optimum at a later time under the assumed modes of deformation.

We rewrite (III.2) as follows:

$$(III.17) \quad \frac{p}{k} \leq \frac{1}{\cos \alpha} \left[\frac{1}{\sin \alpha} + \frac{G\xi}{2} \right]$$

The value of α which minimizes this (we call it α_0) satisfies (compare (III.6) and (III.7)).

$$(III.18) \quad \frac{G\xi}{2} \sin^3 \alpha_0 + 2 \sin^2 \alpha_0 - 1 = 0$$

It is clear that α_0 depends on ξ , and that for $\xi < 1$ we have

$$(III.19) \quad \alpha_0(\xi) > \alpha_0(1)$$

Now if the flow is initially constrained,

$$(III.20) \quad \tan \alpha_0(1) > \frac{H_1}{L_1}$$

But for $\xi < 1$, $H(\xi) < H_1$ and $L(\xi) > L_1$. Combining this with (III.19)

and (III.20) we get that for $\xi < 1$

$$(III.21) \quad \tan \alpha_0(\xi) > \tan \alpha_0(1) > \frac{H_1}{L_1} > \frac{H(\xi)}{L(\xi)}$$

The first and last expressions in this continued inequality give us the statement that the flow cannot become optimum for $\xi < 1$, i.e. for $\eta > 0$. This completes the proof.

DISCUSSION

We first make several comments on the results obtained.

(i) For optimum flow, although the estimated indentation pressure decreases during penetration, the total load on the land stays constant, as is apparent from (III.6).

(ii) Generally speaking, increasing G causes the whole curve of pressure history to be raised and increasing C causes the curve to be lowered.

(iii) For the cases where optimum flow occurs initially, the qualitative behavior of the pressure jump is as follows: increasing G decreases the magnitude of the jump and makes it occur earlier in the process, and decreasing C has the same effect.

(iv) We want to re-emphasize that all these results depend first of all on the assumption of no flow in the X -direction. Naturally for sufficiently wide bands and for small clearances this condition will be violated, and we would not expect very good results in these cases. We have carried out calculations for some of these cases, however, because it is of some interest to see how much error is introduced, and because the results may be useful for the case (mentioned previously) where external constraint prevents flow in the X -direction.

It still remains to clarify a point concerning the theory underlying this method of finding the pressure history. The point is that the estimate of the pressure history given here is not necessarily an upper bound on the actual pressure at any stage of indentation except the first instant. The reason is, of course, that at no instant after the first can we be sure that we have the correct geometry. I.e. at each instant we find an upper bound on the pressure necessary to continue indentation from the assumed geometry; there is no positive assurance, however, that the assumed geometry is sufficiently close to the actual geometry so that the pressure found is an upper bound for deformation from the actual geometry except at the initial instant.

Therefore it is desirable to view these results as follows: if we make good estimates of the mode of deformation at each instant, the estimated pressure will be close to the true pressure at any stage although we no longer can say that it is an upper bound. Some unpublished experimental work on normal engraving done at Watertown Arsenal by Mr. E. M. Hegge indicates that the velocity state used in deriving the results of this report is reasonably accurate. We present these results at this time, therefore, as an approximation to the true pressure history for narrow bands.

We may note in passing that Onat and Haythornthwaite [5] have recently (and quite independently) used a method, intuitively identical with the one used here, on the problem of finding load-carrying capacities of circular thin plates at large deflections.

Finally we wish to call attention to some normal engraving experiments being conducted at Watertown Arsenal Laboratory. The results of these experiments should permit a much more sensible assessment of the present results than is now possible.

BIBLIOGRAPHY

- [1] W. Prager and P. A. Hodge, The Theory of Perfectly Plastic Solids, New York, John Wiley & Sons, 1951.
- [2] D. C. Drucker, W. Prager and H. J. Greenberg, Extended Limit Design Theorems for Continuous Media, Quarterly of App. Math. 9, 1952 pp. 381-389.
- [3] R. T. Shield and D. C. Drucker, The Application of Limit Analysis to Punch Indentation Problems, Journal of App. Mech. 20, No. 4, 1953.
- [4] E. W. Ross, Theoretical Investigation of Indentation Pressures on Rotating Bands, WAL Rpt. No. 760/525, 1954.
- [5] E. T. Onat and E. M. Haythornthwaite, The Load Carrying Capacity of Circular Plates at Large Deflection, Brown University Report No. OOR-3172/4 to the Office of Ordnance Research, December, 1954.

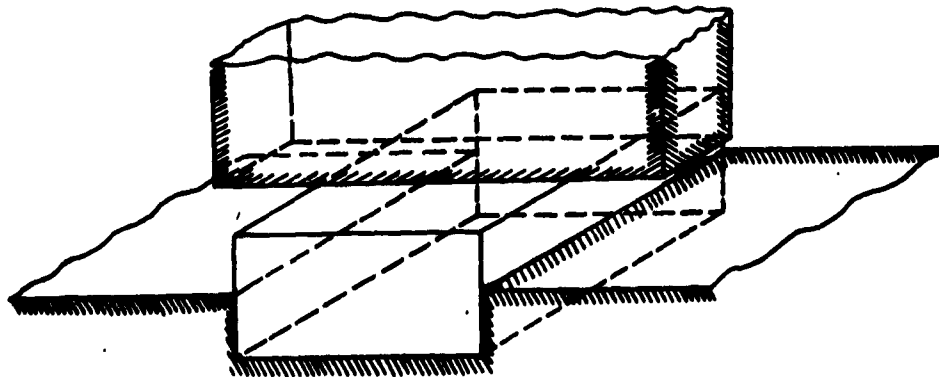


FIGURE 1 : IDEALIZATION OF SOLID ROTATING BAND AND RIFLING.

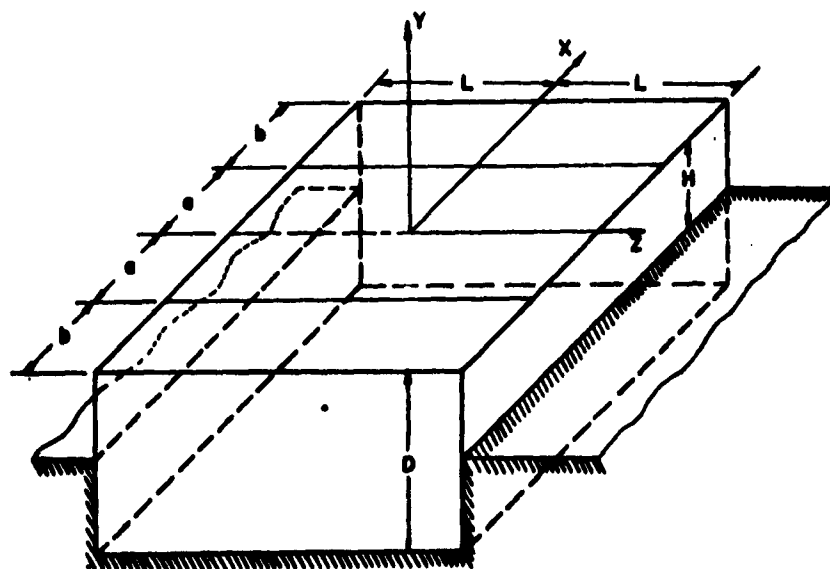


FIGURE 1a : COORDINATE SYSTEM, REFERRED TO THE SHELL,
(Z) IS IN THE LONGITUDINAL DIRECTION, (Y) IS IN THE
RADIAL DIRECTION AND (X) IS IN THE CIRCUMFERENTIAL DIRECTION.

WATERTOWN ARSENAL LABORATORY

Wta. 69-13,239

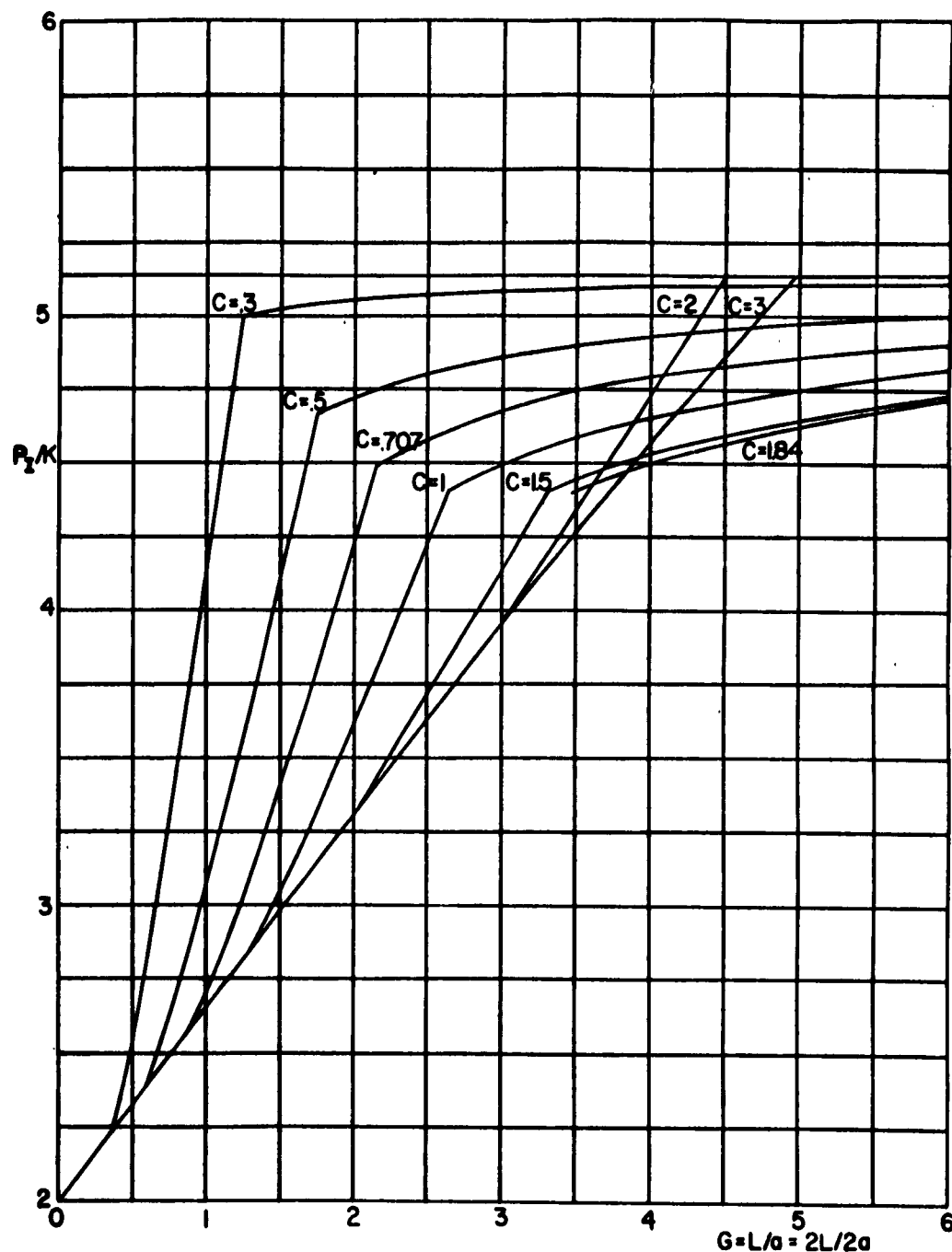


FIGURE 2 : UPPER BOUND ON INITIAL INDENTATION PRESSURE,
 P FOR $D \gg .707a$. H = CLEARANCE, $2L$ = BAND WIDTH,
 $2a$ = LAND WIDTH, $C = H/a$, D = BAND DEPTH.

WATERTOWN ARSENAL LABORATORY

Wtn. 639-13,732

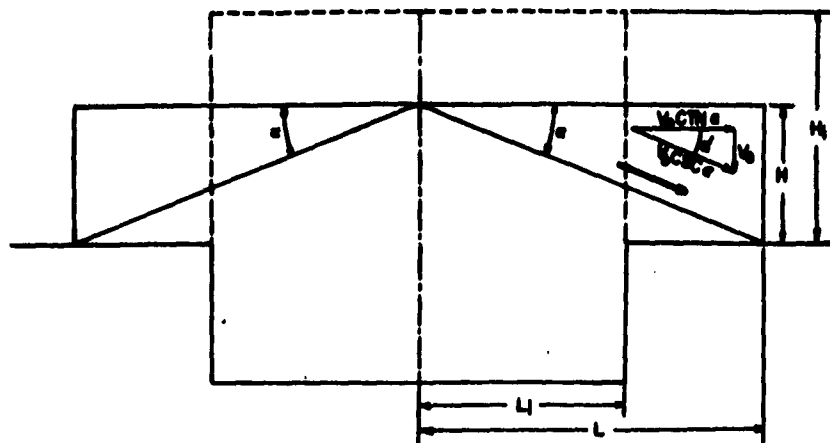


FIGURE 3 : CROSS-SECTION UNDER THE DIE OF THE DEFORMED BAND, SHOWING ASSUMED VELOCITY FIELD FOR CONSTRAINED FLOW. DOTTED LINES SHOW ORIGINAL CROSS-SECTION.

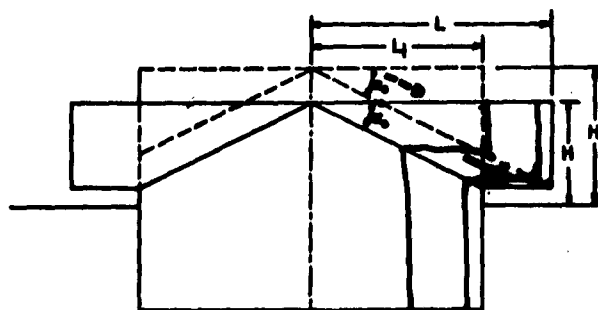


FIGURE 4 : CROSS-SECTION UNDER THE DIE OF THE BAND, SHOWING (SOLID LINES) ASSUMED VELOCITY FIELD AND DEFORMED BAND SHAPE AND (DOTTED LINES) ORIGINAL CROSS-SECTION.

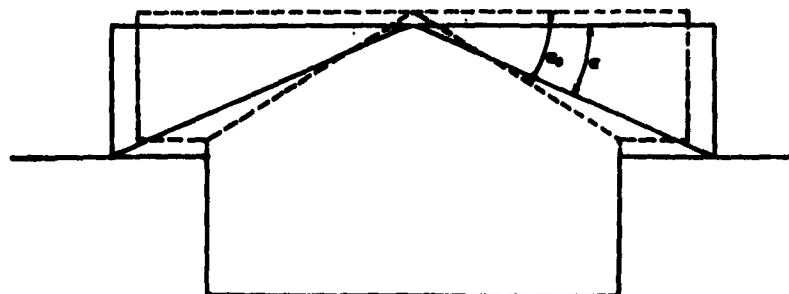


FIGURE 5 : CROSS-SECTION OF BAND UNDER DIE JUST BEFORE (DOTTED) AND JUST AFTER (SOLID) OPTIMUM FLOW BECOMES CONSTRAINED FLOW,
WATERTOWN ARSENAL LABORATORY

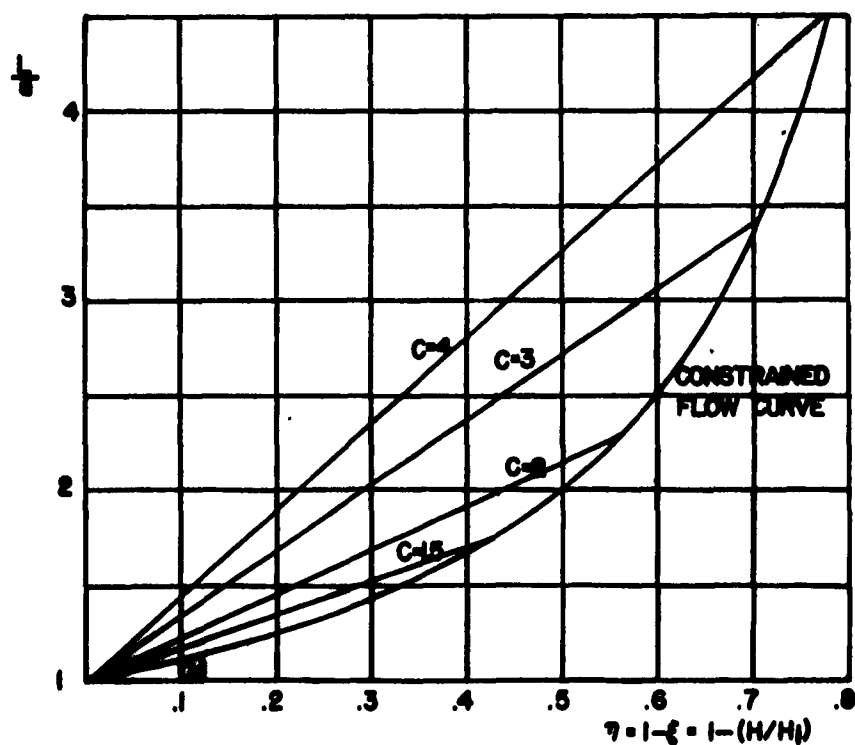
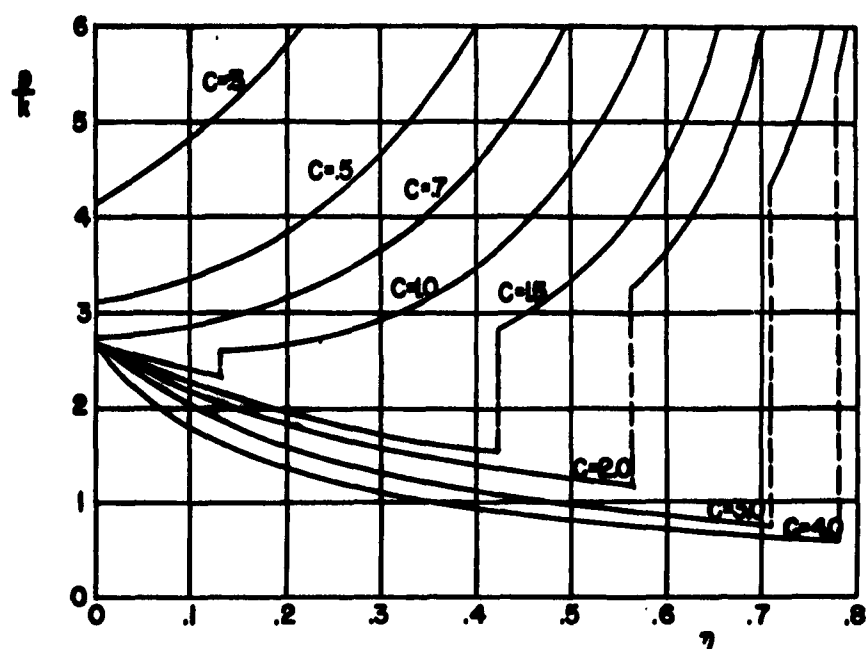


FIGURE 6 : VARIATION WITH PENETRATION (η) OF DIE PRESSURE (p) AND MAXIMUM HALF-WIDTH OF BAND (L) FOR $G=1$.
WATERTOWN ARSENAL LABORATORY

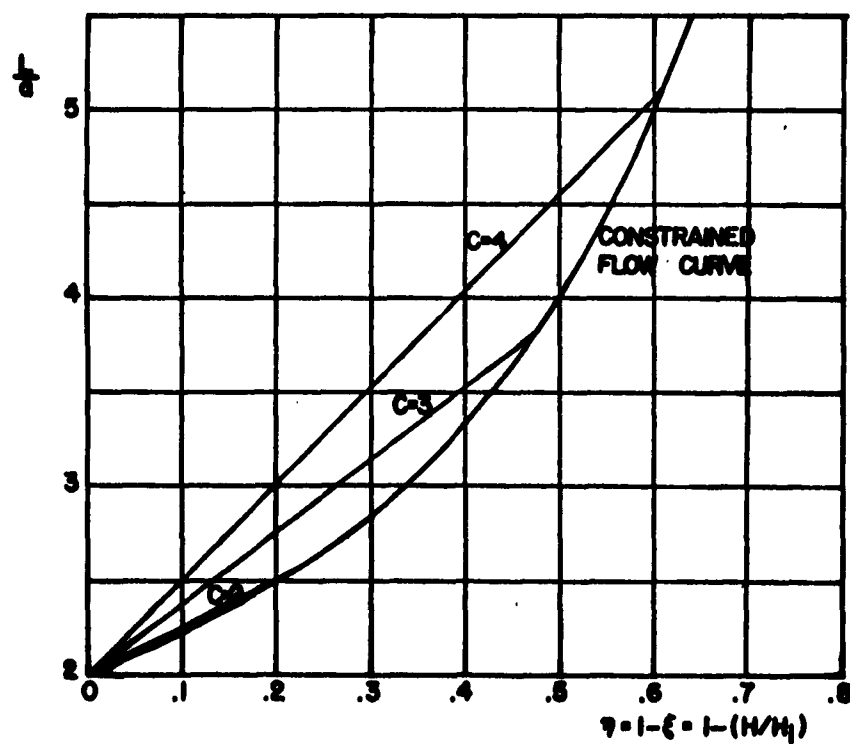
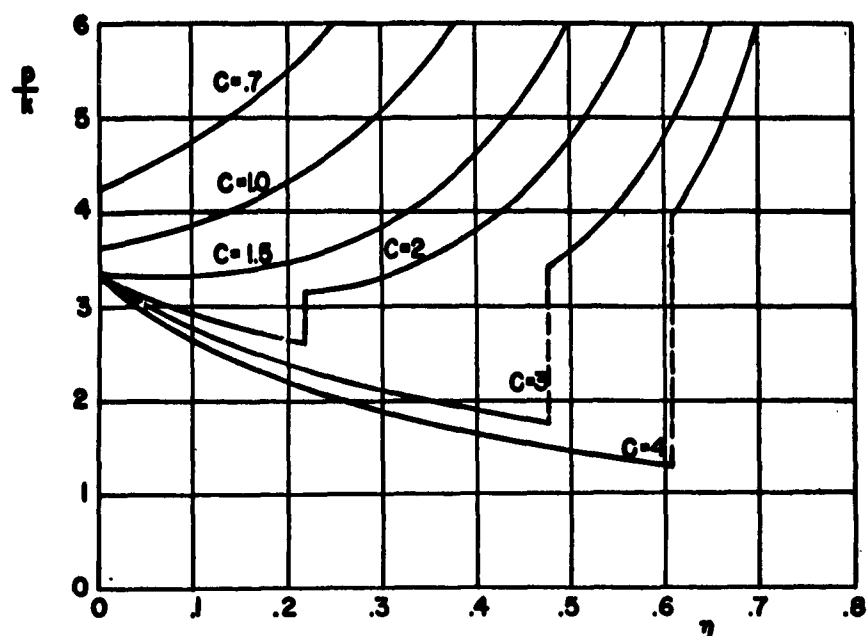


FIGURE 7 : VARIATION WITH PENETRATION (η) OF DIE PRESSURE (p) AND MAXIMUM HALF-WIDTH OF BAND (L) FOR $G=2$.
WATERTOWN ARSENAL LABORATORY

Wtn. 639-13,734

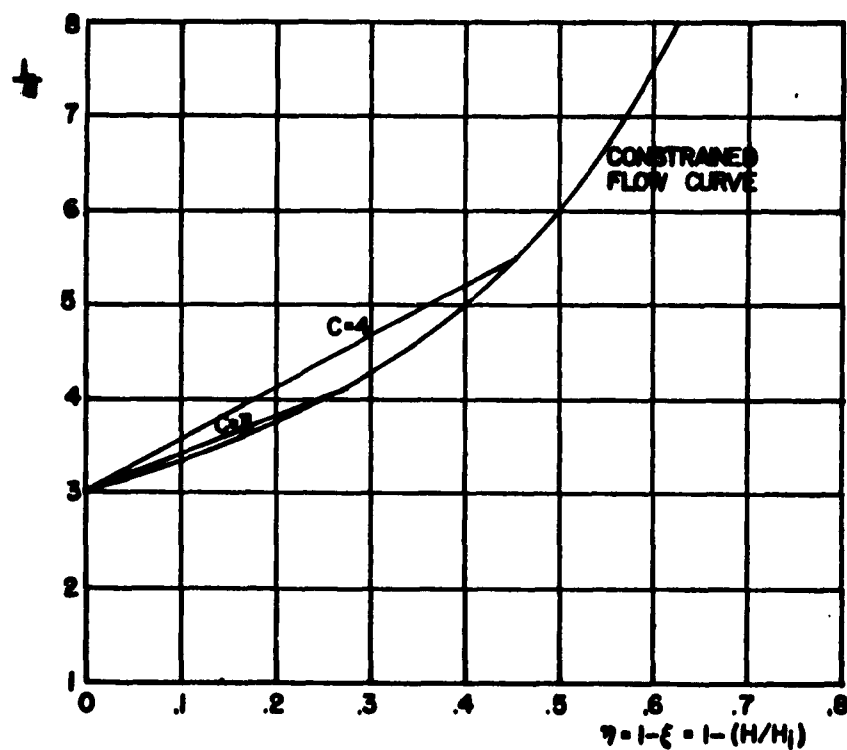
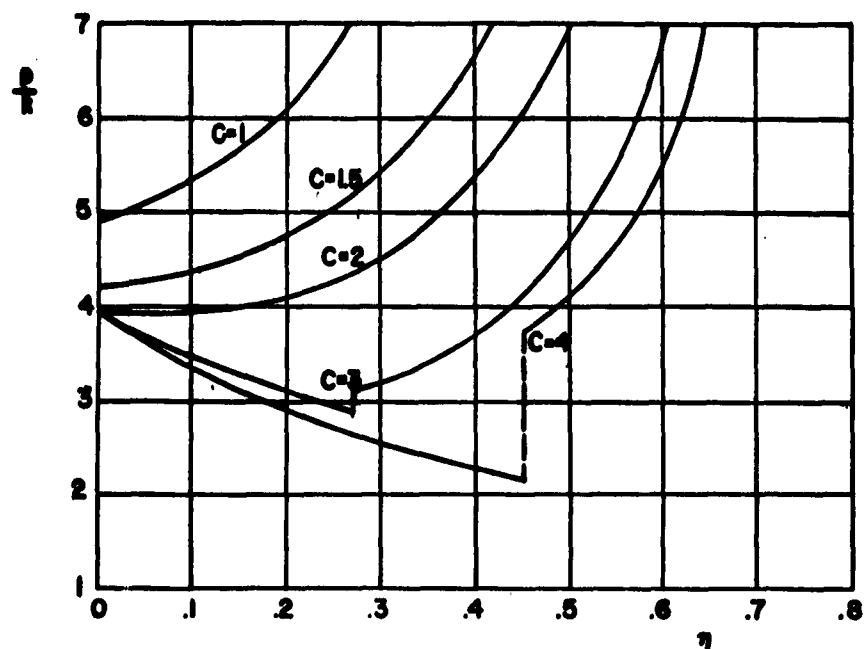


FIGURE 8 : VARIATION WITH PENETRATION (η) OF DIE PRESSURE (p) AND MAXIMUM HALF-WIDTH OF BAND (L) FOR $G=3$.
WATERTOWN ARSENAL LABORATORY

Wm. 409-23,729

ANALOG COMPUTER SIMULATION OF AUTOMATIC WEAPONS

by
E. H. Jakubowski
Springfield Armory

INTRODUCTION. An electronic analog computer is essentially a device used to solve differential equations. The differential equations may be either linear or non-linear.

The computer consists of a collection of circuits and circuit elements, such as amplifiers, relays, passive electric elements, and control circuits, which are capable of being arranged so that the circuit voltages follow a particular differential equation. The computer then becomes an electrical "model" of the mechanical system being studied.

The analog computer is used as a design tool. The process of supplying information to the computer consists of setting potentiometers and other circuit elements, and arranging special function generators. These settings and function generators correspond to coefficients and functions in the equations which describe the system to be studied. The output information, or solution provided by the computer is usually in the form of paper-chart records. In the study of an automatic weapon, displacement, velocity and acceleration of various components of the system are recorded as functions of time.

The heart of an analog computer is a high gain d.c. amplifier, generally referred to as an operational amplifier. When an operational amplifier is used with appropriate combinations of input and feedback impedances, certain mathematical relationships may be obtained.

Figure 1* shows the manner in which an operational amplifier is used to perform a general mathematical operation. When the drift voltage " e_d " and grid current " i_g " are taken into consideration, the application of Kirchoff's Laws

*Figures have been placed at the end of the manuscript.

will yield the general equation for the output voltage " e_o " as a function of the input voltage, drift voltage, and grid current. But as

$$i_g < 5 \times 10^{-11} \text{ amps.}$$

$$e_d < 500 \times 10^{-6} \text{ volts (with stabilization)}$$

$$\text{and } A > 150,000$$

the general equation may be simplified such that

$$e_o = - Z_f / Z_i e_i \quad \text{where } Z_f = \text{feedback impedance}$$

$$Z_i = \text{input impedance}$$

Figure 2 shows the application of this equation. The upper diagram shows the manner in which sign changing and multiplication by a constant may be achieved, while the lower diagram shows the use of an operational amplifier to perform the operations of addition or subtraction.

The upper diagram of Figure 3 shows the manner in which an operational amplifier is used as an integrator. It will be noted that in the integrator there exists a constant " K ". This " K " is equivalent to the initial charge on the capacitor and is analogous to any initial condition which may appear in the problem under consideration.

The lower diagram shows the use of the operational amplifier to perform the operation of differentiation.

WEAPON OPERATION. Figure 4 is a sketch of a revolver type automatic weapon, in which the principal recoiling parts - the drum support, slide, and receiver - are represented by their masses, M_1 , M_2 , and M_3 , respectively. The drum, which is fixed to the drum support but is free to rotate, is represented by I , its moment of inertia.

Springs used in this type of weapon are recoil adapters, driving springs, and mounting leaf which are designated by their stiffnesses K_1 , K_2 , and K_3 , respectively. The displacement of any mass is denoted by " x " with the

proper subscript.

When the weapon is in neutral position, the driving spring holds the slide (M_2) against the drum support (M_1), which consists of the barrel, drum cradle, and drum (I). The drum is fixed in the drum support in such a manner as to prohibit longitudinal motion (relative to the drum support) but permit rotation. The drum has rollers on its periphery, at least one of which is located in a cam which is cut in the slide.

When a round is fired, a force is applied to the drum support, which tends to move the drum support rearward and the projectile forward. As the slide is held against the drum support, the slide displacement must be identical with the drum support displacement; i.e., we can consider the drum support and slide as a lumped mass which exerts a force on the receiver by means of two parallel springs, K_1 and K_2 .

A short time after firing, the moving projectile passes over a gas port, allowing the gas to expand into a gas cylinder, which causes a piston to strike the slide and drive it rearward. When the piston strikes the slide the two masses, M_1 and M_2 , are separated and each mass is now displaced by an amount which is dependent on the summation of the forces on the individual masses. This action is indicated by the force F_2 .

As the slide is being moved rearward, it causes the drum to index. While the drum is being rotated, the slide transfers rotational kinetic energy to the drum and stores potential energy in the driving springs (K_2). When the drum roller reaches the apex of the cam, it limits the rearward displacement of the slide relative to the drum support, causing the slide velocity to be equal to zero; i.e., the slide kinetic energy becomes zero.

With the drum roller at the apex of the cam, the drum now acts as a fly wheel; therefore, the rotational kinetic energy of the drum and potential energy

of the driving spring cause the slide to be moved forward in such a manner that the drum is indexed into battery position. Some instant later, the slide arrives into battery position, firing a subsequent round, thereby initiating another cycle of operation.

During a cycle of operation the slide exerts a force on the receiver by means of the driving spring and any friction that may exist. It also exerts a force on the drum support by means of the cam. The drum support exerts a force on the receiver through the recoil adapter. The summation of these forces causes the receiver to be displaced if the stiffness of the mount (K_3) is not infinite.

Although the various springs are represented by their stiffness K_i , it is not implied that these K 's are constant. Function generators are used to simulate these devices, so that complete variations in spring characteristics are permitted; i.e., complete load-displacement characteristics of the spring can be duplicated and easily varied.

EQUATIONS OF MOTION. The kinematic system under consideration may be described by the following equations of motion:

$$\begin{aligned}
 \text{Case I} \quad & (M_1 + M_2) \ddot{X}_1 + (K_1 + K_2) (X_1 - X_3) = F_1(t) - F_f \\
 & (M_1 + M_2) \ddot{X}_2 + (K_1 + K_2) (X_2 - X_3) = F_1(t) - F_f \\
 & M_3 \ddot{X}_3 + K_1 (X_3 - X_1) + K_2 (X_3 - X_2) + K_3 X_3 = F_f \\
 \text{Case II} \quad & M_1 \ddot{X}_1 + K_1 (X_1 - X_3) = F_1(t) - F_2(t) + F_{\text{cam } X} \\
 & M_2 \ddot{X}_2 + K_2 (X_2 - X_3) = F_2(t) - F_{\text{cam } X} - F_f \\
 & M_3 \ddot{X}_3 + K_1 (X_3 - X_1) + K_2 (X_3 - X_2) + K_3 X_3 = F_f \\
 & F_{\text{cam } X} = I \ddot{\theta} \frac{d\theta}{d(X_2 - X_1)}
 \end{aligned}$$

where M_1 = mass of Drum support
 M_2 = mass of Slide
 M_3 = mass of Receiver

I = Moment of Inertia of Drum

K_1 = Stiffness of Recoil Adapter

K_2 = Stiffness of Driving Spring

K_3 = Stiffness of Mount

X_1 = Displacement of Drum Support

X_2 = Displacement of Slide

X_3 = Displacement of Receiver

θ = Angular Displacement

$F_1(t)$ = Firing Pulse

$F_2(t)$ = Piston pulse

F_f = Coulomb friction between slide and receiver

Case I defines the motion before force $F_2(t)$ is applied, while Case II defines motion during and after the time $F_2(t)$ is applied. These two cases are necessary if the displacements of the slide and drum support are to be identical before the slide is separated from the drum support by the gas piston. As a continuous record of the displacement of each individual component is desired from the analog computer, the computer must transform the equations of Case I into those of Case II by switching circuit parameters. This switching is impractical from the standpoint of available equipment, therefore, to utilize the equipment efficiently one assumption will be made; i.e., between the slide and drum support there exists a single acting spring having a very high rate. This spring will only act in compression and will exert a very high force on the slide and drum support when the slide displacement relative to the drum support tends to be less than zero. Upon introduction of this single acting spring between the drum support and slide, the new equations of motion are as follows:

$$M_1 \ddot{X}_1 + K_c(X_1 - X_2) + K_1(X_1 - X_3) = F_1(t) - F_2(t) + F_{\text{cam } X}$$

$$M_2 \ddot{X}_2 + K_c(X_2 - X_1) + K_2(X_2 - X_3) = F_2(t) - F_f - F_{\text{cam } X}$$

$$M_3 \ddot{X}_3 + K_2(X_3 - X_2) + K_1(X_3 - X_1) + K_3 X_3 = F_f$$

$$F_{\text{cam } X} = I_0'' \frac{d\theta}{d(X_2 - X_1)}$$

It will be noted in these equations that the firing force $F_1(t)$ does not affect the second equation directly, but is introduced into the slide equations by the term $K_c(X_2 - X_1)$ which requires that the slide and drum support displacements will be almost identical when X_2 tends to be less than X_1 .

This relationship involving the cam force has been derived assuming that frictional losses are non-existent. This relationship also shows that manner in which the cam force in the longitudinal direction is dependent upon the cam shape.

PATCH DIAGRAM. A patch diagram is the wiring of the analog computer which is necessary to solve a particular set of equations. Patch diagrams utilize a set of symbols to define mathematical operations as shown in Figure 5. Numbers inside of the block indicate the magnitude of the feedback resistor (in megohms) or capacitor (in microfarads) while numbers outside of the block indicate the reciprocal of the input resistance in megohms. When a number is replaced by the letter "G", it will be taken to mean that the input is tied directly to the grid of the operational amplifier.

The tentative patch diagram of a revolver type automatic weapon is shown in Figure 6. Operation of the simulated automatic weapon is initiated by the momentary closure of the push button switch "SW". The simulated weapon operates automatically due to the pulse actuating circuit which is introduced into the circuit when the slide velocity is negative and the slide displacement relative to the drum support has some predetermined value which is simulated by the voltage "e".

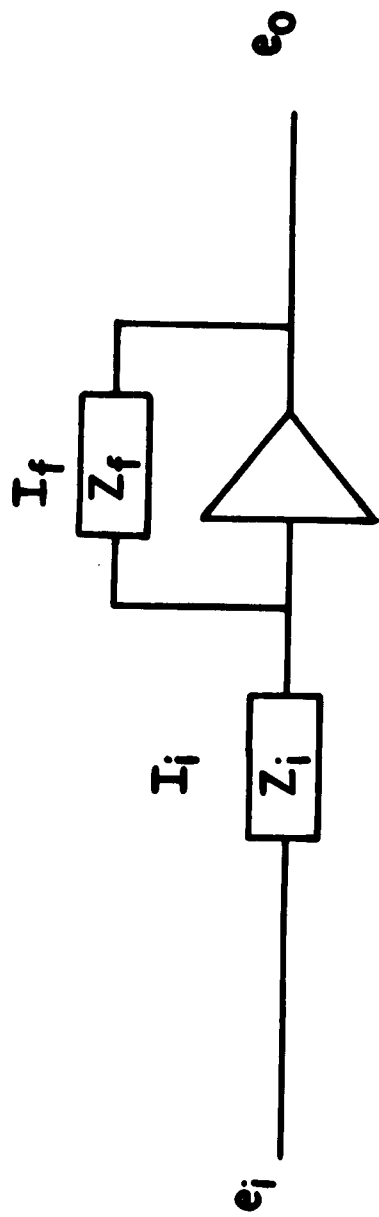
The method used to synthesize the cam force is the same as that used in automatic control systems, where a component is forced to move in accordance with a preconceived demand.

Accelerations, velocities and displacements of the drum support, drum, slide and receiver may be measured at the output terminals of the operational amplifiers indicated in Figure 6.

AID TO A GUN DESIGN. The application of the analog computer to gun design is in the kinematic analyses of the dynamics of the principle recoiling masses of the weapon. This includes vibration problems, trunnion reaction problems, effect of changing parameters on the rate of fire, and similar problems which involve the time-displacement relationship between the moving masses. Once the coupled systems of masses have been set up on the computer, the design engineer is able to adjust the masses, spring constants, losses, and input functions in such a way as to study the relations among these parameters and functions, and their effects on weapon operation. The designer should be able to optimize a set of parameters and make the best compromises to obtain several desirable operating conditions.

The computer is regarded as a designer's aid, not as a replacement for designers. It is not expected to eliminate the construction of prototypes of new weapons. However, it should reduce the number of modifications necessary on each prototype model. The computer should be expected to save money by reducing design, fabrication, and testing time, because it is easier for an engineer to vary a parameter by adjusting a knob on the computer than by having a new component fabricated and tested.

.



$$-e_o = e_i \frac{Z_f}{Z_i} \frac{1}{1 + \frac{1}{A} \left(1 + \frac{Z_f}{Z_i}\right)} + e_o \frac{1 + \frac{Z_f}{Z_i}}{1 + \frac{1}{A} \left(1 + \frac{Z_f}{Z_i}\right)} + i g \frac{Z_f}{1 + \frac{1}{A} \left(1 + \frac{Z_f}{Z_i}\right)}$$

$$e_o \approx -e_i \frac{Z_f}{Z_i}$$

FIG 1
GENERAL OPERATIONAL AMPLIFIER RELATIONSHIP

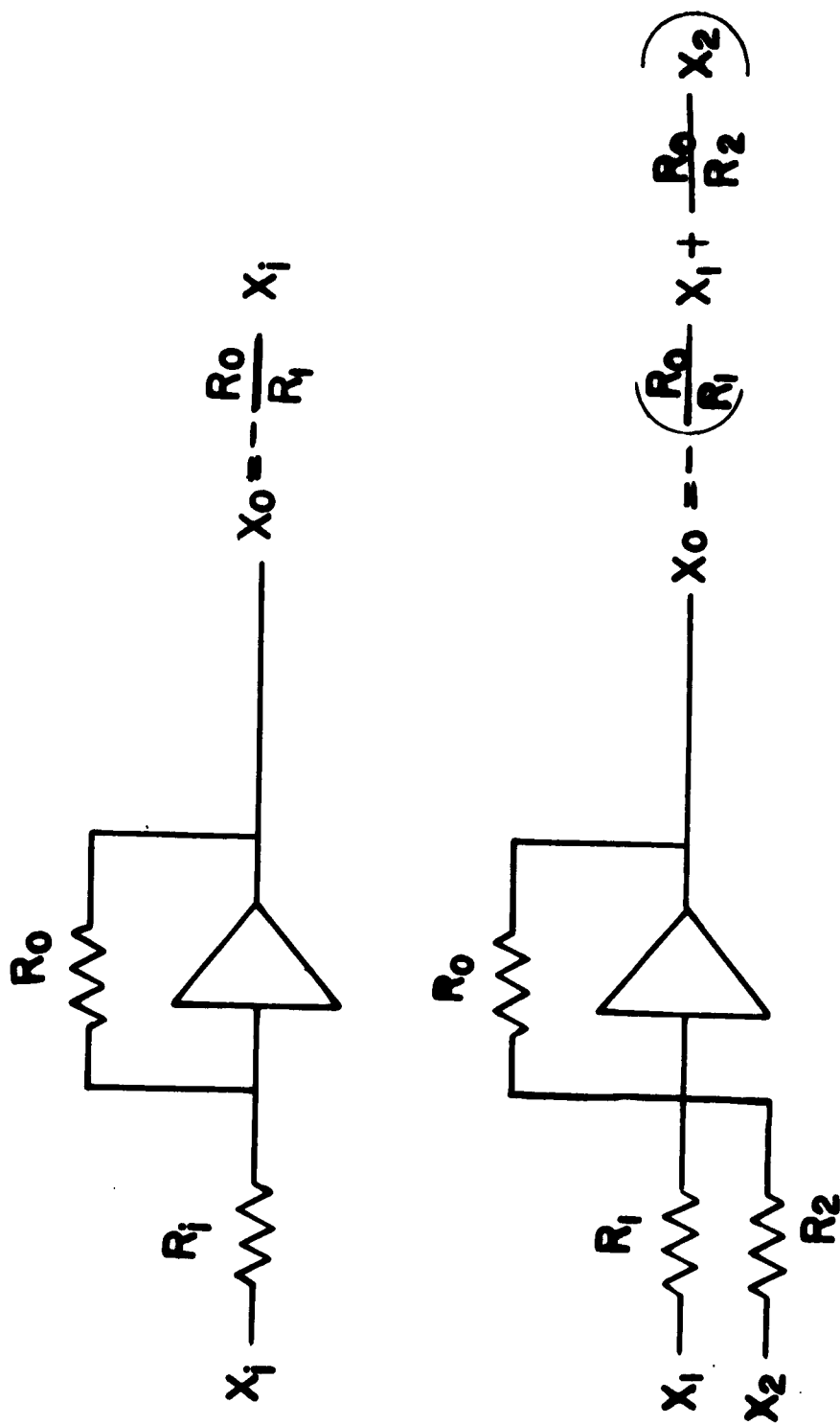


FIG 2

USE OF OPERATIONAL AMPLIFIER TO PERFORM SIGN CHANGING,
MULTIPLICATION, ADDITION AND SUBTRACTION

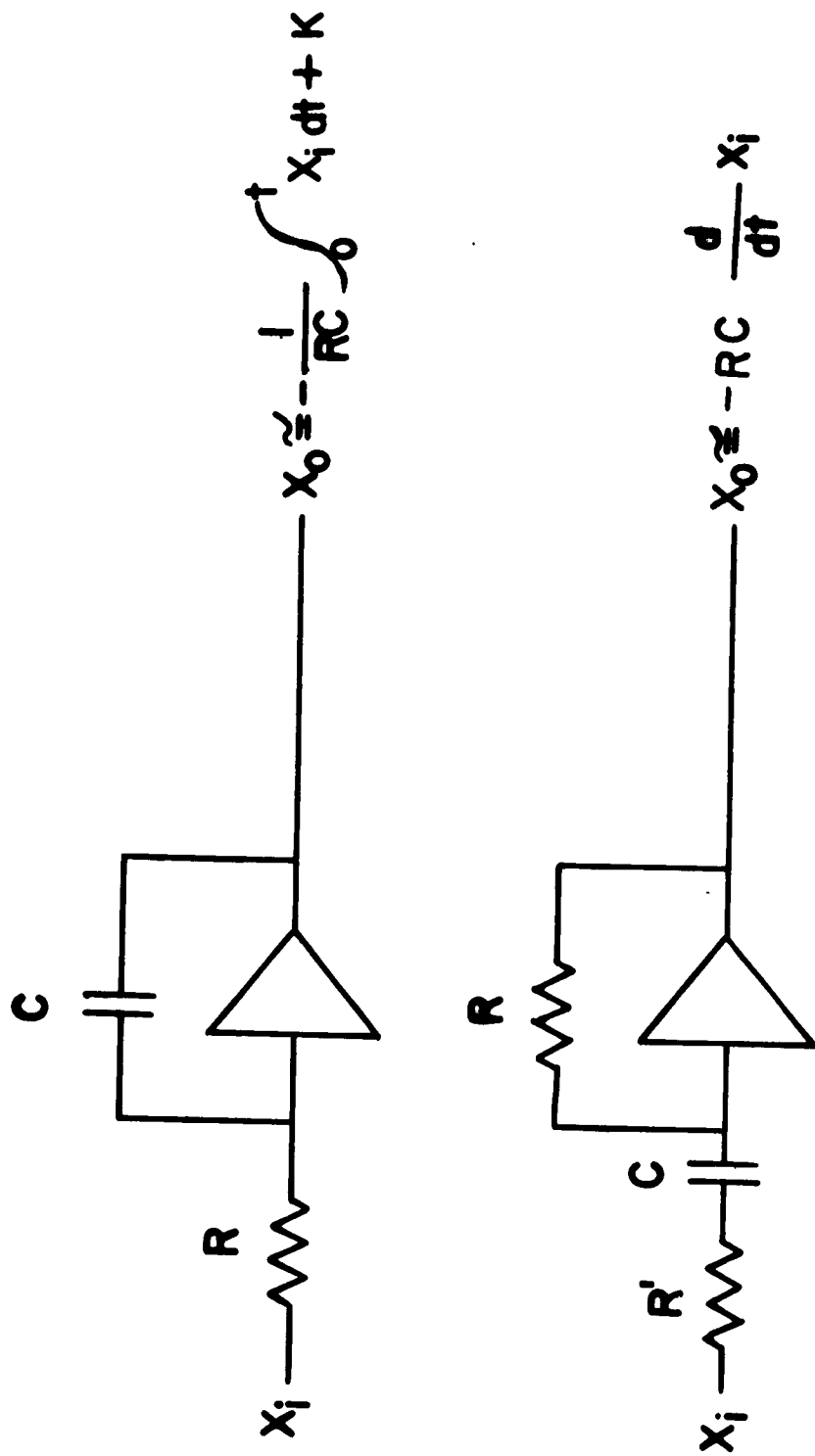
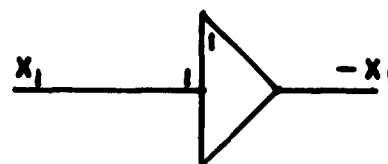
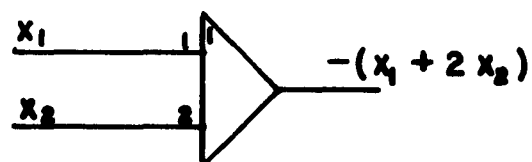


FIG 3
USE OF OPERATIONAL AMPLIFIER TO PERFORM INTEGRATION AND DIFFERENTIATION

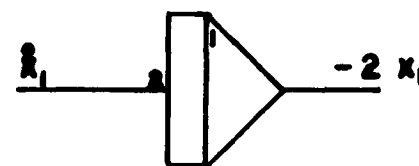
SIGN CHANGER



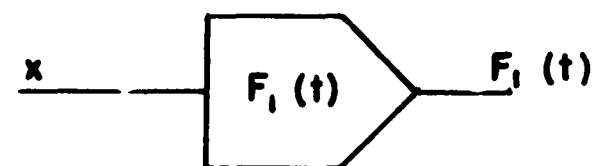
SUMMER



INTEGRATOR



FUNCTION GENERATOR



MULTIPLIER

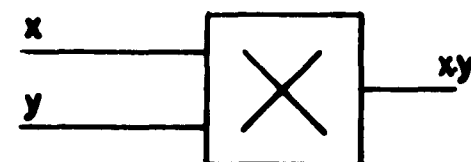


FIG 5

SYMBOLISM USED TO DENOTE VARIOUS SPECIFIC OPERATIONS

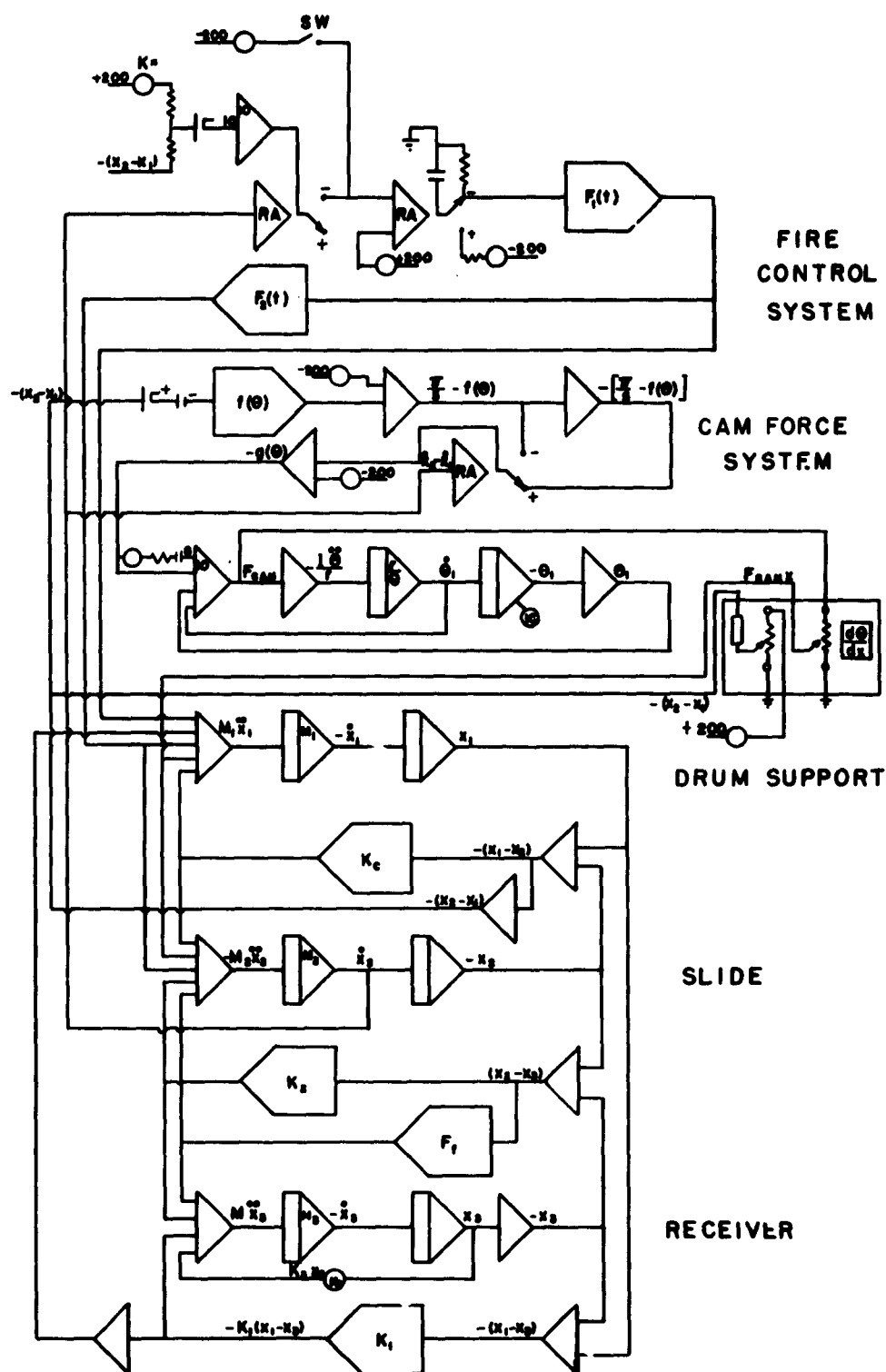


FIG 6

TENTATIVE PATCH DIAGRAM FOR SIMULATION REVOLVER TYPE AUTO WEAPON

SOLIDIFICATION OF MOLTEN MATERIALS IN FINITE REGIONS

by

Amino Nordio
Picatinny Arsenal

1. The Semi-Infinite Molten Mass.¹

The exact analytical solution of the problem of solidification of a semi-infinite mass of molten material has been obtained by N.M.H. Lightfoot. The solution applies to a liquid mass originally at uniform temperature, bounded by the plane $x = 0$, and extending to infinity in the direction of x positive, the plane $x = 0$ being kept at 0°C . Since convective currents are assumed to be negligible, Lightfoot's solution can be applied only to highly viscous molten materials. The author also attempted to solve the problem of solidification of a molten mass in a slab of finite thickness but was unsuccessful except for the case where the initial temperature of the molten material is equal to its melting point.

In order to solve the problem of solidification one must consider the effect on the temperature of the medium resulting from the flow of heat of fusion that evolves during the change from liquid to solid. In the semi-infinite mass, the medium solidifies from the boundary $x = 0$ and, in Lightfoot's analysis, the plane at which the transformation takes place is regarded as a source of heat moving from the boundary toward an increasing value of x . The position of the moving plane at a given time is determined from the condition that its temperature is equal to the melting point of the material. The mathematical solution for this case is obtained as follows. The temperature at a point x , at time t , given initial temperature ϕ , with the boundary surface $x = 0$ maintained at 0°C , and neglecting heat of fusion, is given by

$$V_{\phi} = \phi \operatorname{erf} \frac{x}{2\sqrt{\kappa t}} \quad (1)$$

where κ is the thermal diffusivity of the material.

¹N.M.H. Lightfoot, "The Solidification of Molten Steel," *Proc. London Math. Soc.* (2), 31, (1930) 97

The temperature at the same point x due to the heat of fusion is obtained by integrating from $t = 0$ to t the temperatures due to instantaneous sources of heat:

$$V_L = \frac{L}{2c} \int_0^t \frac{f(t')}{\sqrt{t\kappa(t-t')}} \left[\exp\left(-\frac{x-f(t')^2}{4\kappa(t-t')}\right) - \exp\left(-\frac{x+f(t')^2}{4\kappa(t-t')}\right) \right] dt' \quad (2)$$

In (2), L is the latent heat of fusion and c is the specific heat of the material. The position of the source of heat at time t' is represented by the function $f(t')$ which is determined from the condition

$$V_\phi + V_L = V \quad (3)$$

with V the melting point of the material.

Lightfoot assumed a function

$$x = f(t) = 2k\sqrt{\kappa t} \quad (4)$$

with k unknown. By substituting in (2) and (3) and through successive changes of variable, he established that to satisfy the conditions of the problem, the unknown quantity k is to be evaluated from

$$V = \phi \operatorname{erf} k + \frac{L\sqrt{\pi}}{c} k e^{k^2} \operatorname{erf} k \operatorname{erfc} k \quad (5)$$

which is the mathematical form of condition (3) at the plane of separation of solid and liquid.

While solidification proceeds, the temperature at a point $x_1 < 2k\sqrt{\kappa t}$ (in the solid region) is given by

$$V_1 = \phi \operatorname{erf} \frac{x_1}{2\sqrt{\kappa t}} + \frac{L\sqrt{\pi}}{c} k e^{k^2} \operatorname{erf} \frac{x_1}{2\sqrt{\kappa t}} \operatorname{erfc} k \quad (6)$$

and at $x_1 > 2k\sqrt{\kappa t}$ (through the molten material) by

$$V_1 = \phi \operatorname{erf} \frac{x_1}{2\sqrt{\kappa t}} + \frac{L\sqrt{\pi}}{c} k e^{k^2} \operatorname{erfc} k \operatorname{erfc} \frac{x_1}{2\sqrt{\kappa t}} \quad (7)$$

Equations (5), (6), and (7) consist of two distinct terms and show that during solidification the temperature at any point is obtained by superposing the temperature due to the initial supply of heat (ϕ) and the temperature due to the heat of fusion (L) evolved during solidification. A brief analysis of Lightfoot's results indicates other properties of the flow of heat during solidification which can be applied to the solution of the problem for other cases.

Equation (5) shows that at the surface of separation of solid and liquid, temperature V , the melting point of the material, results by addition of two terms independent of x and t : the two temperatures V_ϕ and V_L at the moving surface will be constant regardless of the distance of this surface from the boundary.

In equation (6) the ratio of the two terms V_ϕ/V_L is a constant for all points in the solid region and coincides with the ratio V_ϕ/V_L at the plane of solidification. Therefore the ratio of flow of initial heat and of heat of fusion,

$$\frac{dV_\phi}{dx} / \frac{dV_L}{dx}$$

is also a constant at all points in the solid. The value of this ratio depends only on the values of ϕ , V , L , and c of the material.

In equation (7), which applies to the molten region, the second term at the right does not indicate flow of heat of fusion through the molten material, but evaluates the amount of initial heat retained by the molten material as a result of added flow of heat of fusion through the solid region to the boundary. This second term will be referred to as $(V_L)_\phi$. Since the first term at the right is identically equal to ϕ only at infinity ($x = \infty$, $\operatorname{erf} x = 1$), one would obtain $(V_L)_\phi = 0$ only when $x = \infty$. A more definite value V_ϕ at a point x_1 , with $x_1/2\sqrt{\kappa t} \geq 3$, is obtained if the point is regarded as the center of a slab of thickness $2x_1$. In this case the temperature is given by

$$V_\phi = \frac{4\phi}{\pi} \sum_{n=0}^{\infty} \frac{1}{2n+1} \sin \frac{(2n+1)\pi}{2} e^{-(2n+1)^2 \pi^2 \kappa t / 4x_1^2} \quad (8)$$

With $x_1/2\sqrt{\kappa t} \geq 3$, the result of (8) will always be equal to ϕ . But the temperature at x_1 in the semi-infinite region cannot be lower than the temperature computed for x_1 as if it were the center of a slab of finite thickness and we may correctly conclude that when $x/2\sqrt{\kappa t} \geq 3$

$$\left[V_\phi \right]_{x_1} = \phi \quad \left[(V_L)_\phi \right]_{x_1} = 0 \quad (9)$$

An example of the various distributions in a semi-infinite mass during solidification is shown in Figure 1.

2. The Slab 2a

In the case of solidification of a molten mass initially at uniform temperature and bounded by the two plane surfaces $x = 0$ and $x = 2a$ kept at 0°C , the condition $V = V_\phi + V_L$ must be satisfied at the two planes of separation of liquid and solid moving from boundaries $x = 0$ and $x = 2a$ toward the center of the slab; the positions of the two planes (symmetrical about the center $x = a$) at time t must be obtained accordingly. A mathematical treatment of the problem similar to that followed for the case of a semi-infinite mass proves to be quite involved and has not been followed. As suggested by Lightfoot it is assumed instead that in the beginning, solidification proceeds from each boundary independently and that the position of the surface of separation of solid and liquid in the region $0 < x < a$ is given by $x = 2k\sqrt{\kappa t}$ with k obtained from (5) as for the semi-infinite case; the position of the plane surface moving in the region $a < x < 2a$ will be given by $x = 2a - 2k\sqrt{\kappa t}$.

According to this assumption, and using the dimensionless variable

$$r = \frac{\kappa}{a^2} t$$

the three distinct temperatures which are superposed at a point $x/a = 2k\sqrt{r}$ are obtained from the following:

$$V_\phi = \frac{4\phi}{\pi} \sum_{n=0}^{\infty} \frac{1}{2n+1} \sin \frac{(2n+1)\pi x}{2a} e^{-(2n+1)^2\pi^2 r/4} \quad (10)$$

$$(V_L)_\phi = \frac{L\sqrt{\pi}}{c} k e^{k^2} \operatorname{erfc} \operatorname{erfc} \frac{2a-x}{2a\sqrt{r}} \quad (11)$$

$$V_L = \frac{L\sqrt{\pi}}{c} k e^{k^2} \operatorname{erfc} k \quad (12)$$

Because of symmetry, (11) can be regarded as being due to original heat retained at x as a result of heat of fusion flowing to boundary $x = 2a$, and (12) accounts for heat of fusion flowing to boundary $x = 0$. It is found that the sum of (10), (11), and (12) is equal to V , the melting point of the material, up to a maximum value r_0 which depends on the temperature at $x = a$, the center of the slab. During solidification, this total temperature is given by

$$V = \frac{4\phi}{\pi} \sum_{n=0}^{\infty} \frac{1}{2n+1} \sin \frac{(2n+1)\pi}{2} e^{-(2n+1)^2\pi^2 r/4} + 2 \frac{L\sqrt{\pi}}{c} k e^{k^2} \operatorname{erfc} \frac{1}{2\sqrt{r}} \quad (13)$$

The maximum value r_0 for which (13) equals ϕ , the initial temperature, is the limit of the independent stage of solidification. When $r = r_0$, the surface of separation of solid and liquid will be found at

$$x_0/a = 2k\sqrt{r_0} \quad (14)$$

The boundary conditions to be satisfied during this first stage are obtained from (11) and $x = 0$. As indicated previously in (9), when

$$\frac{1}{\sqrt{r}} \geq 3, \quad (15)$$

$(V_L)_\phi$ can be assumed to be identically equal to zero.

From $r = 0$ to $r = r_0$ the total temperature distributions through the solid sections bounded at $x = 0$ and at $x = 2a$ will coincide with the temperature distribution obtained in the solid section of the semi-infinite mass. The ratio of flows and ratio of temperatures, which are constant at the sources and through the solid sections, will be expressed as follows:

$$\frac{d[V_\phi + (V_L)_\phi]}{dV_L} = \frac{V_\phi + (V_L)_\phi}{V_L} \quad (16)$$

The various temperature distributions for a numerical example at $r = r_0$, are shown in Figure 2.

For solidification in the range $x_0 < x \leq a$ it is assumed that the position of the plane of separation of solid and liquid is given by

$$x/a = -b + 2k_a \sqrt{r - r_2} \quad (17)$$

where b , k_a , and r_2 are all unknown and must be determined from the condition that the temperature at the moving plane or planes is always equal to V . Also when $r > r_0$, heat will flow from the center $x = a$ toward both boundaries $x = 0$ and $x = 2a$, and the new function must reflect a rate of solidification higher than the rate given by $x/a = 2k\sqrt{r}$.

The condition of continuity of the two functions of r , $x/a = 2k\sqrt{r}$ and (17), at r_0 , and of their first derivatives, gives two relations between the three unknown quantities

$$r_2 = r_0 \left(1 - \frac{k_a^2}{k^2} \right) \quad (18)$$

$$x_0/a = -b + 2k_a \sqrt{r_0 - r_2} \quad (19)$$

For solidification at $x = a$ we have also

$$1 = -b + 2k_a \sqrt{r_a - r_2} \quad (20)$$

The new parameter r_a appearing in (20) refers to time of solidification at the center of the slab $x = a$ and can be evaluated directly if the value of V_L at the time the two sources merge at $x = a$ can be pre-established.

During the first stage V_L at the source is constant but beyond $x = x_0$ we may observe any one of the following trends:

- (a) Temperature V_L at the source increases
- (b) Temperature V_L at the source decreases
- (c) Temperature V_L at the source remains constant and equal to

$$\frac{L\sqrt{\pi}}{c} k e^{k^2} \operatorname{erfc} k$$

as for the semi-infinite mass.

For case (c), of constant V_L , r_a can be evaluated from

$$V = \frac{4\phi}{\pi} \sum_{n=0}^{\infty} \frac{1}{2n+1} \sin \frac{(2n+1)\pi}{2} e^{-(2n+1)^2 \pi^2 r_a / 4} + 2 \frac{L\sqrt{\pi}}{c} k e^{k^2} \operatorname{erf} k \operatorname{erfc} k \quad (21)$$

It is quite evident that r_a will be greater for trend (a) than in (21) and will be smaller for trend (b). Solving (18), (19), and (20) with the three different values of r_a , it will be found that rate of solidification (a) will be lower than rate (c), while rate (b) will be greater than (c). But both (a) and (b) are inconsistent with (c) since a higher source temperature can be obtained only with a higher rate of evolution of heat of fusion or rate of solidification, and a lower source temperature with a lower rate. The only possible solution left is (c), with temperature V_L at the source constant through the entire process of solidification. This result indicates that, in one-dimensional flow, the value of the ratios

$$\frac{d[V\phi + (V_L)\phi]}{dV_L} \quad \text{and} \quad \frac{V\phi + (V_L)\phi}{V_L}$$

at any point in the solid and at the sources will be maintained till solidification is complete.

In conclusion it can now be stated that, in a freezing mass, initially at uniform temperature ϕ and with bounding surfaces $x = 0$ and $x = 2a$ maintained at 0°C , the position of the plane of separation of solid and liquid in the region $0 < x \leq a$ is given by the two functions

$$\begin{aligned} x/a &= 2k\sqrt{r} \quad 0 < r \leq r_0 \\ x/a &= -b + 2k_a\sqrt{r-r_0} \quad r_0 \leq r \leq r_a \end{aligned} \quad (22)$$

where the various constants and the ranges of r are evaluated from the data of the problem according to the method specified above. The position of the moving plane in (22) is expressed in terms of the dimensionless variable $r = \frac{\kappa}{a^2} t$ where κ is the average thermal diffusivity of the material in the temperature range V to ϕ (in the molten range). The numerical value of κ is to be obtained from experiment.

Complete solution of the problem for the special case $\phi = V$ (that is, when the initial temperature is at the melting point of the material) is given by Lightfoot. In this case the position of the moving plane through the entire range $0 < x \leq a$ is given by

$$x/a = 2k\sqrt{r} \quad (23)$$

where k is obtained from (5) as for semi-infinite mass. Lightfoot's solution implies a constant value of V_L at the moving planes, as can be verified with the following

$$V = \frac{4V}{\pi} \sum_{n=0}^{\infty} \frac{1}{2n+1} \sin \frac{(2n+1)\pi}{2} e^{-(2n+1)^2 \pi^2 r_a/4} + 2 \frac{L\sqrt{\pi}}{c} k e^{k^2} \operatorname{erfc} k \quad (24)$$

and

$$r_a = \left(\frac{1}{2k} \right)^2 \quad (25)$$

Numerical examples of solidification in finite slabs are shown in Figure 3.

3. The Cylinder and the Sphere

The results obtained in the previous section furnish the basis for solving the problem of solidification in an infinite cylinder $0 \leq r \leq a$ and in a sphere $0 \leq r \leq a$ where the initial temperature of the molten material is the same as for the slab $2a$ and the boundary surfaces are kept at 0°C . According to the property observed above, during solidification in one-dimensional flow, the ratio of flow of original heat to heat of fusion and the ratio of temperatures remain constant through the solid from the boundary to the source. Because solidification in a cylinder and in a sphere will proceed by radial flow, we find that at the surfaces of separation of solid and liquid, and regardless of their distance from their respective boundaries,

$$\frac{d[V\phi + (V_L)\phi]_{l,c,s}}{d[V_L]_{l,c,s}} = \frac{[V\phi + (V_L)\phi]_{l,c,s}}{[V_L]_{l,c,s}} \quad (26)$$

and

$$[V_\phi + (V_L)_\phi + V_L]_{l,c,s} = V \quad (27)$$

The subscripts l, c, and s stand for slab, cylinder, and sphere respectively. The $(V_L)_\phi$ in cylinder and sphere is for original heat retained because of heat of fusion evolving at radially opposite point sources. From (26) and (27), we have

$$(V_L)_l = (V_L)_c = (V_L)_s \quad (28)$$

or a constant source temperature at the convergent surfaces of the cylinder and of the sphere. Thus, the time r_c when the cylindrical source finally converges to the axis of the cylinder can be obtained directly from

$$V = 2\phi \sum_{n=1}^{\infty} \frac{1}{a_n J_1(a_n)} e^{-a_n^2 r_c} + 2 \frac{L\sqrt{\pi}}{c} k e^{k^2} \operatorname{erfc} k \quad (29)$$

and the time r_s when the spherical source converges to the center of the sphere is obtained from

$$V = 2\phi \sum_{n=0}^{\infty} (-1)^n e^{-(n+1)^2 \pi^2 r_s} + 2 \frac{L\sqrt{\pi}}{c} k e^{k^2} \operatorname{erfc} k \quad (30)$$

The first terms at the right of (29) and (30) are temperatures due to original heat.

According to another property of heat conduction we observe that when solidification in the slab, in the cylinder, and in the sphere has proceeded an equal distance from the respective boundary, the distributions through the molten region of total temperature and of V_ϕ and $(V_L)_\phi$ individually will be equal. Mathematical proof is obtained with the known solutions

$$(V_\phi)_l = \frac{4\phi}{\pi} \sum_{n=0}^{\infty} \frac{1}{2n+1} \frac{\sin \frac{(2n+1)\pi x}{2a}}{2a} e^{-(2n+1)^2 \pi^2 l/4} \quad (31)$$

$$(V_\phi)_c = 2\phi \sum_{n=0}^{\infty} \frac{J_0(r a_n)}{J_1(a_n)} e^{-a_n^2 r_c} \quad (32)$$

$$(V_\phi)_s = \frac{2a\phi}{\pi r} \sum_{n=0}^{\infty} \frac{(-1)^n}{n+1} \frac{\sin \frac{(n+1)\pi r}{a}}{a} e^{-(n+1)^2 \pi^2 r_s} \quad (33)$$

These solutions give temperature distributions throughout the three geometries being considered, neglecting heat of fusion. With any given gradient $(V_\phi)_1$ in a range

$$\frac{x_1}{a} \leq \frac{x}{a} \leq \frac{2a - x_1}{a}$$

we can always find particular values of r_c and r_s such that the three distributions coincide at all points within ranges

$$\frac{a - r}{a} \geq \frac{x_1}{a}$$

as shown in Figure 4. The three distributions will never cross each other regardless of the values r_1 , r_c and r_s .

The distributions of total temperature through corresponding molten ranges coincide because they depend on the temperature at the limiting surfaces. This temperature is V , the melting point of the material for all three cases.

The distributions of $(V_L)_\phi$ coincide because they reflect delay in cooling due to the heat of fusion evolved during solidification. At the limiting surfaces or sources $(V_L)_\phi$ is equal to V_L while the ratio of flows at points outside the ranges is the same for the three cases.

Finally, since the distributions $(V_L)_\phi$ are continuous across the sources opposite their origin, we find that at the limiting surfaces

$$x_1/a = \frac{a - r_1}{a}$$

$$(V_\phi)_1 = (V_\phi)_c = (V_\phi)_s \quad (34)$$

For solidification at a given point, x_1/a in the slab $2a$, we evaluate r from the two formulas of (22), and obtain from (31) the V_ϕ corresponding to this distance from the boundary. In (32) and (33) we substitute V_ϕ as obtained from (31), and r_1 as obtained from $(a - r_1)/a = x_1/a$, and solve for r .

Numerical examples of solidification in slab, cylinder, and sphere are shown in Figure 5.

The principle of constant ratio of flows throughout the solid regions can be applied to any slab, cylinder, or sphere cooling by radiation into a medium at constant temperature. Comparison of the distributions V_ϕ and V_L with the distribution obtained originally for the slab shows that the property of coincident distribution through the molten ranges applies also for these cases. The thermal properties of a container may be given in terms of a heat transfer coefficient and the solution for the freezing material obtained by the method outline above.

4. The Finite Cylinder and the Parallelepiped

Solidification at a point $P(r, z)$ in the finite cylinder l, a , with center at the origin, will occur when the temperature V_ϕ is equal to that obtained for the slab with the smaller of the two quantities

$$\begin{cases} \frac{l-z}{l} \\ \frac{a-r}{a} \end{cases} \quad (35)$$

This method results from a comparison of the finite cylinder with the infinite cylinder and the slab. Initially, at a point $z = 0$ and $r = a$ solidification will proceed as in an infinite cylinder. At a point $z = l$ and $r = 0$ it will proceed as in a slab $2l$.

A numerical example computed with

$$V_\phi = \frac{8\phi}{\pi} \sum_{n=1}^{\infty} \frac{J_0(ra_n)}{a_n J_1(a_n)} e^{-a_n^2 r} \sum_{n=0}^{\infty} \frac{(-1)^n}{2n+1} \cos \frac{(2n+1)\pi z}{2l} e^{-(2n+1)^2 \pi^2 \left(\frac{a}{2l}\right)^2 r}$$

is shown in Figure 6.

Solution for a parallelepiped is obtained similarly.

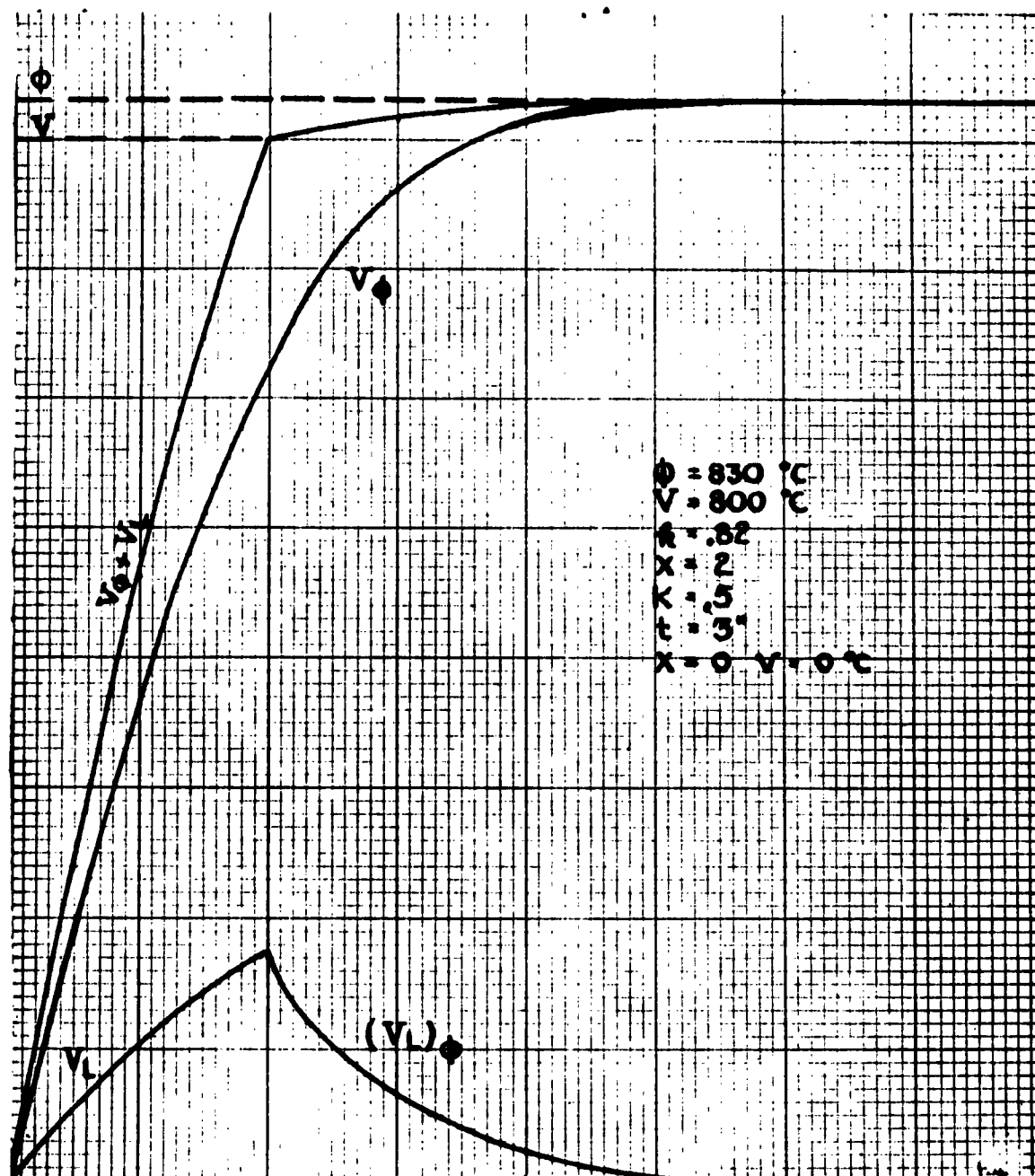


Fig 1 Temperature Distributions During Solidification in a Semi-Infinite Mass.

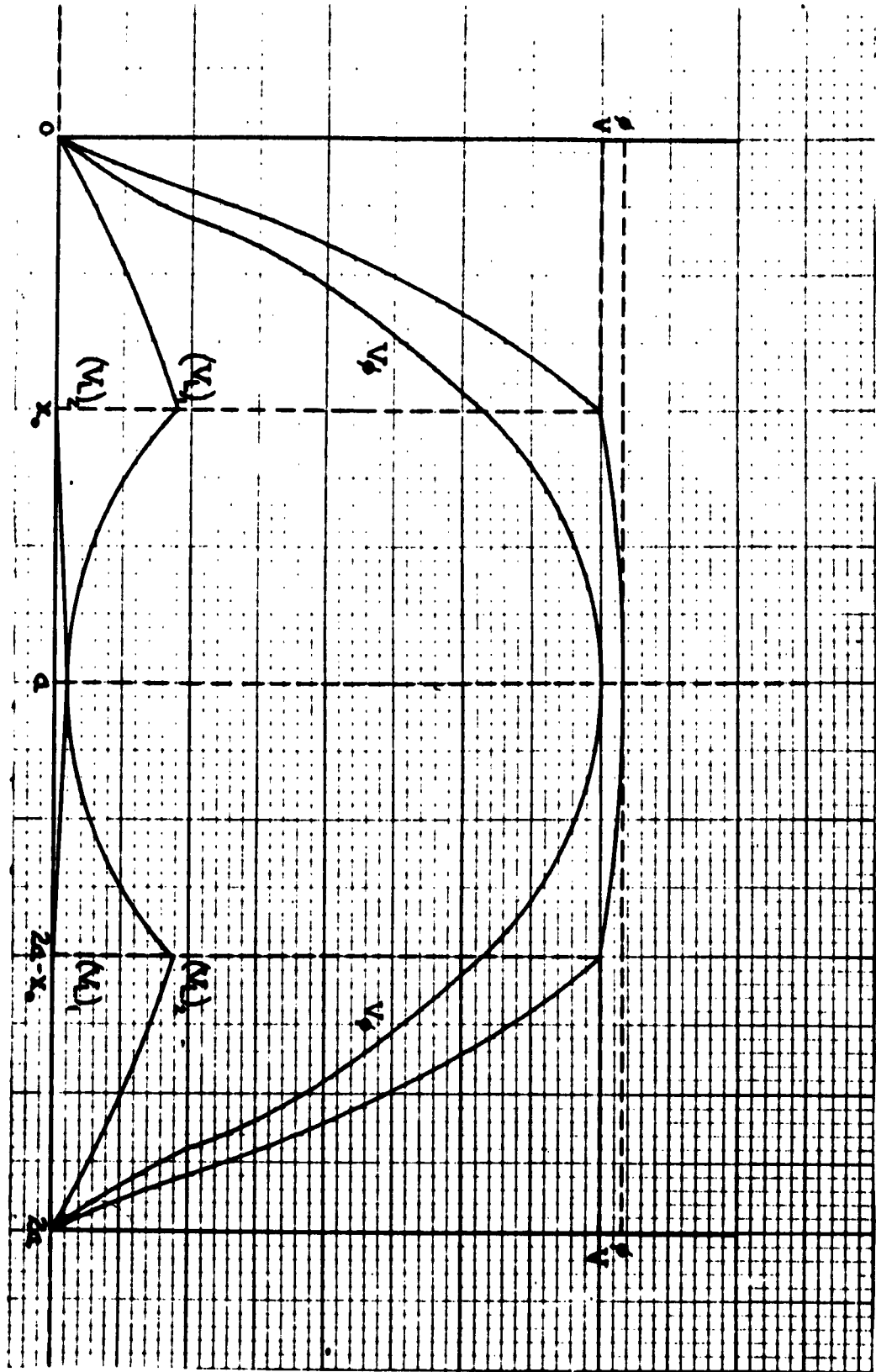


Fig 2 Temperature Distributions in Slab 2a with $r = r_0$



Fig 3 Time of Solidifications in Slabs 2a, with the same V For all Slabs and ϕ and L/c varying for each Slab.

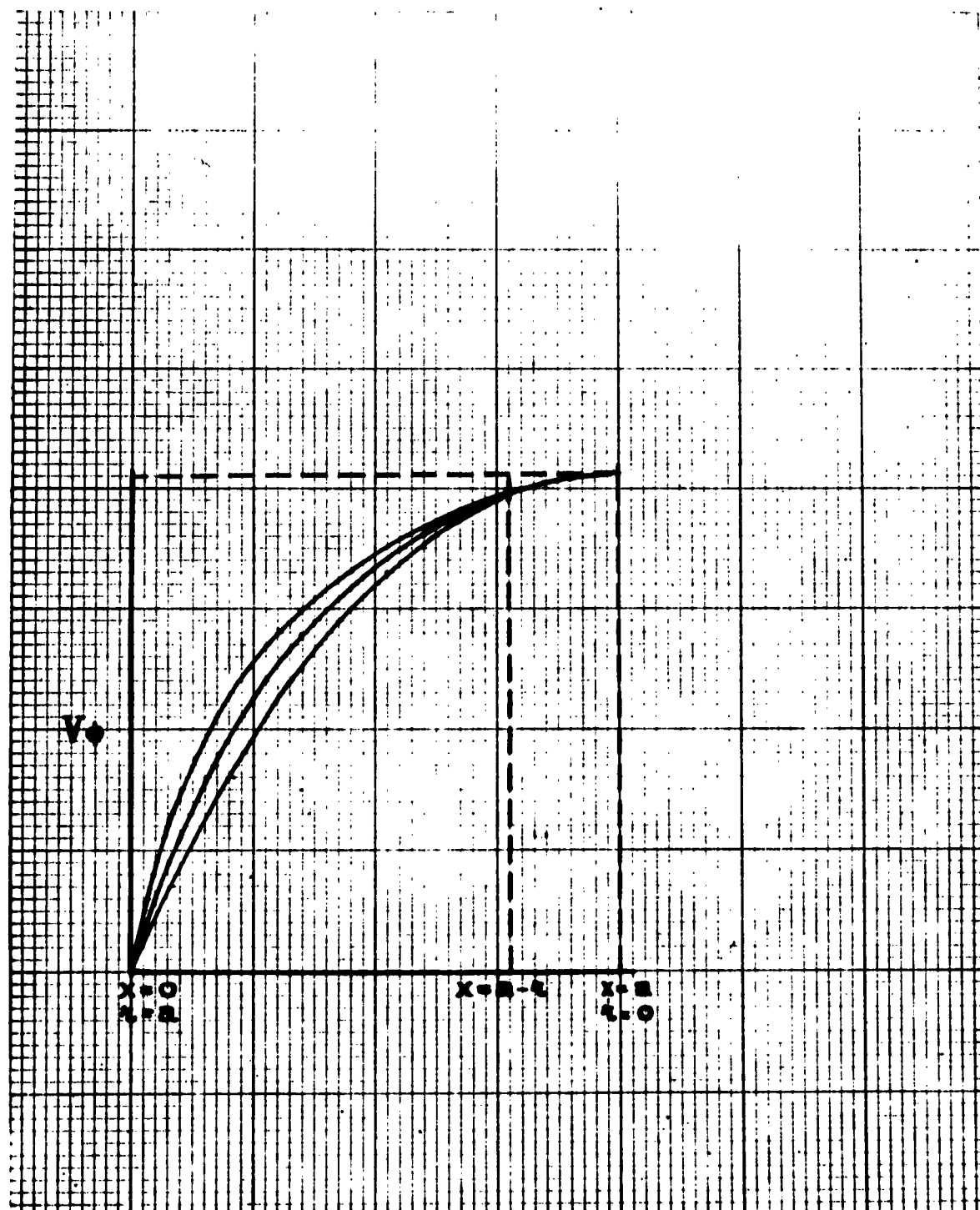


Fig 4 Temperature Distribution V_ϕ in Slab, Cylinder, and Sphere for Particular Values r_b , r_c , and r_a .

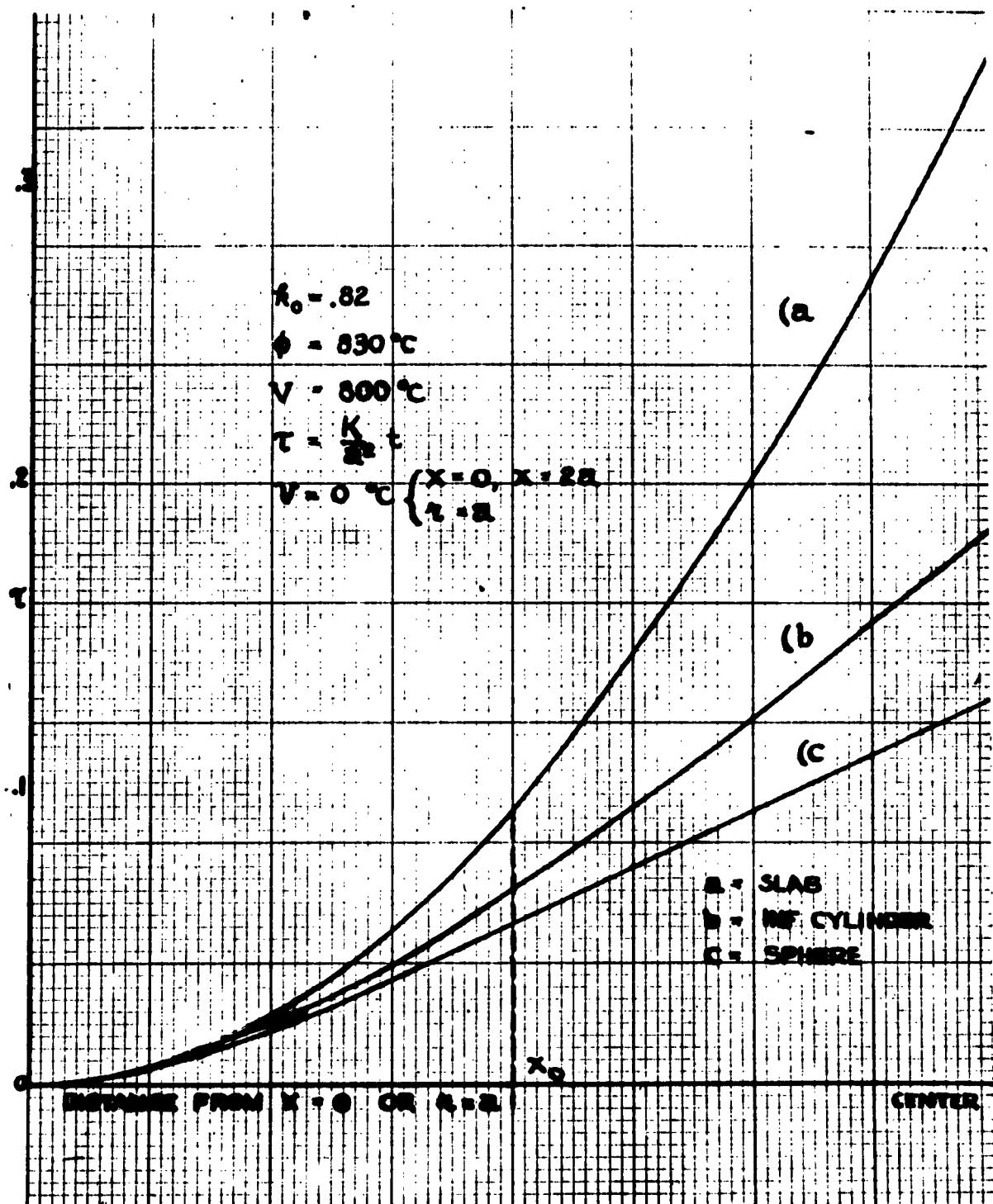


Fig 5 Time of Solidification in Slab, Cylinder, and Sphere with Equal ϕ , V , and L/c .

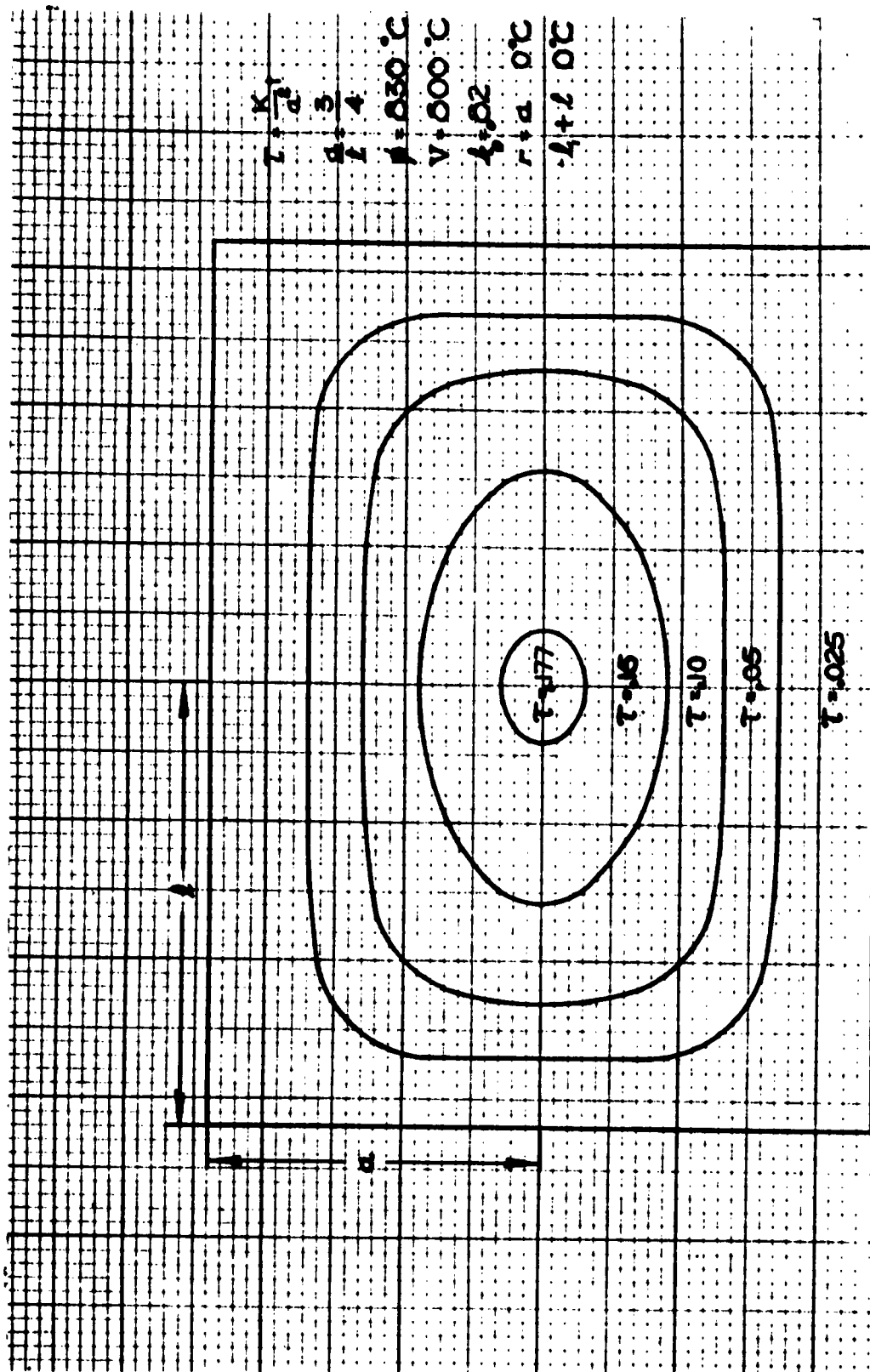


Fig 6 Surfaces of Solidification in Finite Cylinder

**ON THE FLY-OFF OF ROTATING BANDS
UNDER CENTRIFUGAL LOADING**

By

F. I. BARATTA

J. I. BLUM

O.O. Project: TA1-5005, Artillery Ammunition - Banding and Rifling
D/A Project: 504-03-061
Report No.: WAL 760/536.
Filing Title: Rotating Bands

**WATERTOWN ARSENAL
WATERTOWN 72, MASS.**

ABSTRACT

One of the necessary design features of a projectile rotating band is that it must not be discarded in flight by virtue of the centrifugal forces acting. One of the common methods of retaining the band consists of utilizing undercut band seats thus in effect, restraining the band from outward movement. In the present paper the elastic stresses in a band, thus constrained, are determined for both the quasi-static loading condition (i.e., slowly applied centrifugal forces) and for the dynamic case (i.e., suddenly applied centrifugal forces). As expected, the dynamic case yields stresses just twice the quasi-static case. In both these analyses the band is considered as a beam on an elastic foundation.

As a limited extension of these elastic analyses, the non-elastic case of an unconstrained band (applicable also to a long constrained band) is analyzed assuming a stress-strain curve of the form $\sigma = k\epsilon^n$, giving rise to a non-linear differential equation. A hodograph is plotted and the required information related to failure or retention of the rotating band is obtained.

FRANCIS I. BARATTA
Mathematician

APPROVED:

JOSEPH I. BLUM
Mechanical Engineer

J. F. SULLIVAN
Associate Technical Director
Watertown Arsenal Laboratories

RUSSELL F. SCOTT, Jr.
Major, Ord Corps
Director
Watertown Arsenal Laboratories

NOMENCLATURE

- σ = Stress*
 ϵ = Strain
 κ, η = Constants in the stress-strain law
 y = Radial deflection of mean radius of band
 x = Longitudinal position along band
 E = Young's modulus
 ν = Poisson's ratio
 I' = Moment of inertia of cross-section of beam of width $\frac{D}{2} \Delta \alpha = \frac{Dh^3}{24} \Delta \alpha$
 I = $I' / \Delta \alpha = \frac{Dh^3}{24}$
 $\Delta \alpha$ = Angle subtended by beam element
 D = Instantaneous mean diameter of band
 D_0 = Initial mean diameter of band
 $p(x, t)$ = Loading on beam (lbs/inch)
 $a(x, t)$ = Centrifugal contribution to $p(x, t)$
 $b(x, t)$ = Restoring load contribution to $p(x, t)$
 $c(x, t)$ = Inertial contribution to $p(x, t)$
 q = Centrifugal loading (lbs/in.²) = $\frac{1}{2} \frac{\rho D h}{g} \omega^2$
 q_1 = Generalized coordinate
 h = Thickness of band
 ρ = Density of band material
 g = Gravitational constant
 t = Time
 t_0 = Time for $\frac{dy}{dt}$ (or $\frac{dU}{dt}$) in Case III to initially become zero

*Subscripts l and t indicate longitudinal and tangential, respectively; subscript Max indicates maximum value of stress.

ω = Rotational speed of band (radians/sec.)

M, N = Constants (see. Eq. 5)

$$\gamma = \sqrt{\frac{4 \cdot 12(1-\nu^2)}{D_0^2 h^2}} \frac{l}{2}$$

ξ = Radial distance from middle surface

P.E. = Potential energy

K.E. = Kinetic energy

Q_1 = Generalized force

$$p_1^2 = \frac{\pi^4}{l^4} \frac{Egh^2}{12\rho} \left[1^4 + 4\left(\frac{2}{\pi}\right)^4 x^4 \right]$$

U = Displacement parameter = $\left(1 + \frac{2y}{D_0}\right)$

λ = Load parameter = $\frac{\rho D_0^2 \omega^2}{4kg}$

INTRODUCTION

The present paper is concerned with the problem of the failure of rotating bands during the firing of projectiles. The primary function of such bands is to engage the gun tube rifling and impart its twist to the projectile in order to maintain stable flight. Inherent in the satisfactory fulfillment of this primary function is the creation of centrifugal loading of these bands. Figure 1 shows the nature of the band deformation and some of the pertinent notation. The resulting stresses may then cause undesirable premature failure of the band upon emergence from the gun tube, i.e., as soon as the constraints of the tube are no longer applied. Frequently, this failure is characterized by rupture and the band takes leave of the projectile.

In many applications, this "fly-off" is not desirable and various attempts have been made, consequently, to prevent it. All of the common methods of accomplishing this end involve a "bonding" of the band to the projectile. In most instances where this bonding is attempted, it is restricted only to the ends of the band (as in undercut seats); in other cases, the bonding is effected at closer intervals, as exemplified in the practice of using dovetails in plastic bands; in other instances, this "bonding" is continuous as by depositing the band material by welding onto the projectile (as in welded overlay bands). Figure 2 shows common "bonding" techniques.

To a great extent, the "Fly-off" problem is minimized or eliminated by the use of the latter methods of bonding. However, it is expected that this latter method may not always be feasible; considering the extensive use of the first method of "bonding", it would therefore seem desirable to understand the nature of the stresses induced in such bands in order to minimize the chance of fly-off.

In the present paper, * attention is accordingly focused upon a smooth, unrifled band which is permitted to be constrained only at its ends. The band is assumed (a) to be thin enough to allow use of "thin wall" theory and (b) to be long enough so that ordinary beam theory is applicable to a segment of the band.

It is evident that, as the band becomes long with respect to its other dimensions, the effects of the end constraints become negligibly small at regions remote from its ends, so that the central portion of the band can be considered as a band without end constraints, i.e., as a "hoop", wherein the only significant stresses are the tangential stresses. On the other hand, short bands (i.e., bands in which the end constraints are the primary reactions to the applied centrifugal loading) are subject primarily to longitudinal bending stresses. There is also considered to exist an intermediate geometry of the band in which both tangential and longitudinal stresses are significant.

*The results presented in the current paper have been culled from the following Watertown Arsenal laboratory reports: a. "On the Influence of End Constraints on Stresses in Rotating Bands under Centrifugal Forces", WAL No. 700/520-2; b. "Elastic Stresses in a Rotating Band subjected to a Suddenly Applied Centrifugal Force", WAL No. 700/531, and c. "Stresses beyond the Yield Point in: a) A Long Rotating Band Loaded by a Suddenly Applied Centrifugal Force, b) A Long Thin Cylinder Loaded by a Suddenly Applied Internal Pressure", WAL No. 700/532.

In the following analysis, the differential equation is first presented and is then specialized to apply to each of three specific cases as follows:

Case I: Static State - Elastic Behavior

Case II: Dynamic State (Suddenly Applied Load) - Elastic Behavior

Case III: Dynamic State (Suddenly Applied Load) - Inelastic Behavior

These three cases are distinguished, one from the other, by the nature of the response, of the band material, to load and by the time rate of application of this load. The effect of time will be adequately covered later in the paper, so we consider here only the significance of the material properties, best characterized by the representative stress-strain curve shown in Figure 3. Figure 3a shows the general behavior of many engineering materials; it will be observed that for small loads the material behaves elastically and linearly. Cases I and II conform to response restricted to this region of elastic behavior of such materials. Case III, on the other hand, is aimed at the response of a completely inelastic material such as shown in Figure 3c. Several characteristics of the behavior of materials stressed into the plastic state are of interest and are pertinent to the present problem. We note in Figure 3a, for example, that the nominal stress reaches a maximum value and that an instability ensues in that the strain continues to increase with diminishing stress. This instability, which is accompanied by a localized contraction of the specimen, is known as "necking" and is associated with the fact that the rate of strain hardening is inadequate to compensate for the decreasing cross-section of the specimen. When such stress-strain curves are plotted in terms of true stress and natural* strain, the curves can generally be expressed in the form $\sigma = k\epsilon^{\eta}$ ** for monotonically increasing σ and necking or the instability point can then be shown to be governed by the criterion $\frac{d\sigma}{d\epsilon} = \sigma$. Applying this criterion to the suggested stress-strain law leads to the conclusion that necking occurs when the natural strain ϵ equals the strain hardening coefficient η , i.e., $\epsilon = \eta$. Figure 3b shows a conventional stress-strain curve in which premature fracture has precluded the necking possibility.

FORMULATION OF DIFFERENTIAL EQUATIONS

Consider the longitudinal element of the band shown in Figure 1.*** Treating this as a beam on an elastic foundation subjected to static loading $p(x)$ directed radially outward, we may express the deflections in terms of the following familiar differential equation:

$$\frac{d^4 y(x)}{dx^4} = \frac{1-\nu^2}{EI} p(x) \quad \dots \dots \dots (a)$$

*True stress is the load divided by the instantaneous area rather than the original area, and natural strain is defined by the relation $\epsilon = \ln l/l_0$ where l and l_0 are the instantaneous and initial infinitesimal gage lengths respectively.

**This form with $k > 0$ and $0 < \eta < 1$ has been demonstrated to apply to most engineering materials, particularly for the plastic state.

***The rifling shown is so very shallow with respect to the thickness of the band; hence is neglected.

where I' is the moment of inertia of the beam

E is Young's modulus

ν is Poisson's ratio

More generally, if the external loading is a function of time, this equation should more appropriately be written

$$\frac{\partial^4 y(x,t)}{\partial x^4} = \frac{1-\nu^2}{EI'} p(x,t) \dots \dots \dots (1)$$

where $p(x,t)$ may be expressed in the form

$$p(x,t) = [a(x,t) + b(x,t) + c(x,t)] \Delta \alpha$$

and the quantities a , b , c are respectively the centrifugal, restoring and inertial contributions to $p(x,t)$ and $\Delta \alpha$ is the angular width of the beam as noted in Figure 1.

We now specialize the general differential equation (Eq. 1) to conform with the specific cases described earlier. In the next section, we shall solve these resulting explicit differential equations for the motion of the band and derive therefrom the general behavior of the band.

Case I: Static State - Elastic Behavior

In this case y and p are functions only of position x ; hence, the inertial contribution to the external loading is absent and remaining contribution $a(x)$ and $b(x)$ can be shown to be given by

$$a(x) = \frac{qD_0}{2}$$

$$b(x) = -\frac{2Eh}{D_0} y(x)$$

where q is the centrifugal loading per unit area, h is the beam thickness, and D_0 is the initial mean diameter of the band. It will also be obvious that the partial derivative

$$\frac{\partial^4 y(x,t)}{\partial x^4}$$

can be replaced with the complete derivative. Then Equation 1 can be shown to reduce to the form

$$\frac{d^4 y(x)}{dx^4} = \frac{(1-\nu^2)}{EI'} \left[\frac{qD_0}{2} - \frac{2Eh}{D_0} y(x) \right] \Delta \alpha \dots \dots \dots (2)$$

Case II: Dynamic State (Suddenly Applied Load) - Elastic Behavior

For this case, we observe that y and p are functions of both position x and time t , and it is necessary to include the inertial contribution in the loading term $p(x, t)$. It can accordingly be demonstrated that

$$a(x, t) = \frac{qD_0}{2}$$

$$b(x, t) = -\frac{2Eh}{D_0} y(x, t)$$

$$c(x, t) = -\frac{\rho}{g} \frac{D_0 h}{2} \frac{\partial^2 y(x, t)}{\partial t^2}$$

whence Equation 1 becomes

$$\frac{\partial^4 y(x, t)}{\partial x^4} = \frac{1-\nu^2}{EI'} \left[\frac{qD_0}{2} - \frac{2Eh}{D_0} y(x, t) - \frac{\rho D_0 h}{2g} \frac{\partial^2 y(x, t)}{\partial t^2} \right] \Delta \alpha \dots (3)$$

Case III: Dynamic State (Suddenly Applied Load) - Inelastic Behavior

Here we restrict our attention to a long band, i.e., a band of sufficient length so that end constraints, if present, do not significantly influence the maximum deflections of the band. Consequently, we note that in the critical region of the band, i.e., away from the ends, the loading term p and deflection y are functions only of time t and are independent of position x .

We further depart from the earlier simplifying conditions of elastic behavior and permit extensive plastic deformation of the band. In the present case, it is assumed that the material obeys the exponential true stress-natural strain law $\sigma = k\epsilon^\eta$ (for monotonically increasing σ). It will be recalled that such materials exhibit the so-called necking or instability phenomenon at a strain ϵ governed by the result $\epsilon = \eta$.

Within the scope of the above restrictions, it can be shown that

$$\frac{\partial^4 y(x, t)}{\partial x^4} = 0$$

$$a(x, t) = \frac{qD}{2}$$

$$b(x, t) = -kh \left[\ln \left(1 + \frac{2y(t)}{D_0} \right) \right]^\eta$$

$$c(x, t) = -\frac{\rho D h}{2g} \frac{d^2 y(t)}{dt^2}$$

where D is the instantaneous mean diameter of the band, i.e.,

$$D = D_0 \left[1 + \frac{2y}{D_0} \right]$$

Equation 1 may then be expressed as

$$0 = \frac{1-\nu^2}{EI'} \left\{ \frac{qD}{2} - kh \left[\ln \left(1 + \frac{2y(t)}{D_0} \right) \right]^\eta - \frac{\rho Dh}{2g} \frac{d^2 y(t)}{dt^2} \right\} \Delta a \quad \left(\frac{dy}{dt} > 0 \right) \quad \dots \dots \dots (4a)$$

Noting, then, that q may be written $\frac{1}{2} \frac{\rho h D}{g} \omega^2$ this becomes

$$0 = \left[1 + \frac{2y}{D_0} \right] \frac{D_0}{2} \omega^2 - \frac{2kg}{\rho D_0} \left\{ \frac{\left[\ln \left(1 + \frac{2y}{D_0} \right) \right]^\eta}{\left(1 + \frac{2y}{D_0} \right)} \right\} \frac{d^2 y(t)}{dt^2} \dots \dots \dots (4b) \quad \left(\frac{dy}{dt} > 0 \right)$$

Equations 2, 3 and 4 have been summarized in Table I, along with the appropriate boundary and initial conditions.

GENERAL ANALYSIS

We proceed now with the solution of Equations 2, 3 and 4 for the pertinent boundary conditions shown tabulated in Table I.

Case I:

Deflections

We had (Equation 2), (recalling that $I' = \frac{D_0 h^3}{24}$)

$$\frac{d^4 y(x)}{dx^4} + \frac{48(1-\nu^2)}{D_0^2 h^2} y(x) = \frac{12(1-\nu^2)}{Eh^3} q \quad \dots \dots \dots (2)$$

^aEquation (4a) is not the exact differential equation of equilibrium in that it is assumed $\bar{D} = D$ in the term $\frac{qD}{2}$, where \bar{D} is twice the centroidal radius of an elementary section.

Solution for the case of simply supported ends leads to the expression*

$$y(x) = + \frac{D_0^2 q}{4EH} \left[M \cos \frac{2\gamma x}{l} \cosh \frac{2\gamma x}{l} + N \sin \frac{2\gamma x}{l} \sinh \frac{2\gamma x}{l} + 1 \right] \quad (5)$$

where

$$M = - \frac{\cos \gamma \cosh \gamma}{\sin^2 \gamma \sinh^2 \gamma + \cos^2 \gamma \cosh^2 \gamma}$$

and

$$N = - \frac{\sin \gamma \sinh \gamma}{\sin^2 \gamma \sinh^2 \gamma + \cos^2 \gamma \cosh^2 \gamma}$$

and

$$\gamma = \sqrt[4]{\frac{12(1-\nu^2)}{D_0^2 h^2}} \frac{l}{2}$$

Stresses

The strains in the longitudinal and tangential directions at a distance ξ from the middle surface of the band are then given by

$$\epsilon_L = -\nu \frac{2y(x)}{D_0} - \xi \frac{d^2 y(x)}{dx^2}$$

and

$$\epsilon_T = \frac{2y(x)}{D_0}$$

The corresponding stresses follow directly, i.e.: (a)

$$\sigma_L = - \frac{E\xi}{1-\nu^2} \frac{d^2 y(x)}{dx^2}$$

and

$$\sigma_T = \frac{2Ey(x)}{D_0} - \frac{\nu E}{1-\nu^2} \xi \frac{d^2 y(x)}{dx^2}$$

*It should be noted here that x is measured from the center of the band.

The maximum value of the stresses occur at the band surface at mid-span and can be shown by appropriate substitution to be given by

$$\sigma_{L_{\max}} = \frac{\sqrt{3} D_0 q}{2(1-\nu^2)} \frac{\sin \gamma \sinh \gamma}{\sin^2 \gamma \sinh^2 \gamma + \cos^2 \gamma \cosh^2 \gamma}$$

and

$$\sigma_{T_{\max}} = \frac{D_0 q}{2h} \left[1 + \frac{\sqrt{3\nu}}{\sqrt{1-\nu^2}} \frac{\sin \gamma \sinh \gamma - \cos \gamma \cosh \gamma}{\sin^2 \gamma \sinh^2 \gamma + \cos^2 \gamma \cosh^2 \gamma} \right] \quad \dots \dots \dots (6)$$

To facilitate interpretation of Equation 6, it is convenient to normalize $\sigma_{L_{\max}}$ and $\sigma_{T_{\max}}$ with respect to the corresponding value obtained utilizing simple wide-beam theory and "boiler" theory, respectively. We consequently define the ratios S_L and S_T as follows:

$$S_L = \frac{\sigma_{L_{\max}}}{\sigma_{L_{\text{beam}}}}$$

and

$$S_T = \frac{\sigma_{T_{\max}}}{\sigma_{T_{\text{hoop}}}}$$

where $\sigma_{L_{\text{beam}}}$ is the stress computed using conventional (wide beam) theory, i.e.

$$\sigma_{L_{\text{beam}}} = \frac{3}{4} \frac{l^2}{h^2} q$$

and

$$\sigma_{T_{\text{hoop}}} = \frac{D_0}{2h} q.$$

Appropriate substitution then yields the following equation for S_L and S_T .

$$S_L = \frac{1}{\gamma^2} \frac{\sin \gamma \sinh \gamma}{\sin^2 \gamma \sinh^2 \gamma + \cos^2 \gamma \cosh^2 \gamma}$$

$$S_T = 1 + \frac{\left(\frac{\sqrt{3\nu}}{\sqrt{1-\nu^2}} \right) \sin \gamma \sinh \gamma - \cos \gamma \cosh \gamma}{\sin^2 \gamma \sinh^2 \gamma + \cos^2 \gamma \cosh^2 \gamma} \quad \dots \dots \dots (7)$$

These quantities, plotted in Figure 4* for $\nu = 0.3$, may be used as correction factors for determining the actual stresses in a band by multiplying the appropriate normalizing stress by the factor. For example, suppose a band such that S_l and S_r are 0 and 1.1 respectively; then, the tangential stress is the simply computed hoop or boiler stress multiplied by 1.1. Obviously, the longitudinal stress is zero in this case. (This merely means that the band is quite long, and behaves essentially like an unconstrained hoop.)

Case II:

We had (Equation 3)

$$\frac{\partial^4 y(x, t)}{\partial x^4} = \frac{1-\nu^2}{EI'} \left[\frac{qD_0}{2} - \frac{2Eh}{D_0} y(x, t) - \frac{\rho D_0 h}{2g} \frac{\partial^2 y(x, t)}{\partial t^2} \right] \Delta a \quad \dots (3)$$

Using the method of generalized coordinates** we write

$$y = \sum_{i=1}^{\infty} q_i \sin \frac{i\pi x}{l}$$

where q_i is the generalized coordinate and x is measured from the end of the band***. We form the potential and kinetic energies thusly:

$$P.E. = \frac{EI\pi^4}{4l^3} \sum_{i=1}^{\infty} i^4 q_i^2 + \frac{Eh\Delta a}{2D_0} \sum_{i=1}^{\infty} q_i^2$$

$$K.E. = \frac{\rho D_0 h \Delta a}{8g} \sum_{i=1}^{\infty} \dot{q}_i^2$$

Substitution into LaGrange's equation then yields the following differential equation for q_i :

$$\frac{d^2 q_i}{dt^2} + \frac{\pi^4}{l^4} \left(\frac{Egh^2}{12\rho} \right) \left[i^4 + 4 \left(\frac{2}{\pi} \right)^4 \gamma^4 \right] q_i = \frac{4g}{\rho D_0 h l} \frac{Q_i}{\Delta a}$$

where Q_i is the generalized force corresponding to the coordinate q_i .

In the present case, we assume an external running load (centrifugal loading) of intensity $q \frac{D_0}{2} \Delta a$ suddenly applied at time $t = 0$ and there-

*Some slight inaccuracy is introduced in the dashed region due to shear deformation of the beam. For length to thickness ratio greater than 5, however, this error is less than 10%.

**Timoshenko, S.; "Vibration Problems in Engineering". D. Van Nostrand Co., Inc., 2nd Ed., pp. 398-370, 1937.

***In Case I, x was measured from the midspan position.

after maintained constant. Under these conditions, Q_1 can be shown to be given by

$$Q_1 = -\frac{qD_0\Delta a\ell}{2i\pi} (\cos i\pi - 1).$$

The general solution then for this case may be written

$$y(x, t) = + \frac{qD_0\Delta a\ell^4}{EI'\pi^3} \sum_{i=1}^{\infty} \frac{[\cos(i\pi)-1][\cos p_i t - 1]}{i \left[i^4 + 4\left(\frac{2}{\pi}\right)^4 \gamma^4 \right]} \sin \frac{i\pi x}{\ell} \dots (8)$$

where

$$p_i^2 = \frac{\pi^4}{\ell^4} \left(\frac{Egh^2}{12\rho} \right) \left[i^4 + 4\left(\frac{2}{\pi}\right)^4 \gamma^4 \right]$$

Appropriate substitution into the stress-deflection equation (a) leads to the following maximum stress formulations at $x = \ell/2$, and $t = \pi/p_i$;

$$\sigma_{l_{\max}} = + \frac{24q\ell^2}{(1-\nu^2)h^2\pi^3} \sum_{i=1}^{\infty} \frac{i[1 - \cos i\pi]}{i \left[i^4 + 4\left(\frac{2}{\pi}\right)^4 \gamma^4 \right]} \sin \frac{i\pi}{2}$$

and

$$\begin{aligned} \sigma_{T_{\max}} = & + \frac{96q\ell^4}{D_0\pi^3h^3} \sum_{i=1}^{\infty} \frac{[1 - \cos(i\pi)]}{i \left[i^4 + 4\left(\frac{2}{\pi}\right)^4 \gamma^4 \right]} \sin \frac{i\pi}{2} \\ & + \frac{24q\ell^2\nu}{(1-\nu^2)h^2\pi^3} \sum_{i=1}^{\infty} \frac{i[1 - \cos i\pi]}{i \left[i^4 + 4\left(\frac{2}{\pi}\right)^4 \gamma^4 \right]} \sin \frac{i\pi}{2} \dots (9) \end{aligned}$$

Evaluation of Equation 9 and comparison with Equation 6 show that the stresses are just twice the former stresses. This is as should have been expected for the sudden loading of an elastic system. The curves of Figure 4 are therefore directly applicable, provided the normalization is recognized to have been taken in this case with respect to the dynamic loading stresses in a wide beam or simple hoop.

Case III:

Finally, we had (Equation 4b)

$$0 = \left[1 + \frac{2y}{D_0} \right] \frac{D_0}{2} \omega^2 - \frac{2kg}{\rho D_0} \left\{ \frac{\left[\ln \left(1 + \frac{2y}{D_0} \right) \right]^\eta}{\left(1 + \frac{2y}{D_0} \right)} \right\} - \frac{d^2 y(t)}{dt^2} \quad \dots (4b)$$

$$\text{for } \frac{dy(t)}{dt} > 0$$

Letting $U = \left(1 + \frac{2y}{D_0} \right)$, and rearranging, this becomes

$$\frac{d^2 U}{dt^2} + \frac{4kg}{\rho D_0^2} \frac{\left[\ln U \right]^\eta}{U} - U \omega^2 = 0 \quad \dots (4c)$$

for $0 < t < t_0$ where t_0 is the first time for which $\frac{dU}{dt} = 0$.

The complete solution of this non-linear equation is not readily obtained by ordinary methods; however, by single integration, the velocity-displacement relation is readily obtained and considerable insight to the characteristic behavior of the band may be derived therefrom. We thus obtain by the initial integration of Equation 4c (with the initial condition

$$\frac{dU}{dt} = 0 \text{ at } U = 1)$$

$$\frac{1}{\omega} \frac{dU}{dt} = \sqrt{(U^2 - 1) - \frac{2}{A} \frac{\left[\ln U \right]^\eta}{(\eta + 1)}} \quad \dots (10)$$

$$\text{for } 0 < t < t_0$$

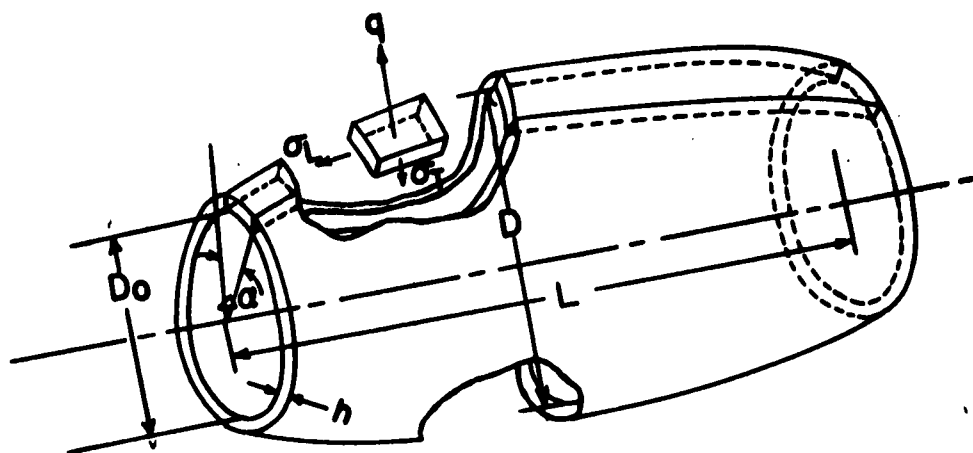
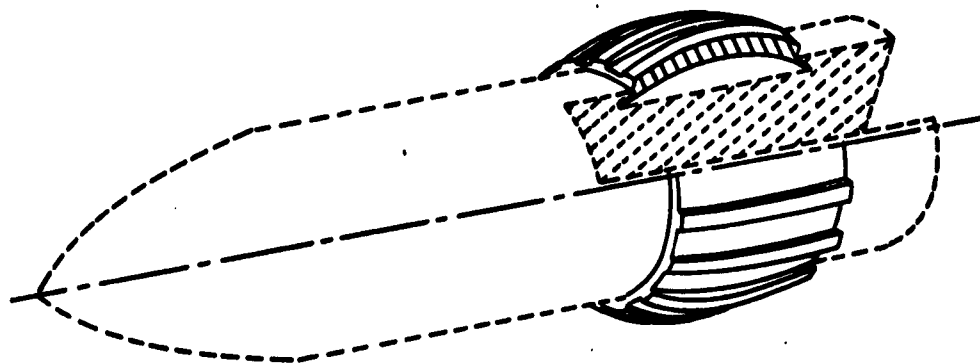
where the loading term A is defined as follows:

$$A = \frac{1}{4} \frac{\rho D_0^2 \omega^2}{gk}$$

A plot of this velocity-displacement relation is shown in Figure 5 for a fixed value of η (i.e., a given material) and for a range of values of the load parameter A . The arrows indicate the direction of increasing time. Only the plastic behavior of the band is presented. (The dash lines

indicate the start of elastic vibratory behavior, but we shall not discuss this aspect of the band motion here.*) It will be noted that for small values of the load parameter Λ (i.e., $\Lambda < \Lambda_{crit}$) the band expands but eventually slows down to a halt at some finite value of displacement U_{max} . On the other hand, at higher values of Λ (i.e., $\Lambda \geq \Lambda_{crit}$), the band becomes unstable and extends indefinitely until fracture occurs. This instability is attributable to the necking phenomenon discussed earlier. We designate the value of U_{max} attained at Λ_{crit} as U_{crit} . In Figure 6, we plot the displacement U_{max} against the load parameter Λ for different values of η . The end points of these curves shown by the dash line represent the critical conditions Λ_{crit} and U_{crit} . In Figure 7, we have plotted this critical load parameter for different materials as defined by the stress-strain relation $\sigma = k\epsilon^n$. We recognize in Figure 7 that for loads or speeds less than Λ_{crit} the band is retained; for higher loads or speeds, failure can be anticipated.

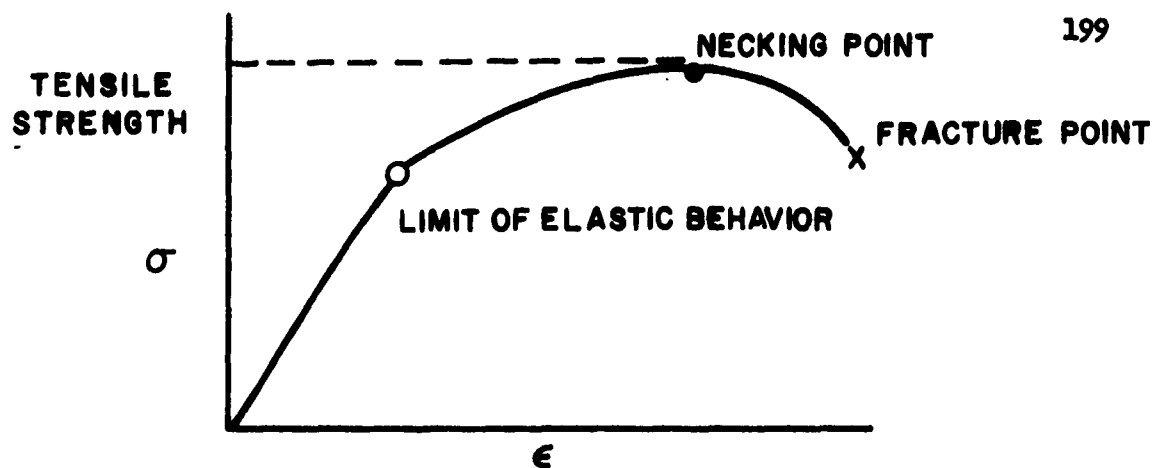
*For details, see NAL Report No. 700/532, "Stresses Beyond the Yield Point in: a) A Long Rotating Band Loaded by a Suddenly Applied Centrifugal Force, b) A Long Thin Cylinder Loaded by a Suddenly Applied Internal Pressure."



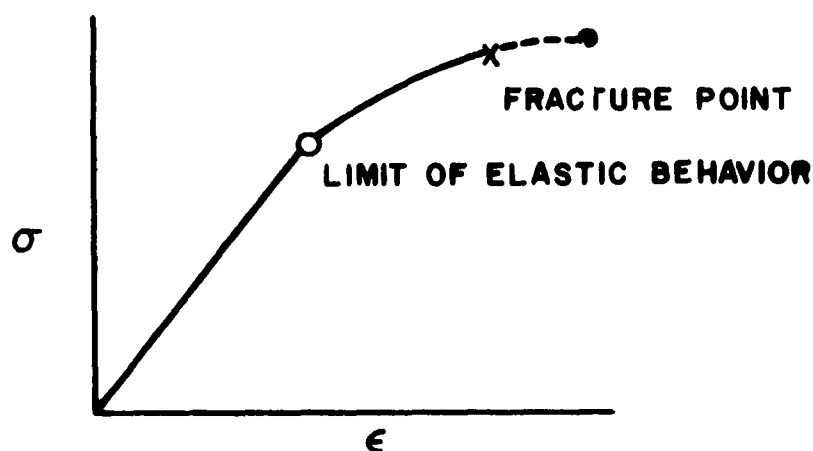
ROTATING BAND GEOMETRY

**A.M. 1820
5-21-56**

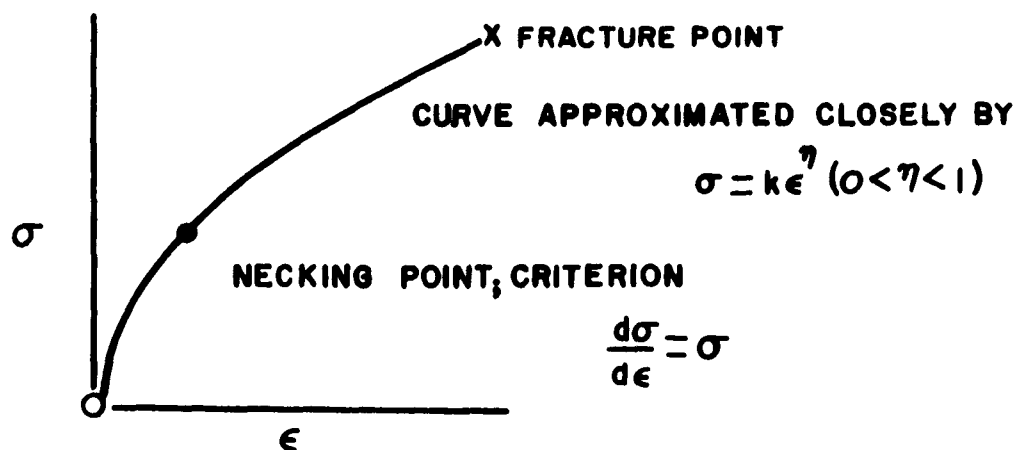
FIGURE 1



a) ORDINARY ENGINEERING STRESS-STRAIN CURVE SHOWING NECKING



b) ORDINARY ENGINEERING STRESS-STRAIN CURVE - NO NECKING



c) TRUE STRESS-TRUE STRAIN CURVE

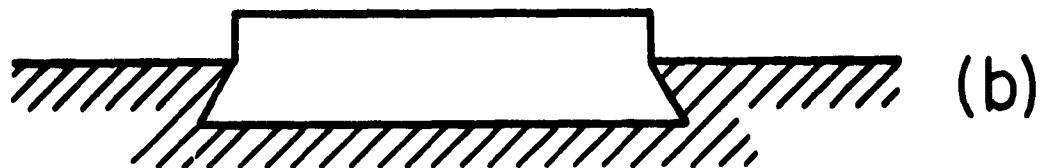
STRESS-STRAIN CHARACTERISTICS OF BAND MATERIALS

AM 1821
5-21-56

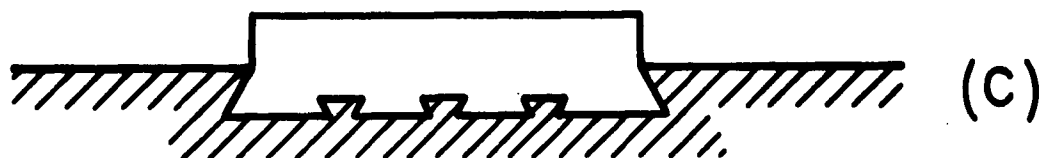
FIGURE 2



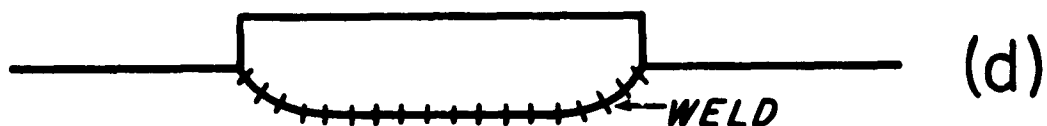
SIMPLE SWAGED ON BAND



UNDERCUT SEAT — SWAGED ON BAND



DOVE-TAIL SEAT — CAST BAND



WELDED OVERLAY BAND

METHODS OF BONDING BAND TO SHELL

A M. 1822
5-21-56

FIGURE 3

LEGEND

$$S_L = \frac{\sigma_L \text{ SHELL}}{\sigma_L \text{ BEAM}}$$

$$S_T = \frac{\sigma_T \text{ SHELL}}{\sigma_T \text{ HOOP}}$$

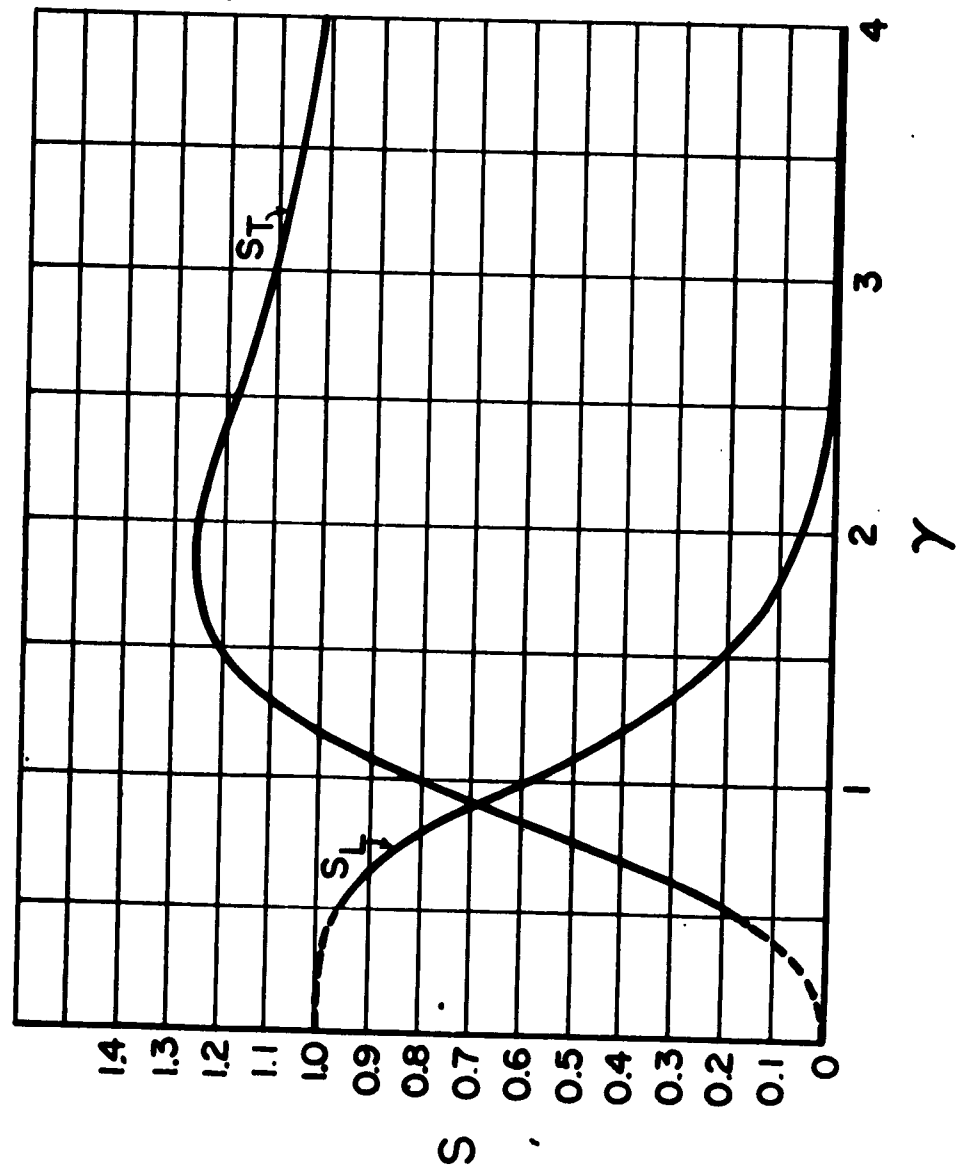
WHERE

σ_L SHELL = MAX. LONGITUDINAL STRESS IN ROTATIONALLY SYMMETRIC BAND

σ_L BEAM = MAX. LONGITUDINAL STRESS IN BEAM HAVING SAME APPLICABLE DIMENSIONS AS BAND

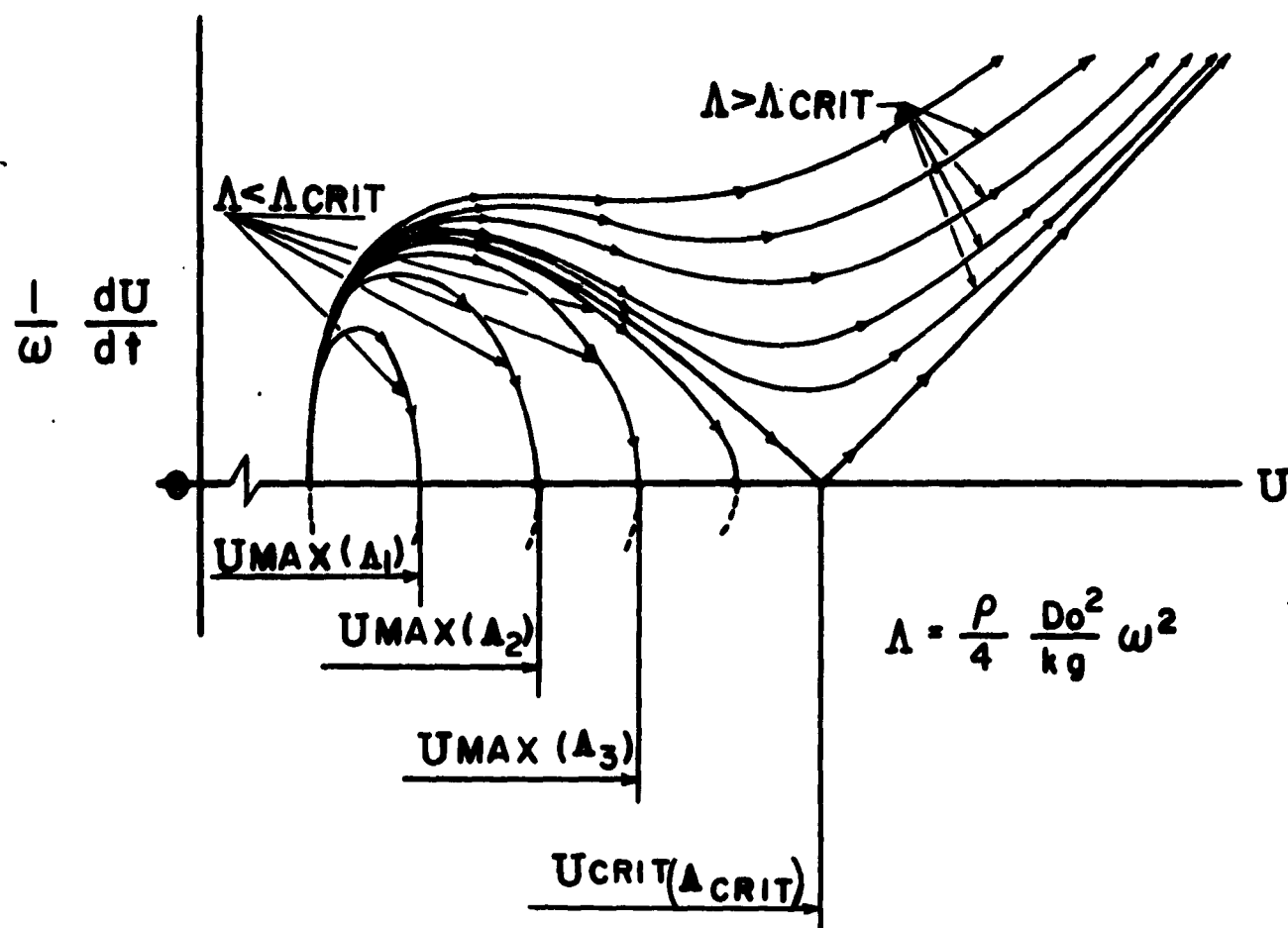
σ_L SHELL = MAX. TANGENTIAL STRESS IN ROTATIONALLY SYMMETRIC BAND

σ_L HOOP = MAX. TANGENTIAL STRESS IN ROTATIONALLY SYMMETRIC BAND ASSUMING NO END CONSTRAINT



MAXIMUM ELASTIC STRESSES IN SMOOTH SIMPLY SUPPORTED ROTATING BANDS

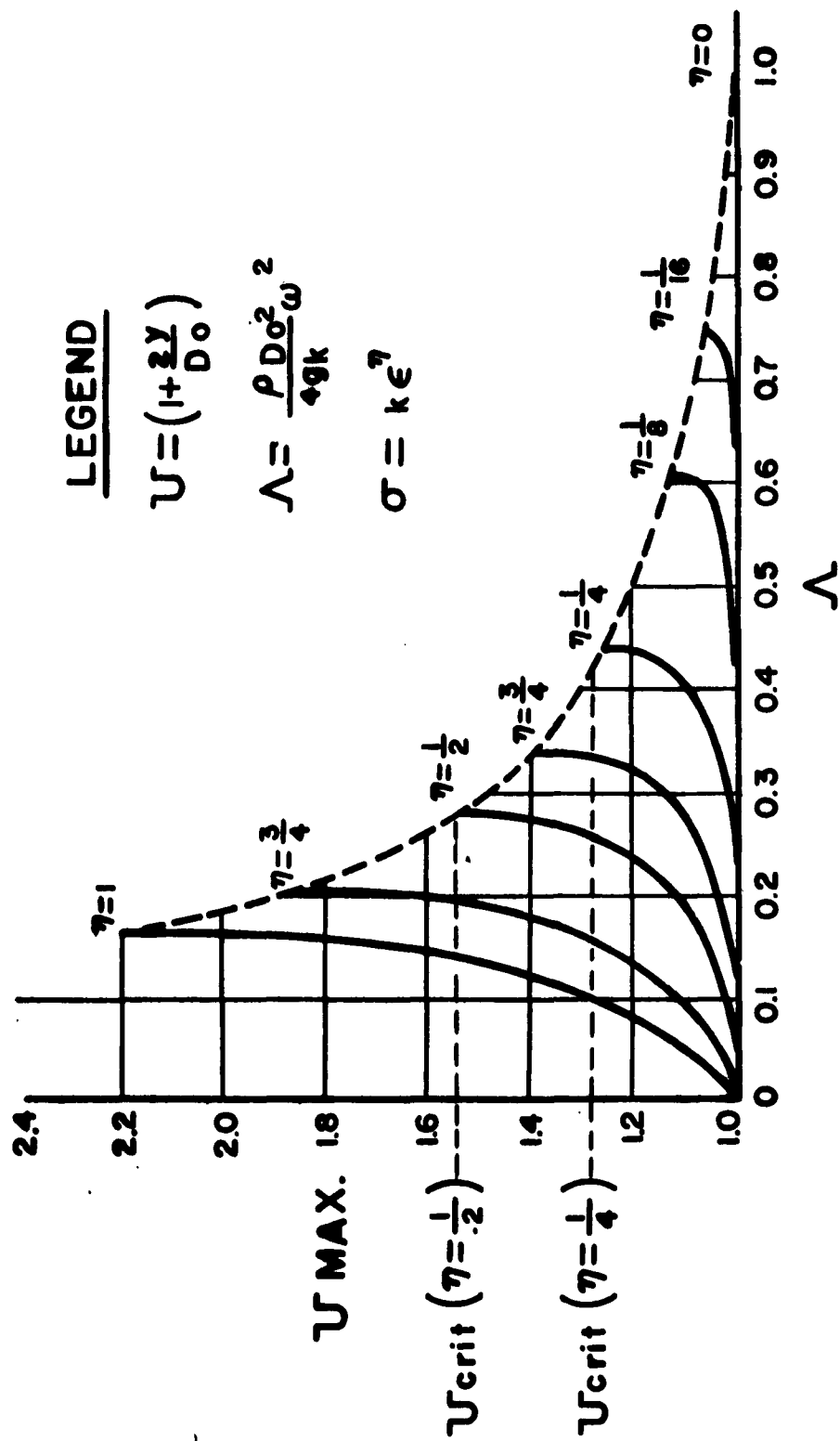
$$\gamma = \sqrt{\frac{12(1-\nu^2)}{D^2 h^2}} \frac{l}{2}$$



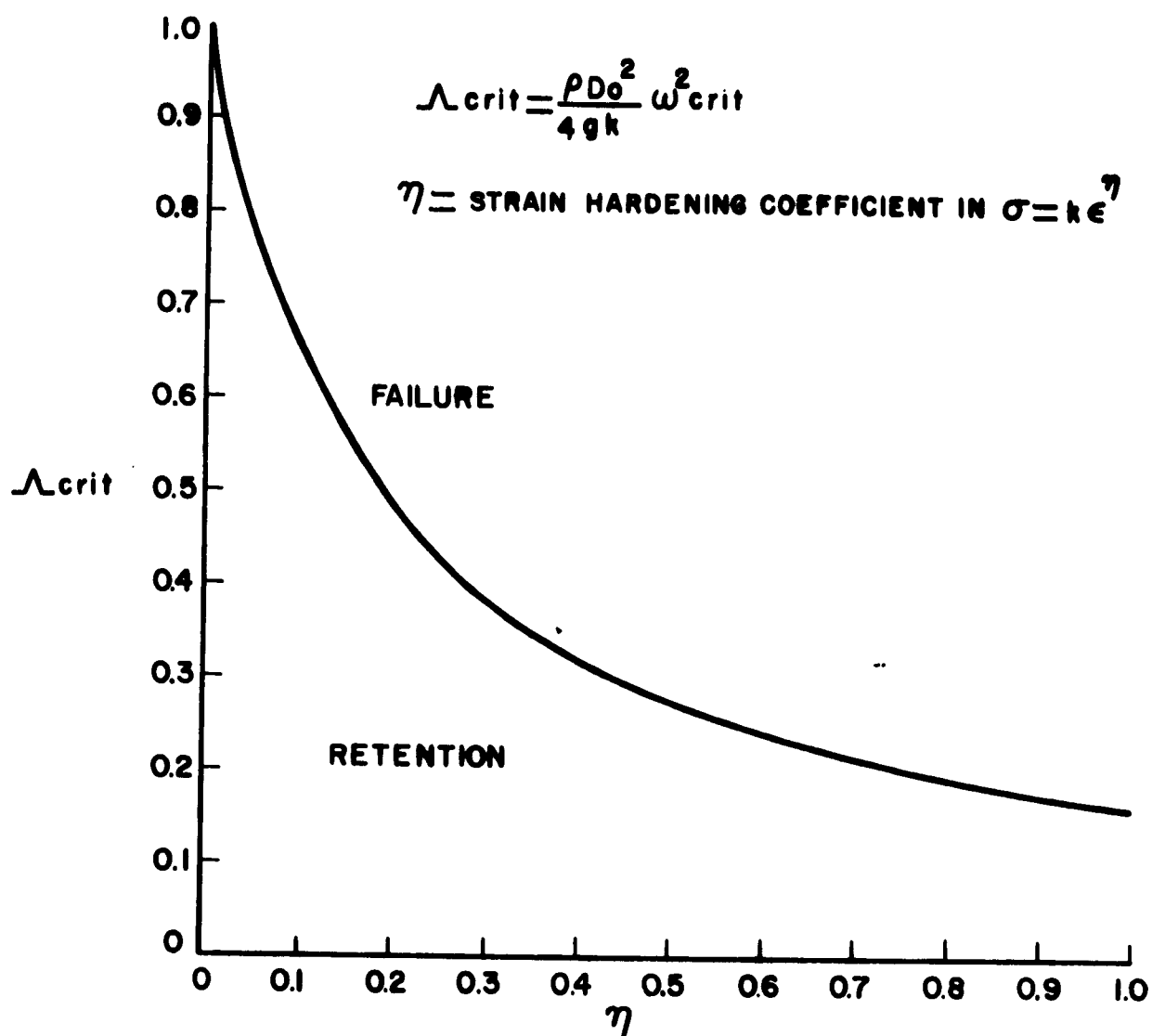
TYPICAL VELOCITY - DISPLACEMENT CURVES
(FOR GIVEN MATERIAL)

A.M. 1824
5-21-56

FIGURE 5



RELATION BETWEEN MAXIMUM RADIAL DISPLACEMENT $U_{MAX.}$
OF BAND AND LOAD PARAMETER Λ FOR VARIOUS VALUES
OF THE STRAIN HARDENING COEFFICIENT η



VARIATION OF THE CRITICAL LOADING (OR SPEED) PARAMETER Λ
WITH STRAIN HARDENING COEFFICIENT η

A.M. 1826
5-21-56

FIGURE 7

THE EFFECT OF PARTICLE SUSPENSIONS ON THE FLOW OF A GAS

Hugh N. Brown*

A suspension of small particles in a gas may produce important changes in the flow of that gas by virtue of the drag forces exerted on the particles and of the exchange of heat between the particles and the gas. Of particular interest is the propagation of a shock wave in such a medium.

For simplicity, let us assume that the particles are spherical and of uniform size. The drag forces and heat transfer properties can then presumably be calculated from experimental data on single spheres. (Refs. 1 and 2) This assumption will be most questionable for large dust concentrations and/or high Mach numbers. If the dust concentration is not too high, the effect of particle collisions may be ignored and the volume occupied by the particles neglected. In this case, the equations for plane flow may be written as

$$n_t + un_x + nu_x = 0, \quad (1)$$

$$u_t + uu_x - \frac{D}{m} = 0, \quad (2)$$

$$\rho_t + v\rho_x + \rho v_x = 0, \quad (3)$$

$$\rho(v_t + vv_x) + p_x + nD = 0, \quad (4)$$

$$mc_p(T_t + uT_x) + K(T - \theta) = 0, \quad (5)$$

$$\rho\theta(S_t + vS_x) - nK(T - \theta) = 0. \quad (6)$$

The symbols used above are

n = number of particles per unit volume,

u = velocity of dust particles,

D = drag force on a single particle,

m = mass of a single particle,

ρ = gas density,

v = gas velocity,

p = gas pressure,

c_p = specific heat of a particle,

T = dust particle temperature,

K = effective heat transfer coefficient,

θ = gas temperature,

S = gas entropy.

* Ballistic Research Laboratories

Subscripts x and t denote differentiation with respect to x and t . The gas will, in the following, be assumed to be an ideal polytropic gas whose equation of state is

$$p = A e^{\frac{s}{c_v}} \rho^\gamma = R \rho \theta$$

where c_v is its specific heat at constant volume, R is gas constant, and γ is the ratio of specific heats.

Equations (1) and (3) are, of course, simply mass conservation equations for the dust and gas respectively. (2) equates the rate of change of momentum of a particle along its streamline to the drag force D acting on it. Similarly, (4) relates the rate of change of gas momentum along a gas streamline to the pressure gradient force and to the reaction of the dust on the gas caused by the drag. Equation (5) states that the rate of loss of heat by a particle along its streamline is proportional to the difference between the mean internal particle temperature and the surrounding gas temperature. The last relation, (6), simply equates the heat given up by the particles in a unit volume to that gained by the gas in the same volume.

These equations can be transformed into the characteristic form (Ref. 3). Let σ be a characteristic curve parameter. Then the characteristic equations C and compatibility equations Γ are

$$\begin{cases} C+ : x_\sigma - (v + c) t_\sigma = 0, \\ \Gamma+ : \rho c v_\sigma + p_\sigma + n \left[Dc - K(\gamma - 1) (T - \theta) \right] t_\sigma = 0, \end{cases} \quad (8)$$

$$(9)$$

$$\begin{cases} C- : x_\sigma - (v - c) t_\sigma = 0, \\ \Gamma- : \rho c v_\sigma - p_\sigma + n \left[Dc + K(\gamma - 1) (T - \theta) \right] t_\sigma = 0, \end{cases} \quad (10)$$

$$(11)$$

$$\begin{cases} C_g : x_\sigma - v t_\sigma = 0, \\ \Gamma_g : s_\sigma - \frac{nK}{\rho\theta} (T - \theta) t_\sigma = 0, \end{cases} \quad (12)$$

$$(13)$$

$$\begin{cases} C_p : x_\sigma - u t_\sigma = 0, \\ \Gamma_p : \begin{cases} u_\sigma - \frac{D}{n} t_\sigma = 0, \\ T_\sigma + \frac{K}{mc_p} (T - \theta) t_\sigma = 0, \\ n_\sigma + n u_x t_\sigma = 0 \end{cases} \end{cases} \quad (14)$$

$$(15)$$

$$(16)$$

$$(17)$$

Here, c is the velocity of sound defined by $c^2 = \left(\frac{\partial p}{\partial \rho}\right)_{S = \text{const.}}$

Note that, unlike the others, equation (17) cannot be reduced to unidirectional derivatives. This is a consequence of the two-fold nature of the particle path $x_0 - ut_0 = 0$, i.e., the parabolic nature of this path.

Let us apply the preceding results to a specific flow problem. Consider the case of a plane, step function shock in free air impinging upon a semi-infinite mass of stationary air in which dust particles are uniformly distributed. In the mixture, the shock-front jump conditions for the air variables will be the same as in pure air. The dust concentration n , velocity u , and temperature T will be taken to be continuous through the front, since drag forces and heat transfer rates remain finite through the front. The conditions to be imposed at a shock front in the mixture are, therefore, for initially stationary air,

$$\frac{p_1}{p_0} = 1 + \frac{2\gamma}{\gamma + 1} \left(\frac{U^2}{c_0^2} - 1 \right), \quad (18)$$

$$\frac{v_1}{c_0} = \frac{2}{\gamma + 1} \left(\frac{U}{c_0} - \frac{c_0}{U} \right), \quad (19)$$

$$\frac{\rho_0}{\rho_1} = 1 - \frac{v_1}{U}, \quad (20)$$

$$u_1 = u_0 = 0, \quad (21)$$

$$n_1 = n_0, \quad (22)$$

$$T_1 = T_0, \quad (23)$$

where subscripts 0 and 1 refer to quantities ahead of and just behind the shock front respectively, and U refers to the shock-front velocity.

Figure 1 gives the flow process in the x, t plane. For $t \leq 0$, the region to the left of the origin Q contains pure air, while that to the right contains an air-dust mixture at the same temperature, pressure, and gas density as the pure air. The path of the incident shock front is along the shock-line. For $t \geq 0$, the air-mixture boundary, originally at $x = 0$, begins to move along the dust streamline C_p through Q , while the shock velocity begins to change steadily due to the influence of the dust.

Consider a point A on the shock line as shown. The unknowns here may be approximated by use of the jump conditions and the relation (9) applied along

the forward sound path C+ drawn to A from a point B on the x-axis in the dust-free air. Equation (9) shows that, under the assumed conditions, the shock strength initially decreases from Q to A. In fact, $\left(\frac{dU}{dt}\right)_Q$ may be calculated from (8) and (9) and the shock conditions. It must be remembered, in integrating (9), that $n = 0$ to the left of the air-mixture boundary. Hence, from (8) and (9),

$$\rho_Q c_Q (v_A - v_B) + (p_A - p_B) = -n_Q \left[D_Q c_Q - K_Q (\gamma - 1) (T_Q - \theta_Q) \right] \frac{U_Q}{v_Q + c_Q} \delta t. \quad (24)$$

Here, ρ_Q , c_Q , v_Q , etc. are the values at the origin appropriate to the initial shock velocity U_Q .

Now, since the incident shock is a step function, $v_B = v_Q$, etc. Therefore, the differences above may also be expressed in terms of the rate of change of U along the transmitted-shock line from Q to A:

$$v_A - v_B = v_A - v_Q = \left(\frac{dv_1}{dU} \right)_Q \left(\frac{dU}{dt} \right)_Q \delta t, \quad \text{approximately,} \quad (25)$$

$$p_A - p_B = p_A - p_Q = \left(\frac{dp_1}{dU} \right)_Q \left(\frac{dU}{dt} \right)_Q \delta t, \quad \text{approximately,} \quad (26)$$

where $\frac{dv_1}{dU}$ and $\frac{dp_1}{dU}$ are evaluated from (18) and (19). Substituting these expressions into (24), we find that

$$\left(\frac{dU}{dt} \right)_Q = - \frac{U_Q}{v_Q + c_Q} \frac{n_Q \left[D_Q c_Q - K_Q (\gamma - 1) (T_Q - \theta_Q) \right]}{\rho_Q c_Q \left(\frac{dv_1}{dU} \right)_Q + \left(\frac{dp_1}{dU} \right)_Q}. \quad (27)$$

Now since T is continuous through the shock front, according to (23), $T_0 = T_Q < \theta_Q$ and so $\left(\frac{dU}{dt} \right)_Q$ is negative.

For a typical case, let us assume a dust particle radius of $a = 10^{-4}$ cm, a dust density (n_m) equal to that of the undisturbed air, ρ_0 , and incident shock velocity of 1.4 c (corresponding to a 1.12 atmosphere overpressure). Taking suitable values for air viscosity, specific heat, dust thermal conductivity, etc., it is found that

$$\frac{1}{U_Q} \left(\frac{dU}{dt} \right)_Q = -0.014/\mu\text{sec.}$$

Thus, the shock relaxation time is of the order of 70 μsec .

An idea of the early behavior of the flow may be obtained from a first-order series approximation. Expanding the shock velocity as a function of time in a series

$$U = U_Q + \sum_{\nu=1}^{\infty} U_{\nu} t^{\nu}$$

and the dependent variables in series such as

$$v(x,t) = \sum_{\mu\nu} v_{\mu\nu} t^{\mu} x^{\nu}$$

The equations of flow, (1) - (6), may be solved correctly to first power terms in x and t . It is necessary to employ different series in each of the flow regions I, II, and III indicated in Figure 1, imposing the initial and boundary conditions in each domain. The flow in domain IV is known.

The value of U_1 so obtained is the same as $\left(\frac{dU}{dt}\right)_Q$ determined above from the characteristic equations. For a given small time δt after the shock enters the mixture, the first-order solutions give the results shown in Figure 2. The numerical values indicated are for the same example mentioned previously; i.e., $a = 10^{-4}$ cm, $U_Q = 1.4 c_0$, $n_0 m = \rho_0$. The ordinates are distorted for the sake of clarity.

It is seen from these curves that, at the origin, the pressure and density increase to a value greater than that in the incident shock even though the shock front has decayed in strength. Clearly, a compression wave is set up which will travel backward into the shocked pure air, eventually developing into a second finite amplitude reflected shock at a point near the backward sound path C- through Q. The flow up to this point can be calculated once the solutions on the air-mixture boundary $C_{P,Q}$ are known, since all the backward characteristics extending into the pure air region are straight. The point of origin of the reflected shock may be estimated by finding the limiting point of intersection of an arbitrary C- with the C- line through Q using the first order approximation already obtained. That is, for a given time δt , the C- line originating on the air-mixture boundary at E is extended to its intersection with C-Q as shown in Fig. 1.

The limiting position of this intersection is then determined when δt approaches zero. Provided that higher order terms do not change the result too radically, it appears that the reflected shock forms far enough from the origin that it can be ignored while starting a numerical integration of the problem. For example, in the special case already considered, the estimated point of origin of the second shock is at $t \approx 40 \mu\text{sec}$ and $x \approx 0.7$ cm, whereas the time and space

increments used in a numerical solution should be less than 2 μ sec and .035 cm respectively.

Hence, a numerical solution to this problem might proceed as indicated in Figure 3, which illustrates a finite difference scheme which could be used in the mixture region. Assuming that all quantities are known as a function of x at a certain time t , the solution may be advanced to $t + \delta t$ by choosing a point A on $t + \delta t$ and extending the four characteristic paths, C_+ , C_- , C_+ , and C_- back to intersect the line $t = \text{constant}$ at the points B, D, E, F. These four unknown values of x plus the six unknown dependent variables at A may be approximated by solving the ten finite difference equations based on equations (8) through (17). Of course, modifications must be made whenever one of the characteristics intersects the air-mixture boundary or the shock line. If, for instance, point A is on the shock line, only equations (8) and (9) need be used in conjunction with the shock-front jump conditions.

An alternative scheme would be to replace the independent variable x by some quantity Z , say, which could be the mass of the gas or of the dust contained between a fixed streamline and the one through an arbitrary point (x, t) . Then Z is constant along a streamline so that, in the Z, t plane, the particular streamlines in question are straight, vertical lines. Thus, the integration net could be simplified without greatly complicating the remaining characteristics.

For the case of a plane, step shock incident upon the mixture, it is conceivable that an asymptotic condition might be approached wherein a wave of constant profile propagates into the mixture at a constant velocity. (Ref. 4) A consideration of the requirements of conservation of mass, momentum, and energy across such a wave shows that, for sufficiently large asymptotic pressure, a wave consisting of an air shock followed by a continuous pressure rise to the final total pressure would be possible. The continuous part of the wave would correspond to the interval required for the dust to come to thermal and dynamic equilibrium with the gas. The strength of the "air shock" would be such that its velocity would be equal to the velocity of the wave as a whole as determined by the total pressure rise, thereby maintaining a constant profile. Whether the equations of motion discussed above actually lead to this situation is not known.

For total pressure rises less than a certain amount, the velocity of a constant profile wave would have to be less than c_0 , the ambient sound speed. Hence, no preceding air shock would be possible, as in the foregoing case, and the wave cannot maintain its shape; the wave would probably be a continuous pressure rise whose "thickness" increases with time.

Under the conditions of the numerical example given previously, the critical overpressure in the mixture is 1.51 atmospheres which corresponds to an incident, pure air shock of 1.26 atmospheres. The assumed pure air shock was only 1.12 atmospheres, which means that the asymptotic wave in the mixture would be continuous; the discontinuous "air shock" front would decay completely to zero strength.

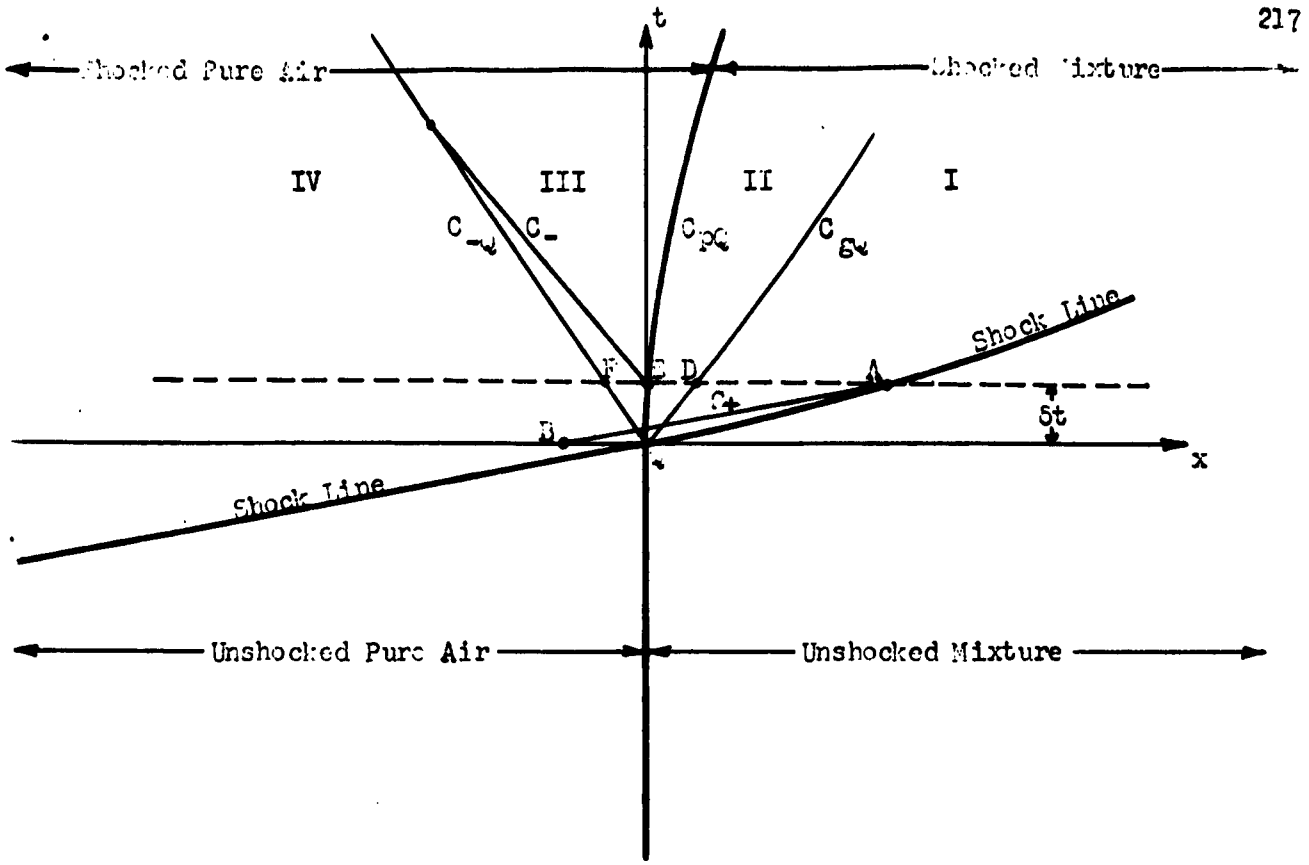


Figure 1.

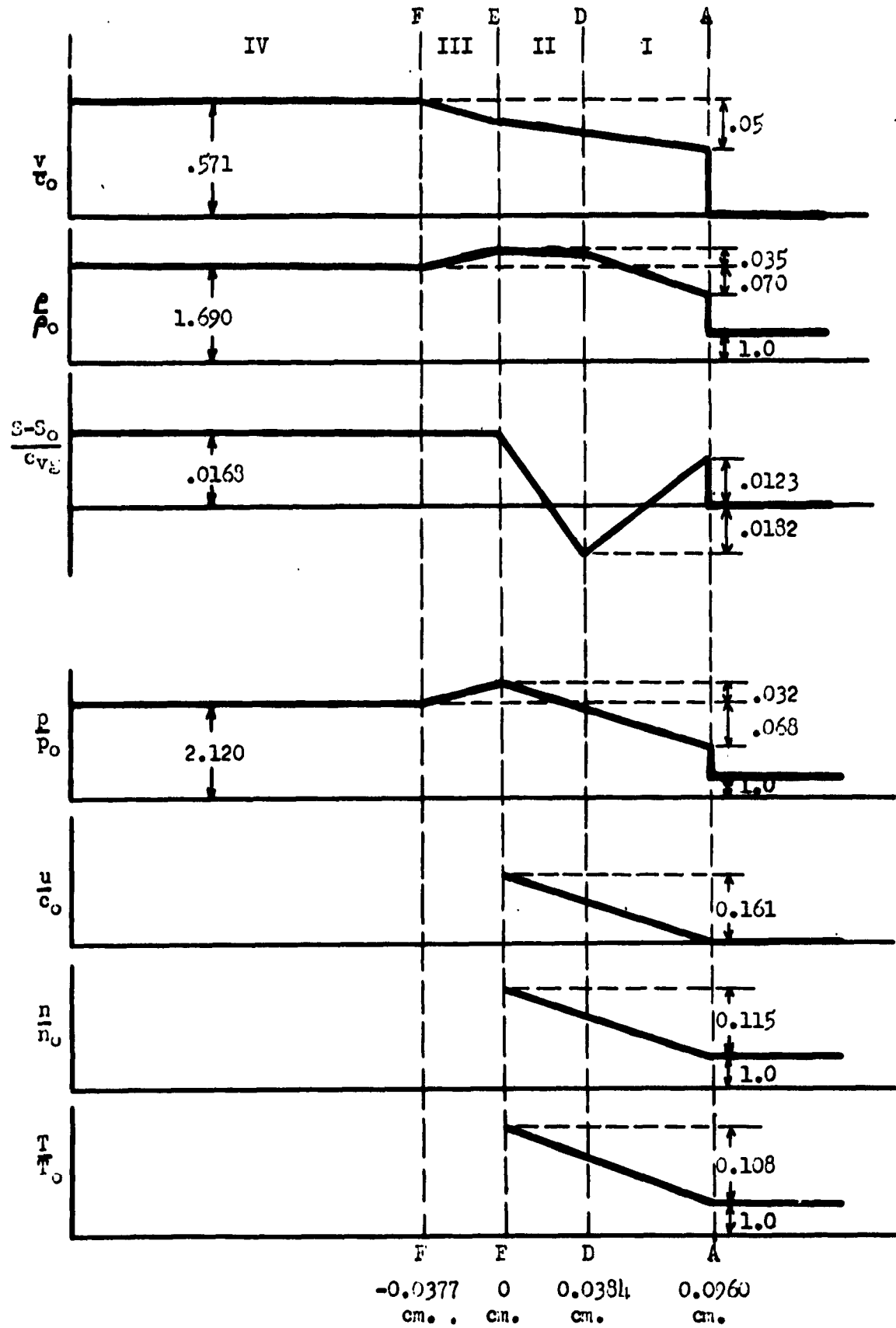


Figure 2.

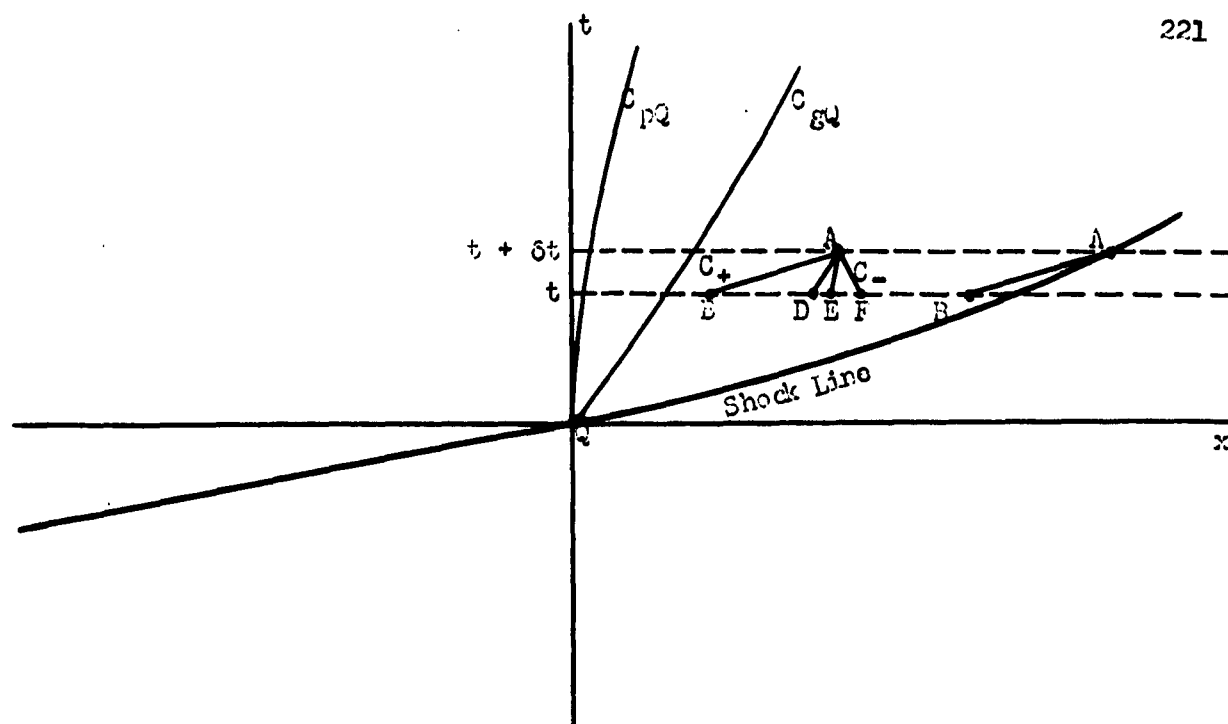


Figure 3.

REFERENCES

1. S. Goldstein, "Modern Developments in Fluid Dynamics," Vol. I, Oxford University Press, London, 1952.
2. Y. S. Tang, J. M. Duncan, and H. E. Schwyer, "Heat and Momentum Transfer between a Spherical Particle and Air Streams," NACA Technical Note 2867, Washington, 1953.
3. R. Courant and H. O. Friedrichs, "Supersonic Flow and Shock Waves," Vol. I. Interscience Publishers, Inc., New York, 1948.
4. L. H. Thomas, "An Approach to the Theory of Shock Waves in Air-Sand Mixtures." BRL Memorandum Report No. 871, Ballistics Research Laboratories, Aberdeen Proving Ground, Maryland, February, 1955.

WATERTOWN ARSENAL LABORATORIES

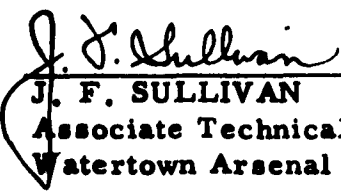
28 February 1956

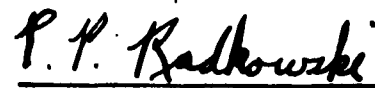
**DETERMINATION OF ELASTIC STRESSES
IN CHAMBER SECTION OF RECOILLESS RIFLES****ABSTRACT**

From the results presented in this report one may, in general, determine the elastic stresses, strains and displacements in arbitrary, but rotationally symmetric, thin shells. The linear theory of thin shells is used in this development. This theory is sufficiently described in the appendices to indicate how all the results are obtained. As an illustrative example, the surface stress distribution is presented for an idealized bell-shaped chamber section (106MM T137) of recoilless rifles.

Membrane stresses, given by a solution which neglects the shearing stresses and bending moments, are presented for comparison purposes.

APPROVED:


J. F. SULLIVAN
Associate Technical Director
Watertown Arsenal Laboratories


P. P. RADKOWSKI
Mathematician



RUSSELL F. SCOTT, Jr.
Major, Ord Corps
Director
Watertown Arsenal Laboratories

TABLE OF CONTENTS

	Page
Abstract	
I. Introduction.....	229
II. Summary of Formulae, Conventions and Notations.....	230
A. Geometry.....	230
B. Notations and Conventions for the Strains, Stresses and Displacements.....	232
C. Solutions of the Basic Differential Equation.....	234
D. Membrane Solution.....	235
III. Application of Results to Bell-Shaped Chamber Section....	236
A. Geometry.....	236
B. Loading Conditions.....	238
C. Solution (Method of Specifying the Constants).....	239
IV. Stress Distribution in the 106MM T 137 (Bell-Shaped) Chamber Section.....	239
Figure 5 - Circumferential Surface Stresses.....	243
Figure 6 - Meridional Surface Stresses.....	244
Figure 7 - Membrane Stresses.....	245

APPENDICES*

Introduction.....

Appendix

A	Finite Deformation.....
A-I	Assumptions of Thin-Shell Theory.....
A-II	Geometry of a Shell.....
A-III	Stress Resultants and Couples.....
A-IV	Conditions of Equilibrium.....
A-V	Displacements and the Analysis of Strain.....
A-VI	Stress-Strain Relations.....
A-VII	Compatibility Equation.....
B.	Linearized (Small Deformation) Theory.....
B-I	Assumptions.....
B-II	Summary of Results.....
B-III	Basic Equations as a Complex Differential Equation.....

*These appendices are given in WAL Report No. 731/407.

Table of Contents (Continued)		Page
Appendix		
C	Asymptotic Solutions of the Complex Differential Equation.....	
C-I	Asymptotic Integration.....	
C-II	Homogeneous Solution of the Complex Differential Equation.....	
C-III	Particular Solution of the Complex Differential Equation.....	
Bibliography.....		247

WATERTOWN ARSENAL LABORATORIES

I. INTRODUCTION

A considerable amount of effort has been made in recent years towards lighter ordnance materiel. In many cases, this has resulted in making component parts, such as gun tubes and chamber sections, thinner.

It is well known that the maximum stresses in tubes or chamber sections will, in general, increase as the thickness with respect to a reference radius decreases. Thus, it is useful to know the stress distribution, a priori, in these component parts so that under- as well as over-designing may be avoided. In this report mathematical results are given which may be used to determine such stress distributions in thin, elastic, isotropic shells ⁽¹⁾ which are axisymmetrically loaded, are of known axisymmetrical shape, and have small deformations.

While much work has been done on the elastic theory of shells, ⁽²⁾ the greatest progress in the development of its application has been accomplished only in the past few years. Most previous applications ⁽³⁾ have been of the membrane ⁽⁴⁾ type, where bending and shearing stresses have been neglected. This latter analysis, in general, is theoretically valid only for paper-thin shells of revolution (i. e., paper-thin in comparison to the least radius of curvature). However in many instances this analysis does give sufficiently accurate results for thin shells which are not paper-thin. In the case of chamber sections of recoilless rifles the membrane solution is questionable, for here the curvature changes sharply and the chamber wall is not paper-thin.

In this report a more refined thin-shell theory is applied to determine the stress distribution occurring in chamber sections of recoilless rifles. This thin-shell theory ⁽⁴⁾ is presented in the appendices. A solution of the equations derived from this theory is presented in Appendix C and is valid for many types of thin shells. (These appendices are given in WAL Report No. 731/407.)

⁽¹⁾ A shell is said to be thin if its thickness h is small in comparison to its least radius of curvature.

⁽²⁾ An exact three-dimensional analysis of thin shells, generally speaking, is not practical, because a thin-shell analysis is usually more expedient and usually gives answers which are sufficiently accurate for their intended purposes.

⁽³⁾ Whether or not a shell is a membrane depends, not only on the stress-free form of the shell, but also on the nature of the load.

⁽⁴⁾ The appendices list the conditions, as formulated by E. Reissner, of thin-shell theory.

The solutions⁽¹⁾ for sections of conical, cylindrical, and toroidal (donut shape) shells are extracted from the appendix and are presented more explicitly in the body of this report. These solutions may be used for determining the stresses in conical, cylindrical and bell-shaped chamber sections. The case of the bell-shaped chamber section is considered here in some detail (the 106MM T137 chamber section was chosen as an example).

One of the great values of thin shell theory (linear) is that, under certain restrictions, component sections, such as cones, tori, etc., can be considered separately for analysis purposes and then pieced together. The results of the analysis for each component section can be written down as the sum of a) terms which include the loading conditions on the surface of the shell (called the particular solution) and b) terms which are used to satisfy the end or junction conditions (called the homogeneous solution).

II. SUMMARY OF FORMULAE, CONVENTIONS AND NOTATIONS

In this section, a summary is made of results, gathered in the Appendix, that are necessary for calculating stresses, strains and displacements in shells of various shapes. In particular, these results may be applied to determine the stress distribution occurring in various types of chamber sections. These results are based on a linear theory of shells, which is sufficiently described in the appendices of Section II. The information that is of importance in applying the contents is the geometry of the shell, loading and end conditions. This application is illustrated in Section III for bell-shaped chamber sections by means of a numerical example in Section IV.

A. Geometry:

The middle surface of a shell, illustrated in Figure 1, can be represented by

$$r = r(\xi), \quad z = z(\xi),$$

so that ξ together with the angle θ in the (x, y) plane determine a point on the middle surface. It is convenient to define ξ in terms of the arc length of a meridional curve of the surface in the (r, z) plane, as follows:

$$\text{or} \quad a^2 = \left(\frac{ds}{d\xi} \right)^2 = (r')^2 + (z')^2$$

and

$$r' = a \cos \phi, \quad z' = a \sin \phi,$$

⁽¹⁾ The extracted solutions are valid for other types of shells provided that, over the considered region of the shell, (a) there exists no tangent perpendicular to the center line and (b) the thickness is constant. The cases involving a tangent perpendicular to the center line and/or a non-constant thickness are discussed briefly in the appendix.

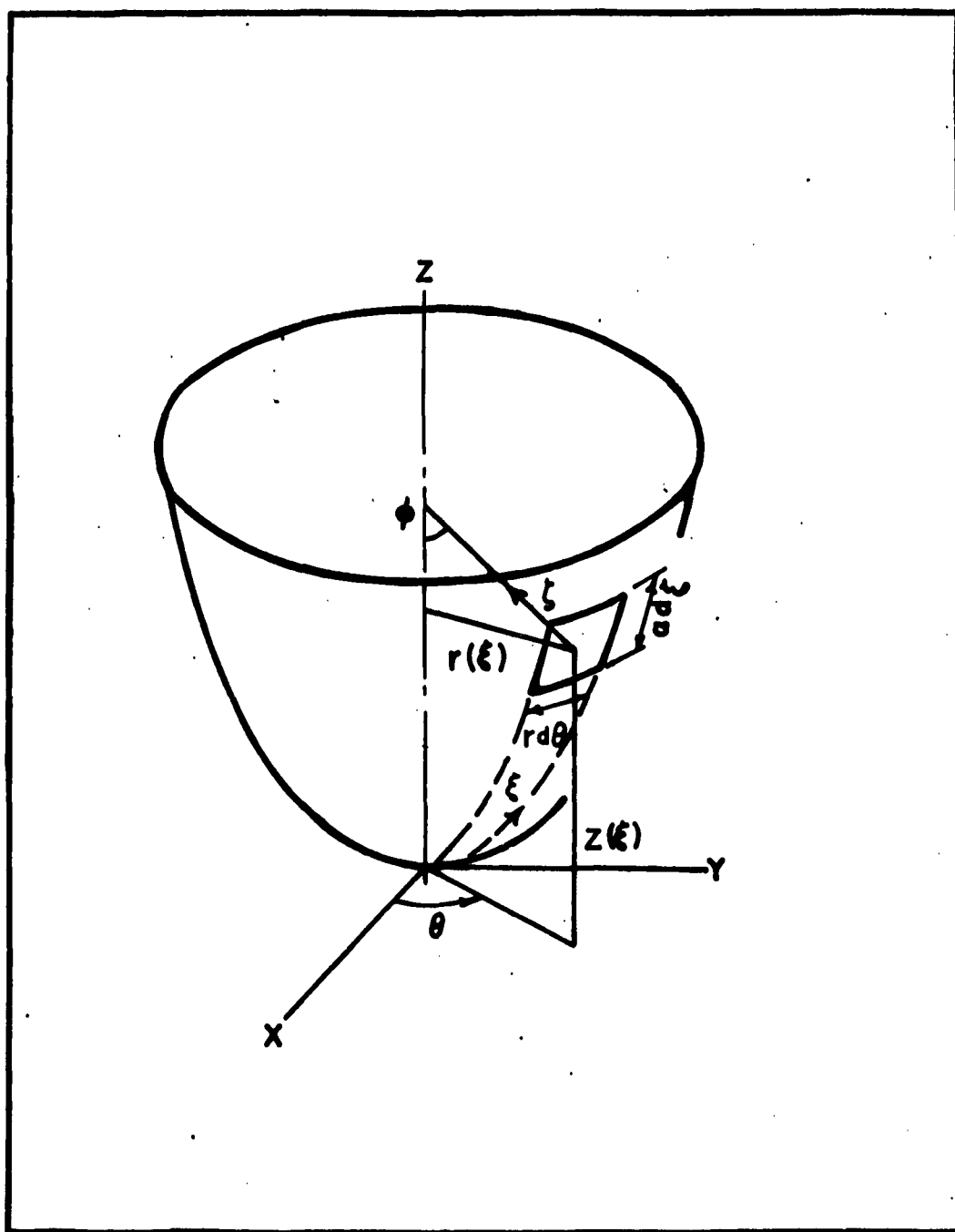


FIGURE 1

where $\tan \phi$ is the slope of the tangent line to the meridian as illustrated in Figure 1 and primes designate differentiation with respect to ξ . It is assumed that ξ is such that a is of the order of magnitude of a reference dimension of the shell, such as a reference radius of curvature of the middle surface of the shell. The coordinate ζ with axis directed along the inward normal to the middle surface is used to determine points relative to the middle surface.

B. Notations and Conventions for the Strains, Stresses and Displacements:

The strains, stresses and displacements are defined more explicitly in Appendix A; but for the purposes of determining the same, only the following are needed:

(1) Strains

$$\begin{aligned} E \epsilon_{\theta} &= \sigma_{\theta} - \nu \sigma_{\xi} = E \times \text{circumferential strain} \\ E \epsilon_{\xi} &= \sigma_{\xi} - \nu \sigma_{\theta} = E \times \text{meridional strain} \end{aligned}$$

(2) Stresses

$$\begin{aligned} \sigma_{\theta} &= \frac{N_{\theta}}{h} + \frac{12}{h^3} \zeta M_{\theta} = \text{circumferential stress} \\ \sigma_{\xi} &= \frac{N_{\xi}}{h} + \frac{12}{h^3} \zeta M_{\xi} = \text{meridional stress} \\ \tau &= (3Q)/(2h) = \text{shearing stress} \end{aligned}$$

where

a) Stress Resultants (taken in accordance with Figure 2)

$$\begin{aligned} N_{\theta} &= \frac{1}{a} \left[(rH)' + raP_H \right] \quad , \quad a^2 = (r')^2 + (z')^2 \\ N_{\xi} &= \frac{1}{a} \left[\frac{r'}{r} (rH) + \frac{z'}{r} (rV) \right] \\ Q &= \frac{1}{a} \left[-\frac{z'}{r} (rH) + \frac{r'}{r} (rV) \right] \\ rV &= -\int raP_V d\xi \end{aligned}$$

b) Moments (taken in accordance with Figure 2)

$$\begin{aligned} M_{\theta} &= \frac{D}{a} \left(\frac{r'}{r} \beta + \nu \beta' \right) \\ M_{\xi} &= \frac{D}{a} \left(\beta' + \nu \frac{r'}{r} \beta \right) \end{aligned}$$

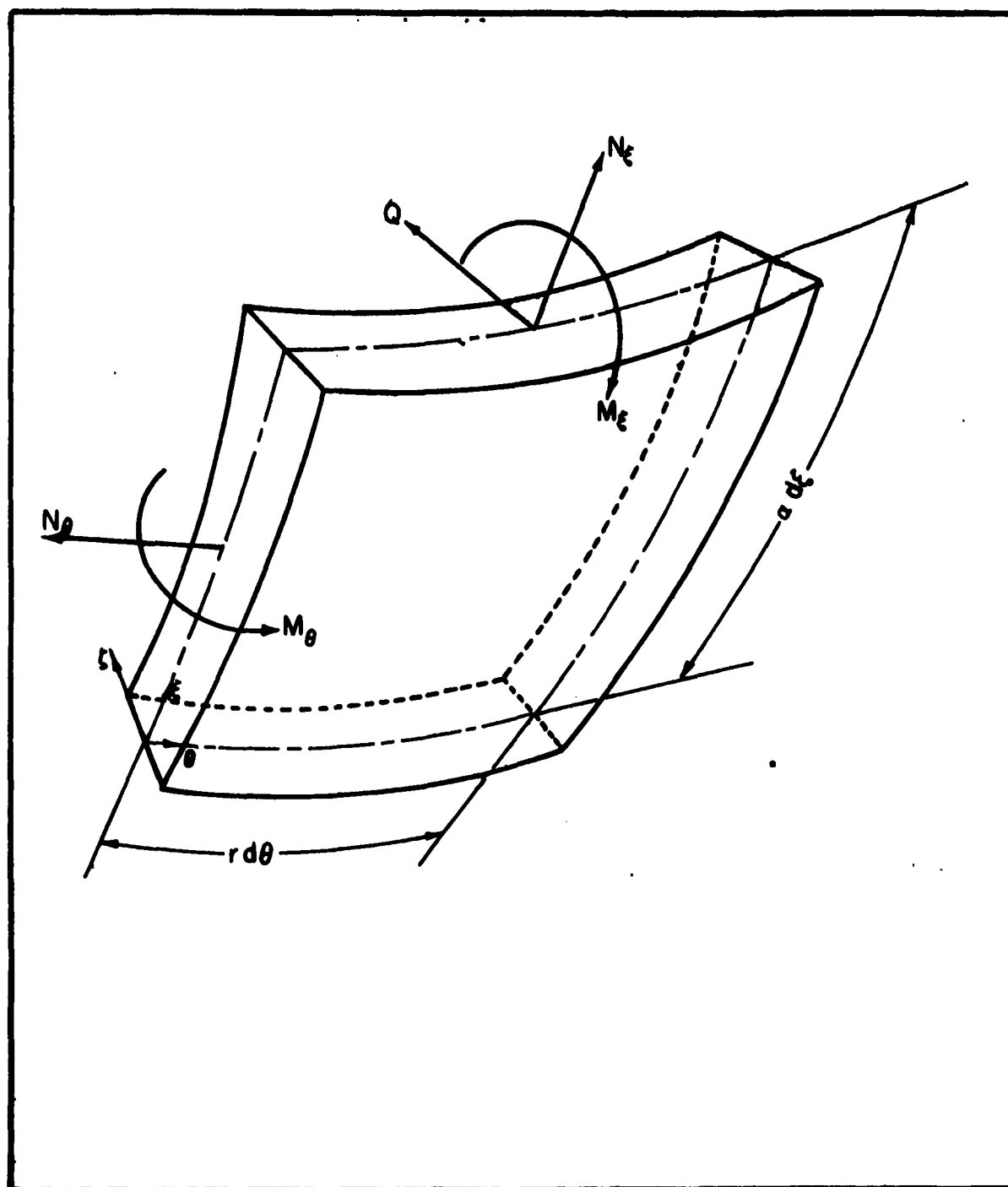


FIGURE 2

(3) Displacements

$$u = \frac{r}{C} (N_\theta - \nu N_\xi) = \text{radial (horizontal) displacement}$$

$$w = \int \left[\frac{z'}{C} (N_\xi - \nu N_\theta) - r' \beta \right] d\xi = \text{vertical displacement.}$$

(4) Constants

E = Young's modulus

ν = Poisson's ratio

$C = Eh$

$D = Eh^3/m^2$

$m^2 = 12(1-\nu^2)$

h = thickness

The quantities P_H and P_V denote the components of load intensity in the r and z directions, respectively; while H and β are the horizontal stress resultant and the angle enclosed by the tangents to the deformed and undeformed meridian of the middle surface at one and the same material point, respectively.

C. Solution of the Basic Differential Equation:

The basic differential equation of the linear theory of thin elastic shells and a general solution, which is valid for a large class of thin shells, are presented in Appendix B and C, respectively. For the problems at hand (i.e., chamber sections), solutions are extracted from this general solution and are presented in this section for a class of shells that have the following properties over the considered region of ξ :

- 1) the thickness, h , remains constant
- 2) there exists no tangent perpendicular to the axis of rotation

An approximate solution of the differential equations for the class of shells having the above properties is

$$\beta = \left(\frac{a}{r}\right)^{1/2} \left(\frac{r}{z}\right)^{1/4} \left\{ \exp(\mu \bar{\xi}) [A_0 \cos \mu \bar{\xi} - B_0 \sin \mu \bar{\xi}] + \exp(-\mu \bar{\xi}) [A_1 \cos \mu \bar{\xi} + B_1 \sin \mu \bar{\xi}] \right\}$$

and

$$\psi = \frac{m}{Eh^2} (rH) = \left(\frac{a}{r}\right)^{1/2} \left(\frac{r}{z}\right)^{1/4} \left\{ \exp(\mu \bar{\xi}) [B_0 \cos \mu \bar{\xi} + A_0 \sin \mu \bar{\xi}] + \exp(-\mu \bar{\xi}) [B_1 \cos \mu \bar{\xi} - A_1 \sin \mu \bar{\xi}] \right\} + \frac{m}{Eh^2} \frac{r}{z} rV$$

where A_0 , B_0 , A_1 and B_1 are constants that are to be determined from the surface loading, junction and/or end conditions. Here

$$\exp(\mu \bar{\xi}) = e^{\mu \bar{\xi}}$$

$$\exp(-\mu \bar{\xi}) = e^{-\mu \bar{\xi}}$$

$$1) \mu^2 = \frac{a^2 m}{2h}, \alpha' = 0, \quad 2) \mu^2 = \frac{m}{2h}, \alpha' \neq 0$$

$$\text{and} \\ 1) \bar{\xi} = \int_{\xi_0}^{\xi} \left(\frac{r}{z}\right)^{1/2} d\xi, \alpha' = 0, \quad 2) \bar{\xi} = \int_{\xi_0}^{\xi} \left(\frac{r}{z}\right)^{1/2} d\xi, \alpha' \neq 0$$

where ξ_0 is an arbitrarily chosen point that is usually chosen in the considered region of ξ .

D. Membrane Solution:

The membrane solution⁽¹⁾, as mentioned in the introduction, is obtained by neglecting the bending and shearing effect. This implies that $M_\xi = M_\theta = Q = 0$; the equivalent would be the following

$$rH = \frac{r'}{z} rV, \quad \beta = \beta' = 0.$$

The stresses, that result from the above and the relations given in Section II B, would have the simplified form

$$\sigma_\theta = N_\theta/h = \frac{1}{ah} [(rH)' + r\alpha p_H]$$

and

$$\sigma_\xi = N_\xi/h = \frac{a}{hrz} rV.$$

⁽¹⁾ There are a number of so-called membrane theories of which the one above is possibly the simplest.

In general, junction and end effects contribute little, if anything, to the stresses at points whose distances are greater than $(R_0 h)^{1/2}$ from the particular junction or end, that is being considered. (R_0 is a representative dimension of the shell). Hence, in general, the above so-called membrane solution is usually valid for points whose distance is greater than $(R_0 h)^{1/2}$ from junctions and ends.

III. Application of Results to Bell-Shaped Chamber Sections:

A. Geometry

A typical bell-shaped chamber section (see Figure 3) of constant thickness, h , is composed of two truncated cones and segments of two toroidal⁽¹⁾ shells. These truncated cones⁽²⁾ and segments of toroidal shells are assumed to be joined so as that there exists a continuously turning tangent across each of the junctions $z = z_i$.

The middle surface of the shell can be represented as follows:

$$\begin{cases} r = p_1 \bar{r}_1 \xi + \bar{r}_1, & \frac{dz}{dr} = \frac{1}{p_1} \\ z = \bar{r}_1 \xi + \bar{z}_1, & \bar{z}_1 \leq z \leq \bar{z}_2 \end{cases}$$

(Note⁽²⁾: We have a cylindrical section, when $p_1 = 0$)

$$\begin{cases} r = r_2 - S \cos \xi \\ z = z_2 + S \sin \xi, & \bar{z}_2 \leq z \leq \bar{z}_3 \end{cases}$$

$$\begin{cases} r = r_3 + R \sin \xi \\ z = z_3 - R \cos \xi, & \bar{z}_3 \leq z \leq \bar{z}_4 \end{cases}$$

$$\begin{cases} r = p_4 \bar{r}_4 \xi + \bar{r}_4, & \frac{dz}{dr} = \frac{1}{p_4} \\ z = \bar{r}_4 \xi + \bar{z}_4, & \bar{z}_4 \leq z \leq \bar{z}_5 \end{cases}$$

(Note: We have a cylindrical section when $p_4 = 0$)

The terms with a subscript i will imply that they are to be evaluated in the region $\bar{z}_i \leq z \leq \bar{z}_{i+1}$.

⁽¹⁾ The case of a toroidal shell having $b < a$, where b is the radius of the cross-sectional circle and a is the distance from the center of the circle to the center line, was studied by Clark [8]. The case when $b > a$ was solved independently by author and Naghdi [6]. Numbers in brackets refer to the Bibliography.

⁽²⁾ The analysis presented here assumes that the cones are not shallow.

MIDDLE SURFACE OF A TYPICAL BELL-SHAPED CHAMBER SECTION

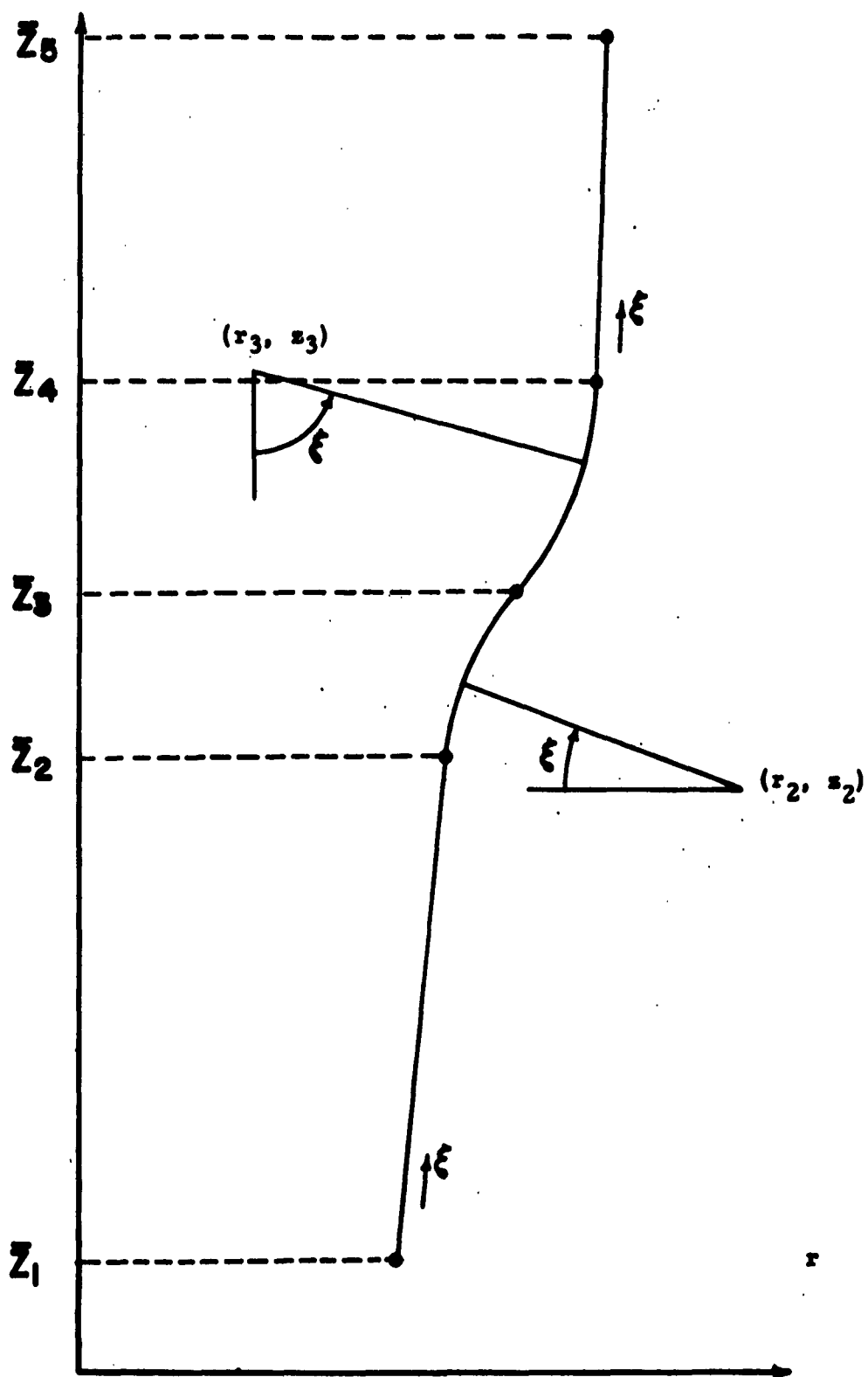


FIGURE 3

AM-1775-6
11-4-55

B. Loading Conditions

This chamber is assumed to be subjected to internal pressure, P , and a supporting tension at the end $z = \Xi_5$. In addition it is assumed that

$$M_\xi = Q = 0 \text{ at } z = \Xi_5$$

and

$$\beta = \beta' = 0, \text{ at } z = \Xi_1.$$

As mentioned in the introduction, one of the great values of thin-shell theory (linear), is that under certain restrictions component sections, such as cones, tori, etc., can be considered separately for analysis purposes and then pieced together. These certain restrictions are the so-called junction conditions, which are obtainable from the conditions of equilibrium and continuity (compatibility) that must exist across the junctions of the component sections. These latter conditions may, in general, be reduced to the following four conditions at the junctions, for a continuously turning tangent (as is the case here):

- a) equality of radial displacements for the middle surface,
- b) a continuous tangent is maintained across the junction (i. e. β is continuous),
- c) equality of shear resultants (i. e. Q)

and

- d) equality of the meridional moments (i. e. M_ξ).

It can be shown that the preceding four conditions are equivalent to the following conditions⁽¹⁾ imposed on β and ψ at the junctions:

$$\begin{aligned} \beta_i &= \beta_{i+1} \quad , \quad \psi_i = \psi_{i+1} \\ \beta'_i/a_i &= \beta'_{i+1}/a_{i+1} \quad , \quad \psi'_i/a_i = \psi'_{i+1}/a_{i+1} \quad , \text{ for } z = \Xi_i + 1, \quad i = 1, 2, 3. \end{aligned}$$

⁽¹⁾ These conditions assume that s' is not negative on one side of the junction point and positive on the other side.

C. Solution (Method of Specifying the Constants)

Now, the strains, stresses and displacements, in view of Sections IIIA and IIIB are dependent on the quantities β and ψ . These quantities are defined in Section II C, where for convenience the constants A_0 , B_0 , A_1 and B_1 are now replaced by the constants A_{0i} , B_{0i} , A_{1i} , B_{1i} ($i = 1, 2, 3, 4$), respectively. (The subscript i has the same implication as mentioned previously, see IIIA). Since all other terms are defined, the stresses, strains and displacements are determined once the above sixteen constants are specified.

From the conditions given in Section IIIB, it is easily seen that there are four equations for the end conditions and twelve equations for the junction conditions. This is in agreement with the fact that we have sixteen constants to specify; that is, we have a system of sixteen equations to solve. These equations can be solved by the classical method of iteration [1], and in many instances by Crout's method [1], if the system of equations can be arranged to get a dominant diagonal. If the diagonal is not dominant, then a scheme devised by O. Bowie [2] may be used to get the required dominance. Further numerical techniques may be found in a text by Hildebrand [1] or in a Bureau of Standards Reference List [3].

The solutions of this system of equations are then substituted into the relations for β and ψ , which in turn are substituted into the relations for the stresses, strains and displacements given in II B.

IV. Stress Distribution in the 106MM T137 (Bell-Shaped) Chamber Section

As an illustrative numerical example, the 106MM T137 chamber section was idealized to fall into the class of so-called bell-shaped chamber sections. (See Figure 4). The length of the chamber is 24 inches, where $x = 0$ is assumed to be at the muzzle end of the chamber. In view of Section III; the pertinent values⁽¹⁾ that are needed for the analysis are as follows:

For the region $i = 1$, we have

$$p_1 = 0.103187, (\bar{r}_1, \bar{x}_1) = (2.96330, 11.4), \bar{x}_2 = 17.32, \alpha_1 = 2.97903$$

and

$$\bar{x} = \int \sqrt{\frac{z}{r}} d\xi = \frac{2}{p\sqrt{\bar{r}_1}} [\sqrt{r} - \sqrt{\bar{r}_1}]$$

⁽¹⁾Since the region of interest is near the toroidal sections, the analysis is restricted to $24 \geq x \geq 11.4$.

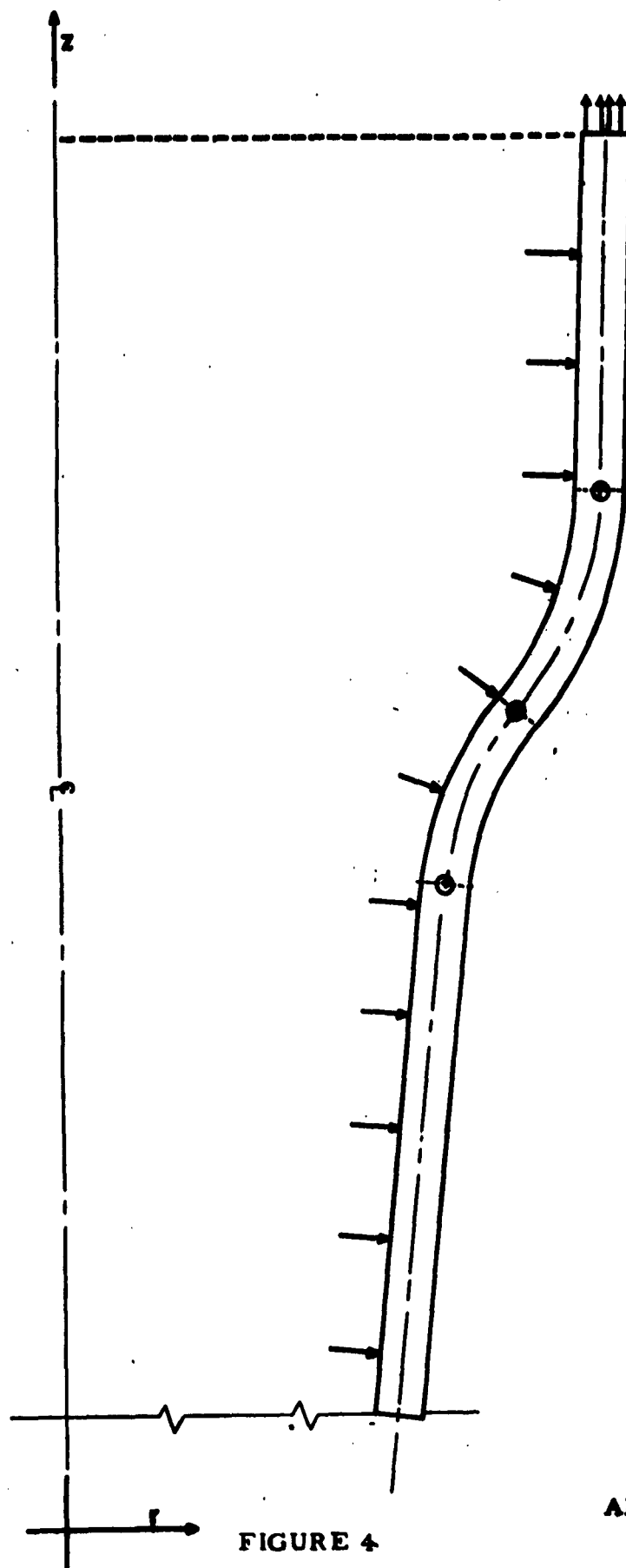


FIGURE 4

AM-1773-G
11-4-55

For the region $i = 2$

$$(r_2, z_2) = (6.26532, 17.0262) \quad S = a_2 = 2.830270, \quad \bar{r}_3 = 18.85$$

The values of \bar{I} for this region were obtained by numerical integration.

For the region $i = 3$

$$(r_3, z_3) = (1.66340, 20.9043) \quad R = a_3 = 3.187840 \quad \bar{r}_4 = 20.82$$

The values of \bar{I} for this region were obtained by numerical integration.

For the region $i = 4$, we have

$$p_4 = 0.0274869, \quad (\bar{r}_4, \bar{r}_4) = (4.85, 20.82), \quad \bar{r}_5 = 24 \quad a_4 = 4.85184$$

and

$$\bar{I} = \frac{2}{p_4 \sqrt{\bar{r}_4}} [\sqrt{r} - \sqrt{\bar{r}_4}]$$

From the normal surface loading, P , we obtain

$$\begin{aligned} r a P_v &= -P r' / a, \quad r V = (-r^2 / 2 + C_1) P \\ r a P_H &= r z' P = \begin{cases} \bar{r}_1 r P, & \text{for } i = 1 \\ r z' P, & \text{for } i = 2, 3 \\ \bar{r}_4 r P, & \text{for } i = 4. \end{cases} \end{aligned}$$

Since the chamber is supported at $z = z_5$, the condition at $z = 0$ would essentially be that of a free end. Hence from the condition that $rV = 0$ at $z = 0$, we find

$$C_1 = -\left. \frac{r^2}{2} \right|_{r=2.289} = -2.62.$$

The needed physical constants are as follows:

$$m = \sqrt{12(1-\nu^2)}$$

$$E = 30 \times 10^6$$

$$\nu = 0.285$$

$$h = 0.43228 = \text{average thickness.}$$

The preceding relations and values are to be substituted into the expressions for β , ψ and their derivatives, which in turn are to be substituted into the end and junction conditions. This latter substitution, as previously mentioned will result in a system of sixteen equations with sixteen constants A_{0i} , B_{0i} , A_{1i} , B_{1i} , $i = 1, 2, 3, 4$. This system of equations was solved by a reordering of the equations to get a partially dominant diagonal and then applying Crout's method. The following results were obtained:

$A_{01} = -2.06 \times 10^{-9}$	$A_{11} = 2.06 \times 10^{-9}$
$B_{01} = 6.86 \times 10^{-10}$	$A_{11} = 4.81 \times 10^{-9}$
$A_{02} = -1.12 \times 10^{-7}$	$A_{12} = 1.52 \times 10^{-7}$
$B_{02} = 2.01 \times 10^{-7}$	$B_{12} = 2.94 \times 10^{-7}$
$A_{03} = -1.69 \times 10^{-8}$	$A_{13} = 9.15 \times 10^{-6}$
$B_{03} = -2.75 \times 10^{-9}$	$B_{13} = -4.03 \times 10^{-6}$
$A_{04} = -2.46 \times 10^{-10}$	$A_{14} = 3.66 \times 10^{-7}$
$B_{04} = -2.83 \times 10^{-9}$	$B_{14} = 6.52 \times 10^{-7}$

These values were then used to evaluate β , β' , ψ and ψ' , which were in turn used to evaluate the resultant stresses and moments, IIB. These latter values were then used to evaluate the surface stresses⁽¹⁾ as presented in Figures 5, 6.

The membrane stresses (IIID) for the chosen example have been evaluated and are presented in Figure 7.

⁽¹⁾ Stresses obtained from experimental firing results for a 100MM appear to agree quantitatively at the points where strain gauges were attached. See Reference [15] listed in the bibliography.

**CIRCUMFERENTIAL STRESS DISTRIBUTION AT THE SURFACES OF A
RECOILLESS RIFLE CHAMBER SECTION (106MM T137)**

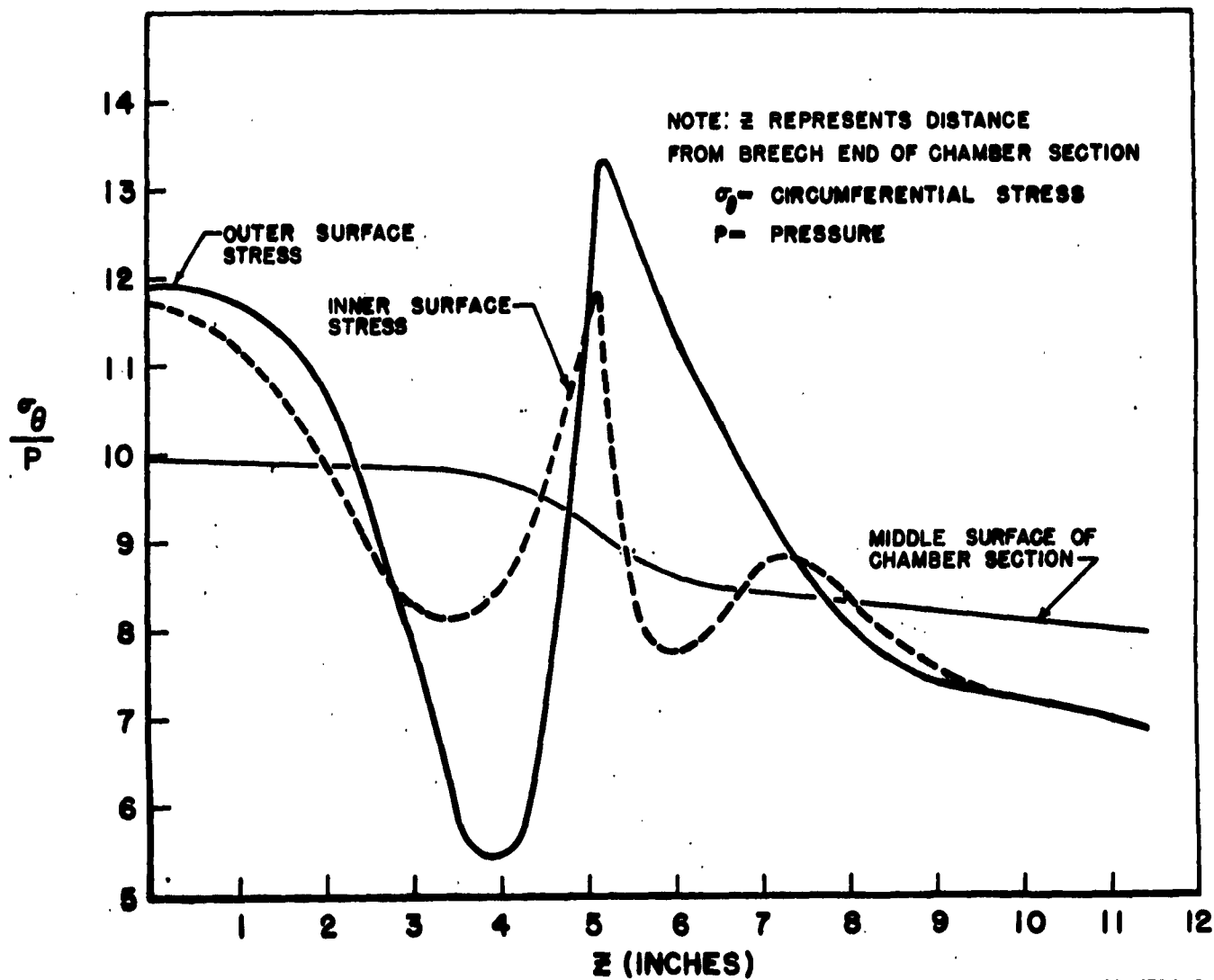


FIGURE 5

AM-1774-8
11-4-85

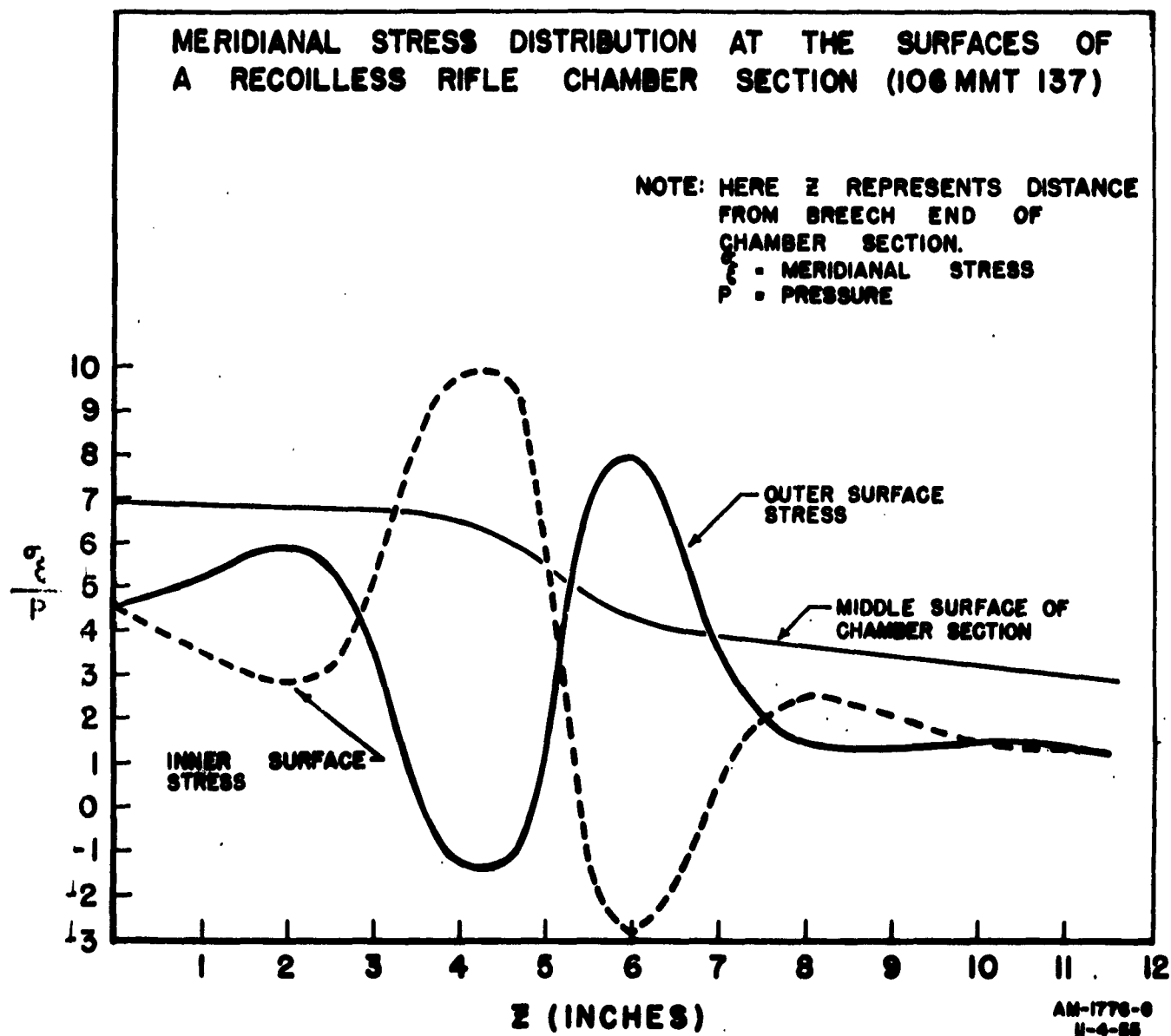


FIGURE 6

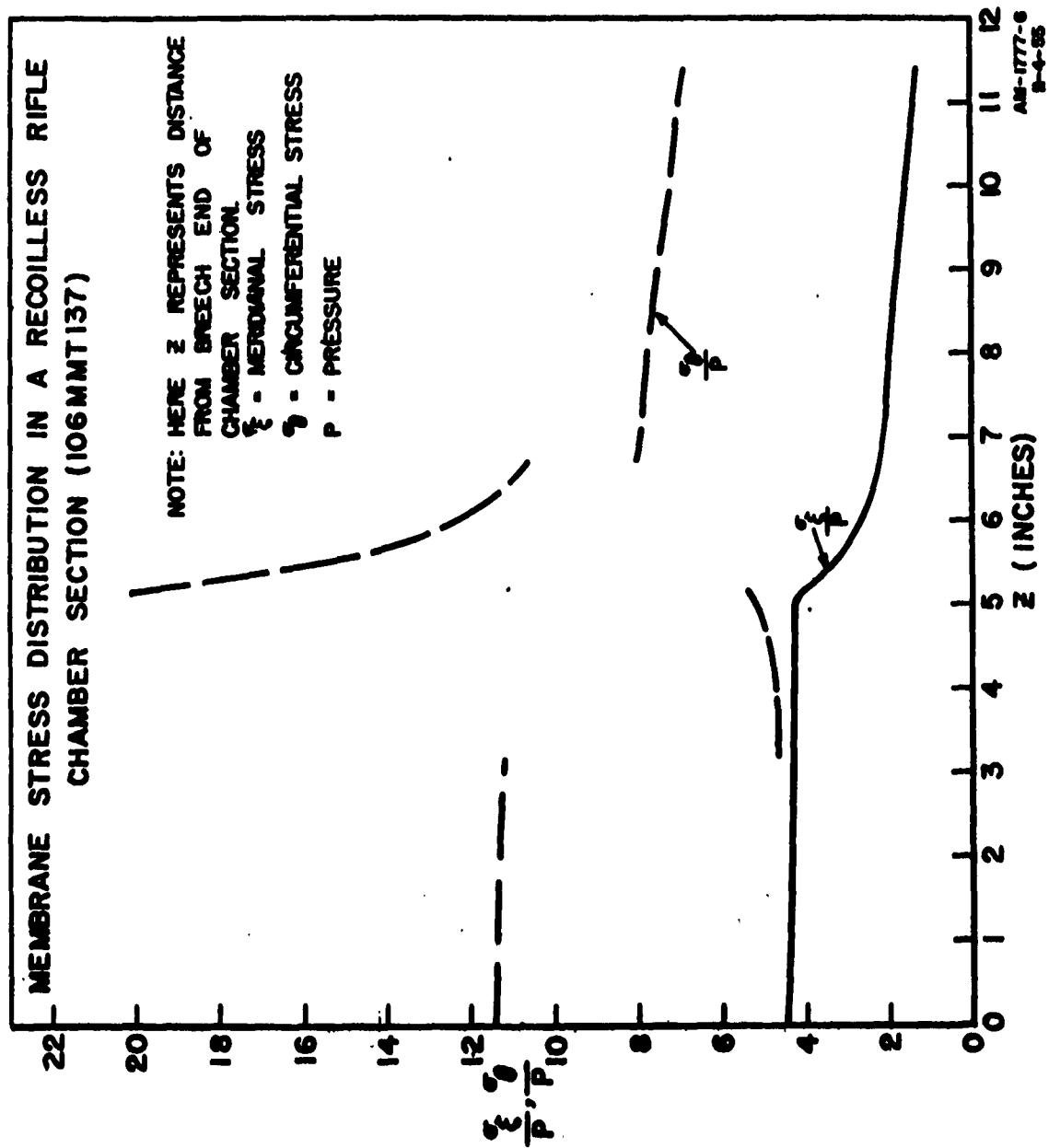


FIGURE 7

BIBLIOGRAPHY

1. F. B. Hildebrand, "Numerical Analysis", McGraw-Hill Book Company, 1 January 1956.
2. O. L. Bowie, "Practical Solution of Simultaneous Linear Equations", Quarterly of Applied Mathematics, January 1951.
3. G. E. Forsythe, "Simultaneous Linear Equations and the Determination of Eigenvalues", National Bureau of Standards Applied Mathematics Series 29, 31 August 1953.
4. E. Reissner, "On the Theory of Thin Elastic Shells", Reissner Anniversary Volume. J. W. Edwards, Ann Arbor, Michigan, 1949.
5. E. Reissner, "On Axisymmetrical Deformations of Thin Shells of Revolution," Proceedings of Symposia in Applied Mathematics, Volume III, McGraw-Hill Book Company, 1950.
6. R. A. Clark and E. Peissner, "A Problem of Finite Bending of Toroidal Shells", Quarterly of Applied Mathematics, January 1953.
7. F. B. Hildebrand, "On Asymptotic Integration in Shell Theory", - ibid Reference 5.
8. P. N. Naghdi and C. N. De Silva, "On the Deformation of Elastic Shells of Revolution", Quarterly of Applied Mathematics, January 1955.
9. R. A. Clark, "On the Theory of Thin Elastic Toroidal Shells", J. Math. Phys. 29, (1950).
10. R. E. Langer, "On the Asymptotic Solution of Ordinary Differential Equations", Trans. Am. Math. Soc. 33, 23-64, (1931).
11. R. E. Langer, "On the Asymptotic Solution of Ordinary Differential Equations, with reference to the Stokes' Phenomenon about a Singular Point", Trans. Am. Math. Soc. 37, 397-416, (1935).
12. R. A. Clark, "Asymptotic Integration of a Non-Homogeneous Differential Equation", OOR-DA-33-019-ORD 1193, June 1954.

Bibliography (Continued)

13. R. A. Clark and E. Reissner, "Bending of Curved Tubes", Advances in Applied Mathematics II, Academic Press; pp 93-122, 1950.
14. E. Reissner, "On Some Aspects of the Theory of Thin Elastic Shells", Journal of the Boston Society of Civil Engineers, Volume XLII, No. 2, April 1955.
15. Aberdeen Proving Ground, Maryland, "Firing Record. No No. M-74445". "Chamber Stresses, 106MM Rifle M40", TS 4-4020, 18 thru 25 August 1954.
16. P. N. Naghdi and C. Nevin De Silva, "Deformation of Elastic Ellipsoidal Shells of Revolution", Proceedings of the Second U. S. National Congress of Applied Mechanics, A.S.M.E. 333-343, 1954.

**LINEAR PROGRAMMING AND HIGH SPEED
COMPUTER APPLICATIONS**

by C. Tompkins

**Prepared under the sponsorship
of the Office of Naval Research,
the Office of Ordnance Research, U. S. Army,
and the University of California**

**Reproduction in whole or in part is permitted
for any branch of the U. S. Government**

**Numerical Analysis Research
University of California
Los Angeles 24, California**

15 June 1956

LINEAR PROGRAMMING AND HIGH SPEED
COMPUTER APPLICATIONS

1. Introduction

In writing of linear programming and high speed computer applications, I have several excellent works from which I can draw material -- the preliminary material relating to the increasing practical importance of linear programming, the mathematical background of methods of solution, and computational aspects of these mathematical ideas. I shall refer mainly to three such sources here, but I must note that I limit my references to these sources only with the understanding that additional references are available in the bibliographies they print. The sources are:

The activity analysis volume edited by T. C. Koopmans [1],
The symposium proceedings edited by H. A. Antosiewicz [2]*,
The expository book by A. Charnes, W. W. Cooper, and
A. Henderson [3].

I shall set myself the task of describing in a general way the generation of problems of linear programming; then I shall proceed to describe these problems in their abstract mathematical and econometric settings;

*It might be remarked that one of the papers most interesting for the present purposes in [2] is that of A. J. Hoffman, p. 397-424, and that many of his bibliographic references are numbered one lower than they should be, so that his references to his [34], [35], and [36] (as they are numbered in the bibliography) frequently appear as references [33], [34], and [35], respectively in the text.

finally, I shall report some numerical attacks on such problems using large machines, indicate some victories and admit some defeats in these computations. In the course of the exposition, I shall allow myself to wander a little afield, particularly with regard to computations requiring integral solutions, and I shall reject other tempting excursions into the interesting work involving efficient sets with respect to several functions to be optimized; my guide in each case is a combination of computational feasibility (or convenience) and economic application.

In particular, I shall limit myself to a single numerical utility function, rather than many such functions (or a vector function) because of the dominating importance of these problems in the present applications which have been reduced to computation. Economically it is true in times of stability that the only item in short supply is money and that the value of every other item can be stated completely in terms of money. Hence the money value is a sound utility function under these (idealized) conditions. In other times other goods are in short supply (thus requiring ration coupons or other items not completely exchangeable for money in order to provide a complete abstract set of values -- hence a vector value rather than a scalar value), but even in these times competitive decisions must be made, and these decisions require ordering of various possible courses of action so that a most desirable one can be chosen. Hence, even in the case of vector utilities each decision may have to be reduced to one based on a (possibly temporary) scalar utility.

2. Generation of linear programming problems

In describing the generation of linear programming problems, I shall look at the matter from the point of view of an administrator -- not a

mathematician. The words I use will be those of an administrator, and we shall have to provide a slight translation in order to get them into their mathematical equivalents -- in which the same words unfortunately have different meanings.

The administrator is faced with a problem in which he must cause accomplishment as highly remunerative as possible to his firm.

If he is a true administrator as opposed to a directly productive member of society, his tools for accomplishing this are a few departments of his firm, each functioning with some degree of autonomy. His technique for using these tools is to relay to each a set of general assignments (which it develops into explicit assignments and carries out). In this assignment, since the administrator is unable to monitor the whole operation of each department (otherwise there would be only one department with the administrator as head), he must suggest general objectives and a means whereby each department can estimate the value of any detailed accomplishment compatible with these general objectives.

In order to do this, the administrator sets some minimal goals of suitable results for each department. Any accomplishment not meeting these minimal standards is to be rejected either because it is not of enough intrinsic value in itself to justify the operation of the department or because it may leave undone some task essential to the integrated accomplishment of the firm and not explicitly assigned to any other department. These minimal standards are known as suitability restrictions, at least to military administrators.

Similarly, the administrator must allocate the resources of the firm. He makes assignments to his various departments in terms of money, shop facilities, labor force, and other means available to the firm. These assignments carry with them implicit restrictions that the courses of action taken by the departments will in no case generate requirements exceeding the means assigned to these departments. These restrictions are known as feasibility restrictions to military administrators.

Now, if the administrator were omniscient and prescient he could carry out his own calculations concerning the best course of action by each department. However, there is a considerable amount of uncertainty involved in the size of a priori planning factors and in the effect of various actions. Since I am discussing linear programming and not organization theory here, I shall not discuss the sources of these difficulties, but rather jump directly to the abstraction.

The department head can, then, expect to receive from his superior a rule of utility -- what various accomplishments mean to the firm. He has himself a set of rules of tactics -- what various activities he can set up in his department will ultimately mean in terms of accomplished output. He has two types of restrictions -- suitability restrictions which have been arbitrarily imposed by his superior to guarantee proper accomplishment of the whole firm, and feasibility restrictions which have been similarly imposed to prevent the firm from taking action which would generate requirements exceeding the means available. To a considerable extent, each of us has such assignments imposed on him explicitly and implicitly, and each of us must plan to maximize the utility of his actions subject to the

prescribed restrictions. In the case of linear programming, the assignments and the rules are stated explicitly, and they are all assumed to be linear.

Thus, each department may have several activities which it can conceivably carry out at various levels. It is assumed that the levels can be stated explicitly and that they are denoted by non-negative activity levels x_a , where the index a ranges over the set of allowable activities: $a = 1(1)m$. (The notation immediately above indicates that a may take on several values, the lowest being 1, the highest being m , and successive values differing by the increment 1 found in the parentheses.)

It is further assumed that there is a set of pertinent effects mentioned in the suitability restrictions, the feasibility restrictions, and the utility function. These effects will be numbered by a greek letter, say α , $\alpha = 1(1)p$. The planning rule which the department head (or his superior) uses is based on planning factors $p_{\alpha a}$; the level of each effect expected to follow from any schedule of activity is denoted by y_{α} , and is given by the formula

$$(1) \quad y_{\alpha} = \sum_a p_{\alpha a} x_a .$$

It is essential in the generation of linear programming problems that the effects be at least approximated by such a linear homogeneous formula; however, devious techniques are allowed in the generation of this formula, and some will be mentioned later.

The feasibility conditions imposed by the administrator may then be written as

$$(2) \quad y_{\alpha} \leq b_{\alpha} , \quad \alpha \in \varphi ,$$

where φ is the set of effects which constitute expenditure of the means assigned to the department and where the quantities b_α , $\alpha \in \varphi$, represent the assignments of these means to the department.

The suitability conditions imposed by the administrator may similarly be written as

$$(3) \quad y_\alpha \geq c_\alpha, \quad \alpha \in \sigma,$$

where σ is the set of effects in the list of minimal suitable accomplishments required.

Finally, the utility is given by a formula

$$(4) \quad u = \sum_{\alpha} d_{\alpha} y_{\alpha}.$$

Here it is assumed that the summation takes place over the whole range

$\alpha = 1(1) \mu$; any inconsequential effects may be omitted more easily by setting the corresponding coefficients equal to zero than by modifying the formula.

It is also convenient, for mathematical reasons, to combine the sets of inequalities (2) and (3) into a single set. I do not want to spend time in details here, but I simply note that all the inequalities may be made to go in the same direction by multiplying those in (3) by -1, and that by suitable expansion of the range of α or by including meaningless inequalities (with zero coefficients) which will disappear later we can replace $p_{\alpha a}$ by $q_{\alpha a}$ where for some values α , $q_{\alpha a} = p_{\alpha a}$, and for other α , $q_{\alpha a} = -p_{\alpha a}$. Following all this, we can combine formulas (2) and (3), throw in formula (1), and add formula (4) with the following results:

the feasibility and the suitability restrictions
are represented by the formula

$$(5) \quad \sum_a q_{\alpha a} x_a \leq f_{\alpha} ,$$

and the utility function is represented by the formula

$$(6) \quad u = \sum_a g_a x_a .$$

As was stated initially, the activity levels x_a are restricted to be non-negative:

$$(7) \quad x_a \geq 0 .$$

The problem of maximizing a form of the type (6) subject to linear inequalities of type (5) and of type (7) is the standard problem of linear programming.

I note here quickly that several other problems can be reduced to this form. If some restrictions are of the form of equalities rather than inequalities as indicated in (5), then each equality may be replaced by two competing inequalities which have the effect of the equality restriction. If some variables are not restricted to be non-negative, they may be replaced by the difference of two non-negative variables. Similarly, by adding non-negative residue variables, it is possible to change the whole set of inequality restrictions (5) to equality restrictions. These are matters of technique which will not enter seriously into the discussion here but which may have considerable effects on actual computations which are carried out. The

simplex method, which figures prominently in computation is usually based on the equality formulation, using non-negative residue variables rather than the inequality formulation stated explicitly above.

3. Geometric aspects of the linear programming problem

In a coordinate space of m dimensions, the inequalities (5) and (7) describe a convex polyhedral set, or they have no solution at all. We call a convex polyhedral set a convex polytope. The form defined by (6), no matter what the nature of the coefficients g_a , is maximized in this set at one of its vertices, or it may have no maximum at all. If there are solutions to the restricting inequalities but no maximum to u , then the function u grows without bound in the (infinite) region described by the inequalities. Such conditions are not consistent with properly set economic problems; despite the complaints of various rabble rousers, almost no one -- not even mathematicians -- has access to infinite wealth.

So we may admit that the utility function u in any interesting problem actually attains a maximum in the polytope described by the inequalities and that this maximum is attained at a vertex. A vertex of the polytope is a point with the property that no line segment containing it as an interior point lies in the polytope.

Our problem is to find the right vertex.

Actually, the recognition of a vertex is not easy computationally, and finding one is even harder. G. B. Dantsig has pointed out that one can identify many points as not being vertices by observing that no vertex has more than μ non-zero coordinates. This follows immediately from an observation that only those inequalities from (5) and (7) which restrict as

equalities at the point in question can enter into the determination as to whether a point satisfying all inequalities is or is not a vertex. If fewer than m of these restrictions are satisfied as equalities (remembering that all inequalities are satisfied at any point of the polytope), then an infinite number of solutions exist and contain a line segment according to standard algebraic theory; then the point considered cannot be a vertex. Since only μ of these equalities can be from the set (5), and since at least m must be satisfied at any vertex, the remaining $m - \mu$ must come from the set (7), which as equalities specify zero coordinates. The observation of Dantzig follows immediately. The statement is clearly valid also if the restrictions of type (5) are stated as equalities instead of inequalities.

The geometric interpretation given above is complete in principle, but in practice it still gives little hint of ways of arriving at the numerical solution of any problem. In this we are helped by what may be a less standard or more subtle geometric interpretation. Without regard to standards, subtlety or ingenuity, however, I want to stress here that it is a different geometric approach. Alone, it might not be any more productive than the first geometric interpretation I indicated, but the two interpretations used together have been remarkably effective in producing numerical results. The joint use of the two geometric interpretations and the introduction of the following interpretation seem to be due to G. B. Dantzig (although the power of the combination in Dantzig's method was first explicitly pointed out -- at least to me -- by D. Gale, H. W. Kuhn, and A. W. Tucker). I do not feel competent here to comment further either on Dantzig's remarkable insight and ingenuity or on the deep research done by Gale, Kuhn, and Tucker in

various joint and individual works in making this insight and ingenuity clearer -- again, at least to me.

The second geometrical approach uses a coordinate space of μ dimensions -- not m dimensions. In this space the rectangular array $q_{\alpha a}$ from the inequalities (5) is considered to be a set of m vectors, one for each value of the index a with components $q_{\alpha a}$, $\alpha = 1(1)\mu$. The non-negative multipliers x_a in inequalities (5) act on these vectors. For all admissible (that is, non-negative) x_a , the left hand members of inequalities (5) generate the coordinates of points of a polyhedral cone in this μ -dimensional space, and the inequalities (5) are satisfied by points of this cone which lie in an orthant of the μ -dimensional space lying "below and to the left" (in a multi-dimensional sense) of the point with coordinates f_{α} .

It should be noted that in this interpretation the utility function is not a point function. Thus, if the vectors $q_{\alpha a}$ are not independent for all a , there may be several representations of any one point of the polyhedral cone described by the left members of inequalities (5). This means that several different sets x_a may correspond to the same point. Furthermore, in formula (6) these various values of x_a may give different values to u , and in order to determine u it is necessary to know not only the point of the μ -dimensional space at which it is to be determined but also the representation of this point in the polyhedral cone described by the left members of (5).

It might be worth noting briefly in passing that the m -dimensional set described by inequalities (5) and (7) might just as well be described as a convex region with prescribed vertices, using multipliers similar to those used in the description of the convex polyhedral cone in μ -space. Similarly,

it is true (but not quite obvious) that the convex polyhedral cone in μ -space represented by (5) and (7) might also be described as an intersection of closed half spaces with boundaries passing through the origin. (A closed half space is a hyperplane and all the points lying on one side of it.)

Much of the recent analysis leading to powerful computational attacks on the linear programming problem is based on this possibility of describing these sets in two different ways. I shall not go into this in detail here, however.

4. A problem whose variables are permutations -- the assignment problem

I now turn from the main course of my paper to mention a famous problem whose variables are permutations and which may be reduced to a linear programming problem. This is a problem of maximizing a function of permutations on n marks; the function to be maximized is from one particular set of functions which contains many utility functions of problems important in econometric applications.

In principle, a problem of maximizing a function of permutations is even easier to solve than the linear programming problem, for there are only a finite number of permutations and one need only try them all. This finite number may, however, become forbiddingly large if the number of marks n is large. For example, the number of permutations on 12 marks is about 4.8×10^8 , but a manufacturer might reasonably inquire as to which of twelve different products he should make each month during the year in a single plant. The number of permutations of 20 marks exceeds 10^{18} .

I shall describe a method used to reduce some permutation problems to linear programming problems, and thus I shall describe by implication the

type of function which must appear as the utility to be maximized. The permutations are first written as matrices. A permutation on \underline{n} marks may be represented by a matrix with \underline{n} rows and \underline{n} columns subject to the condition that each row and each column contains exactly one element which has value 1 and exactly $(n - 1)$ elements with value zero. If such a matrix is r , then it can be interpreted as representing the permutation which takes the mark \underline{i} into the mark \underline{j} for all (i, j) for which $r_{ij} \neq 0$.

This representation of permutations may be embedded in the set of doubly stochastic matrices; these are matrices, also denoted by r_{ij} , whose elements satisfy the following linear restrictions:

$$(8) \quad r_{ij} \geq 0 ,$$

$$(9) \quad \sum_j r_{ij} = 1 ,$$

$$(10) \quad \sum_i r_{ij} = 1 .$$

We might note that one of these last equalities is dependent on the others, for each of the two sets (9) and (10) implies that the sum of all the elements of the doubly stochastic matrix is \underline{n} .

This set of doubly stochastic matrices, then, may be considered as representing a convex polyhedral set in a space of n^2 dimensions. The matrices which represent permutations belong to this set. They are, in fact, the only vertices of the set. This fact has long been known, but Dantsig points out that a simple inductive proof follows from his observation (noted above) that no vertex of the region has more than $(2n - 1)$ non-zero coordinates. (Here the observation that one of the inequalities of (9) and (10)

is redundant has been used.) Not every row of a matrix representing a vertex can have as many as two elements differing from zero, for this would give $2n$ non-zero coordinates in the array; hence at least one row must have a single non-zero component, which must have the value 1 because of relations (9). Because of (8) and (10), all other elements of the column in which the element with value 1 appears must be zero, and the original matrix less this row and column must be a doubly stochastic matrix with $(n - 1)$ rows and columns. Furthermore, if the point in question is a vertex of the original matrix, the new $(n - 1) \times (n - 1)$ matrix must also represent a vertex, and the inductive proof follows easily.

Thus, the introduction of doubly stochastic matrices permits the permutations to be represented as the vertices of a convex polyhedral set; if the utility function to be maximized can be extended to be a linear function over this set, which is the case for an important class of problems, the problem can be stated as a linear programming problem.

An example of this kind arises when n objects are to be assigned to n positions under a suitable utility rule. These objects may be people assigned to jobs, they may be factories assigned to areas, and so on. The restriction on the utility function is that there is a number describing the value of each object in every possible location and that this value is independent of the assignments of the remaining objects to the remaining positions. In short, there is to be an array g_{ij} of utilities to be achieved independently if the i -th object is assigned to the j -th position. The permutations in question are those relating the ordered set of objects to their assigned positions. If these permutations are represented by their

matrix in the manner described above, the total worth of any arrangement is given by the utility function

$$(11) \quad v = \sum_{ij} g_{ij} r_{ij} .$$

This function extends naturally to become a linear function defined (according to the same formula) over the space of doubly stochastic matrices, and the linear programming problem is thus set.

5. Economic equilibrium and a duality theorem

This section will be devoted to a proof, from the point of view of cost and utility, of a theorem which is really geometric in its content. The theorem itself was recognized implicitly by Dantzig and explicit algebraic statements and proofs have been supplied by Gale, Kuhn, and Tucker in various papers. The proof which will be developed here is a specialization of a study of some conditions of economic equilibrium contained in other work to be published by R. E. McShane and the author.

I again consider the major problem stated in terms of the inequalities (5) and (7), $\sum_a q_{\alpha a} x_a \leq f_{\alpha}$ and $x \geq 0$, respectively, and the requirement that the utility function expressed in (6) $u = \sum_a g_a x_a$ be maximized subject to the above feasibility restrictions.

I shall here assume that the numbers f_{α} in restrictions (5) represent actual investments in plant or other facilities and that these restrictions are obtainable under a rental agreement. It will be convenient notationally to consider that f_{α} is a particular set of restrictions which has been bought or rented and that competitive sets have values denoted by \bar{f}_{α} or by other similar marks deviating from f_{α} .

The rent corresponding to a set of restrictions \bar{F}_α (expressed in the scale used in (6) for the utility computation) will be denoted $w(\bar{F})$. In some particular cases I shall be interested in a function w which is a linear form; I shall reserve the symbol v for this function, and I shall always use the marks z_α as coefficients in this form, so that

$$(12) \quad v = \sum_\alpha z_\alpha \bar{F}_\alpha \quad .$$

Now, the point of view will be that a set of facilities abstractly denoted by f_α has been rented at a rate of $w(f)$. Under optimal operations this will yield a utility $u = \sum_\alpha g_\alpha \bar{x}_\alpha$, where \bar{x}_α is an optimal choice of activity level admissible with the given feasibility restrictions. Some other set of facilities abstractly denoted by \bar{F}_α could be rented at a rate $w(\bar{F})$. An obvious question to examine is the question of whether there is an economic force in favor of changing the feasibility restrictions rented.

I shall here point out that for some choices of \bar{F} there may be no solutions at all to the inequalities (5) and (7), I shall rule these candidates out as not admissible. Other choices might conceivably lead to possibly unlimited utility, but I shall ignore these on the same basis as above -- namely, lack of interest. (Actually it will become clear that there is no way a problem with a finite maximum attainable utility can be deformed into one with possibly unlimited utility without changing the coefficients $q_{\alpha a}$.) In order to avoid tedious detail I shall omit most reference to admissibility and to the possibility of unlimited utilities.

However, I shall establish some formal descriptions of terminology in order to ease the job of expressing the simple for extensive remarks which will be pertinent.

DEFINITION. A set of restrictions \bar{F} will be said to be admissible if there exist activity levels x_a which satisfy the feasibility restrictions (5) and (7) with the values \bar{F}_α inserted in the right members of (5):

$$(5) \quad \sum q_{\alpha a} x_a \leq \bar{F}_\alpha ,$$

$$(7) \quad x_a \geq 0 .$$

DEFINITION. A set of activity levels x_a will be said to be admissible with \bar{F}_α if they satisfy the feasibility conditions (5) and (7) as stated above.

DEFINITION. For some fixed f_α let \bar{x}_a be a set of activity levels maximizing the form (6) $u = \sum_a g_a x_a$ subject to the feasibility restrictions (5) $\sum q_{\alpha a} x_a \leq f_\alpha$ and (7) $x_a \geq 0$. Denote by S the subset of these restrictions (5) and (7) which are satisfied as equalities by x_a . A set of restrictions \bar{F}_α is weakly admissible relative to S if it admits a set x_a satisfying the inequalities of S with the numbers \bar{F}_α substituted in the right members of (5).

DEFINITION. A set of activity levels x_a is weakly admissible with respect to restrictions \bar{F}_α which are weakly admissible relative to S (associated with f_α and \bar{x}_a) if it satisfies all the inequalities of S in which \bar{F}_α have been appropriately substituted in the right members.

Then, attention will be restricted to a set (implicitly defined) of admissible or weakly admissible values \bar{F}_α , and functions $t(\bar{F})$ and $\bar{v}(\bar{F})$ will be defined implicitly for these values;

DEFINITION. The function t , defined for every admissible set \bar{F}_α as argument, is the maximum attainable utility in expression (6) associated

with the restrictions \bar{F}_α in the right members of inequalities (5) when these inequalities are used with (7) to define admissible activity levels.

DEFINITION. The function $\bar{t}(\bar{F})$, defined for every weakly admissible set \bar{F}_α relative to some set S of inequalities (5) and (7) is the value of the maximum attained by the utility expressed in the linear form (6) among weakly admissible activity levels relative to S .

LEMMA 1. For any f_α and x_α the function $\bar{t}(\bar{F})$ is defined for all \bar{F}_α for which $t(\bar{F})$ is defined, $\bar{t}(\bar{F}) \geq t(\bar{F})$, and $\bar{t}(f) = t(\bar{F})$.

Proof. The inequality is an obvious result of removing admissibility restrictions from the admissible set to create the weakly admissible set. The final equality follows from the non-restrictive nature of the dropped inequalities at the optimizing solution \bar{x}_α .

LEMMA 2. The set of admissible or weakly admissible activity levels associated with any admissible or weakly admissible set of restrictions \bar{F}_α is the vector sum of any solution of the set plus the set of solutions of the set with $\bar{F}_\alpha = 0$.

Proof. This is a standard result of linear algebra.

LEMMA 3. If x_α is an admissible or weakly admissible set of activity levels for some admissible or weakly admissible \bar{F}_α , then every admissible or weakly admissible set of restrictions f' neighboring \bar{F}_α admits or weakly admits activity levels neighboring x_α .

Proof. The proof is a standard exercise in linear algebra using lemma 2.

LEMMA 4. If any feasible \bar{F}_α or weakly feasible \bar{F}_α exists for which $t(\bar{F})$ or $\bar{t}(\bar{F})$ exists and is finite, then $t(\bar{F})$ and $\bar{t}(\bar{F})$ exist and are finite for every

feasible or weakly feasible \bar{f}_α and in particular $t(0) = \bar{t}(0) = 0$.

Proof. The proof follows immediately from the linear homogeneous nature of the utility u , and from lemma 7 below.

With the definition of $t(\bar{f})$, it is easy to describe a condition of economic equilibrium in which there is no economic force to change an assignment of feasibility means from the values f_α to some new values \bar{f}_α .

DEFINITION. A feasibility assignment f_α is an equilibrium assignment if and only if for every admissible \bar{f}

$$(13) \quad w(\bar{f}) - w(f) \geq t(\bar{f}) - t(f) \quad .$$

This definition says in effect that the cost of changing the feasibility means is no less than the gain which could be attained by the change in potential utility which would be implied.

Several obvious statements will be made about functions which cause f_α to be an equilibrium assignment. They will lead to the duality theorem which will say in effect that in any problem it is possible to give an example of a linear homogeneous function $w = v$ which renders a particular feasible f_α an equilibrium choice. This abstractly possible rent is useful in computation whether it is a realistically attained rent or not.

LEMMA 5. If $w(\bar{f}) = t(\bar{f})$, then f_α is an equilibrium assignment.

Proof. Under the conditions of the lemma, (13) is satisfied identically as an equality.

LEMMA 6. If $w(f) = t(f)$ and $w(\bar{f}) \geq t(\bar{f})$ for every \bar{f}_α , then f_α is an equilibrium assignment.

Proof. Under the conditions of the lemma, inequality (13) is satisfied immediately.

The development will now follow a course in which it will be proved that $t(\bar{f})$ is a convex positive homogeneous function of weight one and that a supporting linear homogeneous function will serve as $w(\bar{f})$.

LEMMA 7. If \bar{f}_α is feasible and if ρ is a positive number, then $\rho\bar{f}_\alpha$ is feasible and $t(\rho\bar{f}) = \rho t(\bar{f})$; that is, $t(f)$ is positive homogeneous of weight one.

Proof. If \bar{x}_α is an optimal solution for \bar{f}_α , then $\rho\bar{x}_\alpha$ is clearly a feasible set of activity levels for restrictions $\rho\bar{f}_\alpha$ and hence, since the utility of any set of feasible activity levels is expressed by a linear homogeneous form and since the particular feasible solution $\rho\bar{x}_\alpha$ is a competitor for the optimizing solution, it follows that $t(\rho\bar{f}_\alpha) \geq t(\bar{f}_\alpha)$. However, if an optimizing solution x^*_α for the feasibility restrictions ρf_α is selected, the same argument with multiplier ρ^{-1} gives $t[\rho^{-1}(\rho\bar{f})] \geq \rho^{-1} t(\rho\bar{f})$, and the equality follows. This completes the proof of the lemma.

LEMMA 8. The statement of lemma 7 is valid for the function \bar{t} and weakly admissible restrictions \bar{f}_α .

Proof. The proof is that of lemma 7.

LEMMA 9. If \bar{f}_α is weakly feasible relative to f_α and \bar{x}_α , then $f'_\alpha = f_\alpha + \rho(\bar{f}_\alpha - f_\alpha)$ is feasible for all $\rho > 0$ and $\bar{t}[f_\alpha + \rho(\bar{f}_\alpha - f_\alpha)] = \bar{t}(f_\alpha) + \rho\bar{t}(\bar{f}_\alpha - f_\alpha)$.

Proof. The proof is that of lemma 7.

LEMMA 10. The function $t(\bar{F})$ is convex; that is, for any admissible restrictions \bar{F}_α and f'_α and for any numbers λ and μ which are both non-negative and whose sum is one it is true that $\lambda \bar{F}_\alpha + \mu f'_\alpha$ is admissible and that

$$(14) \quad t(\lambda \bar{F} + \mu f') \geq \lambda t(\bar{F}) + \mu t(f') .$$

Proof. The admissibility of $\lambda \bar{F}_\alpha + \mu f'_\alpha$ is clear, for if \bar{x}_α is admissible with \bar{F}_α and if x'_α is admissible with f'_α , then $\lambda \bar{x}_\alpha + \mu x'_\alpha$ is admissible with $\lambda \bar{F}_\alpha + \mu f'_\alpha$; this follows immediately by multiplying the inequalities (5) and (7) (with appropriate choices for $x_\alpha = \bar{x}_\alpha$ or x'_α and $f_\alpha = \bar{F}_\alpha$ or f'_α) by the non-negative numbers λ and μ . If the two sets of activity levels are optimizing, each for its associated restrictions, then the utility associated (by (6), which is a linear form) with the admissible activity level $\lambda \bar{x}_\alpha + \mu x'_\alpha$ subject to the new restrictions $\lambda \bar{F}_\alpha + \mu f'_\alpha$ is $\lambda t(\bar{F}) + \mu t(f')$, and inequality (14) follows immediately. This completes the proof of the lemma.

LEMMA 11. The function $\bar{t}(\bar{F})$ is convex.

Proof. The proof is that of lemma 10.

These lemmas prove that $t(\bar{F})$ and $\bar{t}(\bar{F})$ are convex functions which are positive homogeneous of weight one. Readers with an intimate knowledge of such functions and who may be familiar with recent work on econometric theory based on considerations of such functions may jump to immediate conclusions which will be established in the next theorem. Those who are willing to apply Euler's theorem on homogeneous functions ignoring the possible lack

of the required partial derivatives may prove the next theorem shortly by setting

$$w(\bar{F}) = \sum_{\alpha} \left(\frac{\partial t}{\partial \bar{F}_{\alpha}} \right)_{\bar{F}_{\alpha} = f_{\alpha}} \cdot \bar{F}_{\alpha} ,$$

and applying the lemmas above.

THEOREM I. There exist numbers z_{α} associated with any feasible f_{α} such that if for this choice of z_{α} the function $w(\bar{F}) = v(\bar{F}) = \sum_{\alpha} z_{\alpha} \bar{F}_{\alpha}$, then the restrictions f_{α} are equilibrium restrictions.

Proof. First consider the possible case that $t(f) = 0$ and $t(\bar{F}) \leq 0$ for all \bar{F}_{α} . In this case the coefficients may be taken $z_{\alpha} = 0$. With this choice the value of v is identically zero and the theorem follows by lemma 6.

Otherwise consider the following construction. Find the set F^{+} of values \bar{F}_{α} at which $\bar{v}(\bar{F}) = t(f) + h$, where h is a small positive constant. It will be shown later that F^{+} has content and that it is closed. Choose on F^{+} a point closest in the sense of euclidean metric to f_{α} ; call this point f'_{α} . Write $z_{\alpha} = \sigma(f'_{\alpha} - f_{\alpha})$ and choose $\sigma = \frac{h}{\sum (f'_{\alpha} - f_{\alpha})^2}$, where h is the positive number chosen in F^{+} .

Before continuing with the proof, note that the positive content of the set F^{+} follows from the lemmas above. In particular, if $t(f) \neq 0$, some \bar{F}_{α} on the ray joining the origin with f_{α} (on one side or the other of f_{α} depending on the sign of $t(f)$) will lie on F^{+} for small enough h , according to lemma 8. If $t(f) = 0$, and using the assumption already made that there exists some \bar{F}_{α} such that $\bar{v}(\bar{F}) \geq 0$, there must exist a point on the ray from f_{α} through such \bar{F}_{α} on F^{+} , according to lemma 9.

The fact that F^+ is closed follows from the continuity of the form (6) giving the utility function and lemma 3. Hence the point f'_α mentioned above must exist.

Now, if f_α and f'_α are collinear with the origin, it follows from the facts that $v(f') - v(f) = h$, that $v(0) = 0$, that $v(\bar{f})$ is linear, and from lemma 8 that $v(f) = t(f)$ and $v(f') = \bar{v}(f)$. If f_α and f'_α are not collinear with the origin, then the same results can be obtained by noting that lemmas 8 and 9 guarantee the linearity of $\bar{v}(\bar{f})$ when \bar{f}_α is restricted to move in a single two-dimensional plane containing the segment from the origin to f_α .

The rest of this proof depends on noticing that the determination of z_α is independent of the size chosen for h in determining F^+ . This follows immediately from lemma 9 using the same linear reasoning as that employed in lemma 7; that is, if two different values of h gave two different values of z_α then the usual inconsistency shows up that neither of these can be good, for each furnishes a competitive rate of change for the determination of the other.

With this observed an analogue of Euler's theorem, using the z_α instead of partial derivatives (they were computed by formulas suitable for computing the partial derivatives of a linear homogeneous function from the information granted) will give the final desired result. This analogue is that with this choice of z_α used as partial derivatives of $\bar{v}(\bar{f})$, it is true that $\bar{v}(\bar{f}) \leq \sum z_\alpha \bar{f}_\alpha$. This result is a natural one, for the inequality may occur when the restrictions prevent the use of linear interpolation. However, the proof of this theorem does not follow the usual proof of Euler's theorem. Rather it depends on a simpler geometrical argument, which will be sketched.

If the proposition is false, then there must exist a point f''_{α} such that $\bar{v}(f'') > \sum_{\alpha} z_{\alpha} f''_{\alpha}$. Now, this point f''_{α} along with the origin and the point f_{α} determines a two-dimensional plane, and in this plane the function $\bar{v}(f)$ is linear according to lemmas 8 and 9. Since the function $v = \sum_{\alpha} z_{\alpha} f_{\alpha}$ is linear and since the values of \bar{v} and v agree at f_{α} , it follows that \bar{v} must exceed v at all points along the ray from f_{α} through f''_{α} . Now, if this ray intersects or is parallel to the hyperplane $v = t(f) + h$, where h is the positive value used to determine f'_{α} ; then it must be true that f'_{α} is further from f_{α} than some other point determined as follows. The point on the ray at which $\bar{v}(f) = t(f) + h$ is determined, and the segment between this point and f'_{α} is constructed. By assumption, there is a point on this segment closer to f_{α} than is f'_{α} . By lemma 10 the value of \bar{v} at this closer point is at least $t(f) + h$, and if it exceeds this value at this point there is (by lemma 9) a point even closer at which \bar{v} attains the value $t(f) + h$. This completes the contradiction if v is increasing along this ray.

Finally, if the ray from f_{α} through f''_{α} is a direction of decreasing v , then a similar argument relative to the rays from f_{α} through a point of the segment joining f'_{α} and f''_{α} leads to a contradiction, for it is easily shown that \bar{v} exceeds v and increases along such a ray. This completes the proof of the theorem.

We now turn to the duality theorem.

THEOREM II. If the linear form (6), $u = \sum_{\alpha} g_{\alpha} x_{\alpha}$ is maximized at $x_{\alpha} = \bar{x}_{\alpha}$ among admissible variables x_{α} subject to the feasibility restrictions
 (5) $\sum_{\alpha} a_{\alpha\beta} x_{\alpha} \leq f_{\beta}$ and (7) $x_{\alpha} \geq 0$, then the linear form

$$(14) \quad v = \sum_{\alpha} f_{\alpha} z_{\alpha}$$

attains a minimum at some set of values $z_{\alpha} = \bar{z}_{\alpha}$ among admissible variables z_{α} subject to the restrictions

$$(15) \quad z_{\alpha} \geq 0$$

and

$$(16) \quad \sum_{\alpha} q_{\alpha a} z_{\alpha} \geq g_a .$$

Furthermore, $\bar{z}_{\alpha} = 0$ for every α for which $\sum q_{\alpha a} \bar{x}_a < f_{\alpha}$, and $\bar{x}_a = 0$ for every a for which $\sum q_{\alpha a} \bar{z}_{\alpha} > g_a$. Moreover the maximal value of u equals the minimal value of v .

Proof. The minimal value of the form v will be shown to be taken at the values z_{α} computed in the proof of the last theorem.

In the first place it is easy to show that these values are admissible under (15) and (16). Indeed, if $v = \sum z_{\alpha} f_{\alpha}$ is a rent which renders f_{α} an equilibrium restriction, it is obvious that $z_{\alpha} \geq 0$; otherwise the rent would be lowered by increasing the values of f_{α} for any values of α corresponding to negative z_{α} , and this decrease in rent would not be accompanied by any restriction in activity; in fact, it would generally be accompanied by greater freedom of activity, hence no decrease in utility. This proves that the coefficients z_{α} developed in connection with theorem I satisfy condition (15).

Similarly, if condition (16) is violated for some value of a , then the restrictions should be increased by enough to permit a unit increase of the

activity level x_a for this value of a . This increase will require at most an increase of $q_{\alpha a}$ of the α -th restrictions at a total cost of $\sum_{\alpha} q_{\alpha a} z_{\alpha}$; if condition (16) is violated the gain from this, g_a , exceeds the increase in rent and hence the levels of restriction are not equilibrium levels. This completes the proof of the admissibility of the coefficients z_{α} of theorem I.

Now, if restrictions (5) are multiplied by the non-negative numbers z_{α} and summed and restrictions (16) are multiplied by the non-negative numbers x_a and summed the following inequalities result:

$$v = \sum_{\alpha} f_{\alpha} z_{\alpha} \geq \sum_{\alpha} a_{\alpha} z_{\alpha} x_a \geq \sum_a g_a x_a = u.$$

Thus, for no admissible choice of x_a and z_{α} is u larger than v . However, for the existence of no force proved in connection with the choice of z_{α} in theorem I, there can be no force toward the feasible income of zero connected with restrictions set at the zero level; that is, there will be force to go out of business unless $u \geq v$. Thus, for the optimal choice of $x_a = \bar{x}_a$ and the choice of z_{α} made in the last theorem, it must be true that $u = v$; this proves the equality advertised in the last sentence of the statement of the theorem.

Finally, we need only notice that any strict inequality among the set (5) is preserved as a strict inequality if it is multiplied by a positive number z_{α} and is preserved as an equality if it is multiplied by a zero number z_{α} , whereas equalities are preserved as equalities when multiplied by any z_{α} . A similar remark applies to the inequalities (16) and multipliers x_a . In order to have the equality preserved, the condition stated in the next to last sentence is necessary. This completes the proof of the theorem.

6. Numerical solution of problems

The application of theorem II above in many ingenious ways has led to realistic computational attacks on problems. One of the most ingenious and successful of these is the simplex method which has been developed by G. B. Dantzig and his coworkers and which is described in some of the publications already cited.

The description of the simplex method in a short space has defied good expositors, and there is no intention of presenting a full or even a workable account of computational methods in this paper.

However, it should be noted that methods are developed to a point where they are applicable completely automatically on high speed computers, and that problems with a hundred or more variables and a hundred or more restrictions are now feasibly attackable through the use of these systematic attacks on the larger machines now available.

I shall include a short example. It will be solved by methods not generally applied to the numerical solutions of problems, but the solution will illustrate some of the points of theorem II above.

The example pertains to the function

$$(17) \quad u = x_1 + 2x_2 + 3x_3 + 4x_4 \quad ,$$

which is to be maximized subject to the feasibility conditions

$$(18) \quad \begin{aligned} 2x_1 + 1x_2 + 4x_3 + 1x_4 &\leq 6 \quad , \\ 3x_1 + 2x_2 + 2x_3 + 3x_4 &\leq 9 \quad , \\ 1x_1 + 4x_2 + 3x_3 + 2x_4 &\leq 7 \quad , \end{aligned}$$

and the non-negativity conditions

$$(19) \quad x_a \geq 0 .$$

The dual problem to this involves the form

$$(20) \quad v = 6z_1 + 9z_2 + 7z_3 ,$$

which is to be minimized subject to the feasibility conditions

$$(21) \quad \begin{aligned} 2z_1 + 3z_2 + 1z_3 &\geq 1 , \\ 1z_1 + 2z_2 + 4z_3 &\geq 2 , \\ 4z_1 + 2z_2 + 3z_3 &\geq 3 , \\ 1z_1 + 3z_2 + 2z_3 &\geq 4 , \end{aligned}$$

and the non-negativity conditions

$$(22) \quad z_a \geq 0 .$$

Before the illustrative problem is continued, let it be perfectly clear that the complete unanimity of positive signs among the coefficients is a great help (but it is a help which may appear in many problems of practical significance — and unfortunately be missing in many others of at least as great significance).

Since it is established that vertices of the regions of feasible solutions will maximize or minimize the functions considered, a first attempt will be made to find vertices. In the problems at hand, this is easy (again the positive coefficients help). An initial start for x_a is $x_a = (0, 0, 0, 0)$.

This is a vertex of the region (the unique solution of the four equations got from (19) by rejecting the possibility of inequality), and a simple test shows that it satisfies all the conditions (18) as strict inequalities. The value attained by u at this point is 0.

Turning to the dual problem, the solution of the three equations which can be got by rejecting the possibility of inequality in (22) is not feasible; indeed, it satisfies none of the relations (21). However, a feasible solution can be obtained by readmitting one of the inequalities from this set and extracting an equation from (21). If we set $x_1 = x_2 = 0$ arbitrarily as the equations retained from (22), it develops that the fourth of inequalities (21) is most binding on x_3 , and we get a vertex at $(0, 0, 2)$.

Now according to theorem II these two vertices would constitute solutions of the problem and its dual if and only if the value attained by u and that attained by v are equal. The value attained by v at this vertex, however, is 14, which is greater than the zero value attained by u . Consistent with theorem II, we note that a non-zero value of x_3 appears even though the third of the inequalities (18) is satisfied as a strict inequality rather than as an equality. This furnishes some guide to a means of improving the values obtained.

Since the fourth of the inequalities (21) is satisfied by the z -vertex in hand as an equality, theorem II would encourage the enlargement of x_4 . Thus we replace the fourth of the restrictions (19) by an inequality and seek an equality among the set (18). The most binding of these inequalities (18) under this conditions, $x_1 = x_2 = x_3 = 0$ is the second, and we are led to a new vertex $x_4 = (0, 0, 0, 3)$. At this vertex, the value of u is 12.

Since the second of the inequalities (18) is now satisfied as an equality, we are encouraged to permit the value of z_2 to become positive in seeking a better vertex in the z -space. The earlier restriction $z_2 = 0$ will be replaced by an equality extracted from one of the first three inequalities of (21) — the fourth of these inequalities is already satisfied as an equality. The third equality is adequate, and the vertex it gives (with the other restrictions) is $z_\alpha = (0, 6/5, 1/5)$; for this vertex, $v = 61/5$.

Again, we do not have a solution of the problem and its dual, but there is considerably better agreement between the values of $u = 12$ and $v = 61/5$ than we had attained before. The discrepancy is still due to the fact that the third of the inequalities (18) is satisfied as a strict inequality while $z_3 > 0$.

The z -vertex now in hand satisfies the third and the fourth inequalities (21) as equalities, and hence both x_3 and x_4 are encouraged to seek positive values. Thus we relax the equality $x_3 = 0$ to the inequality $x_3 \geq 0$, and we seek to satisfy another of the inequalities (18) as an equality (meanwhile satisfying all inequalities, of course). We retain the second equality from (18) which is satisfied at the old vertex. The solution obtained by satisfying the third relation of (18) as an equality satisfies the first relation as a strict inequality, and we have a new vertex $x_\alpha = (0, 0, 3/5, 13/5)$.

Actually, this completes the solution of the problem. This follows from the evaluation of $u = 61/5$ at this vertex, a value which agrees with

the value obtained for v at the last z -vertex. Furthermore, we might notice that the positive components of the z -vertex correspond to values of the index for which relations (18) are satisfied as equalities, as theorem II demands, and that the positive components of the x -vertex correspond to values of the index for which relations (21) are satisfied as equalities.

This completes the example.

C. TOMPKINS

Numerical Analysis Research
Department of Mathematics
University of California
Los Angeles 24, California

15 June 1956

Bibliography

1. Tjalling C. Koopmans, Editor, Activity Analysis of Production and Allocation, Proceedings of a Conference, John Wiley and Sons, Inc., New York, 1951.
2. H. A. Antosiewicz, Editor, Proceedings of the Second Symposium in Linear Programming (January 27-29, 1955), volumes 1 and 2, National Bureau of Standards, Washington, D.C., 1955.
3. A. Charnes, W. W. Cooper, and A. Henderson, An Introduction to Linear Programming, John Wiley and Sons, Inc., New York, 1953.

The Basic Principles of a Two Dimensional Slide Rule

Clarence R. White*

The primary objective of this paper is to present a Two Dimensional Slide Rule which combines the features of special purpose graphpaper, nomograms, slide rules and the like. Such a device will consist of two transparent surfaces.

The first surface will be called the 'base surface' or 'body' upon which are drawn appropriate function scales and a set of curves in color, the rectangular coordinates of which are given by

- | | |
|--|-------------------------|
| 1. $(\phi, \log \text{ trig } \phi)$ | in figure 1 |
| 2. $(x, \log x)$ | in figures 2, 3, 4, 5 |
| 3. $(x = \log \tan \phi, \log \text{ trig } \phi)$ | in figure 6 |
| 4. $(f(\phi), \log \text{ trig } \phi)$ | in figures 8, 9, 10, 11 |
| 5. $(\phi, \log \text{ trig } \phi)$ | in figures 13, 14 |

This surface corresponds to the 'body' of the one dimensional slide rule.

The second surface will be called the 'sliding surface' or 'slide' upon which are drawn sets of scales colored to match not only the co-operating curves of the base surface but also the quantity under consideration. The division marks of each scale are perpendicular to the straight line axis which theoretically is infinite in extent. The index of a scale is that mark which denotes the number 1. This surface corresponds to the 'slide' of the one dimensional slide rule. See figures 1 and 12.

The fundamental principle of this Two Dimensional Slide Rule results when a sliding surface comes to rest upon a base surface in such a way that the slope of an axis when referred to the coordinate system of the base surface is 90 degrees, i.e. perpendicular to the horizontal direction, since each apparent intersection of a base surface curve with a sliding surface axis determines a point on curve and on axis. Identification of results is also accomplished by the introduction of alignment algebra which gives coding symbols for the location of desired solutions.

The Two Dimensional Slide Rule may be regarded as a special case of alignment charts which is limited to real positive numbers and represent solutions to $x(y)^{-n}z = 1$. The use of a base surface and a transparent sliding surface, upon each of which the horizontal rulings are linear and the vertical rulings are logarithmic (corresponding to the y-scale and z-scale respectively) affords a ready means for the construction of alignment charts for all values of n.

*Ballistic Research Laboratories

See figures 2 and 3.

It also gives a solution when any three of the four numbers are specified provided that the sliding z-surface whose index is the index of its z-scale be superimposed upon the base y-surface at the point $(n, \log x)$ for n and x given; at the point $(1, \log x)$ for n not given. Consider the following cases for the solution of $x(y^{-n})z = 1$.

1. Given $(n, x, y) = (2, 4, 6)$ with index location at $(n, \log x)$, find $z = 9$
See figure 4
2. Given $(n, x, z) = (2, 4, 9)$ with index location at $(n, \log x)$, find $y = 6$
See figure 4
3. Given $(x, y, z) = (4, 6, 9)$ with index location at $(1, \log x)$, find $n = 2$
See figure 5

The index location of the sliding z-surface is thus a two dimensional parameterization and gives rise to the motion of the sliding surfaces of the Two Dimensional Slide Rule. The alignment solution for case (1) results from the alignment of $y = 6$ on the y-scale with the point $(0, \log 1)$ to give the answer $z = 9$ on the z-scale. The alignment solution for the case (2) results from the alignment of $z = 9$ on the z-scale with the point $(0, \log 1)$ to give the answer $y = 6$ on the y-scale. The nomographic solution for case (3) results from finding the point z on the z-surface along the line determined by the points $(0, \log 1)$ and the position of $y = 6$ on the y-scale at the point $(1, \log y)$. The abscissa of z is the desired value of $n = 2$ on the n-scale which is horizontal. It is convenient to insert a piece of thread at the pivot point $(0, \log 1)$ on the base y-surface to serve as the unmarked straight edge or axis.

The repeated use of such an axis in nomography suggests the introduction of an algebra of alignment charts which will be illustrated from the Line Coordinate Chart given in figure 4.

The symbolism to be introduced stems from the fact that an alignment chart is made up of Scales, Axes and division Marks. If now these three elements be identified by means of the capitalized letters in the order just given, then symbolically

$S_1)A(M_j$

represents a point on the Axis determined by division Marks on the Scale so that M_j represents a number which is in one-to one-correspondence with the points of axis.

An algebraic symbolization of procedures is made possible by

205

$$S_1)A(M_A \doteq S_1)B(M_B)$$

denotes the horizontal translation of a point from axis A to axis B

$$S_1)A(M_A : S_1)B(M_B)$$

denotes the axis determined by two points

$$S_1)A(M_A : S_1)B(M_B :: S_1)C(M_C)$$

denotes the alignment of a third point with two other points

The designations for axes fall into two categories (1) a number associated with its intersection upon the horizontal axis and (2) a literal expression based upon its functional representation. A similar analysis follows for a point on such an axis: (1) a number associated with its position on the axis which is vertical and (2) a literal expression based upon its functional representation, thus

$$S_1)A(M_A = f(x)$$

denotes the value of $f(x)$

The alignment algebra gives for Case (1) figure 4

$$\text{Blue}0(1 : \text{Blue}1(y=6 :: \text{Yellow}1(z=9)$$

Coding symbols for the location of a point on a sliding surface will be denoted by a number triad, where the first number refers to a function scale; the second number, to a vertical axis; and the third number, to a point on the axis. The symbolic expression is $S_1)A(M_j$.

Coding symbols belonging to a base surface will be preceded by ^{the symbol} \wedge . Horizontal scales will be denoted by three symbols, the first of which is 's'; the second, a number; the third 'c', such as $\wedge s2c$, $\wedge s2c$, etc. A point m_2 on such a scale will be denoted by $\wedge s2c(m_2$.

Curves for I-Base Surface-I (figure 1) are constructed from points whose Ordinate = $\log F_n(x)$ and whose Abscissa = $\log \text{hav } \phi$ or $\log \text{Hav}(\phi + 90^\circ)$ where

$$F_a(x) = \csc \phi = (L + S)/2\sqrt{LS}$$

$\wedge a$

$$F_b(x) = \cot \phi = (L - S)/2\sqrt{LS}$$

$\wedge b$

$$F_c(x) = \sec \phi = (L + S)/(L - S)$$

$\wedge c$

$$F_d(x) = \text{one}$$

$\wedge d$

$$F_e(x) = \cos \phi = (L - S)/(L + S)$$

$\wedge e$

$$F_f(x) = \tan \phi = 2\sqrt{LS}/(L - S)$$

$\wedge f$

$$F_g(x) = \sin \phi = 2\sqrt{LS}/(L + S)$$

$\wedge g$

$$F_h(x) = \text{hav } \phi = S/(L + S)$$

$\wedge h$

$$F_H(x) = \text{Hav}(\phi + 90^\circ) = L/(L + S)$$

$\wedge H$

for 0 is less than S is less than L and for 10° is less than ϕ is less than or equal to 90° .

Coding symbols for the Two Dimensional Slide Rule

Blue)2(M₂ /a

denotes a point on Axis)2(
determined by the division
marks of its blue scale which
point is on curve /a of base
surface.

Blue)2 /s5c(50°

aligns axis)2(into a one
dimensional slide rule movement
along the division 50° of the
horizontal scale, s5c.

Blue)2 /s5c(50°

also means that the vertical
axis)2(is perpendicular to
the horizontal axis of s5c at
point 50° on it.

Blue)2(20° /a : Blue)2 /s5c(50°

fixes the position of the sliding
scale)2(by means of a number
on it and the number on scale,
s5c.

Green)1(L /H : Green)1(S /h

fixes the position of the sliding
scale)1(by means of two
numbers on it.

Green)1(L /H : Green)1(S /h :: Green)1(M /d

determines the answer M at the
intersection of the axis)1(
with the curve /d

Blue)2(20° /a : Blue)2 /s5c(50° :: Orange)2(M /d

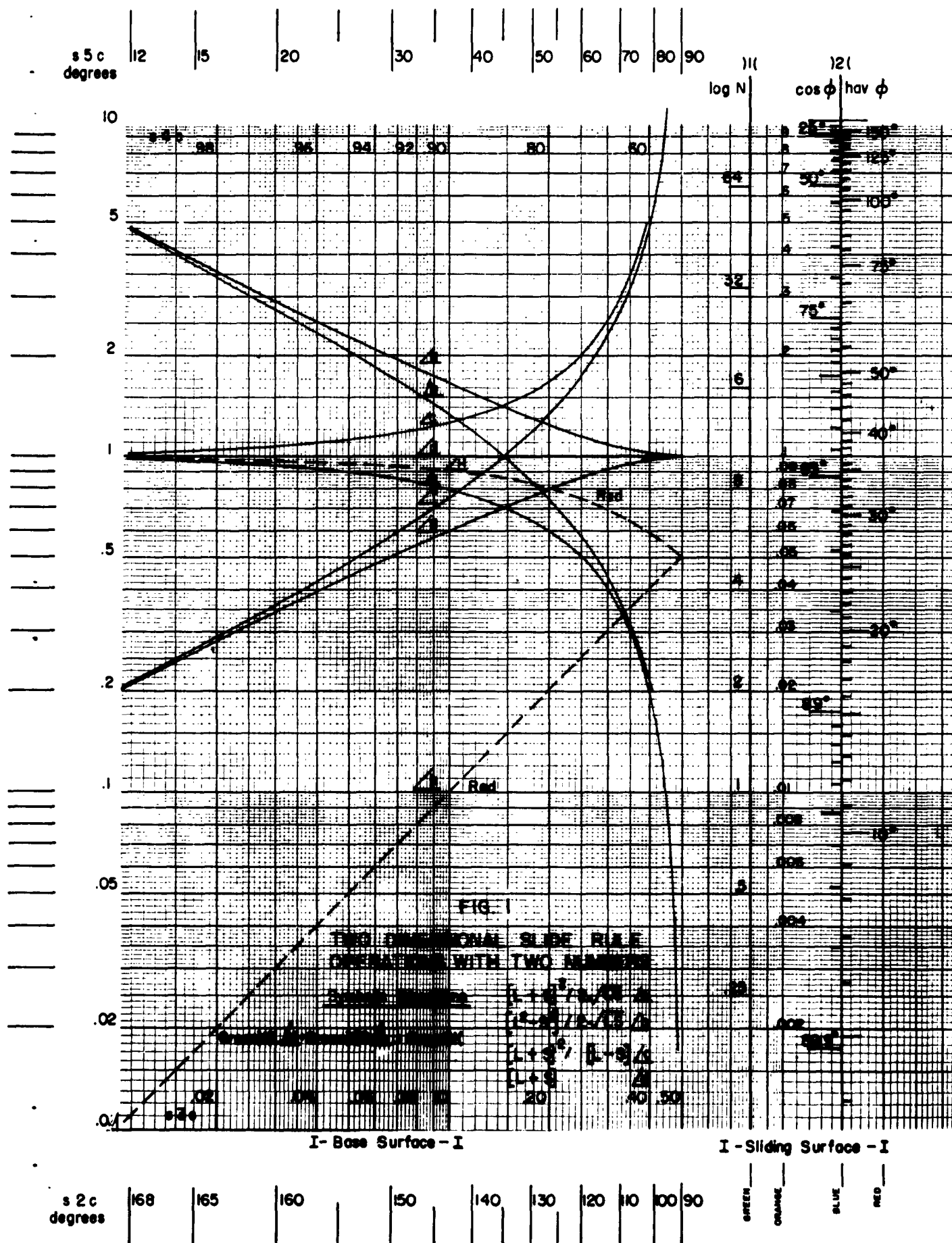
determines the answer M at the
intersection of the axis)2(
with the curve /d

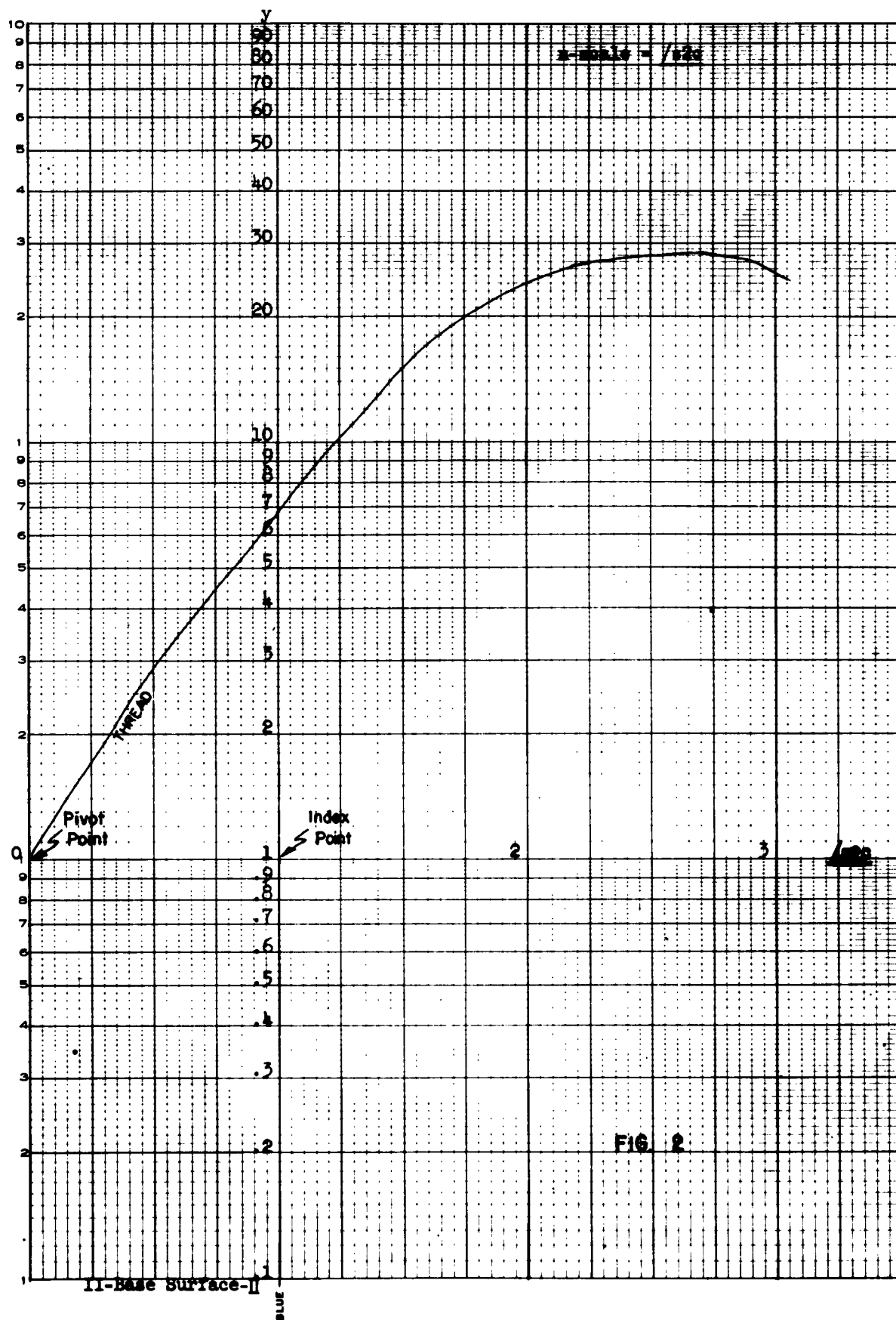
Figures 6 through 14 represent Two Dimensional Slide Rule Solutions
to the problems therein defined.

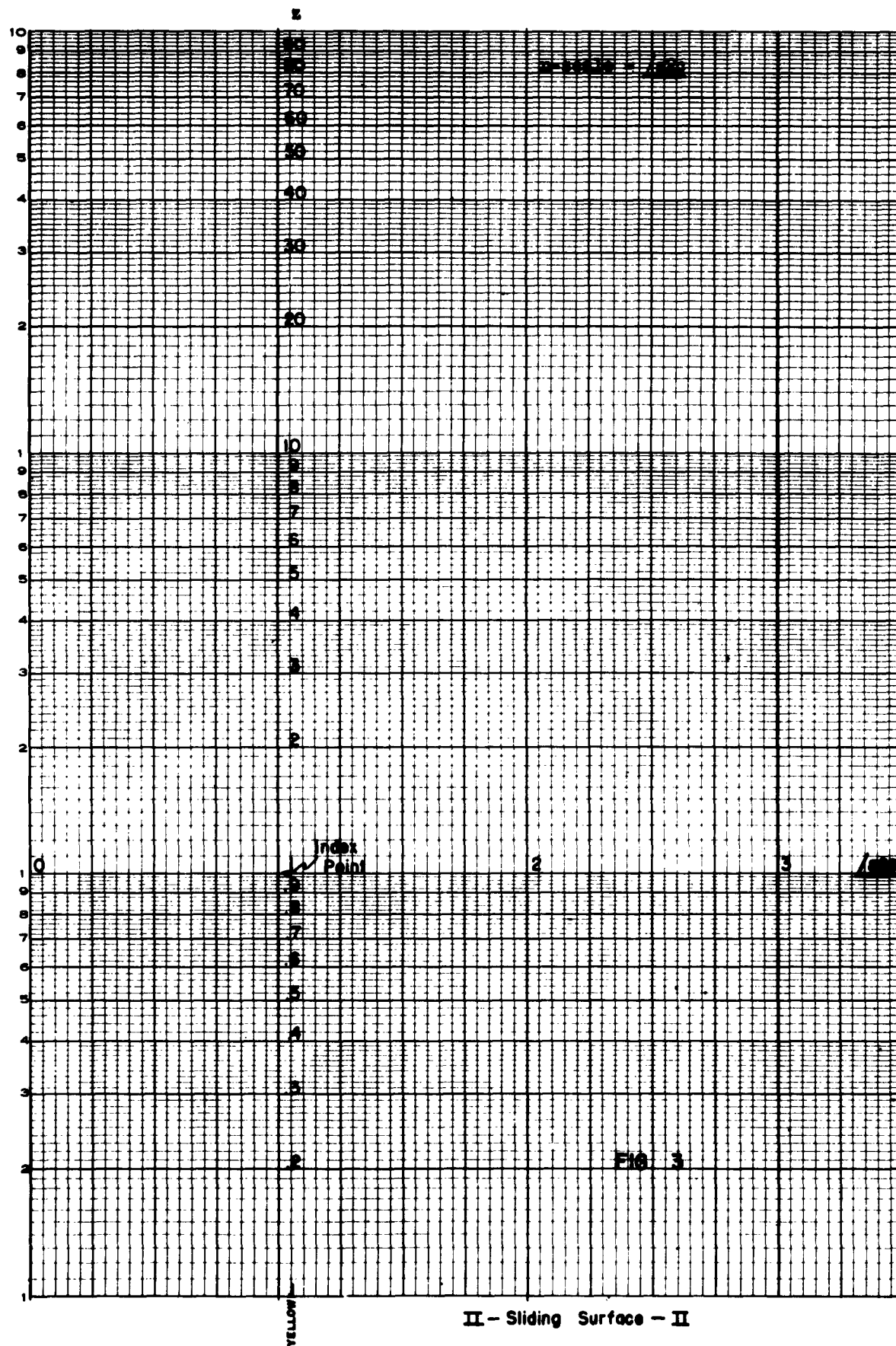
My thanks to co-workers who had a part in the preparation and in the
publication of this paper.

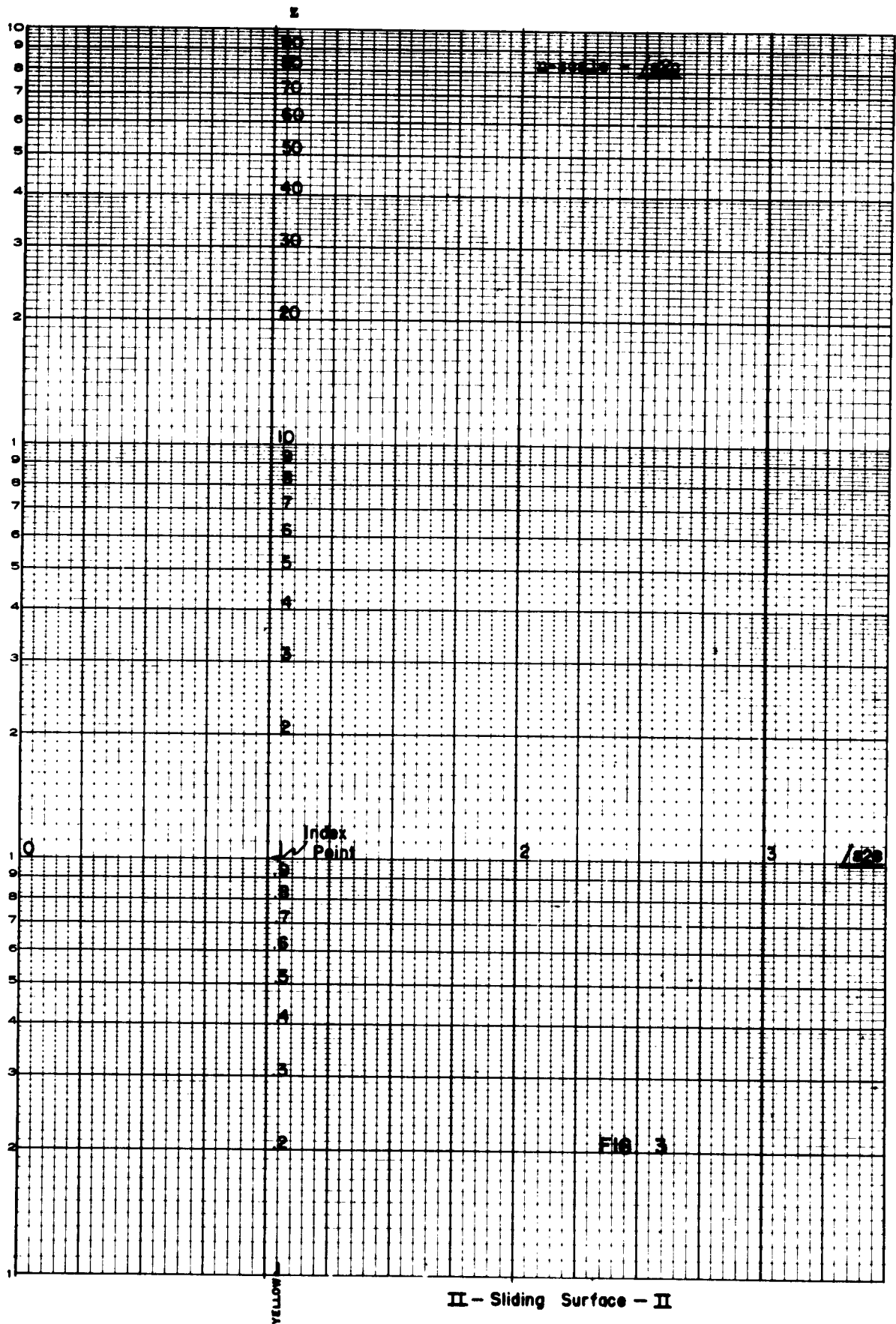
BIBLIOGRAPHY

1. Allcock, H., and Jones, J., "The Nomogram", London, Sir Isaac Pitman and Sons, 1932
2. Burrows, W., Graph Papers as Instruments of Calculation, American Journal of Physics, March, 1949
3. Clement, P., High Frequency Transmission Line Chart, Electronics, August, 1949
4. D'Ocagne, M., "Traite de Nomographie", 1st ed. Gauthier-Villars, Paris, 1899
5. Donnell, L., A Chart for Plotting Relations between Variables over Their Entire Real Range, Quarterly of Applied Mathematics, October, 1943.
6. Douglass, R., and Adams, D., "Elements of Nomography", McGraw-Hill Book Company, Inc., New York, 1947
7. Hansel, C., An Extension of Nomography, Philosophical Magazine, Volume 34, January 1943
8. Hewes, L., and Seward, H., The Design of Diagrams for Engineering Formulas, McGraw-Hill Book Company, Inc.
9. Lipka, J., "Graphical and Mechanical Computation", New York, John Wiley and Sons, 1921
10. Mackey, C., "Graphical Solutions", John Wiley and Sons, Inc., New York, 1936
11. Markus and Zeluff, Electronics for Engineers, McGraw-Hill, New York
12. Middleton, D., Theory and Applications of Nomographs, November 1943, Radio-Electronics Magazine
13. Muffly, Gary, Impedance-Combining Chart, Electronics, March 1944
14. Silverman, E., A Unified Treatment of Certain Santa Corporation Nomographs, Combat Development Department, Ft. Sill, Oklahoma, August, 1955
15. White, C., Field Strength Calculator for Vertical Coverage Patterns and Propagation Curves, CESL Technical Memorandum No. 154-E, December, 1944
16. White, C., Two-Dimensional Slide Rule, Copyright 1951
17. Van Voorhis, M., "How to Make Alignment Charts," McGraw-Hill, Inc., New York, 1937









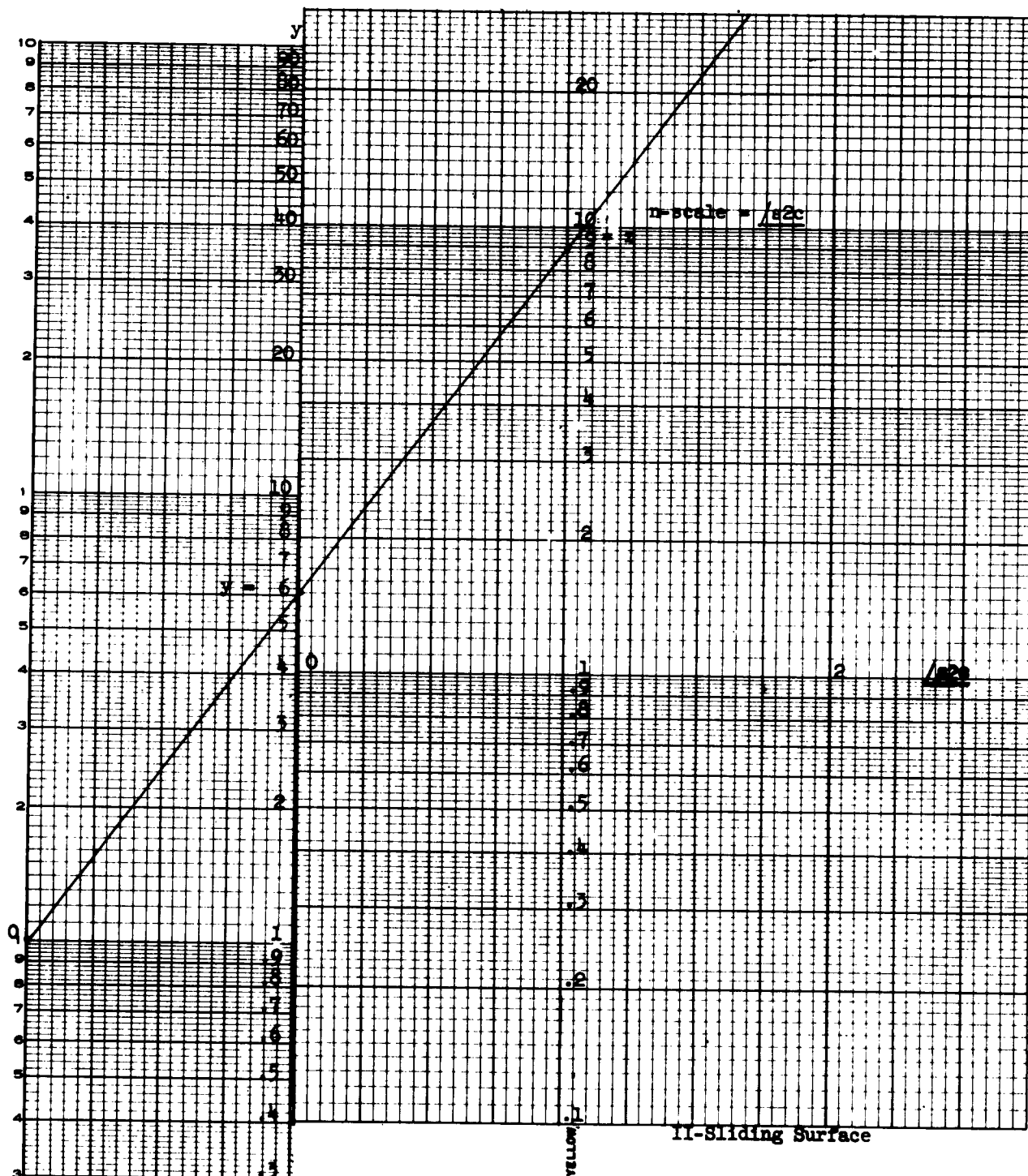


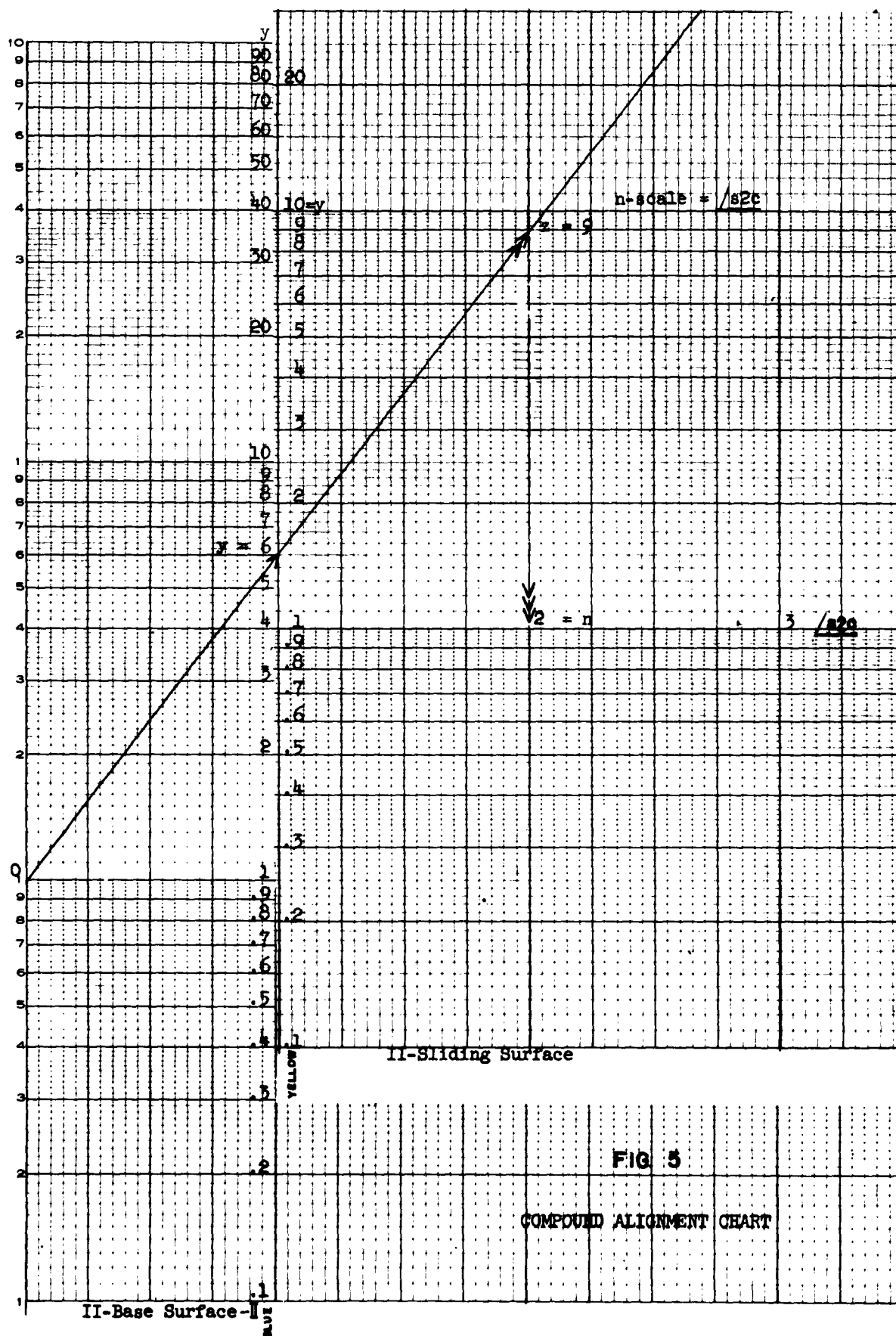
FIG. 4

LINE COORDINATE CHART

Symbolic	$\sqrt{\text{Blue}}D(1) : \sqrt{\text{Blue}}L(y+6)$	Yellow)1(z+9)	Case (1)
Directions	$\sqrt{\text{Blue}}D(1) : \text{Yellow}1(z+9)$	$\sqrt{\text{Blue}}L(y+6)$	Case (2)

II-Base Surface-II

slur



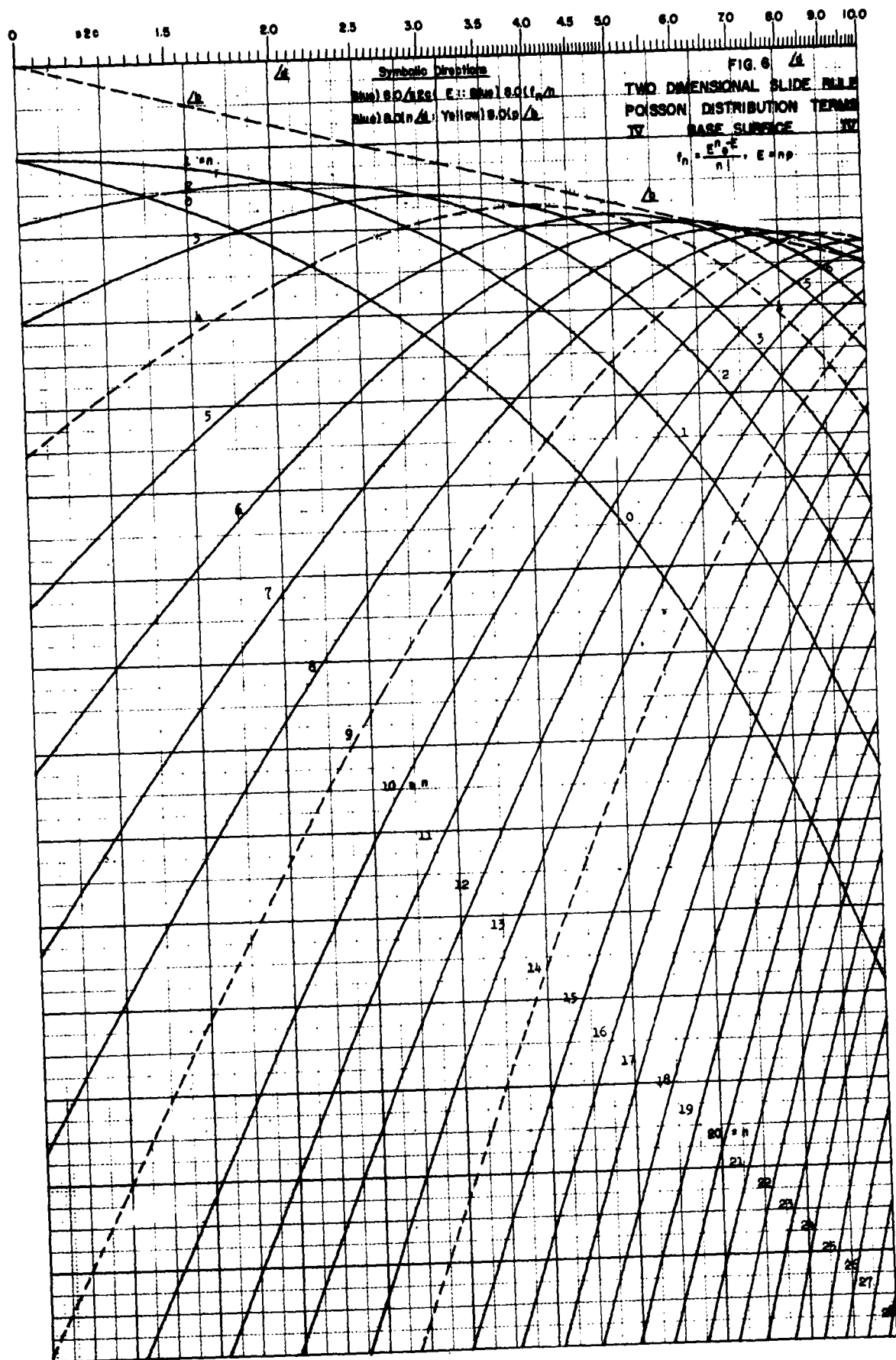
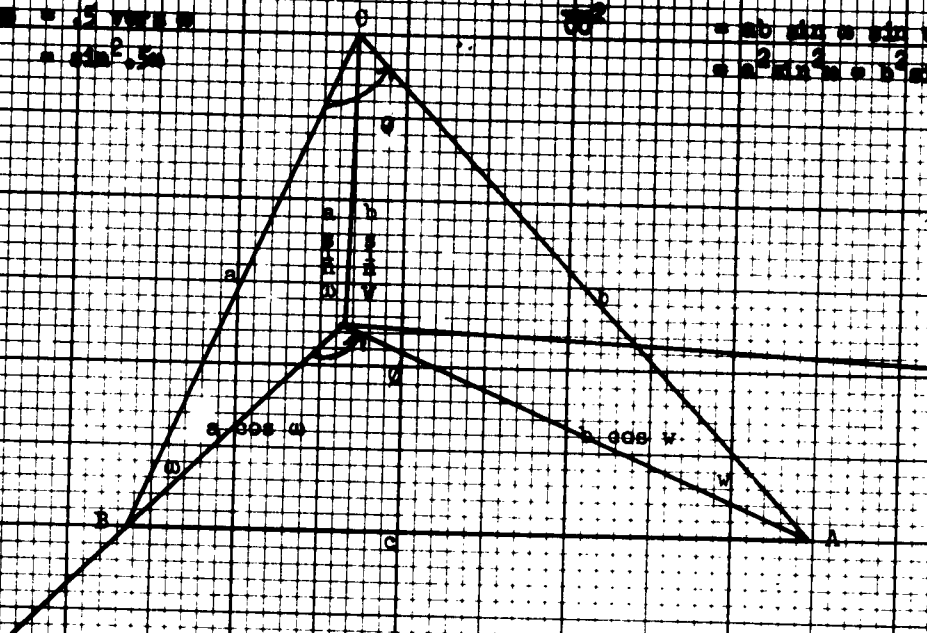


FIG 7
The Reversing Formula

$$\begin{aligned} \text{vers } \phi &= 1 - \cos \phi \\ \text{hav } \phi &= .5 \text{ vers } \phi \\ &= \sin^2 \frac{\phi}{2} \end{aligned}$$

$$\begin{aligned} \cos(\phi - w) &= \sin \phi \sin w + \cos \phi \cos w \\ \frac{1}{\cos^2} &= \frac{ab \sin \phi \sin w}{\cos^2} + \frac{ab \cos \phi \cos w}{\cos^2} \\ &= \frac{a^2 \sin^2 \phi}{\cos^2} + \frac{b^2 \sin^2 w}{\cos^2} \end{aligned}$$



1. AREA $a^2 = b^2 + c^2 - 2ab \cos \phi$

2. AREA $c^2 = a^2 \cos^2 \phi + b^2 \sin^2 \phi - 2ab \cos \phi \cos w \cos \phi$

DIFFERENCE: $0 = 2ab \sin \phi \sin w + 2ab \cos \phi \cos w \cos \phi - 2ab \cos \phi$

3. $\cos \phi = \sin \phi \sin w + \cos \phi \cos w \cos \phi$

4. $1 = 1$

5. $\cos \phi = \cos(\phi - w) + \cos \phi \cos w \text{ vers } \phi$

DIFFERENCE:

6. $\text{vers } \phi = \text{vers}(\phi - w) + \cos \phi \cos w \text{ vers } \phi$

7. $\text{hav } \phi = \text{hav}(\phi - w) + \cos \phi \cos w \text{ hav } \phi$

Let

$N_1 = \cos w \cos \phi$

$N_2 = \cos w \cos \phi \text{ hav } \phi$

$N_3 = \text{hav}(\phi - w)$

$N_4 = N_2 + N_3$

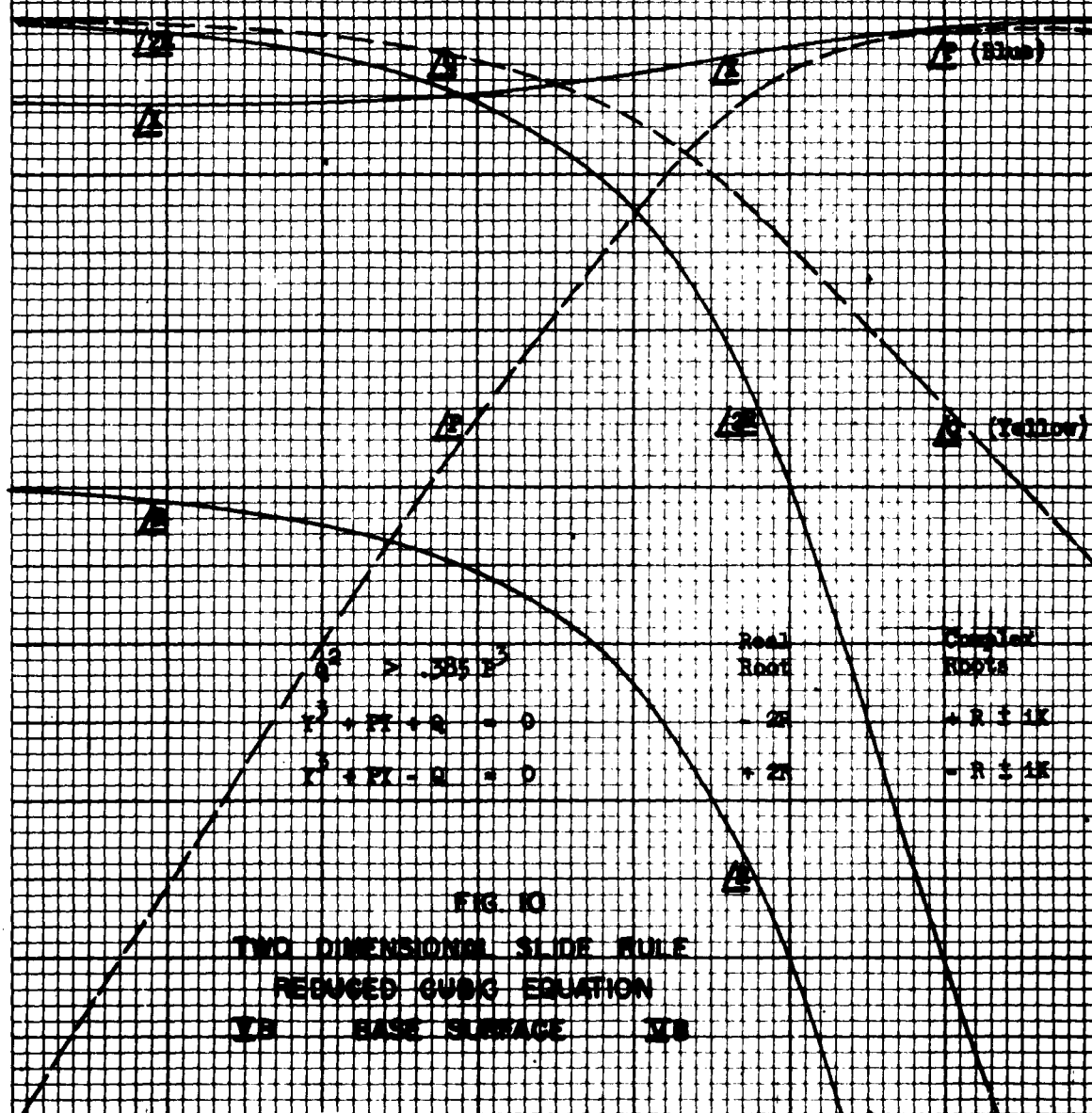
$\phi = \text{arc hav } N_4$

Symbolic Directions for solution of (7) from figure 1

Blue $2(20^\circ/3) : \text{Blue} 2/45c(50^\circ) : \text{Green} 2(M_1/a)$

Orange $2(M_1/a) : \text{Red} 2/45c(50^\circ) : \text{Orange} 2(M_2/h \text{ or } H)$

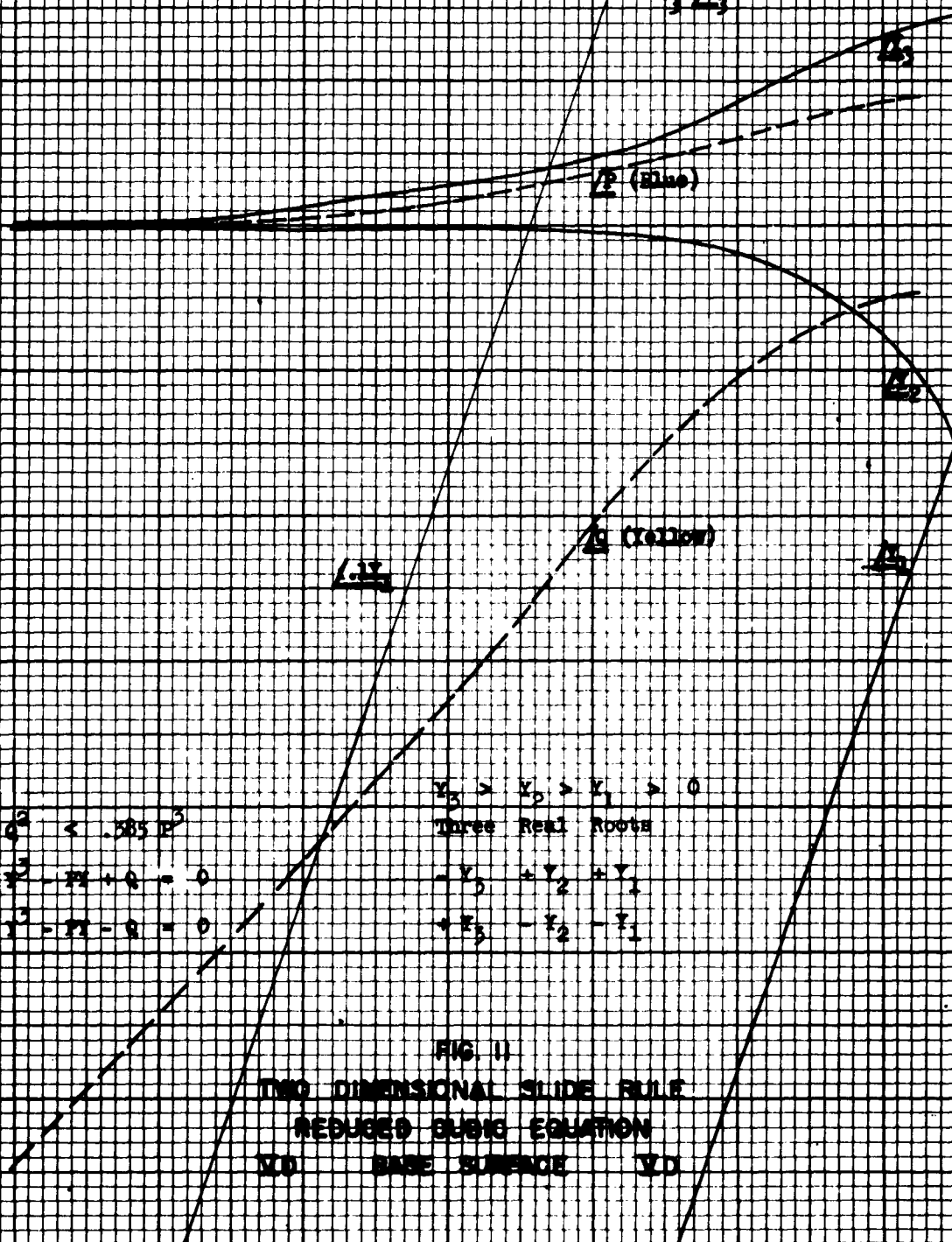
Orange $2(M_2/h \text{ or } H) : \text{Red} 2(w-v/H \text{ or } H) : \text{Red} 2(a/a)$



Symbolic Directions

Blue) 2.6(P) $\frac{1}{3}$; Yellow) 2.5(Q) $\frac{1}{3}$; Black) 2.5(

$\frac{Y_3}{E_3}$
 $\frac{Y_2}{E_2}$
 $\frac{Y_1}{E_1}$



$$Q^2 < .585 P^3$$

$$Y^3 - PY + Q = 0$$

$$Y^3 - PY - Q = 0$$

$$Y_3 > Y_2 > Y_1 > 0$$

Three Real Roots

$$-Y_3 + Y_2 + Y_1$$

$$+Y_3 - Y_2 - Y_1$$

FIG. II

TWO DIMENSIONAL SLIDE RULE

REDUCED SLIG EQUATION

NO BASE SURFACE NO

SLIDING SURFACES

FIG. 12

TWO DIMENSIONAL SLIDE RULE

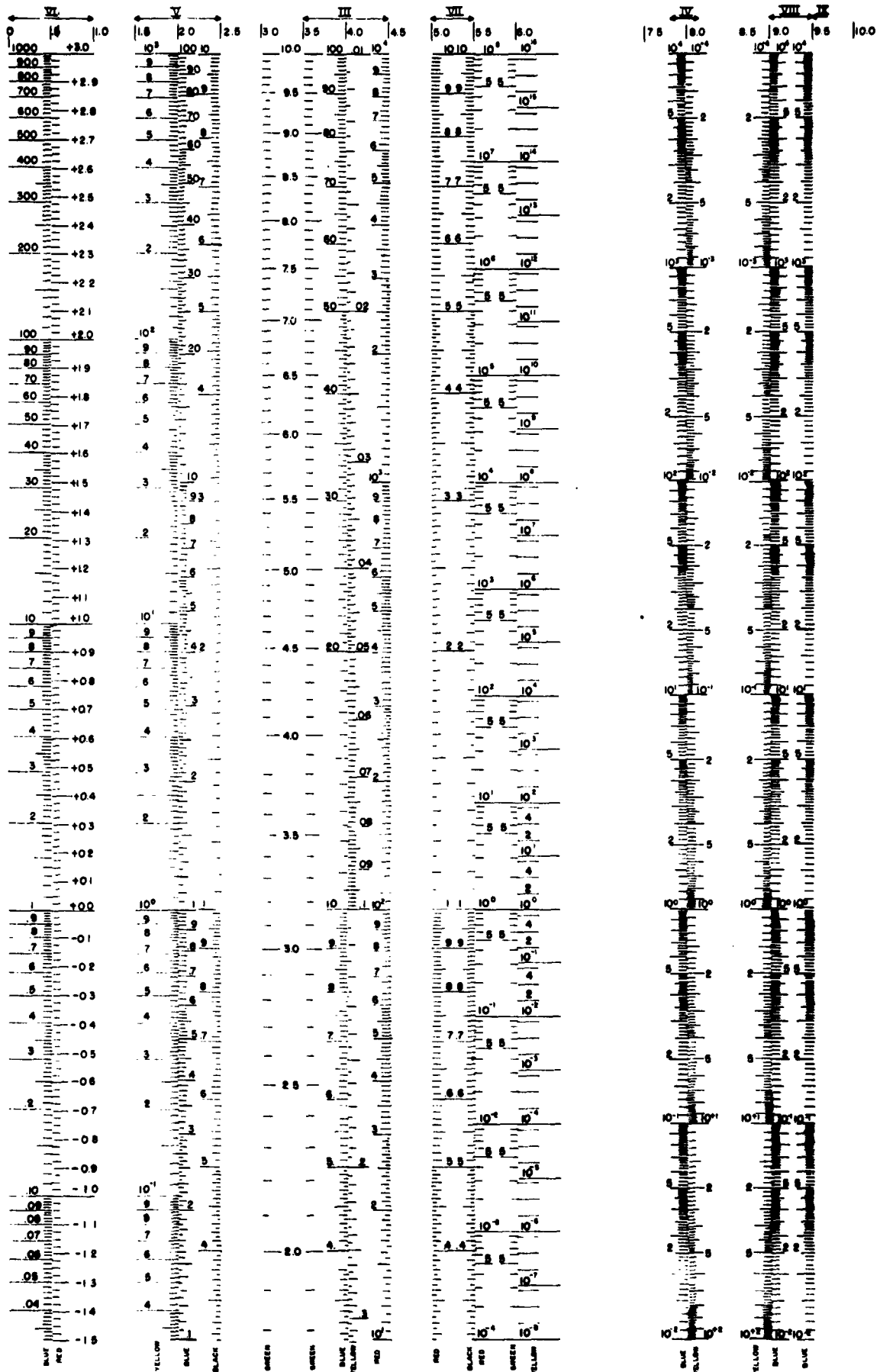


FIG. 12

SLIDING SURFACES

TWO DIMENSIONAL SLIDE RULE

